Serving Correlated Users in Line-of-Sight Massive MIMO Systems for 5G and Beyond

Serving Correlated Users in Line-of-Sight Massive MIMO Systems for 5G and Beyond

A. Farsaei

A catalogue record is available from Eindhoven University of Technology Library.
ISBN: 978-94-6421-366-9

Cover design by M. Nasri
Printed by Ipskamp Printing
Typeset using LaTeX

The research presented in this dissertation was conducted in the Information and Communication Theory Lab (ICTLab) of the Signal Processing Systems (SPS) group at the department of Electrical Engineering, Eindhoven University of Technology (TU/e).

The research project was part of SILIKA consortium. SILIKA has received funding from the European Union's Horizon 2020 research and innovation programme under the Marie Sklodowska-Curie grant agreement No 721732.

Serving Correlated Users in Line-of-Sight Massive MIMO Systems for 5G and Beyond

THESIS

ter verkrijging van de graad van doctor aan de Technische Universiteit Eindhoven, op gezag van de rector magnificus prof.dr.ir. F.P.T. Baaijens, voor een commissie aangewezen door het College voor Promoties, in het openbaar te verdedigen op dinsdag 15 juni 2021 om 16:00 uur

door

Amirashkan Farsaei

geboren te Teheran, Iran

Dit proefschrift is goedgekeurd door de promotoren en de samenstelling van de promotiecommissie is als volgt:

Voorzitter:	prof.dr.ir. J. P. M. Voeten
1e promotor:	prof.dr.ir. F. M. J. Willems
2e promotor:	dr. A. Alvarado
Leden:	prof.dr.ir. S.M. Heemstra
	prof.dr. R. Fischer (Ulm University)
	prof.dr. C. Studer (ETH Zürich)
Adviseur:	dr. U. Johannsen
	dr. U. Gustavsson (Ericsson Research)

Het onderzoek of ontwerp dat in dit proefschrift wordt beschreven is uitgevoerd in overeenstemming met de TU/e Gedragscode Wetenschapsbeoefening.

To the meaning of my life

Maedeh and *my family*.

Summary

Massive multiple-input-multiple-output (MIMO) technology plays a crucial role in the fifth-generation (5G) of cellular communication systems. One of the key properties exploited in massive MIMO systems is favorable propagation (FP). FP is defined as mutual orthogonality among the channel vectors of users. It has been shown in the literature that line-of-sight (LOS) environments and independent and identically distributed Rayleigh fading exhibit FP. However, in LOS environments, there is a nonnegligible probability that the channel vectors of a small number of users become correlated, which makes the environment non-favorable. Correlated users lead to a reduction in the achievable sum-rates of known linear precoders, e.g., conjugate beamforming (CB) or zero-forcing (ZF) and nonlinear precoders, e.g., Tomlinson-Harashima Precoding (THP). In two LOS scenarios, which are identified as important for future 5G systems, "open exhibition" and "crowded auditorium", a large number of users are physically co-located, and thus, many users may have correlated channel vectors. Dealing with these correlated scenarios in LOS environments is of great importance for future 5G and beyond systems. In this thesis, we study three different strategies to deal with correlated scenarios for time-division-duplexing single-cell LOS massive MIMO.

In the first strategy, we focus on using low-complexity precoders. We propose a low-complexity linear precoder and a low-complexity *hybrid* linear and nonlinear precoder (HLNP). The idea of the reduced-complexity linear precoder is to switch between two known linear precoders, i.e., CB and ZF, based on the channel condition. The proposed linear precoder has the sum-rate performance better than both CB and ZF, and has a complexity lower than ZF. The idea of the low-complexity HLNP is to use nonlinear precoding for a limited number of users and to use linear precoding for the rest of the users. By employing the proposed HLNP, the complexity of nonlinear precoding in massive MIMO systems is reduced, while a close to nonlinear precoding performance is achieved. We propose a grouping method to divide the users into two groups. For the first group a proposed modified THP is employed and for the second group linear precoding is used. The proposed HLNP offers a tunable trade-off between computational complexity and performance by varying the number of users in the first group.

In the second strategy, we propose to employ a uniform linear array (ULA) at the BS with optimized inter-element spacing. For a given ULA with an arbitrary inter-element

spacing, we derive the probability that the correlation among the channel vectors of two users being above a threshold. The inter-element spacing of the proposed ULA is the one for which the derived probability is minimized. The proposed ULA is optimized and has the best outage performance for the case when there are only two users. For more users, we present simulation results to show the effectiveness of the proposed array compared to the conventional half-wavelength ULA with a known linear precoder, i.e., ZF.

In the third strategy, we investigate dropping algorithms to drop and reschedule some of the correlated users. It has been shown in the literature that by dropping some users with a spatial correlation higher than a predefined threshold, one can improve the cumulative distribution function of the effective signal to noise ratio (SNR) of the users considerably. However, in the literature, the threshold on the spatial correlation has been found throughout simulations. We derive a threshold for the spatial correlation for a specific channel, and show that we can use it for general cases with a small loss in performance. Particularly, we derive the thresholds for two known linear precoders, i.e., CB and ZF, and for a known non-linear precoder, i.e., THP. We further propose a neural network based dropping algorithm that achieves better sum-rate performance compared to the previous correlation-based dropping algorithms. Finally, we propose an iterative filter-based dropping algorithm (IFDA), which achieves near-optimal performance with limited complexity. In contrast to the previous algorithms in the literature, our proposed IFDA does not require a predefined threshold for the spatial correlation of the users and does not require any preprocessing.

List of Publications

This thesis is based on the following publications.

Journal Papers

[J1] A. Farsaei, A. Alvarado, F. M. J. Willems, and U. Gustavsson, "A low-complexity hybrid linear and nonlinear precoder for line-of-sight massive MIMO with max-min power control," *submitted to IEEE Transactions on Wireless Communications*

[J2] A. Farsaei, N. Amani, R. Maaskant, U. Gustavsson, A. Alvarado, and F. M. J. Willems, "Uniform linear arrays with optimized inter-element spacing for LOS massive MIMO," *IEEE Communications Letters*, vol. 25, no. 2, pp. 613–616, Feb. 2021

[J3] A. Farsaei, A. Alvarado, F. M. J. Willems, and U. Gustavsson, "An improved dropping algorithm for line-of-sight massive MIMO with max-min power control," *IEEE Communications Letters*, vol. 23, no. 6, pp. 1109–1112, Jun. 2019

[J4] ——, "An improved dropping algorithm for line-of-sight massive MIMO with Tomlinson-Harashima Precoding," *IEEE Communications Letters*, vol. 23, no. 11, pp. 2099–2103, Nov. 2019

[J5] A. Farsaei, A. Sheikh, U. Gustavsson, A. Alvarado, and F. M. J. Willems, "DropNet: an improved dropping algorithm based on neural networks for line-of-sight massive MIMO," *IEEE Access*, vol. 9, pp. 29 441–29 448, 2021

[J6] A. Farsaei, N. Amani, R. Maaskant, U. Gustavsson, A. Alvarado, and F. M. J. Willems, "A near-optimal dropping algorithm for line-of-sight massive MIMO with max-min power control," *submitted to IEEE Communications Letters*

Conference Paper

[C1] A. Farsaei, F. Willems, A. Alvarado, and U. Gustavsson, "A reduced-complexity linear precoding strategy for massive MIMO base stations," in *2018 25th International Conference on Telecommunications (ICT)*, Jun. 2018, pp. 121–126

Patent Applications

[P1] A. Farsaei, A. Alvarado, F. M. J. Willems, and U. Gustavsson, "Multi-user precoding: Low-complexity precoding for highly correlated scenarios," PCT patent application,PCT/EP2020/059238, April 1, 2020

[P2] ——, "Multi-user precoding: Low-complexity precoding, compute the correlation-limit," PCT patent application, PCT/EP2020/059241, April 1, 2020

[P3] A. Farsaei, A. Sheikh, A. Alvarado, F. M. J. Willems, and U. Gustavsson, "Neural network for MU-MIMO user selection," PCT patent application, PCT/EP2021/053718, February 16, 2021

[P4] A. Farsaei, A. Alvarado, F. M. J. Willems, and U. Gustavsson, "User selection for MU-MIMO," PCT patent application, PCT/EP2021/053713, February 16, 2022

The following publications are not included in the thesis.

Other Publications

[O1] A. Farsaei, N. Amani, A. Alvarado, F. M. J. Willems, U. Gustavsson, and R. Maaskant, "On the outage performance of line-of-sight massive MIMO with a fixed-length uniform linear sparse array," in *2019 IEEE-APS Topical Conference on Antennas and Propagation in Wireless Communications (APWC)*, 2019, pp. 345–348

[O2] T. A. H. Bressner, A. Farsaei, M. Fozooni, U. Johannsen, M. N. Johansson, and A. Bart Smolders, "MIMO performance evaluation of isotropic, directional and highly-directional antenna systems for mm-wave communications," in *2019 13th European Conference on Antennas and Propagation (EuCAP)*, 2019, pp. 1–5

[O3] T. Marinovic, A. Farsaei, R. Maaskant, A. L. Lavieja, M. N. Johansson, U. Gustavsson, and G. A. E. Vandenbosch, "Effect of antenna array element separation on capacity of MIMO systems including mutual coupling," in *2019 IEEE International Symposium on Antennas and Propagation and USNC-URSI Radio Science Meeting*, 2019, pp. 415–416

[O4] N. Amani, A. Farsaei, U. Gustavsson, T. Eriksson, F. M. J. Willems, M. V. Ivashina, and R. Maaskant, "Array configuration effect on the spatial correlation of MU-MIMO channels in NLoS environments," in *2020 14th European Conference on Antennas and Propagation (EuCAP)*, 2020, pp. 1–4

[O5] N. Amani, A. Farsaei, S. Rezaei Aghdam, T. Eriksson, M. V. Ivashina, and R. Maaskant, "Sparse array synthesis including mutual coupling for MU-MIMO average capacity maximization," *submitted to IEEE Transaction on Antennas and Propagation*

List of Abbreviations

Symbol	Description
4G	fourth generation
5G	fifth generation
3GPP	third generation partnership project
AWGN	additive white Gaussian noise
BER	bit error rate
BLER	block error rate
BS	base station
CB	conjugate beamforming
CDF	cumulative distribution function
CSI	channel state information
DPC	dirty paper coding
eMBB	enhanced mobile broadband
i.i.d	independent and identically distributed
IoT	internet of things
LOS	line of sight
LTE	long-term evolution
MMSE	minimum mean square error
MRT	maximum ratio transmission
MTC	massive machine-type communication
NR	new radio
OFDM	orthogonal frequency-division multiplexing
PA	power amplifier
QPSK	quadrature phase-shift keying
SE	spectral efficiency
SIC	successive interference cancellation
SINR	signal to interference and noise ratio
SNR	signal to noise ratio
TDD	time-division duplexing
URLLC	ultra-reliable low-latency communication
ZF	zero-forcing

Table of Contents

Part I

Overview

CHAPTER 1

Introduction

1.1 Background

Information and communication technologies (ICTs) have transformed societies, cultures, and economies over the past four decades. ICTs have improved quality of life and contributed to economic growth and innovation. From early 2020 and the rise of the Covid-19 pandemic, ICTs have helped individuals and companies to deal with social distancing and working remotely.

Cellular networks have evolved significantly since the first-generation (1G) of mobile communication systems in the early 1980s. Mobile systems in 1G were analog and capable of providing only voice calls. Nowadays, mobile systems are digital and mainly provide data rather than voice. The fifth-generation (5G) of mobile communication systems known as New Radio (NR) was standardized by the third-generation partnership project (3GPP) in 2017 and 2018 [17]. To date, there have been more than seventy five 5G commercial launches across the world [18]. A wide range of use cases have emerged in 5G, e.g., augmented and virtual reality (AR/VR) and video streaming, autonomous vehicle control, and factory automation [19]. 5G targets three main use case families with different connectivity requirements, i.e., enhanced mobile broadband (eMBB), ultra-reliable low-latency communication (URLLC) and machine-type communication (MTC) [20], which are illustrated in Fig. 1.1. Mobile broadband is related to human-centric use cases, e.g., mobile phones and mobile personal computers/tablets. In contrast, MTC and URLLC are related to machine-centric use cases, e.g., low-cost sensors and autonomous vehicles [21]. Typical requirements of each family of 5G use cases are shown in Fig. 1.1.

By the end of 2025, the number of mobile subscriptions is forecast to be 8.9 billion (2.8 billion are 5G, see Fig. 1.2) of which 88% are for eMBB [18]. To address the throughput requirements of eMBB, new wireless technologies are required for 5G NR. The new wireless technologies should be scalable for serving more and more users with

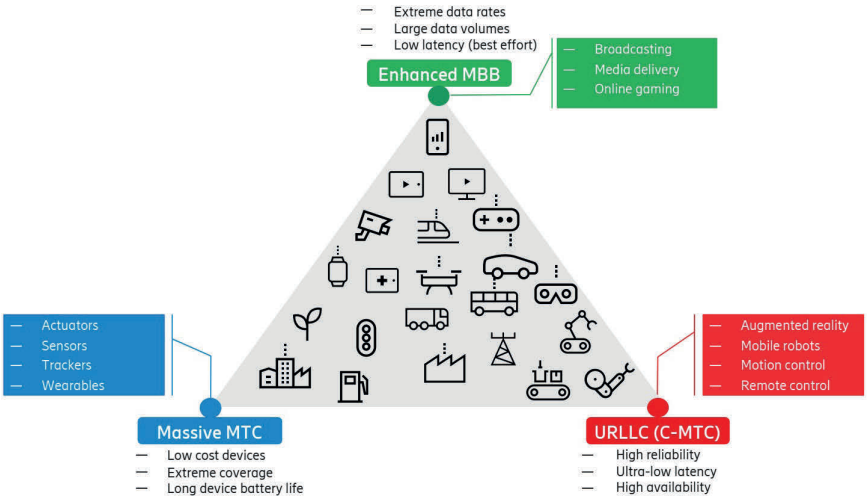

Figure 1.1: The main families of 5G use cases [21]

a higher throughput [22]. Many wireless standards cannot meet this requirement, since they do not have enough bandwidth. One approach to analyze the throughput requirements of eMBB is by studying the area throughput [23]. The area throughput is defined as the number of information bits per unit time that can be delivered to a given area, measured in bits/s/km^2. To increase the area throughput one can increase the cell density (the number of cells per square kilometer), spectral efficiency (SE), or bandwidth. Typically, increasing cell density is quite costly and entails high deployment and maintenance costs [23].

To increase SE, multiple-input-multiple-output (MIMO) technology can be used. MIMO technology has been used in 4G [24] and 5G NR [17, 25]. MIMO technology provides spatial multiplexing by transmitting multiple data streams at the same time-frequency resource to a single user (SU) or multiple users (MU), where each data stream can be beamformed. Beamforming in transmitting mode is the ability to direct energy toward a specific receiver, which increases the received signal level of the user, and consequently, increases its throughput. In SU-MIMO, multiple data streams are transmitted from a multi-antenna base station (BS) to a single user with multiple antennas. In MU-MIMO, multiple data streams are simultaneously transmitted from the BS to multiple single-antenna or multiple-antenna users. The MU-MIMO with a large number of active elements at the BS (much larger than the number of users) is often referred to as massive MIMO [26] also known as large-scale antenna systems. Massive MIMO plays a critical role in the evolution of 4G to 5G [27]. The world's first commercially available 5G NR, i.e., AIR6468 is unveiled in 2016 with 64 transmit and 64 receive antennas supporting massive MIMO. Furthermore, there are emerging massive MIMO technologies for beyond 5G, e.g., cell-free massive MIMO and holographic massive MIMO [28].

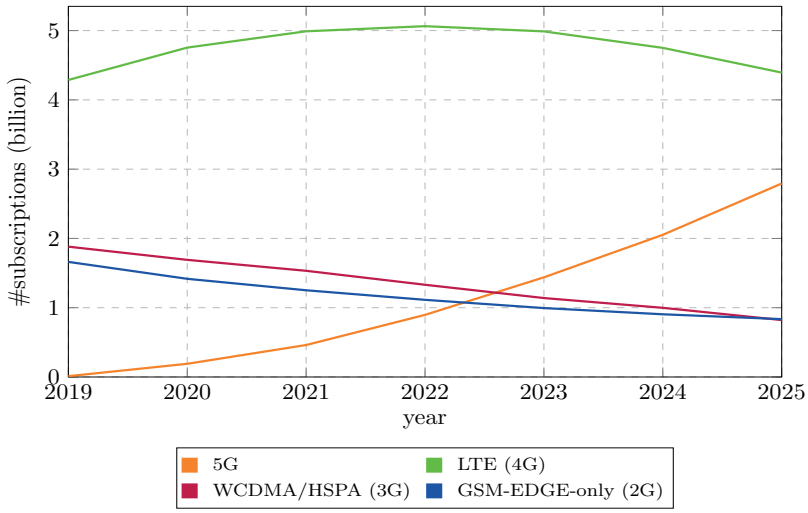

Figure 1.2: Mobile subscriptions by technology [18].

One of the key properties of the radio channel that is exploited in massive MIMO systems is favorable propagation (FP). FP is defined as the mutual orthogonality of the channel vectors of users. By increasing the number of antennas at the BS of a massive MIMO system, the channel vectors of the users become mutually orthogonal, which leads to FP. The mutual orthogonality of the users implies that the inter-user interference is removed and linear processing becomes optimal. Adding more antennas in massive MIMO systems is always beneficial for increased throughput, reduced radiated power, uniformly good service everywhere in the cell, and more simplicity in signal processing [29]. To achieve these improvements, time-division duplex (TDD) operation is employed in massive MIMO systems for which channel reciprocity holds. By using channel reciprocity, the estimated uplink channel is used for the transmitter over the downlink channel, which limits the channel state information (CSI) overhead. These properties make massive MIMO systems a scalable technology that can come up with higher throughput requirement for larger networks [29].

Another solution to address the throughput requirement of eMBB is to increase the bandwidth by exploiting the spectrum that is currently unused. In 5G NR, two frequency ranges are used: “sub 6GHz” and “millimeter-wave” [30]. By implementing massive MIMO in the millimeter-wave band, one can increase the throughput by using more bandwidth available in millimeter-wave band. However, there are challenges in millimeter-wave communication bands because the channel model is different from sub 6GHz. In millimeter-wave there is lower diffraction, higher scattering, higher penetration loss, high sensitivity to blockage and strong differences between line-of-sight (LOS) and non-LOS propagation conditions [31]. An overview of techniques for dealing with

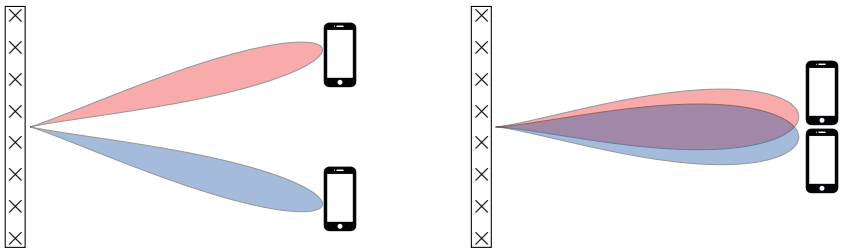

(a) Orthogonal channel vectors. (b) Correlated channel vectors

Figure 1.3: A ULA serves two users when the channel vectors of the users are a) orthogonal and b) correlated. The correlation occurs when the beam intended for a user is overlapped with the beam of the other user.

challenges in millimeter-wave MIMO systems has been given in [31]. Despite these challenges, millimeter-wave found its way in 5G NR, e.g., millimeter-wave Verizon is in the second year of delivering 5G services in the US using the millimeter-wave spectrum [18].

There are challenges in particular 5G use cases. Providing connectivity for the end-user even in very crowded places such as stadiums, shopping malls, open-air festivals, other public events that attract lots of people, unexpected traffic jams and crowded public transportation [32], is of great importance. For instance, consider a BS with a uniform linear array (ULA) that serves two users with a LOS path to the BS in two different scenarios (see Fig. 1.3). The BS creates one beam for each user. In the first scenario (Fig. 1.3a), the users are far apart, and the created beams do not overlap. In this case, the channel vectors from the ULA to the users are orthogonal, leading to a FP environment. In the second scenario (Fig. 1.3b), the users are closely located. The created beams overlap, which means the channel vectors of the users are correlated. A high correlation of the channel vectors leads to a reduction in data throughput.

To alleviate the loss in the data throughput of downlink channel in the correlated scenarios, different strategies can be employed. One strategy is to employ a more advanced signal processing technique at the BS to increase the data throughput. For instance, nonlinear precoding technique can be employed instead of linear precoding to increase the data throughput with the cost of high computational complexity. To trade-off complexity and data throughput, hybrid linear and nonlinear precoding is suggested in the literature. The other alternative is to use an optimized antenna array at the BS instead of conventional half-wavelength antenna array. In this case, the propagation environment changes such that the downlink throughput increases for the optimized antenna arrays compared to conventional BS antenna array. Furthermore, one can use a dropping algorithm to drop some of the correlated users to avoid the correlated scenarios, and increase the data throughput. These three strategies are the main subjects of this thesis.

1.2 Scope of the Thesis

In this thesis, we study the following three research questions (RQs) to address dealing with correlated scenarios in TDD single-cell LOS massive MIMO systems.

- **RQ1:**
  What are the precoding techniques that trade-off complexity vs. performance for LOS massive MIMO systems while improving the performance of linear precoding?

- **RQ2:**
  What is the inter-element spacing for the ULA at the BS that has the optimal outage performance, i.e., minimizes the probability of occurrence of the correlated scenarios?

- **RQ3:**
  What are the dropping algorithms that can achieve near-optimal performance with feasible computational complexity?

Each research question in this thesis deals with the problem of correlated scenarios from a different perspective. In this thesis, we use three different strategies (see Fig. 1.4) to address the research questions. Nevertheless, the goal of all these strategies is to find ways to improve the achievable sum-rate of linear precoders at the BS of a massive MIMO system with half-wavelength inter-element spacing. The first strategy (S1) is to use a low-complexity precoder, the second strategy (S2) is to design a ULA with an optimized inter-element spacing, and the third strategy (S3) is to employ a dropping algorithm. We further elaborate on each research question and each strategy by presenting our contributions in the thesis as follows. A summary of our contributions is depicted in Fig. 1.4.

1.2.1 RQ1, S1 (Low-Complexity Precoders)

[C1] "A reduced-complexity linear precoding strategy for massive MIMO base stations"
A linear precoder is proposed based on switching between two known linear precoders, i.e., conjugate beamforming (CB) and zero-forcing (ZF) for LOS propagation environments. The proposed idea is to predict and use the precoder, which results in the highest sum-rate for a given channel. The achievable sum-rate of the proposed precoder is higher than both CB and ZF, while its computational complexity is lower than that of ZF. Thus, in correlated scenarios, the proposed precoder is a better candidate than CB and ZF. For the proposed precoder, simulations are required in advance to find the regimes where CB or ZF results in a higher sum-rate.
[J1] "A low-complexity hybrid linear and nonlinear precoder for line-of-sight massive MIMO with max-min power control"

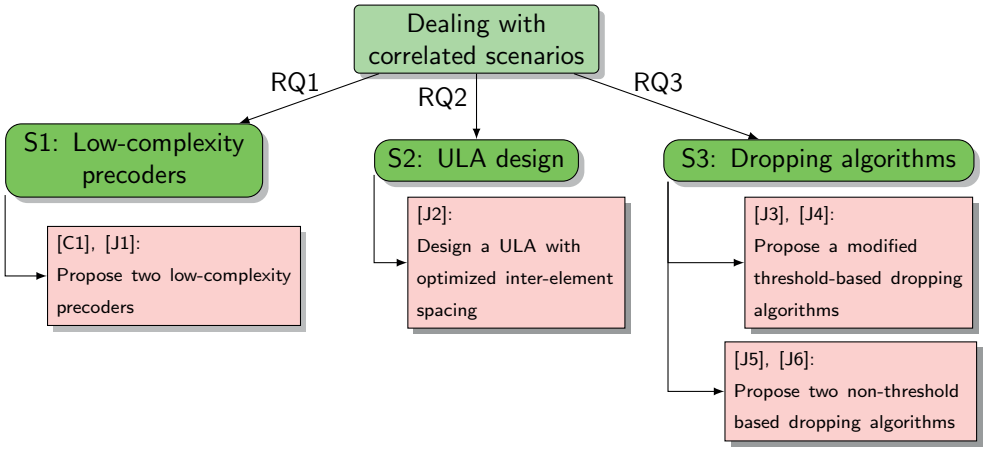

Figure 1.4: The summary of the thesis: the strategy used to address each research question, and the contributions for each strategy.

To alleviate the loss in the sum-rate of linear precoders, nonlinear precoders can be used. However, nonlinear precoding entails a high computational complexity. To reduce the complexity of nonlinear precoders, we propose a hybrid linear and nonlinear precoder with max-min power control based on the proposed modified Tomlinson-Harashima precoding (THP) method. We propose a grouping scheme where users are divided into two groups. For the first group, the proposed modified THP is used, while for the second group, linear precoding is employed. In the end, the precoded vectors of the two groups are combined. The proposed precoder offers a tunable trade-off between computational complexity and performance by varying the number of users in the first group. Besides, we show that in LOS massive MIMO, it is more probable that there are only one or two correlated pairs of users.

1.2.2 RQ2, S2 (ULA Design)

[J2] Uniform Linear Arrays with Optimized Inter-Element Spacing for LOS Massive MIMO

We propose a ULA with an optimized inter-element spacing at the BS to reduce the occurrence of correlated scenarios at the cost of increasing the aperture size at the BS. For a given ULA with an arbitrary inter-element spacing, we derive the probability that the correlation among the channel vectors of two users is above a threshold. The inter-element spacing of the proposed ULA is the one for which the derived probability is minimized. The proposed ULA has the best outage performance when there are only two users. For more users, we present simulation results to show the effectiveness of the proposed array compared to the conventional half-wavelength ULA with a known linear

precoder, i.e., ZF.

1.2.3 RQ3, S3 (Dropping Algorithms)

[J3] "An improved dropping algorithm for line-of-sight massive MIMO with max-min power control"
[J4] "An improved dropping algorithm for line-of-sight massive MIMO with Tomlinson-Harashima Precoding"
In [J3]-[J4], we study the use of a simple dropping algorithm for LOS massive MIMO as previously proposed in [33]. It is shown in [33] that by dropping some users with a spatial correlation higher than a predefined threshold, one can considerably improve the cumulative distribution function (CDF) of the effective signal to noise ratio (SNR) of the users. However, the threshold on the spatial correlation has been found throughout simulations [33]. We derive a threshold for the spatial correlation for a channel with only two users, and show that we can use it for general cases when there are more users with a small loss in performance. Particularly, in [J3] and [J4], we derive the thresholds for two known linear precoders, i.e., CB and ZF, and for a known non-linear precoder, i.e., THP. In these works, we focus on max-min power control at the BS, which is used to provide uniformly good service for the users [34]. In addition, in [4], we derive the threshold for equal received power control.
[J5] "DropNet: An improved dropping algorithm based on neural networks for line-of-sight massive MIMO"
[J6] "A near-optimal dropping algorithm for line-of-sight massive MIMO with max-min power control"
By using an exhaustive search for the dropping problem, we can find the set of users that shall be dropped such that the achievable sum-rate with max-min power control is maximized for the remaining users. By employing the dropping algorithm of [33] with the derived thresholds in [J3, J4] instead of the exhaustive search, the performance is suboptimal in general. We have proposed two dropping algorithms in [J5] and [J6] that do not rely on a predefined threshold and achieve a better performance compared to the dropping algorithm of [33] with the thresholds in [J3, J4].
In [J5], we propose a dropping algorithm based on neural networks (DropNet) to find the users that shall be dropped. By employing DropNet, we can reduce the complexity of the exhaustive search and achieve a better sum-rate performance compared to the previous correlation-based dropping algorithms. We train the neural network in DropNet using a large number of channel realizations, where the input features are the spatial correlation and the norm of the channel vectors of the users. The results show that by employing DropNet, we can trade-off complexity and performance.
In [J6], we propose an iterative filter-based dropping algorithm (IFDA), which achieves near-optimal performance. At each iteration, the user with the highest filter norm is dropped. By comparing the sum-rate of all the iterations, the best set of dropped users is found. In contrast to previous algorithms in the literature, our proposed IFDA does not

require a predefined threshold for the spatial correlation of the users or any preprocessing. Compared to an exhaustive search, the complexity of IFDA is reduced significantly. Simulations results are given in [J6] to show the effectiveness of the proposed IFDA with ZF and THP.

1.3 Organization of Thesis

This thesis is divided into two parts. In the first part (Part I), a background and some general information are given about the topic. The second part (Part II) comprises the included papers. The rest of Part I is organized as follows. In Chapter 2, the principles of LOS massive MIMO systems are reviewed. A review of precoding strategies is presented in Chapter 3. In Chapter 4, we elaborate on the proposed strategies. In Part II, the included papers are presented in Chapter 5 to Chapter 11. In Chapters 5 and 6, the proposed low-complexity precoders are presented ([C1] and [J1]). In Chapter 7, the proposed ULA with optimized inter-element spacing is given ([J2]). Chapter 8 and Chapter 9 improve the previously proposed dropping algorithm of [33] for known linear and nonlinear precoders ([J3] and [J4]). Chapter 10 uses neural networks to improve the dropping algorithm and provides a complexity-performance trade-off ([J5]). Chapter 11 presents a near-optimal dropping algorithm for two known precoders ([J6]). Finally, the conclusion of the thesis is presented in Chapter 12.

1.4 Notation

The following notation is used throughout the thesis. Lowercase, bold lowercase and bold uppercase letters denote scalars, column vectors, and matrices, respectively. The symbols $|\cdot|$, $\|\cdot\|$, $\mathbb{Z}$ and $\mathbb{C}$ denote the absolute value, l^2-norm, the set of integers, and the set of complex numbers, respectively. The superscripts ^{T} and ^{H} denote unconjugated transpose and conjugated transpose, respectively. A diagonal matrix with diagonal entries taken from the vector $\boldsymbol{p}$ is denoted by $\text{diag}(\boldsymbol{p})$, $\boldsymbol{I}_K$ denotes the identity matrix of size $K \times K$, $\text{tr}(\cdot)$ denotes the trace operation, and $\det(\cdot)$ denotes the determinant operation. The symbol $\mathcal{CN}(\boldsymbol{\mu}, N_0\boldsymbol{I}_K)$ denotes a vector of complex Gaussian random variables with mean $\boldsymbol{\mu}$ and covariance matrix of $N_0\boldsymbol{I}_K$. The imaginary unit is denoted by $\jmath$. The operator $\otimes$ denotes the Kronecker product.

CHAPTER 2

2

Line-Of-Sight Massive MIMO

In this chapter, we present the basics of LOS TDD massive MIMO systems, which is the system under study in Part II of the thesis. We assume that the BS uses the same time-frequency resource to serve single-antenna users. We further assume that the communication system operates over a frequency-flat channel, and the hardware components are assumed to be ideal. In the following, first, the LOS propagation environment is reviewed. Then, a review of Shannon capacity is presented. Afterward, single-cell TDD massive MIMO systems are introduced.

2.1 Line-of-Sight Environments

The free-space LOS channel model for ULAs and uniform planar arrays (UPAs) is presented as follows. Assume a BS equipped with a ULA of M antennas located on the x-axis (see Fig. 2.1). Besides, assume that the user i is in the x-y plane, where R_i is the distance from the user to the first element of the array, and ϕ_i is the azimuth angle of the user. The channel vector from the BS antennas to the user i is modeled as (see [35, Sec. 7.2.2] for more details)

$$\begin{aligned}\boldsymbol{h}_i &= (h_{i1}, h_{i2}, \dots, h_{iM})^T \\ &= \sqrt{\beta_i} e^{-\jmath \frac{2\pi}{\lambda} R_i} \left(1, e^{\jmath \frac{2\pi}{\lambda} \delta \cos(\phi_i)}, e^{\jmath \frac{2\pi}{\lambda} 2\delta \cos(\phi_i)}, \dots, e^{\jmath \frac{2\pi}{\lambda} (M-1)\delta \cos(\phi_i)}\right)^T,\end{aligned} \tag{2.1}$$

where β_i is the large-scale fading for user i, λ is the wavelength and δ is the inter-element spacing (typically $\lambda/2$).

A UPA with $M = N_x \times N_y$ elements is shown in Fig. 2.2. The UPA is located on the x-y plane with $z = 0$, which serves a user at the spherical coordinate (R_i, θ_i, ϕ_i). The channel vector for user i in this case is found by (see [36, eq. (5)])

$$\boldsymbol{h}_i = (h_{i1}, h_{i2}, \dots, h_{iM})^T = \sqrt{\beta}_i e^{-\jmath \frac{2\pi}{\lambda} R_i} \boldsymbol{v}_x(\phi_i, \theta_i) \otimes \boldsymbol{v}_y(\phi_i, \theta_i), \tag{2.2}$$

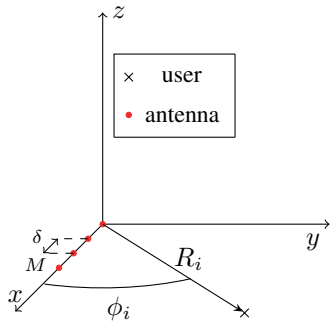

Figure 2.1: Illustration of a ULA with $M = 4$ elements located on x-axis with inter-element spacing of δ. The distance between the first element of the array and the user is R_i.

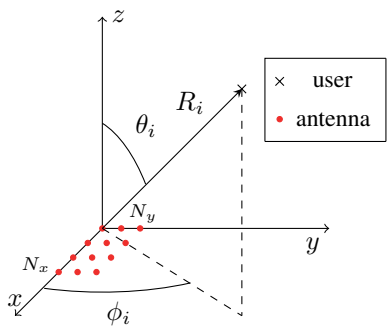

Figure 2.2: Illustration of a UPA with $N_x = 4$ and $N_y = 3$ serving a user at (R_i, θ_i, ϕ_i).

where θ_i is the polar angle of user i as in the spherical coordinates and $\boldsymbol{v}_x(\phi_i, \theta_i)$ and $\boldsymbol{v}_y(\phi_i, \theta_i)$ are

$$\boldsymbol{v}_x(\phi_i, \theta_i) = \left(1, e^{\jmath \frac{2\pi}{\lambda} \delta \sin(\theta_i) \cos(\phi_i)}, e^{\jmath \frac{2\pi}{\lambda} 2\delta \sin(\theta_i) \cos(\phi_i)}, ..., e^{\jmath \frac{2\pi}{\lambda} (N_x - 1)\delta \sin(\theta_i) \cos(\phi_i)}\right)^T, \tag{2.3}$$

$$\boldsymbol{v}_y(\phi_i, \theta_i) = \left(1, e^{\jmath \frac{2\pi}{\lambda} \delta \sin(\theta_i) \sin(\phi_i)}, e^{\jmath \frac{2\pi}{\lambda} 2\delta \sin(\theta_i) \sin(\phi_i)}, ..., e^{\jmath \frac{2\pi}{\lambda} (N_y - 1)\delta \sin(\theta_i) \sin(\phi_i)}\right)^T. \tag{2.4}$$

By using transmit beamforming, the BS antenna array can direct energy toward a specific direction that a user is located. An array with a narrower beamwidth has a better ability to direct energy toward a user, which means the array is more capable of distinguishing two different users. In Fig. 2.3, a ULA with $M = 4$ (Fig. 2.3a) and a ULA

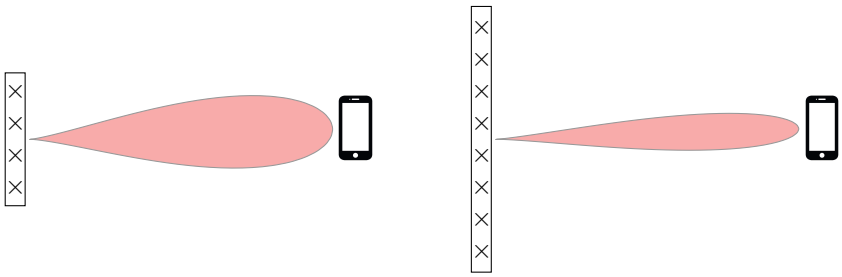

(a) $M = 4$. (b) $M = 8$

Figure 2.3: A ULA with a) $M = 4$ and b) $M = 8$ antennas, both with half-wavelength spacing. The array with $M = 8$ has a narrower beamwidth, and therefore, has a better ability to direct the energy twoard the user.

with $M = 8$ antennas (Fig. 2.3b) both with half-wavelength spacing are serving a user. The array with more number of antennas has a larger aperture size, and therefore, has a narrower beamwidth.

We use the spatial correlation to compare the ability of an array to distinguish two different users. The normalized spatial correlation of the channel vectors of user i and j is found by

$$|\rho| = \left| \frac{\boldsymbol{h}_j^H \boldsymbol{h}_i}{\|\boldsymbol{h}_i\| \|\boldsymbol{h}_j\|} \right|. \tag{2.5}$$

By replacing (2.1) in (2.5), $|\rho_{ij}|$ is found for a ULA with M elements

$$|\rho_{ij}| = \frac{1}{M} \left| \frac{\sin\left(\pi M \frac{\delta}{\lambda} \psi\right)}{\sin\left(\pi \frac{\delta}{\lambda} \psi\right)} \right|, \tag{2.6}$$

where $\psi = \cos(\phi_i) - \cos(\phi_j)$. For a UPA with $N_x \times N_y$ antennas, $|\rho_{ij}|$ is found by replacing (2.2) in (2.5) as

$$|\rho_{ij}| = \frac{1}{N_x N_y} \left| \frac{\sin\left(\pi N_x \frac{\delta}{\lambda} \kappa\right)}{\sin\left(\pi \frac{\delta}{\lambda} \kappa\right)} \right| \left| \frac{\sin\left(\pi N_y \frac{\delta}{\lambda} \zeta\right)}{\sin\left(\pi \frac{\delta}{\lambda} \zeta\right)} \right|, \tag{2.7}$$

where $\kappa = \sin(\theta_i)\cos(\phi_i) - \sin(\theta_j)\cos(\phi_j)$ and $\zeta = \sin(\theta_i)\sin(\phi_i) - \sin(\theta_j)\sin(\phi_j)$.

For a ULA (UPA) with inter-element spacing δ, $|\rho|$ is a function of ϕ_i, ϕ_j (ϕ_i, ϕ_j and θ_i, θ_j) and δ/λ (see (2.6) and (2.7)). Let assume user i and user j are uniformly distributed in the field-of-view. In this case, for a given normalized inter-element spacing of the array δ/λ, $|\rho|$ is a random variable with a certain probability distribution function (PDF). By optimizing the parameter δ/λ the desired PDF for $|\rho|$ can be achieved.

2.2 Shannon Capacity

Before Shannon, it was believed that the only way to achieve reliable communication over a noisy channel, i.e., to make the error probability as small as desired, was to decrease the communication rate [35]. Shannon showed that one can achieve reliable communication below a maximum rate, which he called the capacity of the channel. He showed it is impossible to communicate at a rate above the channel capacity with a vanishing error probability. We review the AWGN channel capacity in the sequel, which can be used as a building block to study the capacity of wireless channels [35, Ch. 5].

2.2.1 AWGN Channel

Consider the following continuous memoryless real-valued AWGN channel at a given time instance

$$y = x + n, \tag{2.8}$$

where $y \in \mathbb{R}$ is the output, $x \in \mathbb{R}$ is the input and $n \in \mathbb{R}$ is the AWGN noise with variance σ^2, i.e., $\mathcal{N}(0, \sigma^2)$, which is independent and identically distributed over time. Typically, there is an average power constraint for the input x, i.e., $\mathbb{E}[|x|^2] \leq P$. The channel capacity of the AWGN channel is found by maximizing the mutual information between the input and output of the channel over all the possible input distributions. Mathematically

$$C = \max_{p(x):\mathbb{E}[|x|^2]\leq P} \quad I(x;y), \tag{2.9}$$

where $p(x)$ is the PDF of x and $I(x;y)$ is the mutual information between x and y. The mutual information between random variables x and y can be stated as the reduction in the amount of uncertainty of y from the observation of x. This is mathematically expressed as

$$I(x;y) = H(y) - H(y|x), \tag{2.10}$$

where $H(\cdot)$ is the entropy function. The capacity of the AWGN channel is achieved by choosing x to have Gaussian distribution, i.e., $\mathcal{N}(0, P)$, which results in [37, Ch. 9.1]

$$C_{\text{AWGN}} = \frac{1}{2}\log_2(1 + P/\sigma^2) \quad \text{bits per real dimension.} \tag{2.11}$$

We further find the capacity of a continuous-time passband AWGN channel with a bandwidth of W (see [35, Fig. 2.7]), input power constraint of P, and the AWGN with power spectral density of $N_0/2$. After passband-baseband conversion and sampling at rate $1/W$ (see [35, Ch. 2]), the discrete-time baseband-equivalent AWGN channel over W complex samples ($2W$ real samples) per seconds is found ((2.8) with $x, y, n \in \mathbb{C}$). For an interval of $(0, T)$, the input energy per real sample is $(PT)/(2WT) = P/(2W)$, and the noise variance per real sample is $(N_0WT)/(2WT) = N_0/2$. Then, using (2.11), the capacity is (see [35, Ch. 5.2.1] for further details)

$$C(W) = 2W\left(\frac{1}{2}\log_2\left(1 + \frac{P}{WN_0}\right)\right) = W\log_2\left(1 + \frac{P}{WN_0}\right) \quad \text{bits/s.} \tag{2.12}$$

The spectral efficiency in bits/s/Hz is then found by

$$C = \log_2 (1 + \text{SNR}) \quad \text{bits/s/Hz}, \tag{2.13}$$

where SNR $= P/(WN_0)$.

2.2.2 Wireless Channel

The results of the AWGN channel (see (2.11)) are used to derive the capacity of different wireless channels [35, Ch. 5]. In this thesis, to derive the capacity of wireless systems, we assume a narrowband channel, where the channel is assumed to be constant, and the coding is implicitly performed over many random realization of the symbols and noise. Consider the following complex single-input-single-output (SISO) system

$$y = hx + n, \tag{2.14}$$

where the channel $h \in \mathbb{C}$ is the channel. The spectral efficiency of (2.14) assuming the receiver has perfect knowledge of the channel, is found by

$$C_{\text{SISO}} = \log_2 (1 + \text{SNR}) \quad \text{bits/s/Hz}, \tag{2.15}$$

with SNR $= P|h|^2/(WN_0)$. The results of (2.15) can be generalized to MIMO systems (see [35, Ch. 5] for more details).

2.3 TDD Massive MIMO Systems

In TDD systems, the uplink and downlink transmissions are at the same frequency spectrum in different time slots. A general TDD frame structure is shown in Fig. 2.4. The K users transmit uplink data together with pilot data to the BS. The pilot data are training signals that are known to the BS. Typically, the pilots are orthogonal sequences of length $\tau_{\text{p}} \geq K$ [29]. Then, the BS uses the pilot symbols to estimate the frequency response of the propagation channel. The acquired CSI is valid for a limited amount of time where the users do not move more than a fraction of a wavelength. Using the acquired CSI, the BS decodes the users' uplink data. Then, the BS uses the acquired CSI to preprocess the downlink data.

In TDD systems, channel reciprocity is exploited. Channel reciprocity implies that mathematically the uplink and downlink channels are identical. Consequently, TDD systems only need uplink pilot data, in contrast to FDD systems, where both uplink and downlink pilots are required. In practice, due to non-reciprocal components in the radio, calibration techniques are required to be able to use channel reciprocity [38].

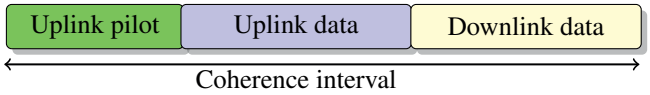

Figure 2.4: A general frame structure for TDD msasive MIMO systems.

2.3.1 Favorable Propagation

Favorable propagation (FP) is defined as the mutual orthogonality of the channel vectors of the users [39]. For a massive MIMO system with M antennas and K users, in FP, $\rho_{ij} = 0, j \neq i, i, j = 1, 2, ..., K$. FP is one of the key properties exploited in massive MIMO systems [33]. It is shown in [33] that both LOS environments and i.i.d. Rayleigh fading exhibit FP. For LOS environments, the expected $|\rho_{ij}|$ decreases at least as fast as $\log(M)/M$ [33]. However, there is a nonnegligible probability that the channel vectors of a small number of users become correlated [39]. To minimize this probability for a given antenna array at the BS, one needs to tune M and K (see the Appendix in Chapter 6 for more details).

2.3.2 Uplink Channel

A general architecture for massive MIMO in uplink is shown in Fig. 2.5. Each user performs baseband processing and uses digital-to-analog converters (DACs) to convert digital signals to analog signals. Then, by employing RF chains and antennas, the baseband signal is upconverted, and is transmitted through the propagation channel. At the BS, the received signals at the antennas are downconverted using the RF chains, and are converted to baseband using analog-to-digital converters (ADCs). Then, the BS performs baseband combining to detect each users' signals.

In uplink, the users transmit pilot symbols and data symbols to the BS. The pilot symbols are known to the BS, which are used at the BS to estimate the uplink channel. The memoryless discrete-time baseband signal received at the BS at a specific time in a given coherence interval is modeled by [35, Ch. 8]

$$\boldsymbol{y} = \boldsymbol{H}^H \boldsymbol{x} + \boldsymbol{n}, \tag{2.16}$$

where $\boldsymbol{y} \in \mathbb{C}^{M\times 1}$ is the vector of received signals of BS antennas, $\boldsymbol{H}^H \in \mathbb{C}^{M\times K}$ is the uplink channel matrix for the given coherence interval, $\boldsymbol{x} = (x_1, x_2, ..., x_K)^T \in \mathbb{C}^{K\times 1}$ is the transmitted signal of the users and $\boldsymbol{n} \in \mathbb{C}^{M\times 1}$ is the AWGN at the BS antennas, which is $\mathcal{CN}(\boldsymbol{0}, \sigma_n^2 \boldsymbol{I}_M)$. For LOS environments we use the models described in Sec. 2.1 to find the elements of $\boldsymbol{H}$. For i.i.d. Rayleigh fading, each element of $\boldsymbol{H}$ is $\mathcal{CN}(0, 1)$. Typically, it is assumed that the transmit power for each user is limited, i.e., $\mathbb{E}[|x_i|^2] = P_{\text{UL}}, i = 1, 2, ..., K$. Assuming a perfect channel state information at the BS, the uplink

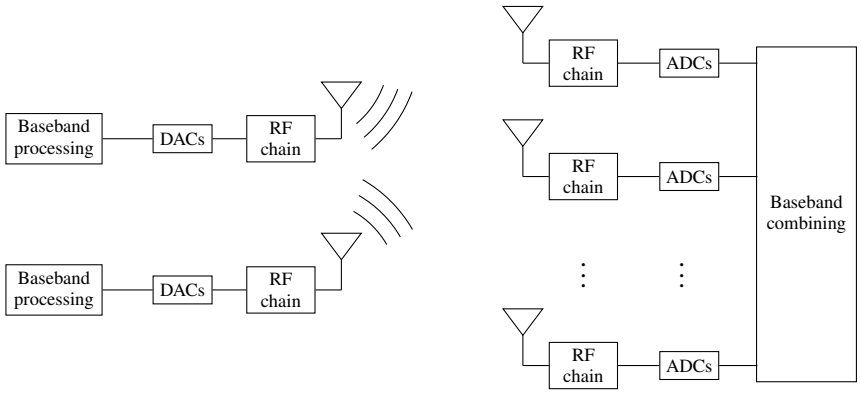

Figure 2.5: Massive MIMO architecture for uplink. Left: two single-antenna users transmit radio signals to the BS. Right: the BS performs baseband combining to estimate each user's signal.

capacity of (2.16) is found by [35, Ch. 8.2.1]

$$C_{\mathrm{UL}} = \log_2 \det \left(\boldsymbol{I}_M + \frac{P_{\mathrm{UL}}}{N_0} \boldsymbol{H}^H \boldsymbol{H} \right) \text{ bits/s/Hz.} \tag{2.17}$$

To achieve the uplink capacity, successive interference cancellation (SIC) technique is required at the BS with MMSE filters [35, Ch. 8]. Besides, to achieve the capacity, the input distribution has to be i.i.d. Gaussian with $\mathcal{CN}(0, P_{\mathrm{UL}})$. In practice, the input signaling is not Gaussian and has a signaling set, e.g., quadrature amplitude modulation (QAM) constellation. In this case, the maximum likelihood detection (optimal detector) problems can be seen as a lattice decoding or closest point problem [40, 41, Ch. 4.5]. Sphere decoding is known to solve the lattice decoding problem more efficiently than the brute-force maximum likelihood detector [40], however, its computational complexity is still high [41, Ch. 4.5.1]. Instead, linear equalization, e.g., zero-forcing or maximum ratio combining, are used in massive MIMO systems.

2.3.3 Channel Estimation

To estimate the uplink channel, each user transmits a sequence of symbols of length τ_{p} with transmit power P_{p} to the BS. It is typically assumed that the pilot sequence of users $\boldsymbol{S}_{\mathrm{p}} \in \mathbb{C}^{K \times \tau_{\mathrm{p}}}$ are mutually orthogonal, i.e., $\boldsymbol{S}_{\mathrm{p}} \boldsymbol{S}_{\mathrm{p}}^H = \tau_{\mathrm{p}} P_{\mathrm{p}} \boldsymbol{I}_K$. Furthermore, the length of a pilot sequence has to meet $\tau_{\mathrm{p}} \geq K$ [29]. The received sequence of users $\boldsymbol{Y} \in \mathbb{C}^{M \times \tau_{\mathrm{p}}}$ at the BS is

$$\boldsymbol{Y} = \boldsymbol{H}^H \boldsymbol{S}_{\mathrm{p}} + \boldsymbol{N}, \tag{2.18}$$

where $\boldsymbol{N} \in \mathbb{C}^{M\times\tau_p}$ is the corresponding AWGN noise sequence. Typically, the BS estimates the channel as follows

$$\hat{\boldsymbol{H}} = \frac{1}{\tau_p P_p}(\boldsymbol{Y}\boldsymbol{S}_{\mathrm{p}}^H)^H = \boldsymbol{H} + \frac{1}{\tau_p P_p}(\boldsymbol{N}\boldsymbol{S}_{\mathrm{p}}^H)^H. \tag{2.19}$$

To further improve the channel estimate, one can use linear MMSE (LMMSE) estimate of the channel for which further statistical information of the channel is required, e.g., the distribution of the channel (see [42, Sec 3.2] or [43, Sec. 3.1] for further details)

In this thesis, perfect channel state information is assumed for LOS environments for the following reasons. First, the channel estimation for LOS environments is easier than i.i.d. Rayleigh because for LOS only the angle of arrival and a complex amplitude have to be estimated [33]. Moreover, the nature of LOS environments prohibits an ergodic analysis of the channel estimation error [33].

2.3.4 Downlink Channel

A general architecture for massive MIMO in downlink is shown in Fig. 2.6. The BS performs baseband precoding to compensate the effects of the propagation channel. Then, DACs and RF chains are used to transmit generated radio signals intended for the users. Each user, downcovert the received radio signals from the antennas, and uses the ADCs to find the baseband signal, and decodes its symbols. Typically, in massive MIMO, it is assumed that each user has access to a side-information, e.g., a statistics of the channel matrix, to decode its symbols.

The discrete-time baseband signal received by the users at a specific time in a given coherence interval is modeled by

$$\boldsymbol{y} = \boldsymbol{H}\boldsymbol{x} + \boldsymbol{n}, \tag{2.20}$$

where $\boldsymbol{y} \in \mathbb{C}^{K\times 1}$ is the vector of received signals of users, i.e., $\boldsymbol{y} = (y_1, y_2, ..., y_K)^T$, $\boldsymbol{H} \in \mathbb{C}^{K\times M}$ is the downlink channel matrix for the given coherence interval, $\boldsymbol{x} \in \mathbb{C}^{M\times 1}$ is the transmitted vector from the BS and $\boldsymbol{n} \in \mathbb{C}^{K\times 1}$ is the AWGN noise at the users' receivers. Typically, the transmit power at the BS has the following constraint

$$\mathbf{E}[\|\boldsymbol{x}\|^2] \leq P_{\mathrm{DL}}, \tag{2.21}$$

where P_{DL} is the average available transmit power at the BS.

The capacity of the multi-user downlink channel in (2.20) is studied in [44–46]. When the BS has perfect CSI, the capacity of the downlink channel in 2.20 is found by [44]

$$C_{\mathrm{DL}} = \sup_{\boldsymbol{d}:\mathbf{1}^T\boldsymbol{d}\leq 1} \log_2 \det\left(\boldsymbol{I}_M + \frac{P_{\mathrm{DL}}}{N_0}\boldsymbol{H}^H \mathrm{diag}(\boldsymbol{d})\boldsymbol{H}\right) \text{ bits/s/Hz}, \tag{2.22}$$

where $\mathbf{1}$ is a $M \times 1$ vector with elements of 1, and $\boldsymbol{d} = (d_1, d_2, ..., d_K)^T$ with $d_i \geq 0$. To achieve the downlink capacity in (2.22), dirty paper coding (DPC) technique is used [47].

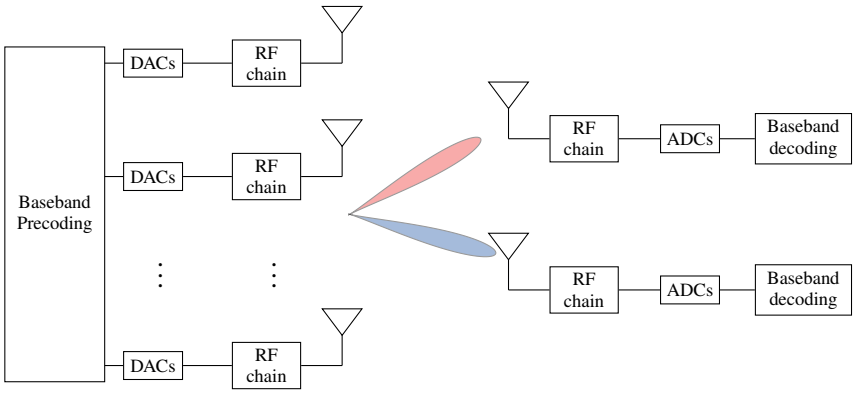

Figure 2.6: Massive MIMO architecture for downlink. Left: the BS performs baseband precoding to generate appropriate radio signals. By employing an appropriate precoding, the BS can generate two separate beams for the users. Right: each user performs baseband decoding to decode its symbols.

The computational complexity of DPC is not affordable for massive MIMO systems because it grows exponentially with the size of the system [29]. It is shown in [29] that using linear precoding instead of DPC leads to a small performance loss in massive MIMO systems. Among linear precoders, zero-forcing and conjugate beamforming a.k.a. maximum ratio transmission, are studied well in the literature [48]. We review important linear precoders and nonlinear precoders in the next Chapter.

CHAPTER 3

Precoding Strategies

3

Precoding refers to preprocessing methods applied at the transmitter that facilitates detection at the receiver. In this chapter, we review known precoding strategies with a focus on max-min fairness power control. Furthermore, we investigate the use of hybrid linear and nonlinear precoding in future communication systems. We then compare the computational complexity of different precoding strategies.

3.1 Linear Precoding

Linear precoding refers to linear preprocessing at the transmitter that makes detection easier at the receiver. To perform linear precoding a precoding matrix and a power control matrix are required. The precoding matrix consists of K unit-norm column vectors of length M, each acts as a precoding vector for each one of the users. In a complex vector space of dimension M, each precoding vector specifies the direction on which the transmitted vector of a user is sent. The power control matrix is a diagonal matrix for which the square of its diagonal elements are the power allocated for each user. In the literature, the power control and precoding matrices are sometimes combined and considered as a single linear precoding matrix.

The schematic of the massive MIMO downlink channel with a general linear precoder is shown in Fig. 3.1. The symbol of the users $\boldsymbol{s} = (s_1, s_2, ..., s_K)^T \in \mathbb{C}^{K\times 1}$ are assumed to be zero-mean, uncorrelated, and unit variance. The diagonal power control matrix $\boldsymbol{D} = \text{diag}(\boldsymbol{d})$ and a linear precoding matrix $\boldsymbol{U} = (\boldsymbol{u}_1, \boldsymbol{u}_2, ..., \boldsymbol{u}_K) \in \mathbb{C}^{M\times K}$ (with unit-norm column vectors $\boldsymbol{u}_i$) precode $\boldsymbol{s}$ to $\boldsymbol{x} \in \mathbb{C}^{M\times 1}$. The power control vector $\boldsymbol{d} = (\sqrt{d_1}, \sqrt{d_2}, ..., \sqrt{d_K})^T$ with $d_i \in \mathbb{R}^+, i = 1, 2, ..., K$ has the total power constraint $\sum_{i=1}^{K} d_i = P$. The transmit vector $\boldsymbol{x}$ is found by

$$\boldsymbol{x} = \boldsymbol{U}\boldsymbol{D}\boldsymbol{s}. \tag{3.1}$$

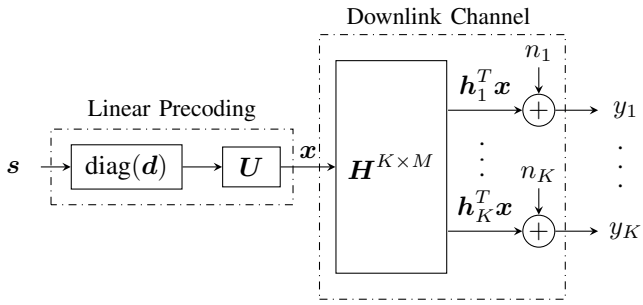

Figure 3.1: The model of the downlink channel with linear precoding.

Then, $\boldsymbol{x}$ is transmitted through the propagation channel $\boldsymbol{H} = (\boldsymbol{h}_1, \boldsymbol{h}_2, ..., \boldsymbol{h}_K)^T \in \mathbb{C}^{K\times M}$, where $\boldsymbol{h}_i$ is the channel vector from the BS antennas to user i.

The received signal at user i is given as

$$y_i = \boldsymbol{h}_i^T\boldsymbol{x} + n_i = \boldsymbol{h}_i^T\boldsymbol{u}_i\sqrt{d_i}s_i + \sum_{\substack{j=1\\ j\neq i}}^{K} \boldsymbol{h}_i^T\boldsymbol{u}_j\sqrt{d_j}s_j + n_i, \tag{3.2}$$

where n_i is zero-mean complex Gaussian noise with the variance of N_0. The first term in (3.2) is the intended signal for user i, the second term is the interference coming from the other users, and the third term is the AWGN noise. If user i has access to the scalar $\boldsymbol{h}_i^T\boldsymbol{u}_i\sqrt{d_i}$, it can estimate its symbol by:

$$\hat{s}_i = \frac{y_i}{\boldsymbol{h}_i^T\boldsymbol{u}_i\sqrt{d_i}} = s_i + \sum_{\substack{j=1\\ j\neq i}}^{K} \frac{\boldsymbol{h}_i^T\boldsymbol{u}_j\sqrt{d_j}}{\boldsymbol{h}_i^T\boldsymbol{u}_i\sqrt{d_i}}s_j + \frac{n_i}{\boldsymbol{h}_i^T\boldsymbol{u}_i\sqrt{d_i}}, \tag{3.3}$$

Assuming perfect channel state information at the BS, the signal to noise plus interference ratio (SINR) for user i denoted by γ_i is given as

$$\gamma_i = \frac{|\boldsymbol{h}_i^T\boldsymbol{u}_i|^2 d_i}{\sum_{j=1,j\neq i}^{K} |\boldsymbol{h}_i^T\boldsymbol{u}_j|^2 d_j + N_0}. \tag{3.4}$$

Various linear precoding strategies are obtained by employing the structure in Fig. 3.1 and using different criteria, e.g., zero-forcing or mean square error. By maximizing the SNR per user, conjugate beamforming (CB) filters $\boldsymbol{G} = \boldsymbol{H}^H$ are obtained. By maximizing the SNR and removing the inter-user interference, zero-forcing (ZF) filters $\boldsymbol{G} = \boldsymbol{H}^\dagger = \boldsymbol{H}^H(\boldsymbol{H}\boldsymbol{H}^H)^{-1}$ are obtained. Other known linear precoders are regularized ZF (RZF) with $\boldsymbol{G} = \boldsymbol{H}^H(\boldsymbol{I}_K + \boldsymbol{H}\boldsymbol{H}^H)^{-1}$ and minimum mean square error (MMSE) precoding with $\boldsymbol{G} = (N_0\boldsymbol{I}_M + \boldsymbol{H}^H\boldsymbol{D}\boldsymbol{H})^{-1}\boldsymbol{H}^H\boldsymbol{D}$, where $\boldsymbol{D}$ is a diagonal power control

matrix that has to be found [49].[1] The precoding matrix $\boldsymbol{U}$ is then found for each precoder by normalizing $\boldsymbol{G}$ to have unit-norm column vectors, i.e., $\boldsymbol{u}_i = \boldsymbol{g}_i/\|\boldsymbol{g}_i\|, i = 1, 2, ..., K$. By replacing CB and ZF filters in (3.4), the following SINR is obtained for a given power control coefficients $d_i, i = 1, 2, ..., K$

$$\gamma_i^{\text{CB}} = \frac{\|\boldsymbol{h}_i^T \frac{\boldsymbol{h}_i^H}{\|\boldsymbol{h}_i\|}\|^2 d_i}{\sum_{j=1,j\neq i}^{K} |\boldsymbol{h}_i^T \frac{\boldsymbol{h}_j^H}{\|\boldsymbol{h}_j\|}|^2 d_j + N_0} = \frac{\|\boldsymbol{h}_i\|^2 d_i}{\|\boldsymbol{h}_i\|^2 \sum_{j=1,j\neq i}^{K} |\rho_{ij}|^2 d_j + N_0}, \tag{3.5}$$

$$\gamma_i^{\text{ZF}} = \frac{|\boldsymbol{h}_i^T \frac{\boldsymbol{g}_i}{\|\boldsymbol{g}_i\|}|^2 d_i}{N_0} = \frac{d_i}{\|\boldsymbol{g}_i\|^2 N_0}, \tag{3.6}$$

where ρ_{ij} in (3.5) is the normalized spatial correlation defined in (2.5) and $\boldsymbol{g}_i$ in (3.6) is the ZF filter. For RZF (or MMSE), the SINR formula is found by replacing the RZF (or MMSE) filters $\boldsymbol{u}_i$ in (3.4).

To find power control coefficients $d_i, i = 1, 2, ..., K$, different power control strategies can be used at the BS, e.g., throughput maximization or fairness maximization. Among those power control strategies, fairness maximization a.k.a. max-min power control has received lots of attention. Employing max-min power control equalizes the SINR of all users [33], i.e., $\gamma_i = \gamma, i = 1, 2, ..., K$. For a given set of filters $\boldsymbol{u}_i, i = 1, 2, ..., K$, the max-min power control coefficients are the ones that maximize the minimum γ_i among the users [42, Sec. 7.1]

$$\boldsymbol{d}^* = \underset{d_1,d_2,...,d_K \in \mathbb{R}^+}{\text{argmax}} \quad \min_{i\in\{1,2,...,K\}} \quad \gamma_i, \tag{3.7}$$

where γ_i is given by (3.4). To solve (3.7) for CB (and RZF and MMSE), we can use the bisection method or other optimization algorithms (see [33, Algorithm 2]). The bisection method is computationally expensive. To reduce the complexity of bisection methods, neural networks are used in [50] to find the power control coefficients. To solve (3.7) for ZF, we use the Lagrangian multiplier, which leads to the following closed-form solutions for the power control coefficient d_i and γ_i

$$d_i = \frac{P\|\boldsymbol{g}_i\|^2}{\sum_{j=1}^{K} \|\boldsymbol{g}_j\|^2}, \tag{3.8}$$

$$\gamma^{\text{ZF}} = \frac{P}{N_0 \sum_{j=1}^{K} \|\boldsymbol{g}_j\|^2}. \tag{3.9}$$

3.2 Tomlinson-Harashima Precoding

THP is a known nonlinear precoder for which nonlinear processing is employed at the BS to make the detection easier at the receiver. The model for THP is shown in Fig. 3.2

[1] The derivation of MMSE precoding filters can be found in [49].

for a given coherence interval. We use ZF criterion for the designed THP in Fig. 3.2. The intended symbols $\boldsymbol{s}$ are encoded to $\tilde{\boldsymbol{s}} = (\tilde{s}_1, \tilde{s}_2, ..., \tilde{s}_K)^T \in \mathbb{C}^{K\times 1}$ by using the feedback filter $\boldsymbol{B} - \boldsymbol{I}_K \in \mathbb{C}^{K\times K}$ and the modulo operator $[\cdot]_\Delta$ with divisor Δ (see Fig. 3.3). When the input to the modulo operator is $x \in \mathbb{C}$, $x = \alpha_x + \jmath\beta_x, \alpha_x, \beta_x \in \mathbb{R}$, the modulo function operates separately on real and imaginary parts of x, meaning $y = \alpha_y + \jmath\beta_y, \alpha_y = \alpha_x - \Delta\lfloor\frac{\alpha_x}{\Delta}\rfloor$ and $\beta_y = \beta_x - \Delta\lfloor\frac{\beta_x}{\Delta}\rfloor$.

A power control matrix $\boldsymbol{D} = \text{diag}(\sqrt{d_1}, \sqrt{d_2}, ..., \sqrt{d_K})$ and feedforward filter $\boldsymbol{Q}^H \in \mathbb{C}^{M\times K}$ are used to generate the precoded vector $\boldsymbol{x} \in \mathbb{C}^{M\times 1}$. To find the filters, the LQ decomposition of the channel $\boldsymbol{H} = \boldsymbol{LQ}$ is employed. Note $\boldsymbol{H}$ is required at the BS for encoding a block of symbols (block-level precoding [51]) in the given coherence interval. The matrix $\boldsymbol{Q}^H$ is used for the feedforward filter, and $\boldsymbol{L}$, which is a lower triangular matrix with positive diagonal elements l_{ii} is used to find $\boldsymbol{B}$ for the feedback filter (for more details on THP see [41, Sec. 5.4.4] and [52, Ch. 3.2.3]). Then, the received signal for user i, i.e., y_i is found by

$$y_i = [\boldsymbol{HQ}^H\boldsymbol{D}\tilde{\boldsymbol{s}}]_i = [\boldsymbol{LQQ}^H\boldsymbol{D}\tilde{\boldsymbol{s}}]_i = [\boldsymbol{LD}\tilde{\boldsymbol{s}}]_i = l_{ii}\sqrt{d_i}\tilde{s}_i + \sum_{j=1}^{i-1} l_{ij}\sqrt{d_j}\tilde{s}_j + n_i, \quad (3.10)$$

where l_{ii} is the ith diagonal element in $\boldsymbol{L}$ and n_i is the complex AWGN noise with variance N_0. By using the scalar $\alpha_i = l_{ii}\sqrt{d_i}$, and using the modulo operator at the receiver, the estimated symbol for user i is found by

$$\hat{s}_i = [y_i/\alpha_i]_\Delta = \left[\tilde{s}_i + \sum_{j=1}^{i-1}\left(l_{ij}\sqrt{d_j}/\alpha_i\right)\tilde{s}_j + \frac{n_i}{\alpha_i}\right]_\Delta. \quad (3.11)$$

To encode $\boldsymbol{s}$ to $\tilde{\boldsymbol{s}}$, the following encoding is used (see the feedback loop in Fig. 3.2)

$$\tilde{s}_i = \left[s_i - \sum_{j=1}^{i-1}\left(l_{ij}\sqrt{d_j}/\alpha_i\right)\tilde{s}_j\right]_\Delta, \quad (3.12)$$

where the element ij of the matrix $\boldsymbol{B}$ is $b_{ij} = l_{ij}\sqrt{d_j}/\alpha_i$. Note that the matrix $\boldsymbol{B}$ represents the interference pattern at the receivers when the precoding in Fig. 3.2 is used to generate $\boldsymbol{x}$. Then, the estimated symbol becomes

$$\hat{s}_i = [s_i + n_i/\alpha_i]_\Delta. \quad (3.13)$$

At high SNRs, where the noise component n_i/α_i is small compared to Δ, the modulo operator (loss) can be ignored [53], and

$$\hat{s}_i = s_i + \frac{n_i}{\alpha_i}. \quad (3.14)$$

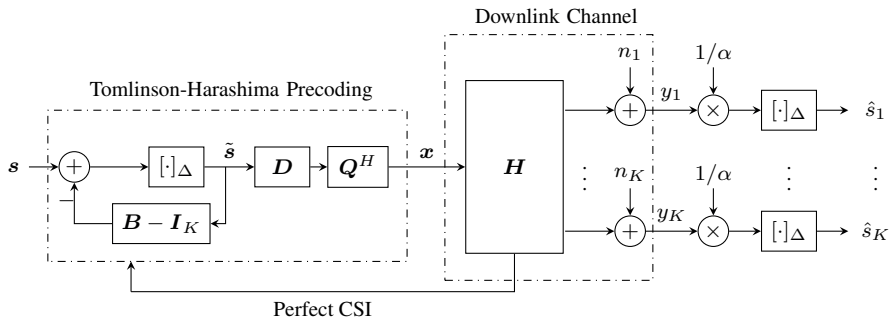

Figure 3.2: The model of the downlink channel with THP. The symbols $\boldsymbol{s}$ are encoded to $\boldsymbol{x}$ using the modulo operator $[\cdot]_\Delta$, the feedback filter $\boldsymbol{B}-\boldsymbol{I}_K$ and the feedforward filters $\boldsymbol{G}$ and $\boldsymbol{Q}^H$. The users has access to the side information α and use the same Δ as in the BS for the modulo operator to estimate their symbols.

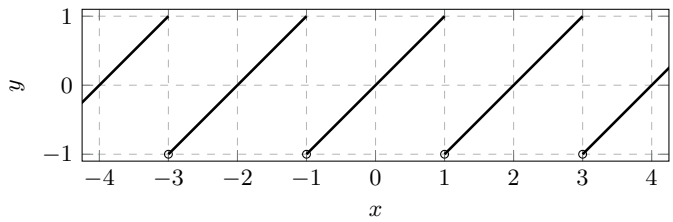

Figure 3.3: Modulo function $y = [x]_\Delta = x - \Delta\lfloor\frac{x}{\Delta}\rfloor$ with $\Delta = 2$ when $x \in \mathbb{R}$.

Thus, using inflated lattice strategies [54] (see Sec. 3.2.2), where the shaping loss is neglected, $\gamma_i = \alpha_i^2/N_0 = l_{ii}^2 d_i/N_0$ can be achieved for user i. The max-min power control coefficients d_i are found by maximizing the minimum γ_i among the users

$$d_i = \frac{P}{l_{ii}^2 \sum_{j=1}^{K} \frac{1}{l_{jj}^2}}, \quad i = 1, ..., K. \tag{3.15}$$

Assuming $\boldsymbol{W} = \boldsymbol{Q}^H \text{diag}(1/l_{11}, 1/l_{22}, ..., 1/l_{KK})$, (3.15) leads to the following γ for each user

$$\gamma = \frac{P}{N_0 \sum_{j=1}^{K} \frac{1}{l_{jj}^2}} = \frac{P}{N_0 \sum_{j=1}^{K} \|\boldsymbol{w}_j\|^2}. \tag{3.16}$$

Note by using (3.15), $b_{ij} = l_{ij}\sqrt{d_j}/\alpha_i = l_{ij}/l_{jj}$. Besides, (3.15) leads to $\alpha_i = \alpha = \frac{P}{\sum_{j=1}^{K} \|\boldsymbol{w}_j\|^2}$. Thus, the scalars α_i that each user requires to estimate its symbol are identical. It is assumed that each user has access to α to estimate its symbols.

The choice of Δ is crucial in achieving (3.14). If Δ is too large, then, the modulo function does not change the input, and this will lead to a transmit power increase because $\tilde{s}_i \in (-\Delta/2, \Delta/2)$ with a large Δ. If Δ is too small, or in other words, if the noise components are not negligible compared to Δ, then, (3.14) can not be achieved from (3.13). In this case, error-free communication becomes impossible even in the absence of AWGN [55]. To achieve a trade-off between transmit power increase and estimation error, we use (9) from [55] for Δ. Δ (equivalent to τ in [55]) is a function of $|s|_{\text{max}}$, i.e., the absolute value of the constellation symbol with the largest magnitude and c, i.e., the spacing between the constellation points

$$\Delta = 2(|s|_{\text{max}} + c/2). \tag{3.17}$$

For THP, the order of users for encoding $\boldsymbol{s}$ to $\tilde{\boldsymbol{s}}$ changes $\|\boldsymbol{w}_j\|^2, j = 1, 2, ..., K$, and consequently, changes γ in (3.16). Each ordering of the users can be represented by a permutation matrix $\boldsymbol{A}$. The optimal permutation matrix $\boldsymbol{A}^\star$ is the one that maximizes γ over all the possible permutation matrices, which is found by

$$\boldsymbol{A}^\star = \underset{\boldsymbol{A}}{\text{argmax}} \ \frac{P}{N_0 \sum_{j=1}^{K} \|\boldsymbol{w}_j\|^2} = \underset{\boldsymbol{A}}{\text{argmin}} \ \sum_{j=1}^{K} \|\boldsymbol{w}_j\|^2. \tag{3.18}$$

In this thesis, we use the VBLAST algorithm described in [41, Fig. 5.18] to solve (3.18), which is reviewed in the sequel. For future works, the VBLAST implementation described in [56] (see [57] for further details) will be used, which entails a lower computational complexity compared to [41, Fig. 5.18].

3.2.1 VBLAST Algorithm

The VBLAST algorithm heuristically finds an order of users to maximize γ for THP (see (3.16)). The best order of users is the one that results in the minimum $\sum_{j=1}^{K} \|\boldsymbol{w}_j\|^2$ as stated earlier in (3.18). VBLAST is a heuristic iterative algorithm that at each iteration selects the user with the minimum $\|\boldsymbol{w}_j\|$. By choosing the user with the minimum $\|\boldsymbol{w}_j\|$ at each iteration, one can expect that $\sum_{j=1}^{K} \|\boldsymbol{w}_j\|^2$ would be small. It turns out that this heuristic algorithm has a close-to-optimal performance [41, Sec. 5.4]. Note the VBLAST algorithm does not explicitly find the LQ decomposition of the channel, instead, it directly finds $\boldsymbol{w}_i$ by computing the pseudo-inverse of the channel at each iteration.

The VBLAST algorithm is presented in Algorithm 1 [41, Fig. 5.18]. The input to the VBLAST algorithm is the channel matrix of users $\boldsymbol{H}$ and the outputs are the feedforward filter of users $\boldsymbol{W}$ and the order of encoding for the users denoted by a permutation matrix $\boldsymbol{A}$. The reordered channel matrix is found by multiplying the permutation matrix $\boldsymbol{A}$ and the input channel matrix $\boldsymbol{H}$. The symbols of the users are reordered using the permutation matrix $\boldsymbol{A}$ found by the VBLAST algorithm before encoding in (3.12).

Algorithm 1 VBLAST for THP [41, Fig. 5.18]

Input $\boldsymbol{H}$
Output $\boldsymbol{W}$, $\boldsymbol{A}$
1: $\boldsymbol{A} = \boldsymbol{0}$
2: $\boldsymbol{H}^{(1)} = \boldsymbol{H}$
3: **for** $j = 1, 2, ..., K$ **do**
4: $\quad \boldsymbol{G}^{(i)} = (\boldsymbol{H}^{(i)})^{\dagger}$
5: $\quad k_i = \text{argmin}_{k \notin \{k_1, k_2, ..., k_{i-1}\}} \|\boldsymbol{g}_k^{(i)}\|^2$
6: $\quad \boldsymbol{w}_{K-i+1} = \boldsymbol{g}_{k_i}^{(i)}$
7: $\quad a_{K-i+1,k_i} = 1$
8: $\quad$ make row k_i from $\boldsymbol{H}^{(i)}$ to $\boldsymbol{0}$
9: **end for**

Algorithm 1 is explained as follows. The permutation matrix is initialized to a zero matrix before starting the iterations (line 1). The channel matrix at iteration i is denoted by $\boldsymbol{H}^{(i)}$. At each iteration of the Algorithm, the pseudo-inverse of the current channel matrix $\boldsymbol{H}^{(i)}$ is computed (line 4). At iteration i, the user with the minimum filter norm denoted by $\|\boldsymbol{g}_{k_i}\|$ is selected (line 5). Therefore, the corresponding filter for the selected user is $\boldsymbol{w}_{K-i+1} = \boldsymbol{g}_{k_i}$ (line 6). The permutation matrix is updated accordingly, i.e., the element a_{K-i+1,k_i} of the permutation matrix is set to 1 (line 7). To proceed to the next iteration, row k_i is removed from $\boldsymbol{H}^{(i)}$ to find the updated channel matrix for the next iteration (line 8). The same procedure is repeated to find the filters $\boldsymbol{W}$ and the ordering $\boldsymbol{A}$ for all the users.

We further explain the VBLAST algorithm in the following example for a channel matrix with 3 users. Consider the channel matrix

$$\boldsymbol{H}^{(1)} = \begin{bmatrix} -1.3077 & 3.5784 & 3.0349 \\ -0.4336 & 2.7694 & 0.7254 \\ 0.3426 & -1.3499 & -0.0631 \end{bmatrix}. \tag{3.19}$$

The pseudo-inverse of the channel $\boldsymbol{G}^{(1)}$ is

$$\boldsymbol{G}^{(1)} = \begin{bmatrix} 0.5899 & 2.8380 & 4.2589 \\ -0.1622 & 0.7019 & 0.2693 \\ 0.2665 & 0.3953 & 1.5176 \end{bmatrix}. \tag{3.20}$$

This results in $\|\boldsymbol{g}_1^{(1)}\|^2 = 0.4453$, $\|\boldsymbol{g}_2^{(1)}\|^2 = 8.7033$, $\|\boldsymbol{g}_3^{(1)}\|^2 = 20.5136$. In this case, the first column of $\boldsymbol{G}^{(1)}$ is selected, i.e., $\boldsymbol{w}_3 = \boldsymbol{g}_1^{(1)}$ and $a_{3,1} = 1$. The corresponding channel row vector of the selected user is removed from the channel matrix, which leads to $\boldsymbol{H}^{(2)}$:

$$\boldsymbol{H}^{(2)} = \begin{bmatrix} 0 & 0 & 0 \\ -0.4336 & 2.7694 & 0.7254 \\ 0.3426 & -1.3499 & -0.0631 \end{bmatrix}. \tag{3.21}$$

The pseudo-inverse of the updated channel $\boldsymbol{G}^{(2)}$ is

$$\boldsymbol{G}^{(2)} = \begin{bmatrix} 0 & 0.6092 & 1.4090 \\ 0 & 0.0891 & -0.5142 \\ 0 & 1.4024 & 2.8053 \end{bmatrix}. \tag{3.22}$$

This results in $\|\boldsymbol{g}_2^{(2)}\|^2 = 2.3459$, $\|\boldsymbol{g}_3^{(2)}\|^2 = 10.1197$. In this case, the second column of $\boldsymbol{G}^{(2)}$ is selected, i.e., $\boldsymbol{w}_2 = \boldsymbol{g}_2^{(2)}$ and $a_{2,2} = 1$. Then, corresponding row of the selected user is removed from $\boldsymbol{H}^{(2)}$, which leads to

$$\boldsymbol{H}^{(3)} = \begin{bmatrix} 0 & 0 & 0 \\ 0 & 0 & 0 \\ 0.3426 & -1.3499 & -0.0631 \end{bmatrix}. \tag{3.23}$$

Thus, $\boldsymbol{G}^{(3)} = [\boldsymbol{0}, \boldsymbol{0}, \boldsymbol{g}_3^{(3)}]$ with $\boldsymbol{g}_3^{(3)} = [0.1763, -0.6945, -0.0324]^T$, which leads to $\boldsymbol{w}_1 = \boldsymbol{g}_3^{(3)}$ and $a_{1,3} = 1$. For the given example, the outputs of the VBLAST algorithm are the same as the solution to (3.18) found by

$$\boldsymbol{W} = \begin{bmatrix} 0.1763 & 0.6092 & 0.5899 \\ -0.6945 & 0.0891 & -0.1622 \\ -0.0324 & 1.4024 & 0.2665 \end{bmatrix}, \quad \boldsymbol{A} = \begin{bmatrix} 0 & 0 & 1 \\ 0 & 1 & 0 \\ 1 & 0 & 0 \end{bmatrix}. \tag{3.24}$$

3.2.2 Inflated lattice Precoding

THP described in Section 3.2 can be further optimized, particularly in low signal to noise ratios [41]. The idea is to remove a scaled version of the interference in encoding $\tilde{s}_i$ in (3.12). This method has been called inflated lattice precoding [54]. In inflated lattice precoding, the encoded symbols are

$$\tilde{s}_i = \left[s_i - \zeta_i \sum_{j=1}^{i-1} \frac{l_{ij}\sqrt{d_j}}{\alpha_i} \tilde{s}_j \right]_{\Delta}, \tag{3.25}$$

where ζ_i is the same as the scalar Costa used for digital watermarking [41]. At the receiver, $\zeta_i y_i$ is used to find $\hat{s}_i$. Using inflated lattice precoding, a higher information rate is achieved [54, Sec. III.F]. THP is a specific case of a more general precoding scheme, i.e., vector precoding, which is reviewed in the sequel.

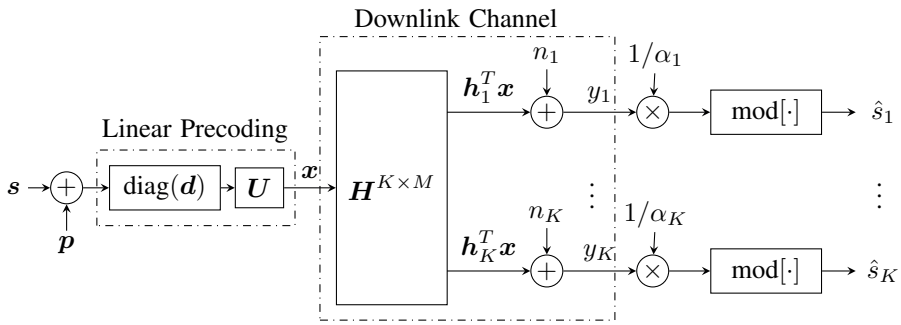

Figure 3.4: The model of the downlink channel with VP.

3.3 Vector Precoding

A similar precoding strategy to THP is vector precoding (VP), which is more general than THP. A ZF implementation of VP is explained as follows.[2] Recall $\tilde{\boldsymbol{s}}$ in (3.12)

$$\tilde{s}_i = \left[s_i - \sum_{j=1}^{i-1} \left(l_{ij}\sqrt{d_j}/\alpha_i \right) \tilde{s}_j \right]_\Delta = s_i - \sum_{j=1}^{i-1} \left(l_{ij}\sqrt{d_j}/\alpha_i \right) \tilde{s}_j + p_i, \tag{3.26}$$

where $p_i = (l_i + \jmath m_i)\Delta, l_i, m_i \in \mathbb{Z}$. The idea in VP is to add a perturbation vector $\boldsymbol{p} = (p_1, p_2, ..., p_K)$ with $p_i = (l_i + \jmath m_i)\Delta, l_i, m_i \in \mathbb{Z}$ and $\Delta \in \mathbb{R}$ to the symbols $\boldsymbol{s} \in \mathbb{C}^{K\times 1}$ such that some desired properties of transmit signal can be achieved [41], e.g., the transmit power for a given γ is minimized. In VP, $\boldsymbol{p}$ is found in a more general way than THP.

One of the simplest precoding strategies using VP is shown in Fig. 3.4. A perturbation vector $\boldsymbol{p}$ is added to the symbols $\boldsymbol{s}$, and linear precoding is done using power control matrix diag($\boldsymbol{d}$) and precoding matrix $\boldsymbol{U}$. The transmitted vector $\boldsymbol{x}$

$$\boldsymbol{x} = \boldsymbol{U}\text{diag}(\boldsymbol{d})(\boldsymbol{s} + \boldsymbol{p}), \tag{3.27}$$

goes through the propagation channel and is received by the users. Each user uses an appropriate scalar and the modulo operator to remove the perturbation vector and detect its intended symbol. Note the modulo interval Δ has to be tuned for each user for the best performance. Nevertheless, Δ is typically assumed to be the same for the users. If ZF filters are used and $\alpha_i = \boldsymbol{h}_i^T \boldsymbol{u}_i \sqrt{d_i}$ then the received signal for each user is

$$\left[\frac{y_i}{\alpha_i} \right]_\Delta = \left[(s_i + p_i) + \frac{n_i}{\alpha_i} \right]_\Delta = \left[s_i + \frac{n_i}{\alpha_i} \right]_\Delta . \tag{3.28}$$

[2]For MMSE VP see [58].

In high SNRs, where the noise component n_i/α_i is small compared to Δ, the modulo operator (loss) can be ignored in (3.28) and the same γ as in typical ZF is achieved. Note the perturbation vector $\boldsymbol{p}$ is found such that transmit power is minimized

$$\boldsymbol{p} = \underset{\tilde{\boldsymbol{p}}:\tilde{p}_i=(l_i+\jmath m_i)\Delta, l_i, m_i\in\mathbb{Z}}{\operatorname{argmin}} \|\boldsymbol{U}\operatorname{diag}(\boldsymbol{d})(\boldsymbol{s}+\tilde{\boldsymbol{p}})\|^2. \tag{3.29}$$

In contrast to THP, the computational complexity of finding the perturbation vector in (3.29) by an exhaustive search grows exponentially with the number of users and the size of the constellation.

Compared to ZF, using the VP structure in Fig. 3.4 results in the same γ for each user with a reduced transmit power at the BS. To find $\boldsymbol{p}$, lattice decoding techniques, e.g., sphere decoding [40] can be used for a small number of dimensions. Vector precoding, which finds the optimum precoding vector, can be seen as the dual to the maximum likelihood detection problem. The computational complexity burden of VP limits its use in massive MIMO systems. For instance, the problem of quantized precoding explained in [59, Fig. 2.b] requires a complexity that grows exponentially with the number of BS antennas.

3.4 Hybrid Linear and Nonlinear Precoding

To trade-off complexity vs. performance, hybrid linear and nonlinear precoding (HLNP) is suggested in the literature. The goal in designing an HLNP is to achieve a γ close to that of nonlinear precoding with the complexity close to that of linear precoding. HLNP is of great importance for industry because of its low computational complexity and latency compared to nonlinear precoders [60].

Different HLNP strategies are reported in the literature for single-cell and multi-cell multi-user MIMO systems. An HLNP strategy is suggested for 5G [60], where the BS switches between a linear and a nonlinear precoder based on the channel condition. For instance, the BS uses nonlinear precoding when some users become highly correlated and uses linear precoding otherwise. Another example is when the BS measures the instantaneous SNR for the current set of users. If the SNR requirements with linear precoding have not been met, nonlinear precoding is used to meet the SNR requirements. Among HLNP strategies, the ones using THP as the nonlinear precoder, have received more attention from both industry and academia because THP is a low-complexity nonlinear precoder that can be regarded as a simple implementation of DPC [60–62].

An HLNP strategy is reported in [61, 62] for which the users are divided into several groups. A two-stage precoding scheme is then used in [61, 62] to precode symbols of users. In the first stage, THP is used to remove intra-group interference and in the second stage, linear precoding, e.g., ZF is used to remove inter-group interference. To divide the users into several groups, it is assumed in [61] that the users in each group have the same correlation matrix. This grouping is not suitable for channels for which the users do not have the same correlation matrix, e.g., free space LOS environments. Dividing the users

into a number of groups and finding the order of encoding the users in each group are the challenges in this HLNP strategy. An exhaustive search can be used to find a grouping of the users and to find an ordering of the users in each group such that γ with max-min power control is maximized. Designing a low-complexity grouping method is essential for an HLNP strategy to reduce the complexity of an exhaustive search. Two different HLNP strategies are compared in the sequel.

3.4.1 Example: Designing HLNP for LOS Massive MIMO Systems

We design two HLNP strategies using the results in [39] for LOS massive MIMO systems, where it is shown that by dropping a few users, performance close to favorable propagation environments is achieved. This means in LOS massive MIMO systems there are a limited number of users with correlated channel vectors and the remaining users are near orthogonal. Let consider a simple HLNP strategy for a massive MIMO system with K users, where the users are divided into a group of $K-2$ and a group of 2 users. Assume an appropriate grouping method is used to divide the users into these groups. For simplicity, we further assume the users in the first group have low intra-group interference, which means the users are near orthogonal in this group. For a low intra-group interference, linear precoding leads to a performance close to that of nonlinear precoding. Therefore, we use ZF filters to remove the intra-group interference for the users in the first group. The users in the second group with 2 users might have high intra-group interference for which THP is used. Note the inter-group interference is removed by using appropriate filters for the users in the first and second groups. Based on this intuition, we design two different HLNP strategies as follows.

In the designed HLNP strategies, THP or ZF filters are used to remove intra-group interference. For the groups with low intra-group interference, we use ZF filters, and for the groups with high intra-group interference, we use THP filters. For a BS that uses precoding filters $\boldsymbol{W}$, the inter-user interference at the users' receivers is the off-diagonal elements of $\boldsymbol{HW}$, which is shown in Fig. 3.5 for two different HLNP strategies. An off-diagonal element $[\boldsymbol{HW}]_{ij}$ is shown by a square at row i and column j, which is the interference coming from user j to user i. The white square shows that the inter-user interference is removed, the green square shows the intra-group interference and the gray square shows the inter-group interference.

In the first HLNP strategy (see Fig. 3.5a), we find the ZF filters for the users in the first group as follows. The ZF filters for the users in the first group are columns 1 to $K-2$ of the pseudo-inverse of the channel matrix of all the K users, i.e., $\boldsymbol{G} = \boldsymbol{H}^{\dagger} = (\boldsymbol{g}_1, \boldsymbol{g}_2, ..., \boldsymbol{g}_K)$. Thus, we use $\boldsymbol{g}_1, \boldsymbol{g}_2, ..., \boldsymbol{g}_{K-2}$ for the users in the first group. This assures that the inter-group interference from the users in the first group to the users in the second group is removed. If the allocated transmit power for the users in the first group is P_{ZF}, then, assuming there is no inter-group interference from the users in the

second group, γ for the users in the first group is

$$\gamma = \frac{P_{\text{ZF}}}{N_0 \sum_{i=1}^{K-2} \|\boldsymbol{g}_i\|^2}. \tag{3.30}$$

We use conventional THP for the users in the second group. We use the channel matrix of all the K users to compute $\boldsymbol{w}_{K-1}$ and $\boldsymbol{w}_K$ filters. This assures that the inter-group interference from the users in the second group to the users in the first group is removed. If the allocated transmit power for the users in the second group is P_{THP}, γ for the users in this group is

$$\gamma = \frac{P_{\text{THP}}}{N_0 \sum_{i=K-1}^{K} \|\boldsymbol{w}_i\|^2}. \tag{3.31}$$

To equalize γ for the first and second groups, the following power allocation shall be used assuming $P = P_{\text{ZF}} + P_{\text{THP}}$

$$P_{\text{THP}} = \left(\frac{\sum_{i=K-1}^{K} \|\boldsymbol{w}_i\|^2}{\sum_{i=K-1}^{K} \|\boldsymbol{w}_i\|^2 + \sum_{i=1}^{K-2} \|\boldsymbol{g}_i\|^2} \right) P \tag{3.32}$$

This leads to the following γ for all the users in the first HLNP strategy

$$\gamma = \frac{P}{N_0 \left(\sum_{i=K-1}^{K} \|\boldsymbol{w}_i\|^2 + \sum_{i=1}^{K-2} \|\boldsymbol{g}_i\|^2 \right)}. \tag{3.33}$$

In practice, we first start with finding the THP filters for the second group. This will assure that the inter-group interference from the users in the second group to the users in the first group is removed. Then, we find the ZF filters using the channel matrix $\boldsymbol{H}$, which assures that the inter-group interference from the users in the first group to the users in the second group is removed.

The interference pattern for the second HLNP strategy is shown in Fig. 3.5b. In contrast to the first strategy, to find the ZF filters for the first group, we use the channel matrix of $K-2$ users $\tilde{\boldsymbol{H}}$, i.e., $\tilde{\boldsymbol{G}} = \tilde{\boldsymbol{H}}^{\dagger} = (\tilde{\boldsymbol{g}}_1, \tilde{\boldsymbol{g}}_2, ..., \tilde{\boldsymbol{g}}_{K-2})$. Assuming the inter-group interference from the users in the second group to the users in the first group is removed, the following γ for the users in the first group is achieved

$$\gamma = \frac{P_{\text{ZF}}}{N_0 \sum_{i=1}^{K-2} \|\tilde{\boldsymbol{g}}_i\|^2}. \tag{3.34}$$

Note $\sum_{i=1}^{K-2} \|\tilde{\boldsymbol{g}}_i\|^2 \leq \sum_{i=1}^{K-2} \|\boldsymbol{g}_i\|^2$, because when there are only $K-2$ users, there are fewer constraints to find the ZF filters. Employing the channel matrix of $K-2$ users to find the ZF filters for the first group means the inter-group interference from the users in the first group to the users in the second group is not zero, which is shown by gray squares in Fig. 3.5b. To remove inter-group interference for the users in the second

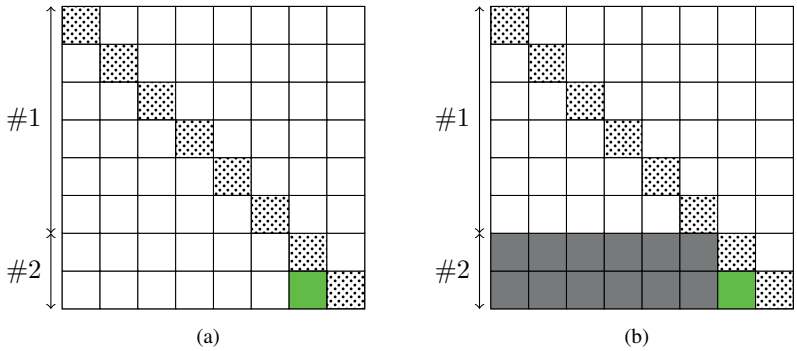

Figure 3.5: The interference pattern for two HLNP strategies when there are $K = 8$ users with 6 users in the first group and 2 users in the second group. The white square shows that inter-user interference is 0, the green square shows the intra-group interference, and the gray square shows the inter-group interference from the users in the first group to the users in the second group.

group, a modified THP is used as follows. Although the THP filters are computed the same as in the first HLNP strategy, we encode the symbols in the second strategy as

$$\tilde{s}_i = \left[s_i - \sum_{j=K-1}^{i-1} b_{ij}\tilde{s}_j - \sum_{j=1}^{K-2} \frac{\boldsymbol{h}_i^T \boldsymbol{u}_j \sqrt{d_j}}{l_{ii}\sqrt{d_i}} s_j \right]_{\Delta}, \quad i = K-1, K, \tag{3.35}$$

where the first sum in (3.35) is the interference as in the conventional THP, and the second sum is the inter-group interference coming from the users in the first group (gray squares in 3.5b). In this way, the same γ as in the first strategy is found for the users in the second group because the filter norms are the same as in the first HLNP strategy. After equalizing γ for the users in the first and second groups, the following γ is found for the second precoding strategy

$$\gamma = \frac{P}{N_0(\sum_{i=K-1}^{K} \|\boldsymbol{w}_i\|^2 + \sum_{i=1}^{K-2} \|\tilde{\boldsymbol{g}}_i\|^2)}. \tag{3.36}$$

In practice, we first start with finding the THP filters successively for the users in the second group. This will assure that the inter-group interference from the users in the second group to the users in the first group is removed. After finding the THP filters, the remaining channel matrix with $K-2$ column vectors, is used to find the ZF filters for the users in the first group. Therefore, the users in the first group will cause inter-group interference for the users in the second group. To remove this inter-group interference, we use (3.35). By comparing (3.33) with (3.36) and taking into account that $\sum_{i=1}^{K-2} \|\tilde{\boldsymbol{g}}_i\|^2 \leq \sum_{i=1}^{K-2} \|\boldsymbol{g}_i\|^2$, it turns out that γ in the second strategy is higher than that of the first strategy.

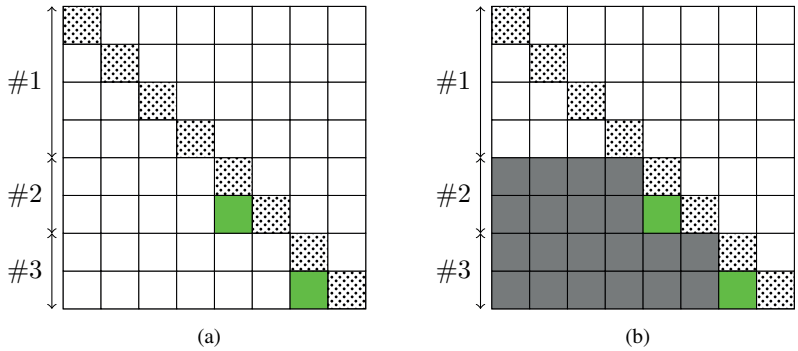

Figure 3.6: The interference pattern for two HLNP strategies of Fig. 3.5 when there are three groups of users. The white square shows that inter-user interference is 0, the green square shows the intra-group interference, and the gray square shows the inter-group interference.

In both strategies, it is of great importance to find an appropriate number of groups, and assign the users appropriately in the groups such that γ with max-min power control is maximized for all the users. To divide the users into a given number of groups, different methods can be used. An exhaustive search can be used, which entails a high computational complexity. Another heuristic grouping method is to separate the highly correlated pairs of users, and assign each of the correlated users into different groups. The other method is to train a neural network that can classify the users into different groups. By feeding appropriate features from the channel matrix of the users, e.g., the spatial correlation ρ_{ij}, one can train a neural network that finds an appropriate grouping for the HLNP strategy.[3]

Furthermore, both HLNP strategies can be applied when there are more groups. For the first strategy, the first HLNP strategy can be generalized by computing appropriate ZF and THP filters for the users in each group. In the second strategy, we find ZF filters based on the channel matrix of the users in each group. To remove the inter-group interference, we use the modified THP. It can be shown that in the second strategy, by keeping the number of groups to 2, and changing the number of users in the two groups, one can trade-off complexity vs. performance. When all the users are assigned to the second group, the second HLNP strategy becomes conventional THP, which leads to the highest γ for an HLNP strategy. On the other hand, when all the users are assigned to the first group, the second HLNP strategy becomes conventional ZF, which leads to the lowest γ for an HLNP strategy. The interference pattern is shown for both strategies when there are three groups in Fig. 3.6. For the second strategy, it can be shown that the same γ is achieved if the second and third groups are combined.

[3]Please see Chapter 6 for the details on the proposed grouping method.

3.5 Computational Complexity of Precoders

In this section, the computational complexity of finding the precoded vector in terms of the required real-valued floating-point operations (FLOPs) are presented. It is assumed that each real-valued addition and each real-valued multiplication require 1 FLOP. Thus, each complex addition and each complex multiplication require 2 and 6 FLOPs, respectively [63, Sec. 2.2]. The computational complexity of precoding strategies has two important terms. The complexity of finding the required filters, i.e., precoding matrix and power control coefficients, and the complexity of finding the transmit vector for a block of n symbols. The computational complexity of these terms are summarized for CB, ZF, THP, the first designed HLNP strategy (HLNP I) and the second designed HLNP strategy (HLNP II) in Table 3.1, where max-min power control is used to find the power control coefficients. For HLNP I and HLNP II, we assume the users are divided into a group of $K-2$ users and a group of 2 users. We further summarize the computational complexity of important operations in Table 3.2.

For CB, the precoding matrix is the complex conjugate of the channel matrix $\boldsymbol{H}$. For ZF, the pseudo-inverse of the channel $\boldsymbol{H}^{\dagger}$ is required to find the precoding matrix. To find the pseudo-inverse of the channel, $\boldsymbol{H}\boldsymbol{H}^{-1}$ is computed and $\boldsymbol{H}\boldsymbol{H}^{-1}$ is then multiplied by $\boldsymbol{H}^{H}$. Thus, for the ZF precoding matrix, an inverse of a $K \times K$ matrix and a multiplication of $M \times K$ and $K \times K$ matrices are required, which leads to $\mathcal{O}(MK^2)$ FLOPs.

To find the power control coefficients for CB, the bisection method is required. The bisection method is computationally expensive because it requires to run many iterations of search to find the power control coefficients. In each iteration of the bisection method, an inverse of a $K \times K$ matrix is computed, which results in $\mathcal{O}(iK^3)$ FLOPs for i iterations. For ZF, we use (3.8) to compute power control coefficients for which $\mathcal{O}(K)$ FLOPs are required assuming the ZF filters are already computed.

For THP, the order of users in encoding the symbols changes γ. Therefore, in addition to the filters and power control coefficients, the order of users has to be found. This is done in an iterative manner using the VBLAST algorithm (see 3.2.1), where at each iteration the pseudo-inverse of the updated channel matrix is computed. In this way, the complexity of finding the filters and the order of users is the complexity of finding the pseudo-inverse of a $K \times K$, $(K-1) \times (K-1)$, $(K-2) \times (K-2)$, ..., 2×2 matrices, which leads to $\mathcal{O}(MK^3)$ FLOPs. For the power control coefficients, we use (3.7) for which $\mathcal{O}(K)$ FLOPs are required assuming THP filters are already computed.

In HLNP I, for the first group of users, we need to find the ZF filters by computing column 1 to column $K-2$ of the pseudo-inverse of the channel. In contrast, in HLNP II, for the first group of users, we need to find the pseudo-inverse of a channel matrix of $K-2$ users. Although, the computations for HLNP II is lower than that of HLNP I, the order of complexity is the same for both precoders, i.e., $\mathcal{O}(MK^2)$ FLOPs. For the users in the second group, we need to find the filters $\boldsymbol{w}_K$ and $\boldsymbol{w}_{K-2}$. For both HLNP I and HLNP II, we need to find two columns from the pseudo-inverse of the channel of K users for $\boldsymbol{w}_K$ and we need to find one column from the pseudo-inverse of the channel of $K-1$

Table 3.1: Complexity order (FLOPs) of CB, ZF, THP, HLNP I and HLNP II

Precoder	Precoding filter	Power control	Transmit vector (n block)
CB	-	$\mathcal{O}(iK^3)$	$\mathcal{O}(nMK)$
ZF	$\mathcal{O}(MK^2)$	$\mathcal{O}(K)$	$\mathcal{O}(nMK)$
THP	$\mathcal{O}(MK^3)$	$\mathcal{O}(K)$	$\mathcal{O}(nMK)$
HLNP I	$\mathcal{O}(MK^2)$	$\mathcal{O}(K)$	$\mathcal{O}(nMK)$
HLNP II	$\mathcal{O}(MK^2)$	$\mathcal{O}(K)$	$\mathcal{O}(nMK)$

M is the number of antennas at the BS, K is the number of users, n is the number of symbols, i is the number of iterations to run the bisection method.

Table 3.2: Computational complexity of important operators for precoding

Operator	Complexity (FLOPs)
matrix-matrix multiplication ($M \times K$ with $K \times K$)	$8MK^2 - 2MK$
matrix-vector multiplication ($M \times K$ with $K \times 1$)	$8MK - 2M$
inverse of $K \times K$ matrix	$4K^3 + 8K^2 + K$

users for $\boldsymbol{w}_{K-1}$. Because in HLNP I and HLNP II, the pseudo-inverse calculations are not done for all the users as in the VBLAST algorithm, the complexity order of finding the filters and power control coefficients is $\mathcal{O}(MK^2)$ FLOPs.

To find the transmit vector for CB, ZF, THP, HLNP I and HLNP II it is required to multiply the precoding filters with the vector of symbols, i.e., multiplication of $M \times K$ matrix by a $K \times 1$ vector. This multiplication is repeated n times to find the transmit vector for a block of n symbols, which leads to $\mathcal{O}(nMK)$ FLOPs. For THP, HLNP I and HLNP II another set of computations is required. For THP, we need to encode symbols $\boldsymbol{s}$ to $\tilde{\boldsymbol{s}}$ as in (3.12), which requires $4nK(K-1)$ FLOPs for a block of n symbols. For HLNP I and HLNP II to encode $\boldsymbol{s}$ to $\tilde{\boldsymbol{s}}$ for a block of n symbols, $8n$ FLOPs and $8n(2K-3)$ FLOPs are required, respectively. Note for HLNP II we need to encode symbols based on (3.35) for which $2(K-2)$ more weights (see the gray squares in Fig. 3.5b) have to be computed.

CHAPTER 4

Dealing with Correlated Scenarios

4

In this chapter, we evaluate the proposed strategies (see Fig. 1.4) that address the research questions in Sec. 1.2. Employing each strategy alleviates the loss in the sum-rate of linear precoders in the correlated scenarios of LOS massive MIMO systems. The proposed strategies can be combined to further improve the performance in the correlated scenarios. In the first strategy, low-complexity precoders are used to provide a trade-off between complexity and performance. Instead of employing nonlinear precoding with high computational complexity, low-complexity precoders are used that improve the sum-rate of linear precoders. In the second strategy, we optimize the inter-element spacing of the BS antenna arrays such that the performance is improved. In the third strategy, we drop a set of users such that the sum-rate of the remaining users is improved. By dropping a set of users, the number of served users is reduced, which makes it easier for the BS to decorrelate the users. The following assumptions are made for the simulation scenarios of this chapter. A UPA with $M = 10 \times 10$ antennas that serves $K = 10$ users are considered. The users are distributed uniformly at the cell-edge (200 m away from the BS with no shadowing) in the field-of-view of $\phi \in (0, 2\pi)$ and $\theta \in (0, \pi/2)$. The carrier frequency is 30 GHz. The minimum acceptable spacing distance between the users is set to 0.01m. The transmit power at the BS is fixed such that when the users are mutually orthogonal, γ (SNR) of 10 dB is achieved for each user employing max-min power control. The simulation is run for 100 K realizations of the channel.

4.1 Outage Performance

To evaluate LOS environments, outage performance is typically studied because the angle of arrival of the user remains substantially constant for a long period of time, and

consequently, the ergodic capacity is unobtainable [43]. When a desired quality of service cannot be met for the users, the system is said to be in the outage. For instance, assume a BS that would like to deliver at least a γ of 10 dB for each user, and for some reasons, this cannot be met. In this example, the outage occurs when γ is less than 10 dB. The outage probability in terms of SNR is defined as follows

$$p(\tilde{\gamma}) = \Pr(\gamma < \tilde{\gamma}), \tag{4.1}$$

where $\tilde{\gamma}$ is the minimum acceptable SNR for the users. It is of great importance to maintain the probability of the outage below a target threshold, e.g., 0.05 or 0.01. This can be seen from a different perspective. For a given outage probability, e.g., 0.05, one can optimize the system to maximize the SNR. We use the 5th percentile γ (SNR) to evaluate the outage performance for each strategy.

4.2 Low-Complexity Precoders

The idea of low-complexity precoders is to provide a trade-off between complexity and performance, i.e., a performance close to that of nonlinear precoding and a complexity close to that of linear precoding. In this section, our focus is on HLNP strategies (see Sec. 3.4). The CDF of γ is shown for different precoders in Fig. 4.1. The horizontal dashed line shows the 5th percentile γ and the vertical dashed line at $\gamma = 10$ dB shows the FP performance[1]. Employing THP (solid black) results in the highest 5th percentile γ compared to the other precoders. By employing THP, the closest performance to the FP performance is achieved. By employing HLNP II (dashed green) using an exhaustive search to find the best grouping of the users, the 5th percentile γ is only 0.29 dB lower than that of THP. Employing HLNP I (orange dashed), ZF (solid blue) or CB (solid red) leads to 0.88 dB, 3.01 dB or 4.95 dB loss in the 5th percentile γ compared to HLNP II. The 5th percentile γ of HLNP II is only 0.29 dB less than that of THP, while HLNP II improves the 5th percentile γ of ZF by 3.01 dB. Taking into account the complexity of HLNP I and HLNP II in Table 3.1 and their outage performance in Fig. 4.1, HLNP strategies are viable candidates for 5G systems.

4.3 Optimized BS Antenna Arrays

The second strategy is to optimize the inter-element spacing of the BS antenna arrays such that the 5th percentile γ is maximized. The optimized array has a better ability to distinguish two different users. The CDF of γ is shown for different precoders in Fig. 4.2 when a UPA with inter-element spacing of 0.99λ[2] is used at the BS instead of half-wavelength UPA (dotted lines in Fig. 4.2). By employing a UPA with inter-element

[1] Recall that in FP, the users are mutually orthogonal.

[2] The value 0.99λ is given as an example, which is chosen close to that of δ_{n_1} in Fig. 7.4.

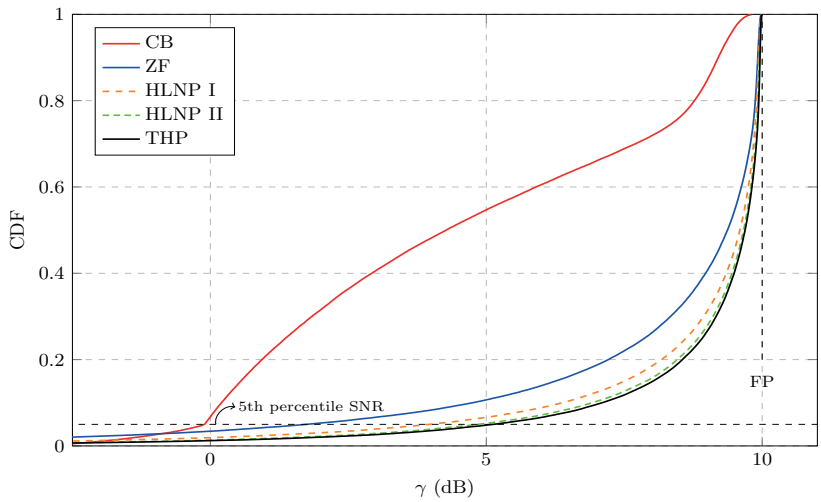

Figure 4.1: The CDF of γ for CB, ZF, THP, HLNP I and HLNP II for $M = 100$ (UPA) with $K = 10$ when a half-wavelength UPA is employed at the BS. The dashed vertical line at $\gamma = 10$ dB shows the FP performance when the users are mutually orthogonal.

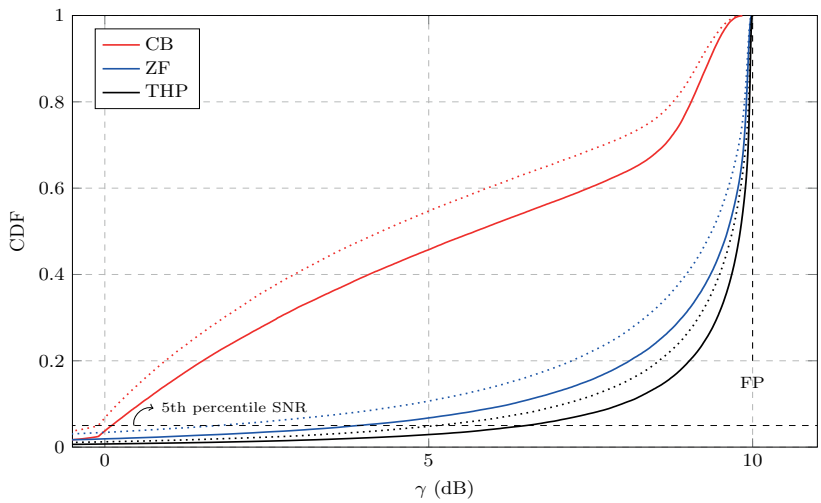

Figure 4.2: Same as Fig. 4.1 for a UPA with inter-element spacing of 0.99λ (solid lines) for CB, ZF, and THP. The dotted lines show the CDF of γ for a half-wavelenth BS antenna array.

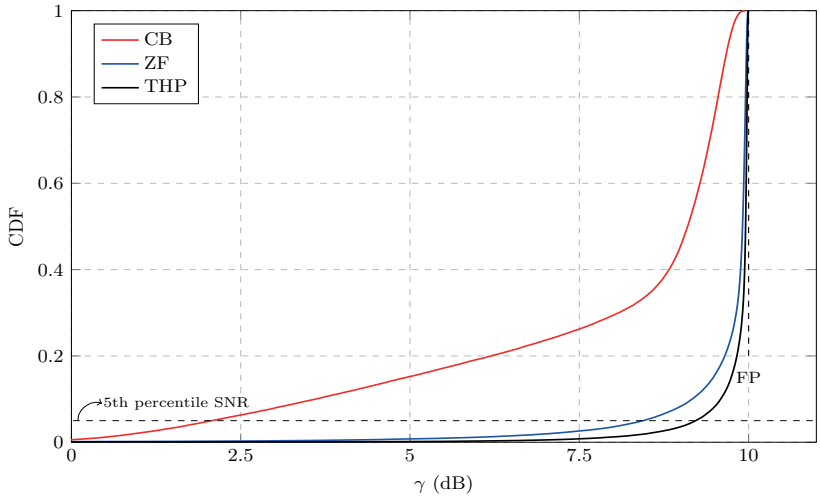

Figure 4.3: Same as Fig. 4.1 for a half-wavelength UPA that uses the dropping algorithm of [3] to drop 1 user.

spacing of 0.99λ, a higher 5th percentile γ is achieved for each precoder, 0.21 dB for CB, 2.16 dB for ZF, and 1.37 dB for THP. For a given precoder, one can find inter-element spacing that maximizes the 5th percentile γ.

4.4 Dropping Algorithms

The third strategy is to employ a dropping algorithm at the BS. The goal of the optimal dropping strategy is to find the set of dropped users such that the sum-rate for the remaining users is maximized, assuming max-min power control is employed. The CDF of γ is shown for different precoders in Fig. 4.3 when a UPA with half-wavelength inter-element spacing is employed at the BS and 1 user is dropped using the dropping algorithm of [3]. Note when 1 user is dropped, the transmit power is set at the BS such that a $\gamma = 10$ dB is achieved in FP for the remaining users. By employing the dropping algorithm to drop 1 user, a performance close to FP is achieved for THP. By dropping users, it is easier for the BS to decorrelate the users.

Part II

Included Papers

CHAPTER 5

Paper A
A Reduced-Complexity Linear Precoding Strategy for Massive MIMO Base Stations

Abstract

Conjugate beamforming (CB) and zero-forcing (ZF) are well-known linear precoders, which have optimized hardware implementations. In this work, a linear precoder is proposed based on switching between CB and ZF for line-of-sight propagation environments. The proposed idea is to predict and use the precoder, which results in the highest sum-rate for a given channel. To this end, three regimes are introduced for the ratio of power per user at the base station (BS) over noise power at a user receiver. For low values of this ratio, CB and for high values, ZF result in the highest sum-rate. For moderate values, a precoding strategy is proposed to switch to the best precoder. The switching mechanism is based on an upper bound for the ZF sum-rate, which we introduced in this work. The proposed precoding strategy achieves a sum-rate higher than both CB and ZF. Simulation results for a massive MIMO system including a 100-antenna BS, show up to 8% improvement on the sum-rate compared to CB and ZF. In addition, the proposed precoder reduces computational complexity up to 16.5% compared to the ZF precoding.

5.1 Introduction

Linear precoders, e.g., conjugate beamforming (CB) and zero-forcing (ZF) are low-complexity precoders, which have a close to capacity performance in massive MIMO systems [29, 39]. Therefore, they are viable candidates for downlink precoding in massive MIMO BSs. Designing a linear precoder includes choosing a precoding matrix and a set of power allocation coefficients. By choosing either CB or ZF precoding matrices, one can find the power allocation coefficients by maximizing a utility function [42], which is subject to practical constraints, e.g., the total power available at the BS [64].

Throughput and fairness are two popular utility functions. However, it has been shown that harmonic mean provides a trade-off between maximizing these two, which is desirable in practice [65]. In this work, by modifying the utility function of harmonic mean, closed-form solutions for power allocation coefficients of CB and ZF are derived. This results in reducing the computational complexity compared to maximizing throughput and fairness, which require complex optimization algorithms. Consequently, a utility function based on the modified harmonic mean is viable for CB and ZF in terms of performance and computational complexity.

In a massive MIMO system with an M-antenna BS and K single-antenna users, by having the channel matrix, finding the ZF precoding matrix has $O(MK^2)$ complexity due to having a matrix inversion and matrix multiplication. However, the CB precoding matrix is available without any processing, since it is equal to the complex conjugate of the channel matrix. Therefore, in terms of complexity, the CB precoding matrix is preferred in massive MIMO BSs. To the best of our knowledge, [66, Section 5.3] and [67] are the only works suggesting switching between CB and ZF to improve the sum-rate. However, no precise method is given, and there is no report on the gain of adaptively using CB and ZF in terms of computational complexity and sum-rate. In our paper, a systematic method is proposed for switching between CB and ZF.

In this paper, three regimes are defined for the ratio of power per user at the BS over noise power at a user receiver, i.e., low, moderate and high value regimes. We show that the CB precoding matrix for low value regime results in the highest sum-rate, whereas ZF results in the highest sum-rate for high value regime. Thus, CB and ZF can be used for low and high value regimes, respectively. For moderate value regime, both CB and ZF do not outperform the other. We propose a precoding strategy that lets the BS adaptively switch between CB and ZF to use the precoder with the highest sum-rate. By switching between CB and ZF, the computational complexity is also reduced compared to a BS that uses ZF. Therefore, the idea of switching between CB and ZF is beneficial in terms of sum-rate and computational complexity. This is the main idea behind the proposed precoding strategy.

The contributions of this work are as follows. First, a reduced-complexity linear precoder is proposed based on switching between CB and ZF. This precoder lets the BS predict and choose the precoder with the highest sum-rate in all regimes. The modified harmonic mean is used as the utility function to derive the power allocation coefficients for CB and ZF. Second, an upper bound is proposed for the ZF sum-rate, which is used

in the proposed switching mechanism to compare the CB and ZF sum-rate. To show the effectiveness of the proposed precoding strategy, and following [33], single-cell LOS scenarios are considered for the simulations. The simulation results show up to 8% improvement on the sum-rate and up to 16.5% reduction in computational complexity.

The structure of this paper is as follows. In Section 5.2, the principles of CB and ZF precoding are explained in detail. In Section 5.3 the proposed precoding strategy is introduced, and in Section 5.4 the simulation results are presented. Finally, Section 5.5 concludes the paper.

The following notation is used throughout the paper. Bold lowercase and uppercase letters denote column vectors and matrices, respectively. Lowercase letters denote scalars. The symbols $|\cdot|$ and $\|\cdot\|$ denote the absolute value and l^2-norm operators, respectively. The superscript * denotes conjugate. The superscripts ^{T} and ^{H} denote unconjugated transpose and conjugated transpose, respectively. The superscript $^{-1}$ stands for the inverse of a matrix. The symbol $\mathbb{C}$ denotes complex numbers. A diagonal matrix with diagonal entries taken from the vector $\boldsymbol{p}$ is denoted by $\text{diag}(\boldsymbol{p})$ and $\boldsymbol{I}_K$ denotes the identity matrix of size $K \times K$. The complex inner product of two vectors $\boldsymbol{a}$ and $\boldsymbol{b}$ is denoted by $\langle \boldsymbol{a}, \boldsymbol{b} \rangle = \boldsymbol{a}^H \boldsymbol{b}$.

5.2 Linear Precoders

In this section, we introduce the system model under consideration. Then, the CB and ZF precoding are reviewed.

5.2.1 System Model

In this paper, we consider the downlink channel shown in Fig. 5.1, where an M-antenna BS transmits symbols to K single-antenna users. Let $\boldsymbol{s} = (s_1, ..., s_K)^T$ be the vector of symbols to be transmitted to the users. These symbols are assumed to be uncorrelated, zero mean and unit variance. To compensate the channel effects and serve all the users, the BS uses a set of power allocation coefficients $\boldsymbol{p} = (\sigma_1, ..., \sigma_K)^T$ and a precoding matrix $\boldsymbol{U} \in \mathbb{C}^{M \times K}$. The transmitted vector $\boldsymbol{x} \in \mathbb{C}^{M \times 1}$ can be expressed as:

$$\boldsymbol{x} = \boldsymbol{U}\text{diag}(\boldsymbol{p})\boldsymbol{s}. \tag{5.1}$$

The precoding matrix is defined as $\boldsymbol{U} = (\boldsymbol{u}_1, ..., \boldsymbol{u}_K)$, which satisfies $\|\boldsymbol{u}_i\| = 1$ for $i = 1, ..., K$. The power allocation coefficients are positive real-values. We assume a total power constraint at the BS, i.e., $\|\boldsymbol{p}\|^2 \leq P_{\text{tot}}$, where P_{tot} is the maximum available power at the BS.

The BS transmits $\boldsymbol{x}$ through the channel, which is then received by the users. The downlink channel is modeled as:

$$\boldsymbol{y} = \boldsymbol{H}\boldsymbol{x} + \boldsymbol{n}, \tag{5.2}$$

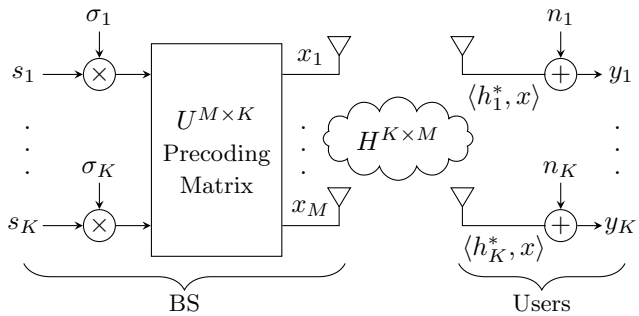

Figure 5.1: General structure of downlink with an M-antenna BS serving K single-antenna users.

5

where $\boldsymbol{y} \in \mathbb{C}^{K\times 1}$ is the received signal vector of the users, $\boldsymbol{n} \in \mathbb{C}^{K\times 1}$ is the noise vector and $\boldsymbol{H} = (\boldsymbol{h}_1, ..., \boldsymbol{h}_K)^T \in \mathbb{C}^{K\times M}$ is the downlink channel matrix. The noise components are modeled as independent, zero mean circularly-symmetric complex Gaussian random variables with covariance matrix of $\sigma_n^2 \boldsymbol{I}_K$. The $\boldsymbol{h}_i$ is the channel vector from the BS antennas to the user i. The ith received signal is given by:

$$y_i = \boldsymbol{h}_i^T \boldsymbol{x} + n_i = \langle \boldsymbol{h}_i^*, \boldsymbol{x}\rangle + n_i, \tag{5.3}$$

which is shown in Fig. 5.1.

For notation simplicity, we use:

$$\boldsymbol{h}_i = c_i \tilde{\boldsymbol{h}}_i, \;\; c_i = ||\boldsymbol{h}_i||, \;\; i = 1, ..., K. \tag{5.4}$$

Thus, $\tilde{\boldsymbol{h}}_i$ is the unit norm channel vector for the user i. The received signal for the ith user can be further simplified (after some simple algebra) as:

$$y_i = c_i \sigma_i \langle \tilde{\boldsymbol{h}}_i^*, \boldsymbol{u}_i\rangle s_i + \sum_{j\neq i} c_i \sigma_j \langle \tilde{\boldsymbol{h}}_i^*, \boldsymbol{u}_j\rangle s_j + n_i, \tag{5.5}$$

where the first term is the desired signal, the second term is the interference from other users, and the last term is noise.

For a given channel, the signal to noise plus interference ratio (SINR) for the user i is defined based on (5.5) as:

$$\text{SINR}_i = \frac{c_i^2 \sigma_i^2 |\langle \tilde{\boldsymbol{h}}_i^*, \boldsymbol{u}_i\rangle|^2}{\sum_{j\neq i} c_i^2 \sigma_j^2 |\langle \tilde{\boldsymbol{h}}_i^*, \boldsymbol{u}_j\rangle|^2 + \sigma_n^2}. \tag{5.6}$$

We define the ratio of the radiated power per user at the BS over the noise power at a user receiver as:

$$\eta = \frac{P_{\text{tot}}/K}{\sigma_n^2}. \tag{5.7}$$

It is worth to mention that $K\eta$ is equivalent to ρ_d in [33]. The η has to compensate the propagation loss in order to satisfy throughput requirements. For a fixed precoding matrix, we use the power allocation coefficients, which maximize the harmonic mean [65] as:

$$\boldsymbol{p} = \underset{\boldsymbol{p}:\|\boldsymbol{p}\|^2 \leq P_{\text{tot}}}{\text{argmax}} \left(\sum_{i=1}^{K} \frac{1}{\text{SINR}_i} \right)^{-1}, \tag{5.8}$$

where SINR_i is given by (5.6). In this paper, the precoding matrix is assumed to be either CB or ZF, which are briefly reviewed in the following sections.

5.2.2 Conjugate Beamforming

The CB precoding matrix $\boldsymbol{U}^{\text{CB}} = (\boldsymbol{u}_1^{\text{CB}}, ..., \boldsymbol{u}_K^{\text{CB}})$ maximizes the inner product of the user component in (5.5). The ith column of CB precoding matrix is obtained by:

$$\boldsymbol{u}_i^{\text{CB}} = \underset{\boldsymbol{u}_i:\|\boldsymbol{u}_i\|=1}{\text{argmax}} \; |\langle \tilde{\boldsymbol{h}}_i^*, \boldsymbol{u}_i \rangle|^2 = \tilde{\boldsymbol{h}}_i^*. \tag{5.9}$$

This leads to $\boldsymbol{U}^{\text{CB}} = (\tilde{\boldsymbol{h}}_1^*, ..., \tilde{\boldsymbol{h}}_K^*)$. To derive the power allocation coefficients of CB, (5.8) can be solved by using water-filling [65], which is computationally expensive. Due to the fact that the channel vectors are nearly orthogonal in massive MIMO systems [39], we propose to solve:

$$\boldsymbol{p}^{\text{CB}} = \underset{\boldsymbol{p}:\|\boldsymbol{p}\|^2 \leq P_{\text{tot}}}{\text{argmax}} \left(\sum_{i=1}^{K} \frac{\sigma_n^2}{c_i^2 \sigma_i^2} \right)^{-1}, \tag{5.10}$$

where $\frac{c_i^2 \sigma_i^2}{\sigma_n^2}$ is the received SNR of each user, which follows from the solution of (5.9). A closed-form solution for (5.10) is found by using the Lagrangian multiplier as:

$$\sigma_i^{\text{CB}} = \sqrt{\frac{P_{\text{tot}}}{\sum_{j=1}^{K} \frac{c_i}{c_j}}}. \tag{5.11}$$

This solution suggests that users with a high c_i should receive less power, whereas users with a low c_i should receive more power. Our proposed power allocation coefficients in (5.10) and (5.11) result in the following SINR for the ith user:

$$\text{SINR}_i^{\text{CB}} = \frac{1}{\sum_{j \neq i} \frac{c_i}{c_j} \rho_{ij}^2 + \frac{1}{K\eta} \sum_{j=1}^{K} \frac{1}{c_i c_j}}, \tag{5.12}$$

where $\rho_{ij} = |\langle \tilde{\boldsymbol{h}}_i^*, \tilde{\boldsymbol{h}}_j^* \rangle|$.

5.2.3 Zero-Forcing

The ZF precoding matrix removes the multi-user interference for all the users in (5.5), while it maximizes the desired signal. The ith column of ZF precoding matrix is found by:

$$\boldsymbol{u}_i^{\text{ZF}} = \underset{\substack{\boldsymbol{u}_i:\|\boldsymbol{u}_i\|=1,\\ \langle\tilde{\boldsymbol{h}}_j^*,\boldsymbol{u}_i\rangle=0,\ j\neq i}}{\operatorname{argmax}} |\langle\tilde{\boldsymbol{h}}_i^*,\boldsymbol{u}_i\rangle|^2. \tag{5.13}$$

The resulting $\boldsymbol{U}^{\text{ZF}} = (\boldsymbol{u}_1^{\text{ZF}},...,\boldsymbol{u}_K^{\text{ZF}})$ given by (5.13), can be found by normalizing the columns of pseudo-inverse of the channel [64] to have unit norm. Unlike CB, ZF removes the multi-user interference, and thus, (5.8) is solved by using the Lagrangian multiplier as:

$$\sigma_i^{\text{ZF}} = \sqrt{\frac{P_{\text{tot}}}{\sum_{j=1}^{K}\frac{c_i\gamma_i}{c_j\gamma_j}}}, \tag{5.14}$$

where $\gamma_i = |\langle\tilde{\boldsymbol{h}}_i^*,\boldsymbol{u}_i^{\text{ZF}}\rangle|$ and $\gamma_j = |\langle\tilde{\boldsymbol{h}}_j^*,\boldsymbol{u}_j^{\text{ZF}}\rangle|$. This results in the following SINR for the user i:

$$\text{SINR}_i^{\text{ZF}} = K\eta\frac{c_i\gamma_i}{\sum_{j=1}^{K}\frac{1}{c_j\gamma_j}}. \tag{5.15}$$

5

5.3 Proposed Precoding Strategy

The proposed precoding strategy lets the BS choose the precoder that results in the highest sum-rate. The selection is based on η and a proposed upper bound for the ZF sum-rate. In this section, we first find two thresholds for η, which determine the best precoder for the low and high η regimes. Then, we derive an upper bound for the ZF sum-rate, which is later used in the switching mechanism of the proposed precoder.

5.3.1 Evaluation Of Precoders

The downlink sum-rate R of a linear precoder for a given channel matrix in bits/second/Hz, can be evaluated as [68, chapter 10], [48]:

$$R = \sum_{i=1}^{K}\log_2(1+\text{SINR}_i), \tag{5.16}$$

where SINR_i is given by (5.6). We replace (5.12) and (5.15) in (5.16) to obtain the CB and ZF sum-rates as:

$$R^{\text{CB}} = \sum_{i=1}^{K}\log_2\left(1+\frac{1}{\sum_{j\neq i}\frac{c_i}{c_j}\rho_{ij}^2+\frac{1}{K\eta}\sum_{j=1}^{K}\frac{1}{c_ic_j}}\right), \tag{5.17}$$

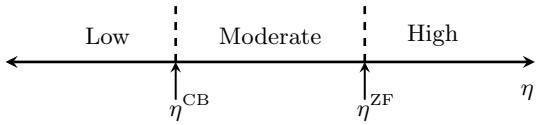

Figure 5.2: The introduced regimes for η.

$$R^{\text{ZF}} = \sum_{i=1}^{K} \log_2 \left(1 + K\eta \frac{c_i \gamma_i}{\sum_{j=1}^{K} \frac{1}{c_j \gamma_j}} \right). \tag{5.18}$$

We compare the SINR_i formulas of these two precoders to find a condition in which CB results in a higher rate for all the users compared to ZF. This is stricter than only having a higher sum-rate. In fact, this condition guarantees that CB has a higher sum-rate. The same condition is found for ZF. The following theorem explains these conditions.

Theorem 5.1. For a given channel realization, when $\eta < \eta^{\text{CB}}$, CB, and when $\eta > \eta^{\text{ZF}}$, ZF result in a higher rate for all the users, where:

$$\begin{aligned} \eta^{\text{CB}} &= \min_{i=1,\ldots,K} a_i, \\ \eta^{\text{ZF}} &= \max_{i=1,\ldots,K} a_i, \end{aligned} \tag{5.19}$$

and a_i is given by:

$$a_i = \frac{1}{K c_i \gamma_i} \left(\frac{1}{\sum_{j \neq i} \frac{c_i}{c_j} \rho_{ij}^2} \right) \sum_{j=1}^{K} \frac{1}{c_j} \left(\frac{1}{\gamma_j} - \gamma_i \right). \tag{5.20}$$

Proof. See Appendix 5.6. □

The interpretation of Theorem 1 is that there are three regimes for η, i.e., low, moderate and high, which are graphically shown in Fig. 5.2. It is concluded from Theorem 1 that for low and high η regimes, CB and ZF result in the highest sum-rate, respectively. For moderate η regime, more analysis is required to find the precoder with the highest sum-rate. This analysis is presented in Section 5.3.3.

The η^{CB} and η^{ZF} are functions of the channel and thus, are random variables. We study the probability density function (PDF) of η^{CB} and η^{ZF} for a large number of channel realizations with a fixed number of users. The PDF plots are used to find two thresholds T_{min} and T_{max}, which define the low and high η regimes, respectively. We define a point on the right tail of η^{CB} as T_{max} for which the probability that CB results in a higher rate for all the users is 0.5%. Thus, above this threshold, CB does not perform well for all the users. Similarly, we define a point on the left tail of η^{ZF} as T_{min}. More details are given in Section 5.4 on how the low and high η regimes can be realized for a fixed or variable number of users.

5.3.2 Correlation Between Channel Vectors

By having the correlation between the channel vectors, i.e., $\rho_{ij}, j \neq i,\ i,j = 1,...,K$, we can calculate the CB sum-rate based on (5.17). The following Lemma shows that the γ_i can be bounded, and thus, the ZF sum-rate can be bounded as well.

Lemma 5.1. The value of γ_i is bounded by:

$$\gamma_i \leq \sqrt{1 - \underset{j:j\neq i}{\operatorname{argmax}}\, \rho_{ij}^2} \qquad i,j = 1,...,K. \tag{5.21}$$

Proof. See Appendix 5.7. □

Lemma 2 states that two users with large ρ_{ij}, have very small γ, which implies that the SINR^{ZF} of those users are very small (see (5.15)). The following Corollary gives an upper bound for the ZF sum-rate. Its proof follows from using the right-hand side of (5.21) in (5.18).

5

Corollary 5.1. The ZF sum-rate is upper bounded by:

$$R^{\text{ZF}} \leq \sum_{i=1}^{K} \log_2 \left(1 + K\eta \frac{c_i \gamma_i^{\text{U}}}{\sum_{j=1}^{K} \frac{1}{c_j \gamma_j^{\text{U}}}} \right), \tag{5.22}$$

where $\gamma_i^{\text{U}} = \sqrt{1 - \underset{j:j\neq i}{\operatorname{argmax}}\, \rho_{ij}^2}$.

The difference between the proposed bound and the ZF sum-rate is very small when the BS serves a low number of users. The accuracy of the proposed bound is studied in Section 5.4. The proposed upper bound is used in the proposed precoding strategy to find the best precoder in moderate η regime.

5.3.3 The Proposed Precoder

The proposed precoder is illustrated in Fig. 5.3. First, given the possible number of users, the PDF plots of η^{CB} and η^{ZF} are used to find T_{min} and T_{max}, or equivalently realize the low and high η regimes. In practice, this can be done either by running a periodic set of measurements or an offline set of measurements. In low η regime, CB and in high η regime, ZF are chosen as explained in Section 5.3.1. In moderate η regime, a switching mechanism is proposed, which is based on the proposed upper bound for the ZF sum-rate. By measuring the channel, all the ρ_{ij} and c_i are found. These values are used to calculate the CB sum-rate based on (5.17) and the upper bound for the ZF sum-rate based on Theorem 2. We use $R_{\text{max}}^{\text{ZF}}$ to denote the right-hand side of (5.22). Whenever R^{CB} exceeds $R_{\text{max}}^{\text{ZF}}$, CB definitely results in the highest sum-rate. Thus, in these cases, the BS switches to CB. Otherwise, the BS uses ZF, due to the fact the proposed upper bound is quite close to the actual ZF sum-rate. In the next section, the results of applying the proposed precoding strategy for a massive MIMO system are presented.

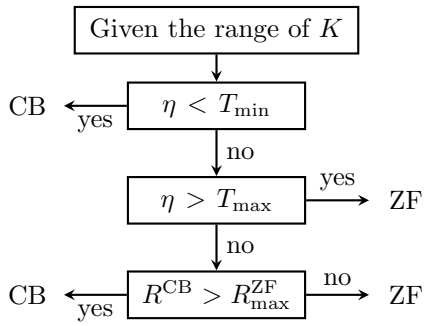

Figure 5.3: Illustration of the proposed precoding strategy, given the possible range of K.

5.4 Simulations

In this section, two examples are given to show the effectiveness of the proposed precoder in moderate η regime. The first example shows how the proposed precoder performs for a fixed number of users. In the second example, the performance of the proposed precoder is evaluated when the number of users changes from $K = 5$ to $K = 25$ for a given η. A massive MIMO system including a linear array with 100 antennas with half-wavelength spacing at the BS is assumed that serves K single-antenna users in a single-cell LOS channel. The channel from the user u to the antenna v at the BS is modeled as $h_{uv} = \sqrt{\beta}e^{-jkR_{uv}}$, where $k = 2\pi/\lambda$ (λ is the wavelength) is the wave number, R_{uv} is the distance from the user u to the antenna v, and β is the average path loss given by the COST-WI model. The following assumptions are assumed:

- The carrier frequency = 1.9 GHz.
- The bandwidth = 20 MHz.
- The BS antenna gain = 0 dBi.
- The mobile antenna gain = 0 dBi.
- The mobile receiver noise figure = 9 dB.
- The users are uniformly distributed in a 120-degree sector, which are 20 m to 2 km far from the BS.
- The minimum distance between the users = 1 cm.

The PDF plots of η^{CB} and η^{ZF} are used to find $T_{\min}$ and $T_{\max}$. In Fig. 5.4, the PDF plots are shown for $K = 5$ and $K = 25$. The moderate η regime for $K = 5$ is found as $(T_{\min}, T_{\max}) = (91\text{ dB}, 111\text{ dB})$ and for $K = 25$ is found as $(T_{\min}, T_{\max}) = (101\text{ dB}, 114\text{ dB})$.

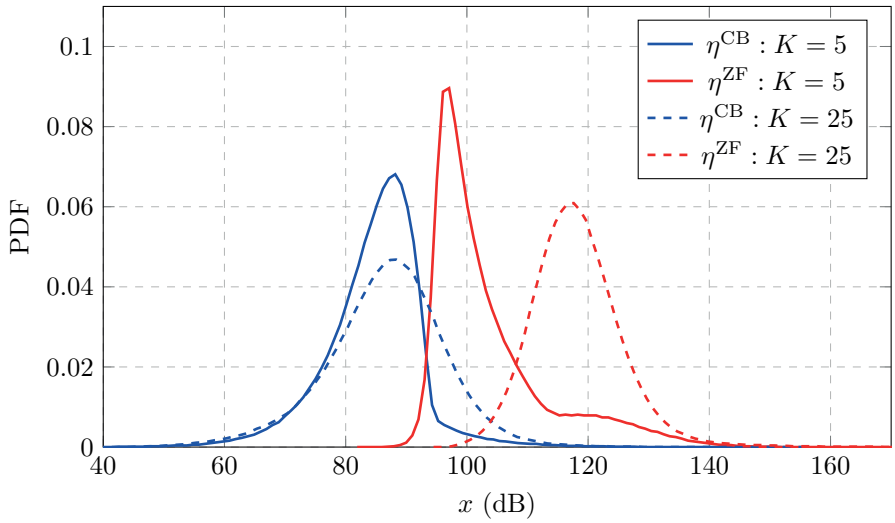

5

Figure 5.4: The PDF plots of η^{CB} and η^{ZF} for 10^6 random realizations when $K = 5$ and $K = 25$.

In moderate η, the proposed upper bound is used to find the best precoder as explained in Section 5.3.3. The proposed upper bound and actual ZF sum-rate are shown in Fig. 5.5 for a different number of users in a wide range of η. For a low number of users ($K = 5$), the difference between the proposed bound and actual ZF sum-rate are negligible. However, by increasing the number of users to $K = 20$ the difference is increased. The sum-rate improvement of the proposed precoder is presented with two examples in the next sections.

5.4.1 Example 1

In this example, the BS serves $K = 20$ users. The moderate η regime is realized by studying the PDF plots of η as $(T_{\text{min}}, T_{\text{max}}) = (98 \text{ dB}, 111.2 \text{ dB})$. Then, the proposed switching mechanism is used to find the best precoder. The effectiveness of the proposed precoder is shown in Fig. 5.6 for a wide range of η, which shows that the proposed precoder improves the sum-rate of CB and ZF. Specifically, the intersection point in Fig. 5.6 shows 7.5% improvement in sum-rate compared to both CB and ZF.

5.4.2 Example 2

In this example, the number of served users is changed from $K = 5$ to $K = 25$. The moderate η regime is found by considering the PDF plots of η^{CB} and η^{ZF} for all the values of $K = 5$ to $K = 25$. The common moderate η regime is found as $(T_{\text{min}}, T_{\text{max}}) =$

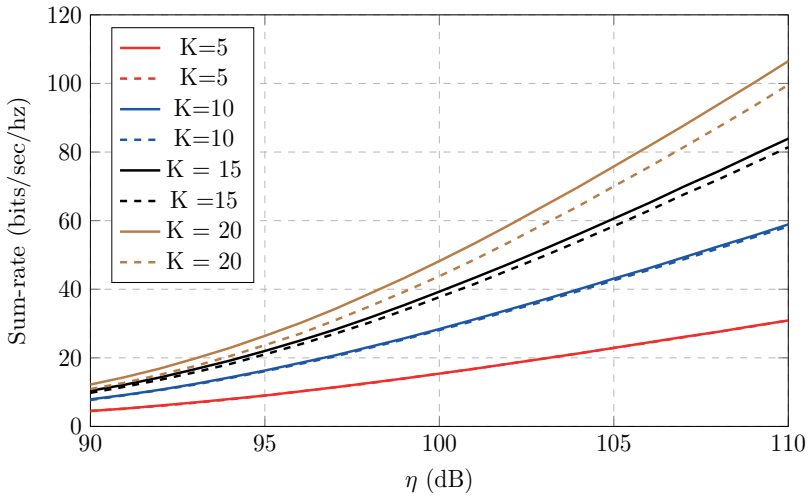

Figure 5.5: The proposed upper bound compared to the ZF sum-rate of (5.18) for 10^5 random realizations, for a different number of users. The solid lines are the upper bound and the dashed lines are the achieved sum-rate.

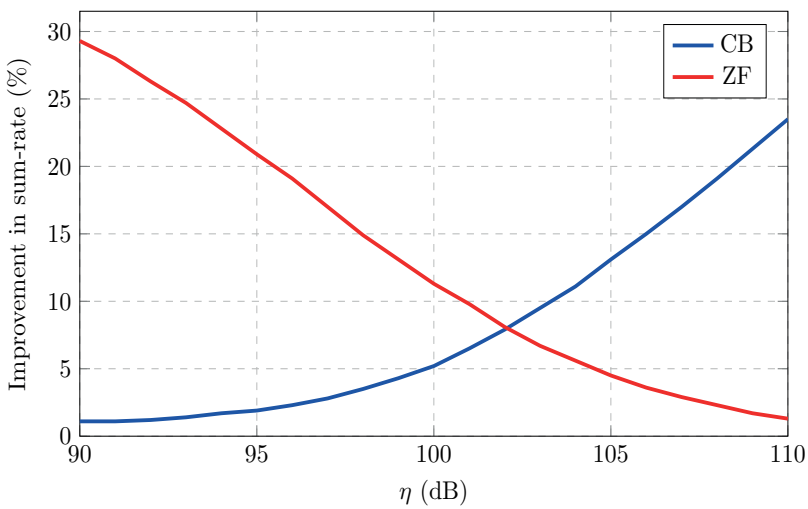

Figure 5.6: The improvement of the proposed precoding strategy for $K = 20$ compared to CB and ZF.

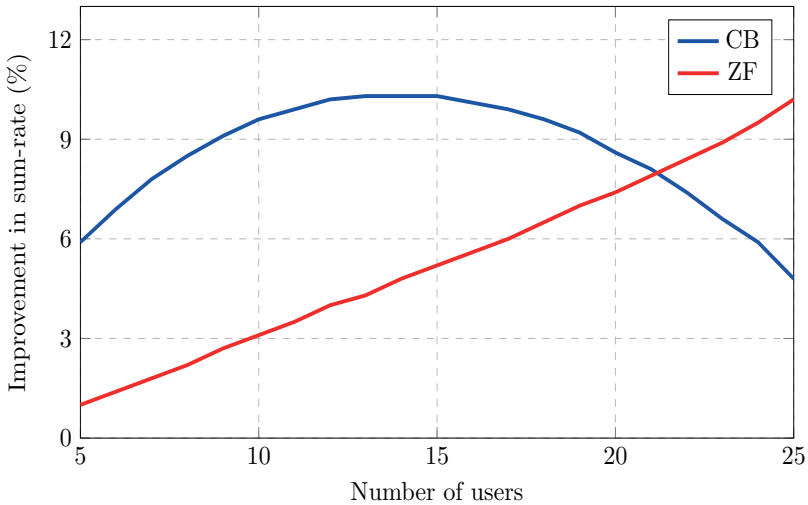

Figure 5.7: The improvement of the proposed precoding strategy in $\eta = 102.5$ dB compared to CB and ZF when the number of users changes from 5 to 25.

$(101 \text{ dB}, 111 \text{ dB})$. The proposed precoder is used in this regime to use the best precoder. The results are shown in Fig. 5.7 for $\eta = 102.5$ dB. The proposed precoder improves the sum-rate up to 8% compared to both CB and ZF (the intersection point). Moreover, the proposed precoder reduces the computational complexity up to 16.5% compared to the case, where a BS uses ZF all the time. This is due to the switching to CB. The proposed precoder has a complexity of $O(MK^2/2)$ when CB is chosen. However, it does not change the order of complexity when ZF is chosen due to the fact that its main processing is a part of the ZF precoder. Therefore, it reduces the total complexity compared to a ZF precoder. The complexity reduction while improving the sum-rate is of great importance for the massive MIMO systems, which is achieved by the proposed precoder.

5.5 Conclusion

In this paper, a linear precoder is proposed based on switching between CB and ZF. The proposed idea is to use the precoder with the highest sum-rate for a given channel realization. An upper bound for the ZF sum-rate is proposed, which is used in the proposed precoding strategy. The proposed precoder improves the CB and ZF sum-rate for moderate η regime, while it reduces the computational complexity. Simulation results show up to 8% improvement on the sum-rate and up to 16.5% reduction in the computational complexity. For future works, we consider applying the proposed idea for millimeter wave massive MIMO systems.

5.6 Proof of Theorem 1

To prove (5.19), we find the condition in which CB results in a higher rate for all the users. This clearly guarantees the CB sum-rate is higher than the ZF sum-rate. For ith user, the condition $\text{SINR}_i^{\text{ZF}} < \text{SINR}_i^{\text{CB}}$ is expressed as:

$$K\eta \frac{c_i\gamma_i}{\sum_{j=1}^{K} \frac{1}{c_j\gamma_j}} < \frac{1}{\sum_{j\neq i} \frac{c_i}{c_j}\rho_{ij}^2 + \frac{1}{K\eta}\sum_{j=1}^{K}\frac{1}{c_ic_j}}. \tag{5.23}$$

Equation (5.23) is simplified as:

$$K\eta c_i\gamma_i \sum_{j\neq i} \frac{c_i}{c_j}\rho_{ij}^2 + \gamma_i \sum_{j=1}^{K} \frac{1}{c_j} < \sum_{j=1}^{K} \frac{1}{c_j\gamma_j}. \tag{5.24}$$

Finally, the following condition is found for each user:

$$\eta < \frac{1}{Kc_i\gamma_i}\left(\frac{1}{\sum_{j\neq i}\frac{c_i}{c_j}\rho_{ij}^2}\right)\sum_{j=1}^{K}\frac{1}{c_j}\left(\frac{1}{\gamma_j} - \gamma_i\right). \tag{5.25}$$

By finding the minimum value of the right-hand side of (5.25) over all the users, η^{CB} is found. The η^{ZF} is found similarly by finding the maximum.

5.7 Proof of Lemma 2

The orthogonal projection of $\tilde{\boldsymbol{h}}_i^*$ onto the subspace of other users' channel vectors, i.e., V, results in the vector $\boldsymbol{a}_i$. The γ_i is the distance from $\tilde{\boldsymbol{h}}_i^*$ to V, which is shown in Fig. 5.8. For a given vector, the orthogonal projection to a sub-space has the minimum distance, compared to the other non-orthogonal projections. Consequently, γ_i has the minimum length, or equivalently $\boldsymbol{a}_i$ has the largest length among the other projections of $\tilde{\boldsymbol{h}}_i^*$ on V. Thus, for any unit vector $\tilde{\boldsymbol{h}}_j^*, j \neq i$ in V, the following holds:

$$||\boldsymbol{a}_i||^2 \geq |\langle \tilde{\boldsymbol{h}}_i^*, \tilde{\boldsymbol{h}}_j^* \rangle|^2 \Rightarrow ||\boldsymbol{a}_i||^2 \geq \rho_{ij}^2 \,. \tag{5.26}$$

Thus, we can conclude that:

$$||\boldsymbol{a}_i||^2 \geq \underset{j:j\neq i}{\text{argmax}}\, \rho_{ij}^2 \qquad i,j = 1,...,K. \tag{5.27}$$

Therefore, considering $||\boldsymbol{a}_i||^2 = 1 - \gamma_i^2$ and (5.27), γ_i is bounded by:

$$\gamma_i \leq \sqrt{1 - \underset{j:j\neq i}{\text{argmax}}\, \rho_{ij}^2} \qquad i,j = 1,...,K, \tag{5.28}$$

which concludes the proof.

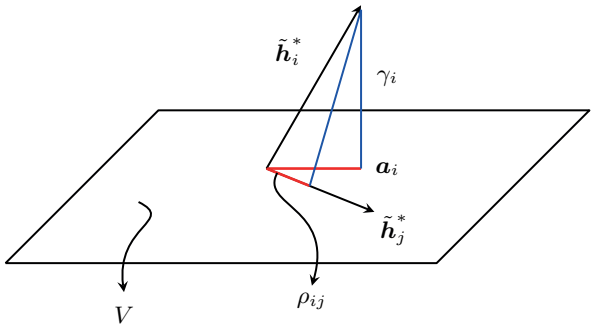

Figure 5.8: The illustration of why $\boldsymbol{a}_i$ has the maximum norm among all the other projections. The blue vectors are orthogonal lines from $\tilde{\boldsymbol{h}}_i^*$ to the directions of red vectors on V subspace.

CHAPTER 6

Paper B
A Low-Complexity Hybrid Linear and Nonlinear Precoder for Line-Of-Sight Massive MIMO with Max-Min Power Control

6

Abstract

In line-of-sight (LOS) massive MIMO, there is a nonnegligible probability that the channel vectors of some users become correlated. In these correlated scenarios, nonlinear precoders can be used instead of linear precoders at the cost of high computational complexity. To reduce the complexity of nonlinear precoders, hybrid linear and nonlinear precoders have been suggested in 5G New Radio (NR). In this paper, we find the probability that there is at least one pair of correlated users and we find the average number of correlated users. We propose a hybrid linear and nonlinear precoder (HLNP) with max-min power control for which the served users are divided into two groups. By employing a proposed modified Tomlinson-Harashima Precoding (THP), we design and combine the transmit vectors of the two groups such that inter-group interference is removed. Simulation results show that by employing HLNP instead of zero-forcing, the required transmit power to assure a given average block error rate (BLER) with 95% probability is reduced. For a 64-antennas BS, when modified THP is used for 3 out of 10 users in HLNP, the

transmit power is reduced by up to 4.70 dB to assure an average BLER of 10^{-2} using 16QAM and 64QAM constellations with NR low-density parity-check codes.

6.1 Introduction

By increasing the number of antennas at the base station (BS) of a massive MIMO system, the channel vectors from the BS to the users become mutually orthogonal [39]. This property is known as favorable propagation (FP), which is one of the key properties exploited in massive MIMO systems [33]. Both line-of-sight (LOS) environments and independent and identically distributed (i.i.d.) Rayleigh fading exhibit FP [69]. In LOS environments, there is a nonnegligible probability that the channel vectors of a small number of users become highly correlated [39], which leads to a reduction of the achievable sum-rates of known linear precoders [70, 71]. For instance, in two LOS scenarios, which are identified as important for future 5G systems, i.e., "open exhibition" and "crowded auditorium", a large number of users are physically co-located [32, 72, 73], and thus, many users will likely have highly correlated channel vectors.

In LOS environments, it is of great importance to provide uniformly good service for all the users, which can be realized by using max-min power control [33]. Employing linear precoding with max-min power control in highly correlated scenarios results in a large loss in the data-rate due to the fairness criterion of max-min power control [3, 33]. To alleviate the large loss associated with linear precoding with max-min power control, there are two alternatives. The first alternative is to use a simple dropping algorithm to reschedule some of the highly correlated users. This approach has been used in [3, 33, 74, 75]. The main drawback of these algorithms is that some of the users are required to be rescheduled for next coherence intervals, which might not be desirable in some applications, e.g., ultra-reliable and low-latency (URLL) applications [76]. The second alternative is to use nonlinear precoders with or without dropping and rescheduling algorithms, e.g., [4, 70]. The main drawback of the second alternative is that nonlinear precoders entail a high computational complexity. To reduce the complexity of nonlinear precoders and their practical issues, hybrid linear and nonlinear precoders are suggested for 5G NR [60, 77]. The hybrid linear and nonlinear precoders are discussed in different 3GPP RAN 1 meetings for the specification of the physical layer of 5G NR [60, 77, 78]. For the nonlinear precoding part, Tomlinson-Harashima precoding (THP) is suggested in [60].

Two structures are suggested for hybrid linear and nonlinear precoding in [60]. In the first structure, the BS dynamically switches between linear and nonlinear precoding, based on the channel condition of the users. The second structure is a hybrid linear and nonlinear precoder similar to [61, 79], where a two-stage linear precoder and nonlinear precoder is used. The users are divided into several groups that all are served at the same time. The intra-group interference is removed by using nonlinear precoding, while the inter-group interference is removed by using linear precoding. In [61, 79], a correlated Rayleigh fading channel model is assumed, where the users in the same group have

an identical channel correlation matrix. Moreover, the simulation results in [61, 79] do not cover the relevant case of massive MIMO systems with a large number of antennas serving few users.

To address the non-ergodic nature of LOS environments [33], a different grouping methodology other than [61, 79] has to be used. To use a hybrid linear and nonlinear precoder for a given channel realization in LOS environments, the optimal grouping of the served users can be found by an exhaustive search, which is not practical when the number of users grows. Thus, in LOS environments, a simple yet efficient grouping algorithm is necessary for a low-complexity hybrid linear and nonlinear precoder based on THP.

In this paper, we study a multi-carrier time-division duplexing single-cell massive MIMO system. We further assume the channel state information (CSI) is perfectly known at the BS for a given coherence interval. The assumptions of single-cell and perfect CSI are justified as follows. The inter-cell interference occurs at longer distances over which the propagation environment is more likely to be i.i.d. Rayleigh than LOS [33] (see Table 7.4.2-1 of [80] for more details). In addition, the nature of LOS environments prohibits an ergodic analysis of the channel estimation error [33]. Moreover, the channel estimation for LOS environments is easier than i.i.d. Rayleigh because for LOS only the angle of arrival and a complex amplitude have to be estimated [33].

In this paper, we first use a simple probabilistic model given in [39] to find the probability that there is at least one pair of correlated users in LOS environments. We further find the average number of users that have correlated channel vectors. We present a probability analysis to show how often and for how many users, nonlinear precoding is beneficial in LOS environments. To the best of our knowledge, this study has not been addressed in the literature.

Second, we propose a novel hybrid linear and nonlinear precoder (HLNP) for a single-cell LOS massive MIMO with max-min power control. In the proposed HLNP, a grouping scheme is proposed to divide the served users into two groups. We design and combine the transmit vectors of the two groups such that inter-group interference is removed. To this end, for the first group, a modified THP is proposed to remove the inter-group interference, while for the second group, linear precoding is employed. Instead of performing nonlinear processing associated with THP for all the users, nonlinear processing is only done for a few users in the proposed HLNP. Consequently, the latency and computation overhead of THP is reduced. Furthermore, linear precoding for the second group of the users is employed for a reduced number of users, which has a less computational complexity than that of finding linear precoding filters for all the users. By changing the combination of the users in the two groups, the signal to noise ratio (SNR) of the users will change. The proposed grouping method heuristically find a combination of the users in the two groups such that the SNR with max-min power control is maximized.

We present different simulations to show the effectiveness of the proposed precoder. We compare the proposed grouping method with a correlation grouping method based

on [33, 74]. Furthermore, we study the block error rate (BLER) performance of the proposed precoder compared to zero-forcing (ZF) and THP for 16QAM and 64QAM constellations using NR-LDPC codes. In addition, we study the sensitivity of the proposed precoder to the channel state information error.

This paper is organized as follows. In Sec. 6.2, preliminaries are given. In Sec. 6.3, the probability analysis is given for LOS environments. In Sec. 6.4, the proposed precoder is presented. In Sec. 6.5, simulation results are presented to show the effectiveness of the proposed precoder. Finally, Sec. 6.6 concludes the paper.

6.2 Preliminaries

6.2.1 System Model

The model for the downlink channel from an M-antenna BS to K single-antenna users with linear precoding is shown in Fig. 6.1. The intended zero-mean, uncorrelated and unit-variance symbols $\boldsymbol{s} = (s_1, s_2, ..., s_K)^T \in \mathbb{C}^{K\times 1}$ are precoded by a diagonal power control matrix $\boldsymbol{D} = \text{diag}(\boldsymbol{d})$ and a linear precoding matrix $\boldsymbol{U} \in \mathbb{C}^{M\times K}$ with unit-norm column vectors $\boldsymbol{u}_i$.[1] The power control vector is $\boldsymbol{d} = (\sqrt{d_1}, \sqrt{d_2}, ..., \sqrt{d_K})^T$, where $d_i \in \mathbb{R}^+$ with $i = 1, 2, ..., K$ are the max-min power control coefficients. The average power constraint for the precoded vector $\boldsymbol{x}$ is $\mathbb{E}[\|\boldsymbol{x}\|^2] = P$, which results in $\sum_{i=1}^{K} d_i = P$. The precoded vector $\boldsymbol{x} \in \mathbb{C}^{M\times 1}$ is found by:

$$\boldsymbol{x} = \boldsymbol{U}\boldsymbol{D}\boldsymbol{s}, \tag{6.1}$$

which is transmitted through the channel $\boldsymbol{H} = (\boldsymbol{h}_1, \boldsymbol{h}_2, ..., \boldsymbol{h}_K)^T \in \mathbb{C}^{K\times M}$, where $\boldsymbol{h}_i$ is the channel vector from the BS antennas to user i. The received signal for user i is:

$$y_i = \boldsymbol{h}_i^T \boldsymbol{x} + n_i = \boldsymbol{h}_i^T \boldsymbol{u}_i \sqrt{d_i} s_i + \sum_{\substack{j=1 \\ j\neq i}}^{K} \boldsymbol{h}_i^T \boldsymbol{u}_j \sqrt{d_j} s_j + n_i, \tag{6.2}$$

where n_i is complex AWGN noise with variance N_0.

Assuming perfect CSI for a given channel realization, the signal to noise plus interference ratio (SINR) for each user can be expressed as:

$$\text{SINR}_i = \frac{|\boldsymbol{h}_i^T \boldsymbol{u}_i|^2 d_i}{\sum_{j=1, j\neq i}^{K} |\boldsymbol{h}_i^T \boldsymbol{u}_j|^2 d_j + N_0}. \tag{6.3}$$

[1] The following notation is used throughout the paper. Lowercase, bold lowercase and bold uppercase letters denote scalars, column vectors, and matrices, respectively. The symbols $|\cdot|$, $\|\cdot\|$, $\mathbb{Z}$ and $\mathbb{C}$ denote the absolute value, l^2-norm, the set of integers, and the set of complex numbers, respectively. The superscripts ^{T} and ^{H} denote un-conjugated transpose and conjugated transpose, respectively. A diagonal matrix with diagonal entries taken from the vector $\boldsymbol{p}$ is denoted by $\text{diag}(\boldsymbol{p})$, $\boldsymbol{I}_K$ denotes the identity matrix of size $K \times K$, $\text{tr}(\cdot)$ denotes the trace operation. The symbol $\mathcal{CN}(\boldsymbol{\mu}, N_0\boldsymbol{I}_K)$ denotes a vector of complex Gaussian random variables with mean $\boldsymbol{\mu}$ and covariance matrix of $N_0\boldsymbol{I}_K$. The imaginary unit is denoted by $\jmath$. The operator $\otimes$ denotes the kronecker product. The permutation matrix $\boldsymbol{P}$ is a square matrix that has exactly one element of 1 in each row and column and 0 elsewhere.

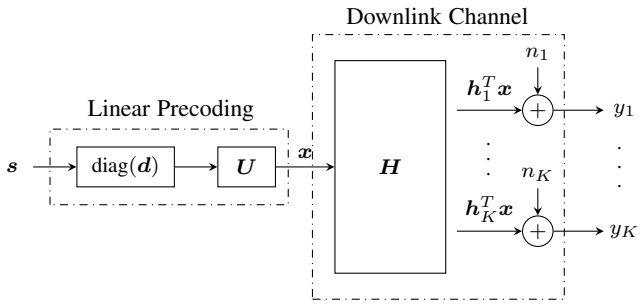

Figure 6.1: The model of the downlink channel with linear precoding. The symbols $\boldsymbol{s} \in \mathbb{C}^{K\times 1}$ are precoded to $\boldsymbol{x} \in \mathbb{C}^{M\times 1}$ by employing the $K \times K$ power control matrix diag($\boldsymbol{d}$) with $d_i \geq 0$ and the precoding matrix $\boldsymbol{U} \in \mathbb{C}^{M\times K}$. Then, $\boldsymbol{x}$ is transmitted through the channel $\boldsymbol{H}$, and is received by each user.

In this paper, for a given set of filters $\boldsymbol{u}_i, i = 1, 2, ..., K$, we are interested in finding the coefficients $d_i, i = 1, 2, ..., K$, that maximize the minimum SINR$_i$ among the users, a.k.a., max-min power control. Using the max-min power control, uniformly good service for all the users is achieved [33]. The values d_i are found by:

$$\begin{aligned} \boldsymbol{d}^\star = \underset{d_1,d_2,...,d_K}{\operatorname{argmax}} \quad \min_{i\in\{1,2,...,K\}} \quad \text{SINR}_i, \\ \text{s.t.} \quad \sum_{i=1}^{K} d_i = P, \end{aligned} \tag{6.4}$$

where SINR$_i$ is given by (6.3).

For linear precoding and nonlinear precoding in the proposed hybrid precoder, ZF filters are used. We find the ZF filters and corresponding max-min power control as follows. The ZF filters $\boldsymbol{u}_i$ are found by normalizing the ith column of the pseudo-inverse of the channel $\boldsymbol{H}^\dagger = (\boldsymbol{g}_1, \boldsymbol{g}_2, ..., \boldsymbol{g}_K) = \boldsymbol{H}^H(\boldsymbol{H}\boldsymbol{H}^H)^{-1}$ to have a unit-norm column vector. By using ZF filters $\boldsymbol{u}_i = \boldsymbol{g}_i/\|\boldsymbol{g}_i\|$, the following max-min power control coefficient d_i and SNR [2] are found for each user using Lagrange multipliers:

$$d_i = \frac{P}{|\boldsymbol{h}_i^T\boldsymbol{u}_i|^2 \sum_{j=1}^{K} \frac{1}{|\boldsymbol{h}_j^T\boldsymbol{u}_j|^2}} = \frac{P\|\boldsymbol{g}_i\|^2}{\sum_{j=1}^{K} \|\boldsymbol{g}_j\|^2}. \tag{6.5}$$

$$\text{SNR} = \frac{P}{N_0 \sum_{j=1}^{K} \frac{1}{|\boldsymbol{h}_j^T\boldsymbol{u}_j|^2}} = \frac{P}{N_0 \sum_{j=1}^{K} \|\boldsymbol{g}_j\|^2}. \tag{6.6}$$

To find $\sum_{j=1}^{K} \|\boldsymbol{g}_j\|^2$, we need to find the trace of $(\boldsymbol{H}^\dagger)^H\boldsymbol{H}^\dagger = (\boldsymbol{H}\boldsymbol{H}^H)^{-1}$. Thus, the elements of $\boldsymbol{H}\boldsymbol{H}^H$ are affecting the SNR in (6.6). The element ij of $\boldsymbol{H}\boldsymbol{H}^H$ can be

[2]Note by using ZF filters, the interference term in 6.3 becomes zero, and SINR becomes SNR.

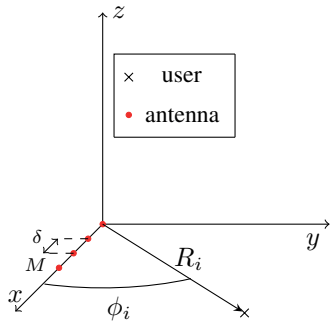

Figure 6.2: Illustration of a ULA with $M = 4$ elements located on x-axis with inter-element spacing of δ. The distance between the first element of the array and the user is R_i.

represented by using the channel norms $\|\boldsymbol{h}_i\|$ and $\|\boldsymbol{h}_j\|$ and the spatial correlation among the channel vectors of user i and user j denoted by ρ_{ij} given by:

$$\rho_{ij} = \frac{\boldsymbol{h}_j^H \boldsymbol{h}_i}{\|\boldsymbol{h}_i\|\|\boldsymbol{h}_j\|}. \tag{6.7}$$

6

To further study correlated scenarios in the next sections, we use the following definition.

Definition 6.1. A pair of users (i, j) with spatial correlation of ρ_{ij} are said to be correlated with a given threshold ρ_{thr} if $|\rho_{ij}| > \rho_{\text{thr}}$, where $0 \leq \rho_{\text{thr}} \leq 1$.

6.2.2 Channel Model

The free-space LOS channel model for uniform linear arrays (ULAs) and uniform planar arrays (UPAs) are given as follows. Assume a BS equipped with a ULA of M antennas located on the x-axis (see Fig. 6.2). Assume also that the user i is in the x-y plane, where R_i is the distance from the user to the first element of the array, and ϕ_i is the azimuth angle of the user. The channel vector from the BS antennas to the user i is modeled as (see [35, Sec. 7.2.2] for details)

$$\boldsymbol{h}_i = \sqrt{\beta_i} e^{\jmath \frac{2\pi}{\lambda} R_i} \left(1, e^{-\jmath \frac{2\pi}{\lambda} \delta \cos(\phi_i)}, ..., e^{-\jmath \frac{2\pi}{\lambda} (M-1)\delta \cos(\phi_i)}\right)^T, \tag{6.8}$$

where β_i is the large-scale fading for user i, λ is the wavelength and δ is the inter-element spacing (typically $\lambda/2$).

A UPA with $N_x \times N_y$ elements is shown in Fig. 6.3. The UPA is located on the x-y plane with $z = 0$, which serves a user at the spherical coordinate (R_i, θ_i, ϕ_i). The channel vector for user i in this case is found by (see [36, eq. (5)])

$$\boldsymbol{h}_i = \sqrt{\beta_i} e^{\jmath \frac{2\pi}{\lambda} R_i} \boldsymbol{v}_x(\phi_i, \theta_i) \otimes \boldsymbol{v}_y(\phi_i, \theta_i), \tag{6.9}$$

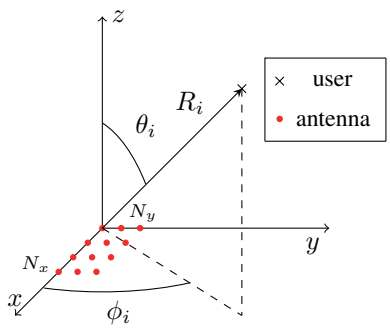

Figure 6.3: Illustration of a UPA with $N_x = 4$ and $N_y = 3$ serving a user at (R_i, θ_i, ϕ_i).

where θ_i is the polar angle of user i as in the spherical coordinates and $\boldsymbol{v}_x(\phi_i, \theta_i)$ and $\boldsymbol{v}_y(\phi_i, \theta_i)$ are:

$$\boldsymbol{v}_x(\phi_i, \theta_i) = \left(1, e^{-\jmath \frac{2\pi}{\lambda} \delta \sin(\theta_i) \cos(\phi_i)}, ..., e^{-\jmath \frac{2\pi}{\lambda} (N_x - 1) \delta \sin(\theta_i) \cos(\phi_i)}\right)^T, \tag{6.10}$$

and

$$\boldsymbol{v}_y(\phi_i, \theta_i) = \left(1, e^{-\jmath \frac{2\pi}{\lambda} \delta \sin(\theta_i) \sin(\phi_i)}, ..., e^{-\jmath \frac{2\pi}{\lambda} (N_y - 1) \delta \sin(\theta_i) \sin(\phi_i)}\right)^T. \tag{6.11}$$

6

6.2.3 Review of THP

The model for THP is shown in Fig. 6.4 for a given coherence interval. The intended symbols $\boldsymbol{s}$ are encoded to $\tilde{\boldsymbol{s}} = (\tilde{s}_1, \tilde{s}_2, ..., \tilde{s}_K)^T \in \mathbb{C}^{K \times 1}$ by using the feedback filter $\boldsymbol{B} - \boldsymbol{I}_K \in \mathbb{C}^{K \times K}$ and the modulo operator $[\cdot]_\Delta$ with divisor Δ.[3] Then, a power control matrix $\boldsymbol{G} = \text{diag}(\sqrt{d_1}, \sqrt{d_2}, ..., \sqrt{d_K})$ and feedforward filter $\boldsymbol{Q}^H \in \mathbb{C}^{M \times K}$ are used to generate the precoded vector $\boldsymbol{x} \in \mathbb{C}^{M \times 1}$. To find the filters, the LQ decomposition of the channel $\boldsymbol{H} = \boldsymbol{LQ}$ is employed. Note $\boldsymbol{H}$ is required at the BS for encoding a block of symbols (block-level precoding [51]) in the given coherence interval. The matrix $\boldsymbol{Q}^H$ is used for the feedforward filter, and $\boldsymbol{L}$, which is a lower triangular matrix with positive diagonal elements l_{ii} is used to find $\boldsymbol{B}$ for the feedback filter (for more details on THP see [41, Sec. 5.4.4] and [52, Ch. 3.2.3]). Then, the received signal for user i, i.e., y_i is found by:

$$y_i = l_{ii} \sqrt{d_i} \tilde{s}_i + \sum_{j=1}^{i-1} l_{ij} \sqrt{d_j} \tilde{s}_j + n_i, \tag{6.12}$$

[3] Δ is equivalent to τ in [55, eq. (9)].

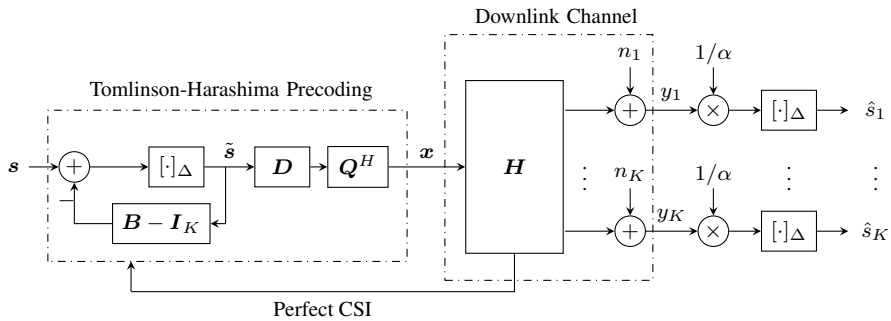

Figure 6.4: The model of the downlink channel with THP. The symbols $\boldsymbol{s}$ are encoded to $\boldsymbol{x}$ using the modulo operator $[\cdot]_\Delta$, the feedback filter $\boldsymbol{B} - \boldsymbol{I}_K$ and the feedforward filters $\boldsymbol{G}$ and $\boldsymbol{Q}^H$. The users has access to the side information α and use the same Δ as in the BS for the modulo operator to estimate their symbols.

where l_{ii} is the ith diagonal element in $\boldsymbol{L}$ and n_i is the complex AWGN noise with variance N_0. By using the scalar $\alpha_i = l_{ii}\sqrt{d_i}$, and using the modulo operator at the receiver, the estimated symbol for user i is found by:

6

$$\hat{s}_i = \left[\frac{y_i}{\alpha_i}\right]_\Delta = \left[\tilde{s}_i + \sum_{j=1}^{i-1} \frac{l_{ij}\sqrt{d_j}}{\alpha_i}\tilde{s}_j + \frac{n_i}{\alpha_i}\right]_\Delta . \tag{6.13}$$

By encoding $\tilde{s}_i = \left[s_i - \sum_{j=1}^{i-1} \frac{l_{ij}\sqrt{d_j}}{\alpha_i}\tilde{s}_j\right]_\Delta$ (see the feedback loop in Fig. 6.4, the element ij of matrix $\boldsymbol{B}$ is $b_{ij} = l_{ij}\sqrt{d_j}/\alpha_i$), the estimated symbol becomes:

$$\hat{s}_i = \left[s_i + \frac{n_i}{\alpha_i}\right]_\Delta . \tag{6.14}$$

At high SNRs, where the noise component n_i/α_i is small with respect to Δ, the modulo operator (loss) can be ignored [53]:

$$\hat{s}_i = s_i + \frac{n_i}{\alpha_i}. \tag{6.15}$$

Thus, using inflated lattice strategies [54], where the shaping loss is neglected, $\text{SNR}_i = \alpha_i^2/N_0 = l_{ii}^2 d_i/N_0$ can be achieved for user i. The max-min power control coefficients d_i are found by maximizing the minimum SNR_i among the users by:

$$d_i = \frac{P}{l_{ii}^2 \sum_{j=1}^{K} \frac{1}{l_{jj}^2}}, \quad i = 1, ..., K. \tag{6.16}$$

Therefore, the following SNR is achieved for each user:

$$\text{SNR} = \frac{P}{N_0 \sum_{j=1}^{K} \frac{1}{l_{jj}^2}} = \frac{P}{N_0 \sum_{j=1}^{K} \|\boldsymbol{w}_j\|^2}, \tag{6.17}$$

where $\boldsymbol{W} = (\boldsymbol{w}_1, \boldsymbol{w}_2, ..., \boldsymbol{w}_K) = \frac{1}{\eta}\boldsymbol{Q}^H\boldsymbol{G}$ with $\eta^2 = \frac{P}{\sum_{j=1}^{K} \frac{1}{l_{jj}^2}}$. Note (6.16) leads to $\alpha_i = \alpha = \frac{P}{\sum_{j=1}^{K} \|\boldsymbol{w}_j\|^2}$. Thus, the scalars α_i that each user requires to estimate its symbol are identical. It is assumed that each user has access to α to estimate its symbols.

For THP, the order of users for encoding $\boldsymbol{s}$ to $\tilde{\boldsymbol{s}}$ affects SNR in (6.17). Each ordering of the users can be represented by a permutation matrix $\boldsymbol{P}$. The optimal permutation matrix $\boldsymbol{P}^\star$ is the one that maximizes SNR over all the possible permutation matrices, which is found by:

$$\boldsymbol{P}^\star = \underset{\boldsymbol{P}}{\text{argmax}} \;\; \text{SNR} = \underset{\boldsymbol{P}}{\text{argmin}} \;\; \sum_{j=1}^{K} \|\boldsymbol{w}_j\|^2. \tag{6.18}$$

We use VBLAST algorithm described in [41, Fig. 5.18] to solve (6.18).

6.3 Probability Analysis

In this section, we use a simple probabilistic model given in [39] to study the correlated scenarios. We first find the probability that at least one pair of users becomes correlated (see Defenition 6.1). Then, we find the average number of correlated users.

6.3.1 Probabilistic Model

The following definition will be used for the analysis in this section.

Definition 6.2. For a given channel with K users and a given correlation threshold ρ_{thr}, ζ is the probability that there is at least one correlated pair of users:

$$\zeta = \Pr\{\exists i, j \neq i, i, j \in \{1, 2, ..., K\} \mid |\rho_{ij}| \geq \rho_{\text{thr}}\}, \tag{6.19}$$

where ρ_{ij} is given by (6.7).

When $|\rho_{ij}|$ increases for a channel with two users, the downlink capacity and achievable sum-rates of linear precoders decrease [3, 70]. Thus, if the two users become correlated with a high threshold ρ_{thr}, the achievable sum-rate of linear precoders is decreased considerably [3, Fig. 2]. For this high threshold, if ζ is nonnegligible, that means there is a nonnegligible probability that a small achievable sum-rate is achieved for the users (due to the fairness criterion). In these scenarios, the system is quite far from FP in which

the channel vectors of the users are mutually orthogonal [39]. Therefore, evaluating ζ for a given massive MIMO system in LOS environments is of great importance.

In what follows, we study two variables for an M-antenna BS serving K users. The first variable is ζ as in (6.19), and the second variable is the average number of users that have correlated channel vectors denoted by $\mathbb{E}[n_{\text{cor}}]$. To find ζ or $\mathbb{E}[n_{\text{cor}}]$ analytically, one should evaluate integrals for a given ρ_{thr}. Instead, we use the following assumptions made in [39]. We assume the BS can create M orthogonal beams. The probability that a user is assigned to a specific beam is independent of the other users and is equal to $1/M$. When two users are assigned to a specific beam, they become correlated with probability $1/M$.

In [39], the average number of users that need to be dropped to achieve a close to favorable propagation performance is found, where some users are dropped such that each beam has either one or no user. The analysis in [39] does not give information on how many users are assigned to a specific beam. For example, when two users are dropped, there are two possibilities. First, it might be the case that there were two pairs of users and second, it might be the case that there were three users assigned to the same beam. In contrast to [39], we focus on the average number of correlated users, which is the number of users that are assigned to a beam with more than one user. We distinguish between the two cases in the mentioned example, i.e., in the first scenario, there were four correlated users while in the second scenario, there were three correlated users.

6.3.2 Study of ζ

We find ζ by computing the probability of its complementary event (see [81, Ch. II. 5]), which is when each user is assigned to a different beam, i.e., there is no beam with more than one user. The complementary event of ζ is equivalent to the probability that no user is dropped [39, Sec. 4.3]. To assign the users in M beams, there are M^K possibilities from which there are $\binom{M}{K}K!$ cases that each user is assigned to a different beam. The probability ζ in (6.19) is then found by:

$$\zeta = 1 - \frac{\binom{M}{K}K!}{M^K} = 1 - \prod_{i=1}^{K-1}\left(1 - \frac{i}{M}\right). \tag{6.20}$$

In Fig. 6.5, we compare ζ found by (6.20) with ζ found by Monte Carlo simulations for two different scenarios for a given M. In the two scenarios, ζ is found by running 100000 Monte Carlo realizations with $K \in \{2, ..., 10\}$ users. The correlated users with $\rho_{\text{thr}} = 0.64$ [4] are found by finding the pairs of users with $\rho_{ij} > 0.64$. In the first scenario (ULA), a ULA of 100 antennas is located at the BS, which serves the users uniformly distributed in an arc from $\phi_{\text{min}} = 0$ to $\phi_{\text{max}} = \pi$. In the second scenario (UPA), a 10×10

[4] The results in [2, Fig. 4] show that the probability that any two users become correlated with $\rho_{\text{thr}} = 0.64$ for relatively large M is close to $1/M$. Thus, to match the assumptions of the probabilistic model, we use $\rho_{\text{thr}} = 0.64$ in the simulations.

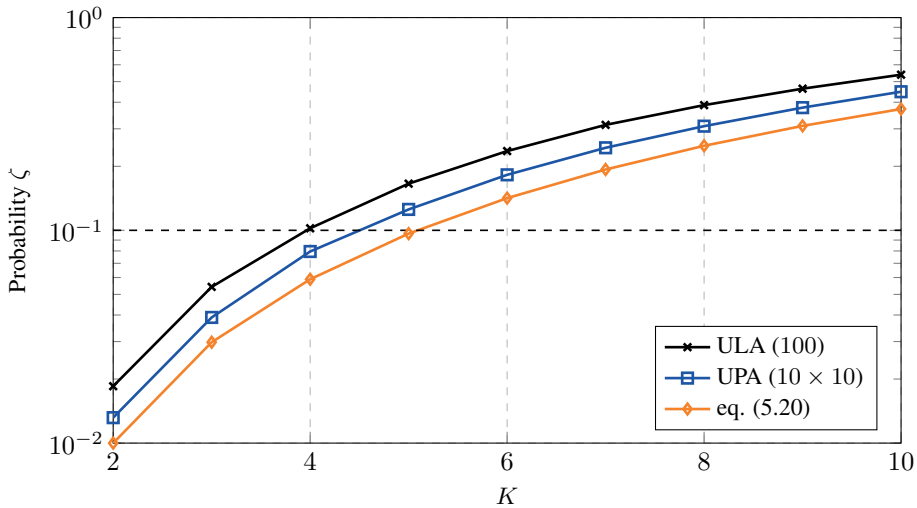

Figure 6.5: The probability that there is at least one pair of correlated users ζ as a function of K cell-edge users for different scenarios for $\rho_{\text{thr}} = 0.64$ obtained via Monte Carlo simulations, i.e., ULA (100) and UPA (10 × 10) compared to ζ found by (6.20).

UPA is assumed at the BS that serves the users uniformly distributed in the field-of-view of $\phi \in (0, 2\pi)$ and $\theta \in (0, \pi/2)$.

The results in Fig. 6.5 show that by increasing the number of users K from 2 to 10, ζ grows rapidly for all three curves, and more importantly, ζ is not negligible. The probability ζ is more than 10% (see the dashed horizontal line in Fig. 6.5) for $K = 4$ and $K = 5$ for ULA and UPA, respectively. The results in Fig. 6.5 show that ζ found by (6.20) underestimates the actual values of ζ, nevertheless, it shows the correct trend. We conclude that in practical scenarios, where there is a small field-of-view in the elevation angle, e.g., UMi-street canyon [80, Table 7.4.1-1], it is expected that ζ grow much faster. Thus, in such practical scenarios, we have correlated scenarios more often.

6.3.3 Study of $\mathbb{E}[n_{\text{cor}}]$

We now find the average number of users that have correlated channel vectors $\mathbb{E}[n_{\text{cor}}]$. To do so, we need to find the probability $\Pr\{n_{\text{cor}} = n\}$. Recall any two users are correlated, when they are assigned to the same beam. Thus, when there are n correlated users ($n_{\text{cor}} = n$), it implies there are $K - n$ beams with exactly one user. We find $\Pr\{n_{\text{cor}} = n\}$

for $n = 0, 1, 2, 3$ as follows

$$\Pr\{n_{\text{cor}} = 0\} = \frac{\binom{M}{K} K!}{M^K}, \tag{6.21}$$

$$\Pr\{n_{\text{cor}} = 1\} = 0 \tag{6.22}$$

$$\Pr\{n_{\text{cor}} = 2\} = \frac{\binom{M}{1}\binom{K}{2}\binom{M-1}{K-2}(K-2)!}{M^K}, \tag{6.23}$$

$$\Pr\{n_{\text{cor}} = 3\} = \frac{\binom{M}{1}\binom{K}{3}\binom{M-1}{K-3}(K-3)!}{M^K}. \tag{6.24}$$

To find (6.21), we find the probability that each user is assigned to a different beam, which is computed to derive ζ in (6.20). Note $\Pr\{n_{\text{cor}} = 1\} = 0$ because the correlation is defined for a pair of users. For $\Pr\{n_{\text{cor}} = 2\}$, we find the probability that there is one beam with exactly two users, $K-2$ beams with exactly one user, and $M-K$ beams with no user. We first choose 1 beam in $\binom{M}{1}$ different ways. Then, we choose 2 users in $\binom{K}{2}$ ways and assign them to the chosen beam. We then choose $K-2$ beams for the remaining $K-2$ users in $\binom{M-1}{K-2}$ ways. These $K-2$ users can be distributed in $K-2$ beams in $(K-2)!$ different ways. Therefore, there are $\binom{M}{1}\binom{K}{2}\binom{M-1}{K-2}(K-2)!$ different scenarios, where there is exactly one pair of correlated users. With the same approach as in (6.23), we find $\Pr\{n_{\text{cor}} = 3\}$. Note $\Pr\{n_{\text{cor}} = 2\}/\Pr\{n_{\text{cor}} = 3\} = 3(M-K+2)/(K-2)$. This shows that the probability that there is only one correlated pair of users is much higher than the probability that all 3 users are assigned to the same beam, e.g., for $M = 100$ and $K = 10$, it is 34.5 times more probable.

For $n_{\text{cor}} > 3$, there is not a single way for the correlated users to occupy the beams. For instance, for $n_{\text{cor}} = 4$, there are two possible sets of events, i.e., when all 4 users are assigned to the same beam and when there are two pairs of users assigned to two different beams. To find the probability of each set of events, we can use the approach as in (6.23). For instance, $\Pr\{n_{\text{cor}} = 4\}$ is found by

$$\Pr\{n_{\text{cor}} = 4\} = \frac{\binom{M}{1}\binom{K}{4}\binom{M-1}{K-4}(K-4)!}{M^K} + \frac{\binom{M}{2}\binom{K}{4}\left(\frac{4!}{2!\ 2!}\right)\binom{M-2}{K-4}(K-4)!}{M^K}, \tag{6.25}$$

where the first term is the probability that all the 4 users are assigned to the same beam, and the second term is the probability that there are two pairs of users assigned to two different beams. Note when dividing the 4 users into two beams, the permutation of the users in each beam does not count. Thus, there are $4!/(2!\ 2!)$ ways to assign the two chosen pairs of users in the two chosen beams. Note the second term in (6.25) is $3(M-K+3)$ times larger than the first term. This shows that the probability that there are two pairs of correlated users is much higher than the probability that all 4 users are assigned to the same beam, e.g., for $M = 100$ and $K = 10$, it is 279 times more probable.

In Fig. 6.6, the probability $\Pr\{n_{\text{cor}} = n\}$ is shown for $n = 2, 3, ..., K$ for $K = 10$ and $M = 64, 100, 144$. The following conclusions are inferred from Fig 6.6. First, the

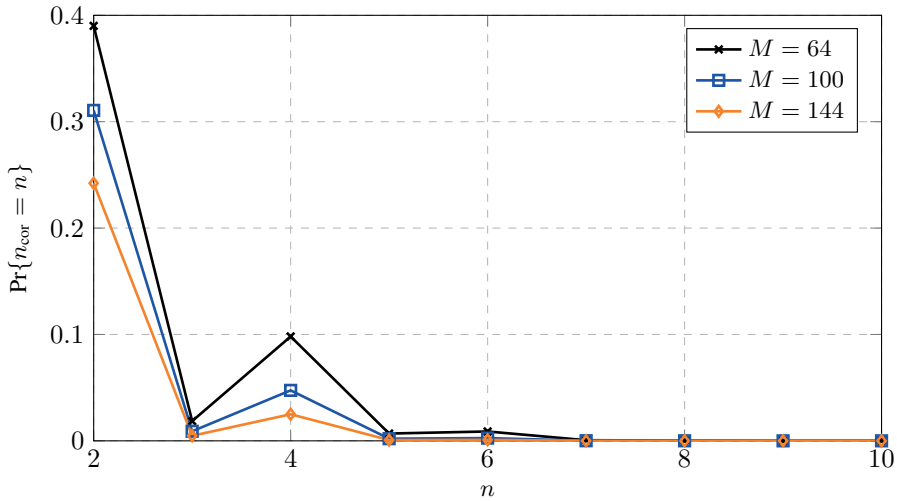

Figure 6.6: $\Pr\{n_{\text{cor}} = n\}$ for $n = 2, 3, ..., 10$ for $K = 10$ for different number of M.

probabilities $\Pr\{n_{\text{cor}} = n\}$ is much higher for $M = 64$ than that of $M = 100$ and $M = 144$. This is because by decreasing the number of antennas at the BS, the ability to distinguish the users is worsened. Second, the probability that there is only one pair ($n = 2$) or only two pairs ($n = 4$) of correlated users is much higher than the other events for all M. Moreover, when n exceeds 6, the probabilities $\Pr\{n_{\text{cor}} = n\}$ are negligible. These results show that it is more likely to have a few correlated users. In the following Theorem, we show that $\Pr\{n_{\text{cor}} = 2\}$ and ζ are asymptotically equivalent as M tends to infinity.

Theorem 6.1. Consider a BS with M antennas that serves K users. As M tends to infinity, $\Pr\{n_{\text{cor}} = 2\}$ and ζ become asymptotically equivalent

$$\Pr\{n_{\text{cor}} = 2\} \sim \zeta, \tag{6.26}$$

which means $\lim_{M\to\infty} \frac{\Pr\{n_{\text{cor}}=2\}}{\zeta} = 1$.

Proof. See Appendix 6.8. □

Theorem 6.1 shows that the probability that there is only one pair of correlated users $\Pr\{n_{\text{cor}} = 2\}$ is dominant when M tends to infinity. For typical massive MIMO systems in the literature, e.g., $M = 100$ and $K = 10$, ζ is 0.37, while $\Pr\{n_{\text{cor}} = 2\}$ is 0.31 ($\frac{\Pr\{n_{\text{cor}}=2\}}{\zeta} = 0.83$). The results in Fig. 6.6 imply that when computing the average number of correlated users as

$$\mathbb{E}[n_{\text{cor}}] = \sum_{n=0}^{K} n\Pr\{n_{\text{cor}} = n\}, \tag{6.27}$$

Table 6.1: Comparison of $\mathbb{E}[n_{\text{cor}}]$ for scenarios of Fig. 6.5 with $K = 10$ to $\mathbb{E}[n_{\text{cor}}]$ found by (6.27)

Scenario	ULA (100)	UPA (10×10)	(6.27)
$M = 64$	2.00	1.60	1.32
$M = 100$	1.41	1.11	0.86
$M = 144$	1.06	0.81	0.61

the term corresponds to $\Pr\{n_{\text{cor}} = 2\}$ and $\Pr\{n_{\text{cor}} = 4\}$ have the most contribution to $\mathbb{E}[n_{\text{cor}}]$ for typical massive MIMO systems.

In Table 6.1, we compare $\mathbb{E}[n_{\text{cor}}]$ for the simulation scenarios of Fig. 6.5 in two different ways. First, we use Monte Carlo simulations to find $\mathbb{E}[n_{\text{cor}}]$ for ULA and UPA. Second, we use $\Pr\{n_{\text{cor}} = n\}$ to find $\mathbb{E}[n_{\text{cor}}]$ as in (6.27). The estimated $\mathbb{E}[n_{\text{cor}}]$ using the probabilistic model is smaller than that of ULA and UPA found by simulations. In other words, similar to the results in Fig. 6.5, using (6.27) underestimates the correlated scenarios. The results in Table 6.1 show that for ULA and UPA, there are a few users with correlated channel vectors. In these scenarios, using nonlinear precoding only for a limited number of users, e.g., 2, could be good enough to achieve the performance of using nonlinear precoding for all the K users. This is the idea of the proposed hybrid precoder, which is presented in the sequel.

6.4 Proposed Hybrid Linear and Non-Linear Precoder (HLNP)

In this section, HLNP and its details are presented. Then, a complexity analysis is given to show the complexity reduction of HLNP.

6.4.1 Details of HLNP

The idea of HLNP is to use nonlinear processing for a few users to limit the complexity overhead of nonlinear precoding. The users are divided into two groups. For the first group of the users, a modified THP precoding, and for the second group of users, ZF are used to find the transmit vectors of each group. Then, the transmit vectors of the two groups are combined to simultaneously serve all the users. For simplicity, we call the users for which THP and ZF are employed by THP users and ZF users, respectively. The proposed hybrid precoder is presented in Algorithm 1. We explain the proposed hybrid precoder assuming that the users are already divided into two groups using Algorithm 2.

The proposed hybrid precoder outputs the precoded vector $\boldsymbol{x}$ using the channel matrix $\boldsymbol{H}$ and the number of users in the THP group, i.e., n_{THP}. The set of THP users $\mathcal{A}_{\text{THP}}$ ($|\mathcal{A}_{\text{THP}}| = n_{\text{THP}}$), feedforward filter for the THP users $\boldsymbol{W}$, precoding matrix for the ZF users $\boldsymbol{U}_{\text{ZF}}$, and power control matrix for the ZF users $\boldsymbol{D}_{\text{ZF}}$ are found by calling the

Algorithm 1 Proposed Hybrid Precoder

Input: $\boldsymbol{H}$, n_{THP}
Output: $\boldsymbol{x}$
1: $(\mathcal{A}_{\text{THP}}, \boldsymbol{W}, \boldsymbol{U}_{\text{ZF}}, \boldsymbol{D}_{\text{ZF}})$ = M-VBLAST($\boldsymbol{H}$, n_{THP})
2: reorder $\boldsymbol{H}$ and $\boldsymbol{s}$ so that rows 1 to $n_{\text{THP}} = |\mathcal{A}_{\text{THP}}|$ corresponds to the THP users
3: find $\boldsymbol{H}_{\text{ZF}}$, $\boldsymbol{H}_{\text{THP}}$, $\boldsymbol{s}_{\text{ZF}}$ and $\boldsymbol{s}_{\text{THP}}$ by removing corresponding rows from $\boldsymbol{H}$ and $\boldsymbol{s}$
4: $\boldsymbol{x}_{\text{ZF}} = \boldsymbol{U}_{\text{ZF}}\boldsymbol{D}_{\text{ZF}}\boldsymbol{s}_{\text{ZF}}$
5: find $\tilde{\boldsymbol{s}}_{\text{THP}}$ by (6.29)
6: $\boldsymbol{x}_{\text{THP}} = \boldsymbol{W}\tilde{\boldsymbol{s}}_{\text{THP}}$
7: $\boldsymbol{x} = \boldsymbol{x}_{\text{ZF}} + \boldsymbol{x}_{\text{THP}}$

proposed grouping method (line 1). Then, the rows of the channel matrix $\boldsymbol{H}$ and symbols $\boldsymbol{s}$ are reordered such that the users in the set $\mathcal{A}_{\text{THP}}$ are associated with rows 1 to n_{THP} of the updated $\boldsymbol{H}$ and $\boldsymbol{s}$. To find the symbols $\boldsymbol{s}_{\text{ZF}}$ for the ZF users, the rows 1 to n_{THP} from the updated symbols $\boldsymbol{s}$ are removed. Using (6.1), $\boldsymbol{x}_{\text{ZF}}$ is found (line 4) for the ZF users, if the allocated power for the ZF users is $P_{\text{ZF}} = \text{tr}(\boldsymbol{D}_{\text{ZF}}^2)$. Using (6.6) and $\boldsymbol{u}_i^{\text{ZF}} = \boldsymbol{g}_i^{\text{ZF}}/\|\boldsymbol{g}_i^{\text{ZF}}\|$, the following $\text{SNR}^{\text{H-ZF}}$ for each of the ZF users is achieved:

$$\text{SNR}^{\text{H-ZF}} = \frac{P_{\text{ZF}}}{N_0 \sum_{i=n_{\text{THP}}+1}^{K} \|\boldsymbol{g}_i^{\text{ZF}}\|^2}, \tag{6.28}$$

where it is assumed that the THP users do not cause any interference to the ZF users. The ZF users may cause interference to the THP users because the ZF filters are found without taking the channel vectors of the THP users into account.

For the THP users, a modified THP is proposed as follows. The reordered channel matrix $\boldsymbol{H}$ is used to find the THP filters $\boldsymbol{w}_i^{\text{THP}}$ to guarantee that the THP users do not cause any interference to the ZF users (line $10-14$ of Algorithm 2). To encode symbols for the THP users $\boldsymbol{s}_{\text{THP}} \in \mathbb{C}^{n_{\text{THP}}\times 1}$, we consider not only the interference based on THP structure, but also the interference coming from the ZF users:

$$\tilde{s}_i = \left[s_i - \sum_{j=1}^{i-1} b_{ij}\tilde{s}_j - \sum_{j=n_{\text{THP}}+1}^{K} \frac{\boldsymbol{h}_i^T \boldsymbol{u}_j \sqrt{d_j}}{l_{ii}\sqrt{d_i}} s_j \right]_{\Delta}, \quad i = 1, ..., n_{\text{THP}}, \tag{6.29}$$

where the first sum in (6.29) is the interference as in the THP structure, and the second sum is the interference coming from the ZF users. To find the interference components (b_{ij} and $\frac{\boldsymbol{h}_i^T \boldsymbol{u}_j \sqrt{d_j}}{l_{ii}\sqrt{d_i}}$) in (6.29), $\boldsymbol{HW}$ is used (see [41, Sec. 5.4.5]). Then, the precoded vector $\boldsymbol{x}_{\text{THP}}$ is found (line 6 of Algorithm 1) using the corresponding feedforward filter. The following $\text{SNR}^{\text{H-THP}}$ is achieved for each of the THP users:

$$\text{SNR}^{\text{H-THP}} = \frac{P_{\text{THP}}}{N_0 \sum_{i=1}^{n_{\text{THP}}} \|\boldsymbol{w}_i^{\text{THP}}\|^2}. \tag{6.30}$$

To assure the max-min criterion among all the users, we equalize the SNR for the ZF users (see (6.28)) and the THP users (see (6.30)). This leads to the following power allocation P_{THP} for the THP users:

$$P_{\text{THP}} = \frac{\sum_{i=1}^{n_{\text{THP}}} \|\boldsymbol{w}_i^{\text{THP}}\|^2}{\sum_{i=1}^{n_{\text{THP}}} \|\boldsymbol{w}_i^{\text{THP}}\|^2 + \sum_{i=n_{\text{THP}}+1}^{K} \|\boldsymbol{g}_i^{\text{ZF}}\|^2} P. \tag{6.31}$$

Employing (6.31) to find the precoded vector for the THP users $\boldsymbol{x}_{\text{THP}}$ and for the ZF users $\boldsymbol{x}_{\text{ZF}}$, the transmitted vector from the BS is found by:

$$\boldsymbol{x} = \boldsymbol{x}_{\text{ZF}} + \boldsymbol{x}_{\text{THP}}. \tag{6.32}$$

Then, the following SNR^{HLNP} is obtained for all the users:

$$\text{SNR}^{\text{HLNP}} = \frac{P}{N_0 \left(\sum_{i=1}^{n_{\text{THP}}} \|\boldsymbol{w}_i^{\text{THP}}\|^2 + \sum_{i=n_{\text{THP}}+1}^{K} \|\boldsymbol{g}_i^{\text{ZF}}\|^2 \right)}. \tag{6.33}$$

In the case of mutual orthogonality of the users, the following SNR is achieved:

$$\text{SNR} = \frac{P}{N_0 \sum_{i=1}^{K} \frac{1}{\|\boldsymbol{h}_i\|^2}}. \tag{6.34}$$

6

By choosing different users in the two groups, SNR in (6.33) will change. For a given n_{THP}, the optimal grouping of users is the one that maximizes SNR in (6.33), which can be found by an exhaustive search. Suppose instead of an exhaustive search, the VBLAST algorithm is used to find the THP and ZF users to optimize (6.33). At each iteration of VBLAST, the user with the lowest $\|\boldsymbol{w}_i\|$ is assigned to the THP group. Thus, after n_{THP} iterations, n_{THP} users with the lowest $\|\boldsymbol{w}_i\|$ are assigned to the THP group, and the rest of the users, which includes the users with the highest $\|\boldsymbol{w}_i\|$, are assigned to the ZF group. In this case, due to the max-min criterion, more power is allocated for the ZF users. Therefore, the THP users are sacrificed for the sake of the ZF users with the highest $\|\boldsymbol{w}_i\|$. One can assign the users with the highest $\|\boldsymbol{w}_i\|$ to the THP group and increase the SNR. Therefore, not all the users with the highest $\|\boldsymbol{w}_i\|$ shall be assigned to the ZF group. In fact, the VBLAST algorithm has to be modified in order to perform well for the proposed hybrid precoder.

We explain the proposed grouping method in Algorithm 2 as follows. In contrast to VBLAST, the pseudo-inverse of the channel matrix of the users $\boldsymbol{H}$ is computed once before the loop (line 10-14) starts. The norms of the filters $\|\boldsymbol{w}_{k_1}\| > \|\boldsymbol{w}_{k_2}\| > \ldots > \|\boldsymbol{w}_{k_K}\|$ are ordered from the highest norm to the lowest. We divide the users into THP and ZF groups by employing a predefined set for the THP users $\mathcal{A}_{\text{proposed}} = \{n_{\text{THP}} + 1, n_{\text{THP}}, \ldots, 3, 2\}$. Similar to VBLAST, the users with a high $\|\boldsymbol{w}_i\|$ shall not be chosen until the last iterations. Thus, at the first iteration, the column $\boldsymbol{w}_{k_{n_{\text{THP}}+1}}$ of the pseudo-inverse of the channel is chosen, and its corresponding row from the channel matrix is made zero to find the updated channel matrix for the next iteration (line 13

Algorithm 2 Proposed Grouping Algorithm: M-VBLAST

Input: $\boldsymbol{H}$, n_{THP}
Output: $\mathcal{A}_{\text{THP}}$, $\boldsymbol{W}$, $\boldsymbol{U}_{\text{ZF}}$, $\boldsymbol{D}_{\text{ZF}}$
1: $\mathcal{A}_{\text{THP}} = \varnothing$
2: $\boldsymbol{W} = \boldsymbol{0} \in \mathbb{C}^{M \times n_{\text{THP}}}$
3: $\boldsymbol{U}_{\text{ZF}} = \boldsymbol{0} \in \mathbb{C}^{M \times (K - n_{\text{THP}})}$
4: $\boldsymbol{D}_{\text{ZF}} = \boldsymbol{0} \in \mathbb{R}^{(K - n_{\text{THP}}) \times (K - n_{\text{THP}})}$
5: $\boldsymbol{H}^{(1)} = \boldsymbol{H}$
6: $\mathcal{A}_{\text{proposed}} = \{n_{\text{THP}} + 1, n_{\text{THP}}, ..., 3, 2\}$
7: $(\boldsymbol{w}_1, ..., \boldsymbol{w}_K) = (\boldsymbol{H}^{(1)})^{\dagger}$
8: sort $\|\boldsymbol{w}_k\|^2$: $\|\boldsymbol{w}_{k_1}\|^2 \geq \|\boldsymbol{w}_{k_2}\|^2 \geq ... \geq \|\boldsymbol{w}_{k_K}\|^2$
9: $\mathcal{A}_{\text{THP}} \leftarrow \mathcal{A}_{\text{THP}} \cup \{k_{n_{\text{THP}}+1}, k_{n_{\text{THP}}}, ..., k_3, k_2\}$
10: **for** $j = 1, 2, ..., n_{\text{THP}}$ **do**
11: $\quad c = \mathcal{A}_{\text{THP}}(j)$
12: $\quad$ find $\boldsymbol{w}_j$ by finding column c from the pseudo-inverse of $\boldsymbol{H}^{(j)}$
13: $\quad$ make row c from $\boldsymbol{H}^{(j)}$ to zero to find $\boldsymbol{H}^{(j+1)}$
14: **end for**
15: given $(\boldsymbol{H}^{(n_{\text{THP}}+1)})^{\dagger}$ and by using $\boldsymbol{W}$ find P_{THP} by (6.31)
16: given $(\boldsymbol{H}^{(n_{\text{THP}}+1)})^{\dagger}$ and $P - P_{\text{THP}}$, find $\boldsymbol{U}_{\text{ZF}}$ and $\boldsymbol{D}_{\text{ZF}}$ as explained in Sec. 6.2.1

of Algorithm 2). Then, at the next iteration, only $\boldsymbol{w}_{k_c}$, which is one column from the pseudo-inverse of the updated channel matrix, is computed. This procedure continues to find all the filters for the THP users. Afterwards, the channel matrix for the ZF users is found $\boldsymbol{H}^{(n_{\text{THP}}+1)}$, which is used to find the allocated power for the THP users (line 15), and ZF precoding and power control matrices (line 16). Using the proposed grouping method, the two users with the highest $\|\boldsymbol{w}_i\|$ are separated into THP and ZF group. For massive MIMO systems, where the average number of users with the correlated channel vectors is limited, the proposed grouping method can work quite well. Simulation results are given in the Sec. 6.5 to show the effectiveness of the proposed HLNP.

6.4.2 Complexity Analysis

The complexity order of finding the filters for ZF, THP, and the proposed hybrid precoder is presented in Table 6.2. The complexity of ZF is $\mathcal{O}(MK^2)$ [82], while the complexity of THP is $\mathcal{O}(MK^3)$ [41, Sec. 4.3.1]. The higher complexity of THP is due to finding the iterative filters and finding an appropriate order of the users for encoding the symbols [41]. The computational complexity of HLNP includes two terms. The first term is the complexity of finding the ZF filters for the ZF users, which is $\mathcal{O}(M(K - |\mathcal{A}_{\text{THP}}|)^2)$. The second term is the complexity of finding the filters and an appropriate order of encoding for the THP users. In contrast to VBLAST, in our grouping method, the order of users is found before starting the iterations by computing the pseudo-inverse of the

Table 6.2: The computational complexity order of the precoders

Precoder	Complexity Order
ZF	$\mathcal{O}(MK^2)$
THP	$\mathcal{O}(MK^3)$
HLNP	$\mathcal{O}(MK^2)$

channel matrix $\boldsymbol{H}$. Then, at each iteration, the filter is found for one user from the updated channel matrix. After n_{THP} iterations, the filters are found for $|\mathcal{A}_{\text{THP}}|$ number of users with the complexity of $\mathcal{O}(MK|\mathcal{A}_{\text{THP}}|)$. Therefore, the dominant complexity is still $\mathcal{O}(MK^2)$, which is the complexity of finding the pseudo-inverse of the channel $\boldsymbol{H}$. Consequently, using HLNP, the complexity of THP is reduced from $\mathcal{O}(MK^3)$ to $\mathcal{O}(MK^2)$.

6.5 Simulations

In this section, simulation results are given in three parts. First, we present the cumulative distribution function (CDF) of the theoretical received SNR for ZF, THP and HLNP. Second, we compare the BLER performance of the precoders using NR-LDPC codes [83]. Third, we present the effects of imperfect CSI on the bit error rate (BER) of the precoders. In the simulations, a BS equipped with a UPA of 8×8 antennas is assumed that serves 10 single-antenna users. The users are distributed uniformly over the entire cell (10-200 m away from the BS with no shadowing) in the field-of-view of $\phi \in (0, 2\pi)$ and $\theta \in (0, \pi/2)$. The carrier frequency is 30 GHz. The minimum acceptable spacing distance between the users is set to 0.01m in the simulations.

6.5.1 SNR

The CDF plots of the received SNR for ZF and THP are compared with HLNP in Fig. 6.7 by generating 100000 realizations of the channel. The transmit power at the BS is fixed for all the precoders such that in favorable propagation, a SNR of 22 dB is achieved for the users located at the cell-edge. The ZF (red line) has the worst CDF curve as expected. By using THP (blue line) instead of ZF, the CDF of SNR is improved considerably, e.g., the 5th percentile SNR is improved by 5.78 dB. The results of HLNP with a different number of users in the THP group $n_{\text{THP}} = 1, 2, 3$, are shown in Fig. 6.7 by dashed lines. The results show that HLNP improves the 5th percentile SNR by 3.50 dB, 4.49 dB, and 4.94 dB for $n_{\text{THP}} = 1$ (HLNP-1), $n_{\text{THP}} = 2$ (HLNP-2), and $n_{\text{THP}} = 3$ (HLNP-3), respectively. If the optimal grouping using an exhaustive search is used with HLNP for $n_{\text{THP}} = 3$ (Opt-3), the dashed black line in Fig. 6.7 is achieved, which has only 0.21 dB loss compared to THP for the 5th percentile SNR. Although using exhaustive search boosts the 5th percentile SNR of HLNP-3 by 0.54 dB, it entails a huge complexity.

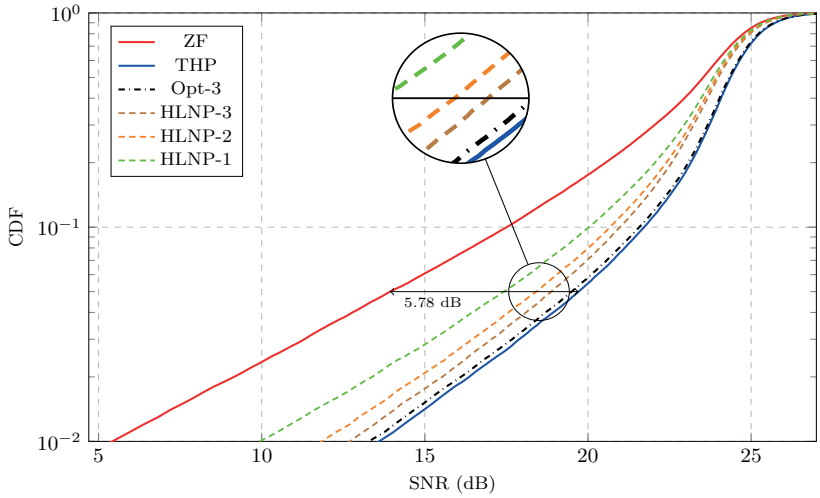

Figure 6.7: The CDF of SNR for ZF, THP, and HLNP with $n_{\text{THP}} = 1, 2, 3$. If optimal grouping is used for HLNP with $n_{\text{THP}} = 3$ (Opt-3), the black line is achieved. The horizontal arrow shows the improvement of 5th percentile SNR for THP compared to ZF.

The results in Fig. 6.7 show that by employing THP for the limited number of users as in HLNP with the proposed grouping, one can achieve a performance close to employing THP for all the users with much less complexity. The improvement of the 5th percentile SNR can be seen from a different perspective. We can find the required transmit power to assure a given 5th percentile SNR for each precoder. For instance, to ensure a 5th percentile SNR of 15 dB, employing THP (or HLNP-3) requires 5.78 dB (or 4.94 dB) less transmit power compared to ZF.

Note for a given channel realization, by changing the transmit power at the BS, the SNR for ZF, THP and HLNP will change. For instance, if the transmit power at the BS increases by 5 dB, the SNR for ZF, THP and HLNP increases by 5 dB as well. This can be explained by looking at (6.6) for ZF, (6.17) for THP, and (6.33) for HLNP. By changing the transmit power, the denominator of the SNR formulas for ZF, THP and HLNP does not change because the denominator is only a function of the channel realization. Note that the ordering of the users for THP or HLNP only depends on the channel realization, and not the transmit power. Consequently, by changing the transmit power for a given channel realization, the SNR for THP and HLNP changes similar to that of ZF. Thus, the gain in the 5th percentile SNR for THP (HLNP-3) compared to ZF will be 5.78 dB (4.94 dB) for any other transmit power at the BS.

We further compare the CDF of SNR for HLNP using our proposed grouping method in Algorithm 2 with a modified correlation grouping method (CGM). The modified CGM is based on the idea of [74], which is to divide the users into groups such that the spatial

correlation of users in each group does not exceed a threshold. To this end, for a given n_{THP}, we modify Algorithm 18 in [33], which was used for the user dropping problem. The CGM is presented in Algorithm 3. Algorithm 3 finds the set of users $\mathcal{A}_{\text{THP}}$ that are assigned to the THP group. User i and user j are found, which have the highest $|\rho|$ among the users (line 4-5). Among user i and user j, the one which has the maximum spatial correlation with the remaining users is assigned to the THP group (line 6-12). This procedure is repeated for the remaining users until n_{THP} users are assigned to the THP group. The rest of the users are assigned to the ZF group.

Algorithm 3 CGM: modification of Algorithm 18 in [33] for user grouping

Input: $\boldsymbol{H}, K, n_{\text{THP}}$
Output: $\mathcal{A}_{\text{THP}}$
1: $\mathcal{A}_{\text{THP}} = \varnothing$
2: $\mathcal{A} = \{1, 2, ..., K\}$
3: **for** $t = 1, 2, ..., n_{\text{THP}}$ **do**
4: using $\boldsymbol{H}$, compute $\rho_{ij}, \forall i, j \neq i \in \mathcal{A}$ (see (6.7))
5: find $i, j \neq i \in \mathcal{A}$ for which $|\rho_{ij}| = \max_{m,n \neq m \in \mathcal{A}} |\rho_{mn}|$
6: **if** $\max_{k \neq i,j} |\rho_{ik}| > \max_{k \neq i,j} |\rho_{jk}|$ **then**
7: $c^\star = i$
8: **else**
9: $c^\star = j$
10: **end if**
11: $\mathcal{A}_{\text{THP}} \leftarrow \mathcal{A}_{\text{THP}} \cup \{c^\star\}$
12: $\mathcal{A} \leftarrow \mathcal{A} \setminus c^\star$
13: **end for**

Recall that Fig. 6.6 shows that is more probable that there are only one or two pairs of correlated users. When there are only one or two pairs of correlated users, using Algorithm 3 assures the correlated users are separated into THP and ZF groups. Consequently, the spatial correlation among the users in ZF (or THP) groups is as small as possible. The CDF of SNR of HLNP using our proposed grouping method is compared with the CGM in Fig. 6.8 for $n_{\text{THP}} = 1, 2, 3$. Employing our proposed grouping method improves the 5th percentile SNR of CGM by 1.21 dB, 1.10 dB and 0.91 dB for $n_{\text{THP}} = 1, 2, 3$, respectively. Although our proposed grouping method is more complicated than the CGM presented in Algorithm 3, the proposed grouping method leads to a higher 5th percentile SNR.

6.5.2 BLER

The results of Fig. 6.7 do not include the modulo loss and power loss of THP-based precoders (THP and HLNP). To study the modulo and power losses of THP-based precoders in this section, we compare the BLER performance of ZF, THP and HLNP-3

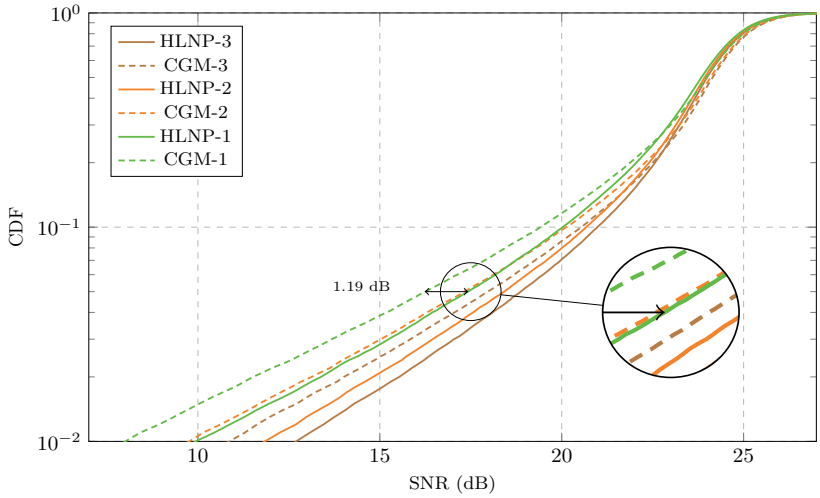

Figure 6.8: The CDF of SNR for CGM compared to HLNP for $n_{\text{THP}} = 1, 2, 3$. The horizontal arrow shows the improvement of 5th percentile SNR for HLNP-1 over CGM-1 THP.

for the same received SNR. We expect the modulo loss and power loss of THP-based precoders to worsen the BLER performance of THP and HLNP compared to ZF. It is reported in [84] that the modulo error of THP for the coded case can lead to performance degradation if a conventional demapper is used. To improve the BLER performance of the conventional demapper, we use the demapper proposed in [85] (see [84, Fig. 6] for more details).

The BLER results over the same received SNR for 16QAM and 64QAM using ZF, THP, and HLNP-3 are shown in Fig. 6.9 and Fig. 6.10, respectively. For 16QAM we use $\Delta = 8/\sqrt{10}$, and for 64QAM we use $\Delta = 16/\sqrt{42}$ based on (9) of [55]. NR-LDPC codes with coding rates of $2/3, 8/10, 9/10$ and 6000 information bits are used in the simulations. The horizontal arrows in Fig. 6.9 and Fig. 6.10 show the loss of THP compared to ZF for a BLER of 10^{-2}. The following conclusions can be drawn from the results in Fig. 6.9 and Fig. 6.10. First, THP-based precoders entail a loss compared to ZF (modulo loss and power loss), which can be seen as the gap between ZF and THP-based precoders. Moreover, the loss of HLNP-3 compared to ZF is slightly lower than that of THP, i.e., 0.1 dB lower for BLER of 10^{-2}. Second, as the constellation size (or the coding rate) increases, the loss of THP-based precoders decreases. For 16QAM, at BLER of 10^{-2} for the coding rate of $2/3$, THP and HLNP-3 have a loss of 1.34 dB and 1.26 dB, respectively. For 64QAM, this loss reduces to 0.78 dB and 0.69 dB, respectively. By increasing the coding rate to $9/10$, the loss of THP and HLNP for 16QAM becomes 0.66 dB and 0.56 dB, whereas, for 64QAM, the loss becomes 0.34 dB and 0.25 dB,

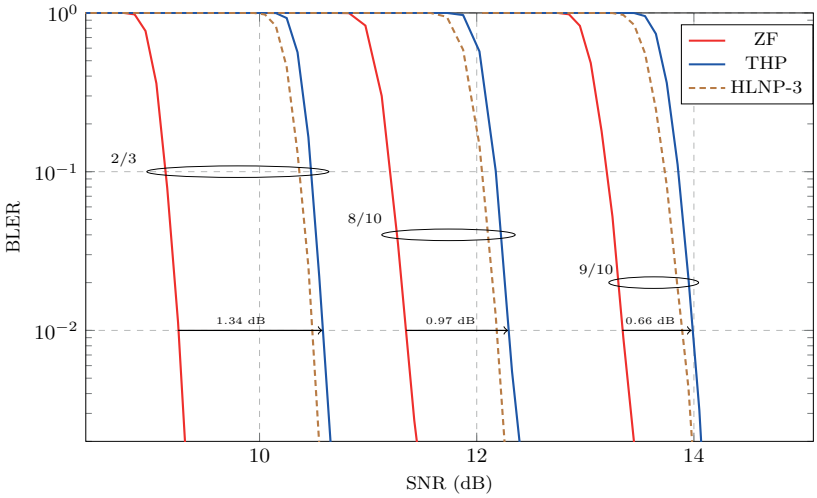

Figure 6.9: Average BLER over received SNR for ZF, THP and HLNP-3 for 16-QAM with coding rates of $2/3$, $8/10$ and $9/10$. The arrows show the loss of THP compared to ZF for BLER of 10^{-2}.

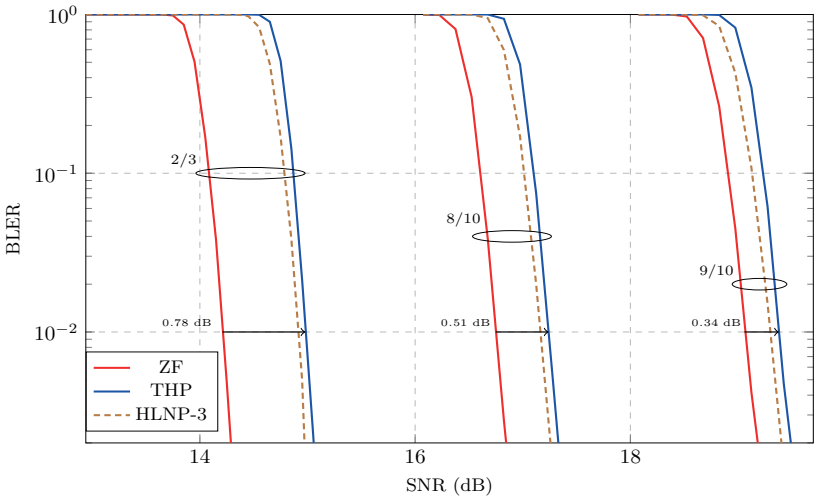

Figure 6.10: Average BLER over received SNR for ZF, THP and HLNP-3 for 64-QAM with coding rates of $2/3$, $8/10$ and $9/10$. The arrows show the loss of THP compared to ZF for BLER of 10^{-2}.

Table 6.3: Transmit power reduction of THP and HLNP compared to ZF to assure average BLER of 10^{-2} with 95%.

Constellation	Coding rate	THP	HLNP-3
16QAM	$2/3$	4.43 dB	3.69 dB
16QAM	$9/10$	5.13 dB	4.37 dB
64QAM	$2/3$	5 dB	4.25 dB
64QAM	$9/10$	5.44 dB	4.70 dB

respectively. Note that by increasing the coding rate or the constellation size, the required SNR to achieve a given BLER is increased. As the SNR increases, the chances of modulo errors reduce [85]. Thus, the loss of THP-based precoders reduces as the constellation size and the coding rate increase.

To take into account the gain of THP-based precoders (see Fig. 6.7) as well as the loss of THP-based precoders (see Fig. 6.9 and Fig. 6.10) compared to ZF, we need a fair comparison. We find the transmit power reduction of THP and HLNP compared to ZF to guarantee an average BLER of 10^{-2} with 95% probability. To this end, we use the results of Fig. 6.9 and Fig. 6.10 to find the SNR denoted by $\gamma^\star$ that gives an average BLER of 10^{-2}. For instance, for ZF using 64QAM and coding rate of 0.9, $\gamma^\star = 19.05$ dB. We can then adjust the transmit power at the BS such that $\gamma^\star$ becomes the 5th percentile SNR (see Fig. 6.7). Therefore, with 95% probability, the received SNR is higher than $\gamma^\star$, and therefore, the average BLER of 10^{-2} is guaranteed by 95%. The transmit power reduction of THP and HLNP compared to ZF for different constellation sizes and coding rates are presented in Table 6.3. The results show that we can benefit in terms of transmit power reduction by employing THP-based precoders compared to ZF using NR-LDPC codes. The transmit power reduction is higher for the higher constellation sizes and larger coding rates. The gap between HLNP-3 and THP in Table 6.3 is around 0.74 dB, which is the loss of HLNP-3 in the 5th percentile SNR compared to THP as in Fig. 6.7, i.e., 0.84 dB $(= 5.78 - 4.94)$ minus the gain of HLNP-3 compared to THP for a BLER of 10^{-2} as in Fig. 6.9 or Fig. 6.10, i.e., around 0.1 dB.

6.5.3 Imperfect Channel State Information

In this section, we study the effects of imperfect channel state information similar to [59, Sec. V.B]. We consider the case that the BS has access to noisy channel matrix $\hat{\boldsymbol{H}}$

$$\hat{\boldsymbol{H}} = \sqrt{1-\epsilon}\boldsymbol{H} + \sqrt{\epsilon}\boldsymbol{Z}, \tag{6.35}$$

where $\epsilon \in [0,1]$ and $\boldsymbol{Z} \in \mathbb{C}^{K\times M}$ has $\mathcal{CN}(0,1)$ [59]. ϵ represents the channel estimation error, $\epsilon = 1$ represents no CSI, $\epsilon = 0$ represents perfect CSI, and any $\epsilon \in (0,1)$ represents partial CSI, e.g., $\epsilon = 0.25$ leads to $\hat{\boldsymbol{H}} = (1/2)\boldsymbol{H} + (1/2)\boldsymbol{Z}$. Note that each user has access to noisy side information $\hat{\alpha}$ computed based on $\hat{\boldsymbol{H}}$.

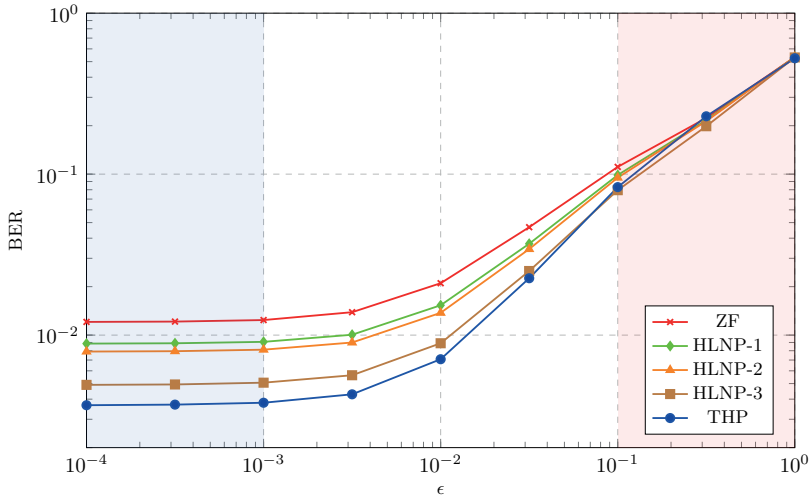

Figure 6.11: The average uncoded BER over ϵ for 64QAM for ZF, HLNP-1, HLNP-2, HLNP-3, and THP. The blue shaded area shows when increasing ϵ does not change the BER considerably, and the shaded red area shows when the BER of all the precoders exceeds 0.05.

6

In Fig. 6.11, the average uncoded BER of ZF, HLNP-1, HLNP-2, HLNP-3, and THP is presented over the channel estimate error ϵ. The simulation is run for 100K channel realizations using 64QAM constellation, and the average BER is computed for each precoder excluding the 5% worst BERs. The transmit power at the BS is fixed for all the precoders such that in FP, a SNR of 20 dB is achieved for each user.

The following conclusions can be drawn from the results in Fig. 6.11. First, by increasing ϵ from 0 to 10^{-3}, the BER of precoders slightly increases (shaded blue area). By increasing ϵ to higher than 10^{-3}, the BER of all the precoders increases rapidly until they all converge at $\epsilon = 1$. In the shaded red area, the BER of all the precoders exceeds 0.05. Second, by employing the proposed precoder (HLNP-1, HLNP-2, HLNP-3), the BER of ZF is improved considerably for small and moderate values of ϵ. For $\epsilon \leq 10^{-3}$, HLNP-3 leads to a higher BER compared to that of THP. However, by increasing ϵ, the BER of HLNP-3 becomes very close to that of THP. That is because for the moderate and high values of ϵ, the loss associated with the modulo operator becomes higher for THP compared to HLNP-3. In THP, the modulo operator is used for all the users, whereas, the modulo operator is used only for three users in HLNP-3. Although the BER of HLNP and THP overlaps with that of ZF for ϵ close to 1, employing HLNP and THP results in a lower BER compared to ZF for other values of ϵ not in the shaded red area.

6.6 Conclusion

In this paper, probability analysis is presented for LOS massive MIMO to study the probability that there is at least one pair of correlated users and to study the average number of correlated users. The presented probability analysis shows that it is more probable that there are only one or two pairs of correlated users in LOS massive MIMO systems. Furthermore, in this paper, a low-complexity hybrid linear and nonlinear precoder is proposed. Simulation results show that the proposed hybird linear and nonlinear precoder reduces the required transmit power at the BS to ensure a given average BLER for NR-LDPC codes using 16QAM and 64QAM compared to zero-forcing. Furthermore, it is shown that the proposed precoder can be used in the presence of channel state information error. By using the proposed precoder the complexity order of the conventional THP is reduced. Taking the performance and complexity reduction of the proposed precoder into account, the proposed precoder is a viable candidate for 5G NR. Future works include studying the effects of imperfect CSI and employing the proposed precoder with scheduling algorithms.

6.7 Acknowledgments

This project has received funding from the European Union's Horizon 2020 research and innovation programme under the Marie Sklodowska-Curie grant agreement No 721732.

6.8 Proof of Theorem 6.1

We first find equivalent expressions for $\lim_{M\to\infty} \Pr\{n_{\text{cor}} = 2\}$ and $\lim_{M\to\infty} \zeta$. In this proof, we use $\lim_{x\to 0} \frac{\log(1+x)}{x} = 1$. We write (6.23) as

$$\Pr\{n_{\text{cor}} = 2\} = \frac{\binom{M}{1}\binom{K}{2}\binom{M-1}{K-2}(K-2)!}{M^K} = \frac{K(K-1)}{2M}\prod_{i=1}^{K-2}(1-\frac{i}{M}). \tag{6.36}$$

Then, we write $\log(\Pr\{n_{\text{cor}} = 2\})$ as

$$\log(\Pr\{n_{\text{cor}} = 2\}) = \log\left(\frac{K(K-1)}{2M}\right) + \sum_{i=1}^{K-2}\log(1-\frac{i}{M}). \tag{6.37}$$

Then, we find an equivalent expression for $\lim_{M\to\infty} \log(\Pr\{n_{\text{cor}} = 2\})$ by

$$\begin{aligned}\lim_{M\to\infty} \log(\Pr\{n_{\text{cor}} = 2\}) &= \lim_{M\to\infty} \log\left(\frac{K(K-1)}{2M}\right) + \sum_{i=1}^{K-2} \log\left(1 - \frac{i}{M}\right) \\ &= \lim_{M\to\infty} \log\left(\frac{K(K-1)}{2M}\right) + \sum_{i=1}^{K-2} -\frac{i}{M} \\ &= \lim_{M\to\infty} \log\left(\frac{K(K-1)}{2M}\right) + \frac{-(K-2)(K-1)}{2M}.\end{aligned} \tag{6.38}$$

Thus

$$\lim_{M\to\infty} \Pr\{n_{\text{cor}} = 2\} = \lim_{M\to\infty} \left(\frac{K(K-1)}{2M}\right) e^{\frac{-(K-2)(K-1)}{2M}}. \tag{6.39}$$

We now find an equivalent expression for $\lim_{M\to\infty} \zeta$. We first find an equivalent expression for $\lim_{M\to\infty} \log(1-\zeta)$ by

$$\lim_{M\to\infty} \log(1-\zeta) = \lim_{M\to\infty} \sum_{i=1}^{K-1} \log(1 - \frac{i}{M}) = \lim_{M\to\infty} \sum_{i=1}^{K-1} -\frac{i}{M} = \lim_{M\to\infty} \frac{-K(K-1)}{2M}. \tag{6.40}$$

Thus:

$$\lim_{M\to\infty} \zeta = \lim_{M\to\infty} 1 - e^{\frac{-K(K-1)}{2M}}. \tag{6.41}$$

Using (6.39) and (6.41), we find $\lim_{M\to\infty} \Pr\{n_{\text{cor}} = 2\}/\zeta$

$$\lim_{M\to\infty} \frac{\Pr\{n_{\text{cor}} = 2\}}{\zeta} = \lim_{M\to\infty} \frac{\frac{K(K-1)}{2M} e^{-\frac{(K-2)(K-1)}{2M}}}{1 - e^{-\frac{(K-1)K}{2M}}} = \lim_{M\to\infty} \frac{K(K-1)\frac{-1}{M^2}}{\frac{-1}{M^2} K(K-1)} = 1, \tag{6.42}$$

where we use L'Hôpital's rule to find the right hand side of (6.42). Thus, $\Pr\{n_{\text{cor}} = 2\}$ and ζ are asymptotically equivalent. This concludes the proof. □

CHAPTER 7

Paper C
Uniform Linear Arrays with Optimized Inter-Element Spacing for LOS Massive MIMO

In this paper, isotropic antenna elements are considered with no mutual coupling. Studying a different radiating element and the mutual coupling effects are considered for future works.

7

Abstract

In this letter, a uniform linear array (ULA) is proposed for line-of-sight massive multiple-input-multiple-output (MIMO). It is assumed that the number of antennas is fixed. For a given ULA with an arbitrary inter-element spacing, the probability that the correlation among the channel vectors of two users being above a threshold value is derived. The inter-element spacing of the proposed ULA is the one for which the aforementioned probability is minimized. To show the effectiveness of the proposed ULA, simulation results for two scenarios are given for a 64-antenna ULA that serves 6 single-antenna users. By using the proposed ULA instead of conventional half-wavelength ULA, 5th percentile sum-rate for zero-forcing precoder is improved by 9.90 bits/channel use in first scenario without dropping, and by 1.43 bits/channel use in second scenario with dropping 1 user.

7.1 Introduction

Massive multiple-input-multiple-output (MIMO) is foreseen as a key enabling technology for fifth-generation wireless networks and beyond [26,38]. It is shown in [33] that in line-of-sight (LOS) massive MIMO, there is a nonnegligible probability that the channel vectors of some users become highly correlated, which results in a non-favorable propagation environment. The high correlation leads to a reduction in the sum-rates of linear and nonlinear precoders [70, Fig. 5]. The reduction of the sum-rate due to the high correlation is considerable for LOS environments with max-min power control as reported in [3,4] (max-min power control is used to provide uniformly good service for the users as reported in [33]). In addition, it is shown in [3, Fig. 2] that when there is only one pair of highly correlated users, the signal to noise ratio with max-min power control will drop significantly. To deal with highly correlated scenarios in LOS environments with max-min power control, [3,4,33] studied dropping algorithms. However, dropping users may not be desirable in the case of latency-sensitive communication.

To avoid dropping and alleviate a high inter-user correlation, one can increase the aperture size to improve the angular resolution of the base station (BS) antenna array. By increasing the aperture size, the minimum resolvability angular resolution of the array, which is defined by the well-known Rayleigh's criterion [86], is improved. Hence, by employing an inter-element spacing (δ) larger than the conventional $\lambda/2$ (λ is a wavelength) the angular resolution of an array with a fixed number of elements is enhanced [35, Sec. 7.2.4]. The major drawback of increasing δ in the uniform linear arrays (ULAs) is the appearance of grating lobes (beamforming ambiguities) [87,88]. The grating lobes may cause a high correlation among the channel vectors of users with a large angular separation (not co-located users). To avoid grating lobes, in [89] a maximum allowable δ, depending on the field-of-view (FOV), is proposed, where the increase in the aperture size is minimal for wide FOVs. Increasing δ is reported beneficial in terms of spectral efficiency for a BS antenna array with a fixed number of antennas [90]. A small LOS spectral efficiency improvement is also reported in [88] by deploying ULAs with larger inter-element spacing. However, none of the above-mentioned studies approaches the problem analytically to compute the probability of correlated users in the absence or presence of grating lobes.

In this letter, a ULA for LOS environments is proposed assuming a fixed number of omnidirectional antennas at the BS. We derive the probability that the correlation among the channel vectors of two users being above a threshold for a ULA with an arbitrary inter-element spacing. The inter-element spacing of the proposed ULA is the one for which the aforementioned probability is minimized. The proposed ULA is optimized for the case when there are only two users. For more users, we present simulation results for two different scenarios, to show the effectiveness of the proposed array compared to conventional half-wavelength ULA with a known linear precoder, i.e., zero-forcing (ZF).

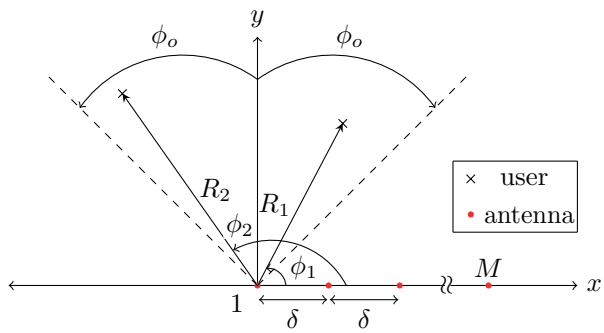

Figure 7.1: ULA with M elements on x-axis with inter-element spacing δ. The distance between the first element of the array and the users are R_1 and R_2.

7.2 System Model

We consider a BS equipped with a ULA of M antennas[1] located on the x-axis (see Fig. 7.1). Two users are assumed to be in the x-y plane, where R_1 and R_2 are the distance from the users to the first element of the array, and ϕ_1 and ϕ_2 are the azimuth angles of the users. It is assumed that ϕ_1 and ϕ_2 are independent random variables that are uniformly distributed in a FoV of $\phi_l \in (\pi/2 - \phi_o, \pi/2 + \phi_o)$, where $\phi_o \in (0, \pi/2)$. The channel between user l ($l \in \{1, 2\}$) and antenna m ($m \in \{1, 2, ..., M\}$) is modeled as [35, Sec. 7.2.2]:

$$h_{lm} = \sqrt{\beta_l} e^{-\jmath k R_l} e^{+\jmath k (m-1)\delta \cos(\phi_l)}, \tag{7.1}$$

where β_l is the large-scale fading for user l, $k = 2\pi/\lambda$ is the wavenumber, and δ is the inter-element spacing of ULA. Typically, δ is assumed to be $\lambda/2$. Using (7.1), the channel vector $\boldsymbol{h}_l = (h_{l1}, h_{l2}, ..., h_{lM})^T$ is found.

The spatial correlation between the channel vectors $\boldsymbol{h}_1$ and $\boldsymbol{h}_2$ is given by:

$$\rho = \frac{\boldsymbol{h}_2^H \boldsymbol{h}_1}{\|\boldsymbol{h}_1\| \|\boldsymbol{h}_2\|}. \tag{7.2}$$

We use the term spatial correlation for (7.2) (following the literature) throughout the paper, although, (7.2) is the inner-product of normalized $\boldsymbol{h}_1$ and $\boldsymbol{h}_2$ for a given coherence interval. By replacing the elements of the channel vectors $\boldsymbol{h}_1$ and $\boldsymbol{h}_2$ using (7.1), in (7.2), $|\rho|$ is found by:

$$|\rho| = \frac{1}{M} \left| \frac{\sin(M k \frac{\delta}{2} \psi)}{\sin(k \frac{\delta}{2} \psi)} \right|, \tag{7.3}$$

[1] Analysis of uniform planar array (3D beamforming) is left for future work.

where $\psi = \cos(\phi_1) - \cos(\phi_2)$. Using (7.3), $|\rho|$ is expressed as a function of ψ with the inter-element spacing of δ as follows:

$$|\rho| = f_\delta(\psi), \;\; \psi \in \left(2\cos(\frac{\pi}{2} + \phi_o), 2\cos(\frac{\pi}{2} - \phi_o)\right). \tag{7.4}$$

Note that $f_\delta(\psi)$ is a periodic function with period $T = \lambda/\delta$ [35, Sec. 7.2.4].

For a given realization of a channel of two users, assume that the angular separation of the users is $\psi = \Delta$. One can find the inter-element spacing δ_1 such that the users become orthogonal, i.e., $|\rho| = f_{\delta_1}(\Delta) = 0$. Suppose the users move and the angular separation of the users becomes $\Delta' \neq \Delta$. In this case, another inter-element spacing $\delta_2 \neq \delta_1$ has to be used to make the users orthogonal. However, changing the inter-element spacing for each realization of users is not practical. Therefore, a probabilistic approach is required to find the best inter-element spacing $\delta^\star$ for which a small $|\rho|$ is achieved with a high probability. In other words, the best inter-element spacing is the one that has the minimum probability that $|\rho|$ becomes larger than a given threshold ρ_o. We use the following definition for the rest of the paper.

Definition 7.1. The probability that a pair of users with the spatial correlation of ρ become correlated with a given ρ_o, is denoted by p, and defined as:

$$p \triangleq \Pr\{|\rho| > \rho_o\}. \tag{7.5}$$

Appropriate probability analysis is required to find the inter-element spacing for the case of two users for which p is minimized, which is given in the sequel.

7.3 Probability Analysis

In this section, we find p for ULAs with $\delta = \lambda/2$ and then for ULAs with $\delta > \lambda/2$ when there are only two users.

7.3.1 ULAs with $\delta = \lambda/2$

In Fig. 7.2, $|\rho| = f_{\lambda/2}(\psi)$ is shown for a ULA of $M = 10$ antennas. The shaded areas show when user 1 and user 2 become correlated with a given $\rho_o = 0.64$ ($\rho_o = 0.64$ is the 3-dB point [87, Sec. 6.3]) or equivalently a given ψ_o. If ψ_o is chosen as in Fig. 7.2, we can derive p as follows using the periodicity of $f_{\lambda/2}(\psi)$ ($T = 2$):

$$p = \Pr\{|\psi| < \psi_o\} + \Pr\{2 - \psi_o < |\psi| < 2\} = \alpha_0 + \alpha_1, \tag{7.6}$$

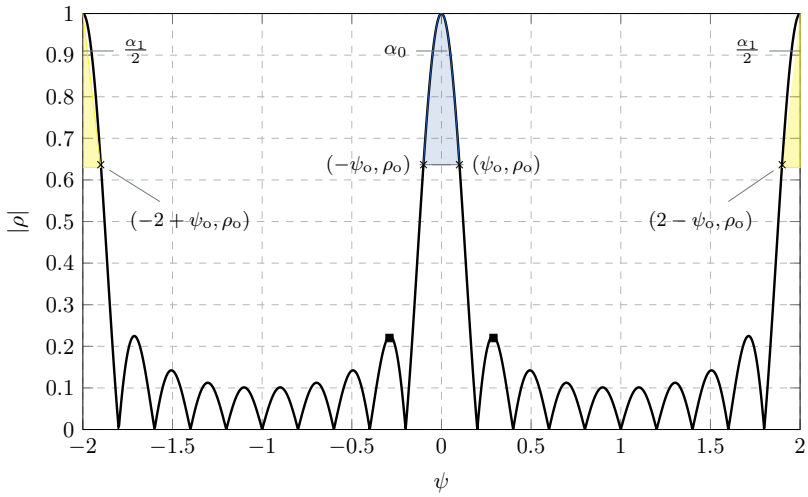

Figure 7.2: The function $|\rho| = f_{\lambda/2}(\psi)$ for a ULA with $M = 10$ and $\psi_o = 0.1$ ($\rho_o = 0.64$) for a FoV of $(0, \pi)$.

where the corresponding area for α_0 and α_1 are shown in Fig. 7.2 by the blue and yellow shaded area, respectively. We find α_0 as follows:

$$\begin{aligned}\alpha_0 &= \Pr\{|\psi| < \psi_o\} = 2\Pr\{0 \leq \psi < \psi_o\} \\ &= 2\Pr\{0 \leq \cos(\phi_1) - \cos(\phi_2) < \psi_o\} \\ &= 2\Pr\{\cos(\phi_2) \leq \cos(\phi_1) < \cos(\phi_2) + \psi_o\} \\ &= 2\Pr\{\cos^{-1}(\cos(\phi_2) + \psi_o) < \phi_1 \leq \phi_2\}.\end{aligned} \tag{7.7}$$

By using the same approach, α_1 is found by:

$$\begin{aligned}\alpha_1 &= \Pr\{2 - \psi_o < |\psi| < 2\} \\ &= 2\Pr\{2 - \psi_o < \psi < 2\} \\ &= 2\Pr\{2 - \psi_o < \cos(\phi_1) - \cos(\phi_2) < 2\} \\ &= 2\Pr\{\cos(\phi_2) + 2 - \psi_o < \cos(\phi_1) < \cos(\phi_2) + 2\}.\end{aligned} \tag{7.8}$$

Note $\cos(\phi_2) + 2 > 1$ for all ϕ_2 in the FoV. Therefore:

$$\begin{aligned}\alpha_1 &= 2\Pr\{\cos(\phi_2) + 2 - \psi_o < \cos(\phi_1) < 1\} \\ &= 2\Pr\left\{\frac{\pi}{2} - \phi_o < \phi_1 < \cos^{-1}(\cos(\phi_2) + 2 - \psi_o)\right\}.\end{aligned} \tag{7.9}$$

Recall that ϕ_l with $l = 1, 2$ are uniformly distributed in the FoV. Consequently, given (7.7)–(7.9), α_0 and α_1 are found by evaluating the following integrals:

$$\alpha_0 = 2 \int_{\frac{\pi}{2}-\phi_o}^{\frac{\pi}{2}+\phi_o} \frac{1}{2\phi_o} \int_{\cos^{-1}(\cos(\phi_2)+\psi_o)}^{\phi_2} \frac{1}{2\phi_o} d\phi_1 d\phi_2, \tag{7.10}$$

$$\alpha_1 = 2 \int_{\frac{\pi}{2}-\phi_o}^{\frac{\pi}{2}+\phi_o} \frac{1}{2\phi_o} \int_{\frac{\pi}{2}-\phi_o}^{\cos^{-1}(\cos(\phi_2)+2-\psi_o)} \frac{1}{2\phi_o} d\phi_1 d\phi_2. \tag{7.11}$$

Whenever ρ_o is higher than the black squares (first side-lobes at $\rho_o = 2/(3\pi)$ [87, Sec. 6.3]) shown in Fig. 7.2, p can be written as a sum of α_0 and α_1 in (7.6), where α_0 and α_1 are found by (7.10) and (7.11), respectively.

7.3.2 ULAs with $\delta > \lambda/2$

In this section, we first find p for a ULA with $\delta = \lambda$. Then, we give an expression for ULAs with any $\delta > \lambda/2$. In Fig. 7.3, $|\rho| = f_\lambda(\psi)$ is shown for a ULA of $M = 10$ antennas. The shaded areas show when user 1 and user 2 become correlated with a given ρ_o. The probability p is found by:

$$\begin{aligned} p &= \Pr\{|\rho| > \rho_o\} \\ &= \Pr\{|\psi| < \psi_o\} + \Pr\{1 - \psi_o < |\psi| < 1 + \psi_o\} + \\ &\Pr\{2 - \psi_o < |\psi| < 2\} = \alpha_0 + \alpha_1 + \alpha_2, \end{aligned} \tag{7.12}$$

where the corresponding area for α_0, α_1, and α_2 are shown in Fig. 7.3 by blue, red, and yellow shaded area, respectively. Similar to case of $\delta = \lambda/2$, we find integrals for α_0, α_1, and α_2. For a ULA with $\delta > \lambda/2$, p for a given ρ_o is found by:

$$\begin{aligned} p &= \Pr\{|\rho| > \rho_o\} = \Pr\{|\psi| < \psi_o\} + \\ &\sum_{i=1}^{n} \Pr\{iT - \psi_o < |\psi| < iT + \psi_o\} = \alpha_0 + \sum_{i=1}^{n} \alpha_i, \end{aligned} \tag{7.13}$$

where n is the number of areas where $\psi > 0$ and $\rho > \rho_o$ excluding the area corresponds to α_0. For instance, $n = 2$ for $\delta = \lambda$. We numerically evaluate integrals to find α_0 and α_i to find p, same as the analysis done for $\lambda/2$.

In Fig. 7.4, p is shown as a function of δ/λ for $M = 10, 20, 64$ for $\delta \leq 2.5\lambda$ [2], $\rho_o = 0.64$ for a FoV of $(0, \pi)$. For each M, $\delta^\star$ shows the inter-element spacing with minimum p, and there are three local minima as shown by colored circles δ_{n_1}, δ_{n_2}, and δ_{n_3}. By increasing δ, p is continuously increasing and then decreasing with decaying behavior. There are two reasons for explaining this behavior. First, by increasing δ, the angular resolution of the array is improved (compare the shaded blue area in Fig. 7.2

[2] The choice of 2.5λ is arbitrary to limit the maximum aperture size.

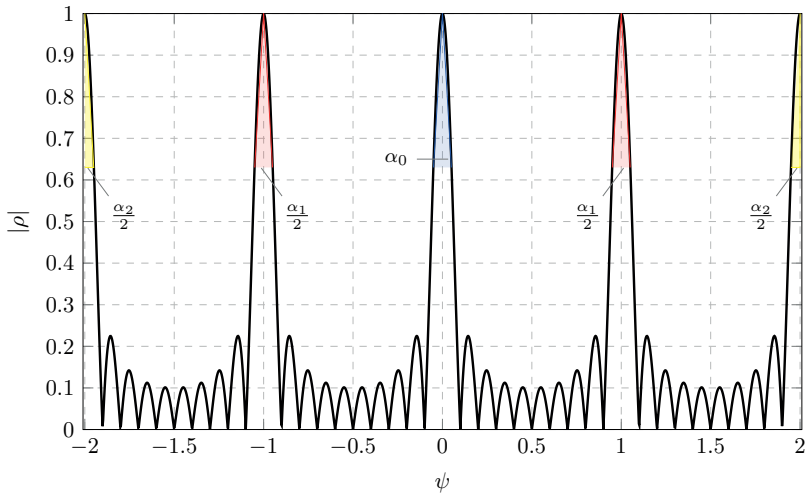

Figure 7.3: $|\rho| = f_\lambda(\psi)$ for $M = 10$, $\rho_o = 0.64$, $\psi_o = 0.05$, and FoV of $(0, \pi)$ with $T = 1$. The blue, red, and yellow shaded area are associated with α_0, α_1, and α_2, respectively.

and Fig. 7.3), which decreases p. Second, by increasing δ, the grating lobes (the peaks correspond to $\alpha_i, i \neq 0$, see Fig. 7.3) gradually appear in the FoV, which increases p. Due to the first reason, p should decrease, and due to the second reason, p should increase. As can be seen, we see a more decrease in p, which shows that increasing the angular resolvability has a stronger effect on p than the grating lobes. Moreover, the effect of increasing the angular resolvability and the appearance of grating lobes is decaying as δ approaches 2.5λ. We further observe that in all the scenarios, p curves approach $p = 1/M$ (horizontal dash-dotted lines).

We approximate δ_{n_i} by the inter-element spacing for which the shaded area associated with $(i+1)$th grating lobe appeared in function $f_\delta(\psi)$ (e.g., in Fig. 7.3, the yellow shaded area is associated with the 2nd grating lobe). For instance, δ_{n_1} is approximated by the inter-element spacing for which the yellow area starts to appear in Fig. 7.3. For a given ψ_o, we approximate δ_{n_i} by solving $\psi_o - (i+1)\lambda/\delta = -2$ for δ, which leads to $\delta_{n_i} \approx \lambda(2M(i+1) - 1)/4M$ for ψ_o of the scenario in Fig. 7.4. The results in Fig. 7.4 shows that the approximations of δ_{n_i} (pink cross) match with the numerical values of δ_{n_i} (colored circle). For a given M, we propose to use $\delta^\star$, which is the inter-element spacing with the minimum p. To reduce the aperture size, one can use $\delta_{n_i}, i = 1, 2, 3$ instead of $\delta^\star$. We assume a narrow-band communication system in this letter. However, the results in Fig. 7.4 can be used for multi sub-carriers systems. By choosing an appropriate spacing for the center sub-carrier, one can make p smaller than a threshold for all the sub-carriers. The performance of using δ_{n_1} and $\delta^\star$ for more number of users is compared

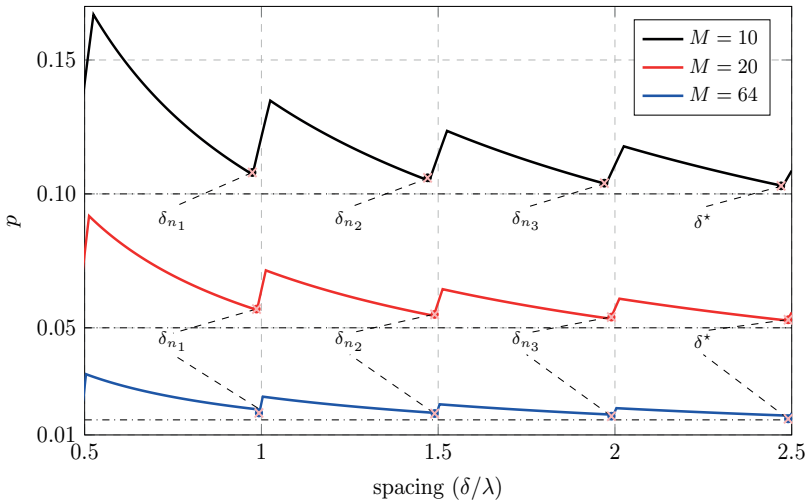

Figure 7.4: p as a function of δ/λ for $M = 10, 20, 64$, FoV of $(0, \pi)$, $\delta \in [0.5\lambda, 2.5\lambda]$ for $\rho_o = 0.64$. For each M, the minimum p occurs at $\delta^\star$. The local minima are δ_{n_1}, δ_{n_2} and δ_{n_3}.

in the next Section. Regarding scenarios where there are paths other than LOS path some insights can be found in [15].

7

7.4 Simulation Results

In this section, the performance of ULAs with $\delta^\star$ and δ_{n_1} (see Fig. 7.4) are compared with half-wavelength ULA for FoV of $(0, \pi)$ in LOS massive MIMO with max-min power control. To study the worst-case scenarios, the users are assumed to be at the cell-edge (no shadowing), which is assumed to be at the far-field of the array. We compare the arrays qualitatively and quantitatively as follows. First, qualitatively, for a given ρ_o, we compare the probability that at least there is one correlated pair of users as a function of the number of users for the three arrays. Second, quantitatively, we compare cumulative distribution function (CDF) of ZF sum-rates of the arrays.

In Fig. 7.5, for a ULA with $M = 64$ antennas, the probability that there is at least one pair of correlated users ($\rho_o = 0.64$) is shown as a function of the number of users K for $\delta = \lambda/2$ (blue), δ_{n_1} (red), and $\delta^\star$ (black). For a given number of users, the ULA with $\delta^\star$ has a smaller probability compared to $\lambda/2$, which means it has a better ability to decorrelate the channel vectors of the users. By using δ_{n_1} instead of $\delta^\star$, we can reduce the aperture size, while the probability that there is at least one pair of correlated users is not that higher than that of $\delta^\star$.

In Fig. 7.6, the CDF of ZF sum-rate is shown for the arrays with $K = 6$ and $M = 64$

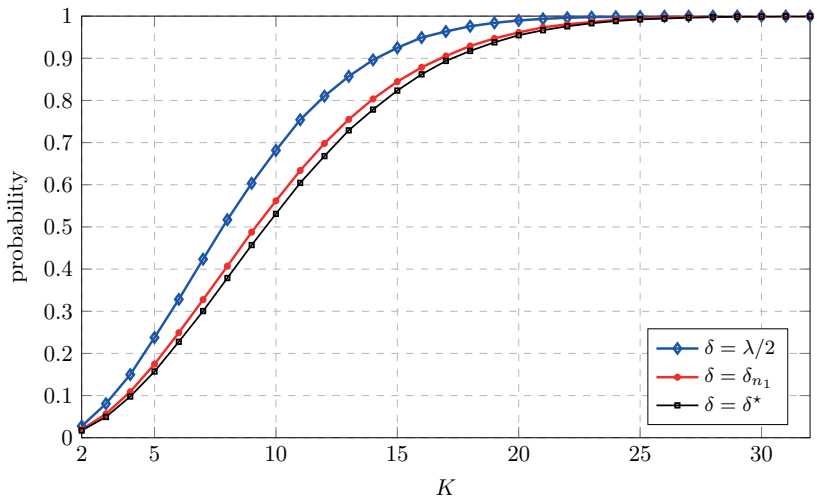

Figure 7.5: The probability that there is at least one pair of correlated users for $\delta = \lambda/2$, δ_{n_1}, $\delta^\star$ when $M = 64$, $\rho_o = 0.64$ for a FoV of $(0, \pi)$.

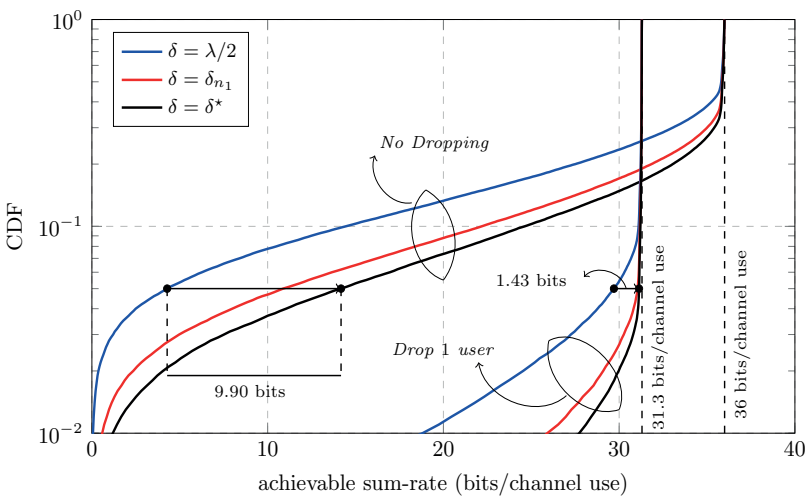

Figure 7.6: The CDF plots of ZF sum-rate for $\delta = \lambda/2$, δ_{n_1}, $\delta^\star$ for two different scenarios, i.e., *No dropping* and *Drop* 1 *user* (based on the algorithm of [33]). The horizontal arrow shows the 5th percentile improvement of the sum-rate by using $\delta^\star$ instead of $\delta = \lambda/2$. The vertical dashed lines show the ZF sum-rate in FP for the two scenarios.

in two different scenarios, where 100K realizations of users' locations are drawn for each scenario. In the first scenario, no user is dropped (*No Dropping*), while in the second scenario one user is dropped (*Drop* 1 *user*) based on the dropping algorithm of [33]. The transmit power at the BS is fixed and is the same in both scenarios such that in the favorable propagation (FP) [39] (when the users are mutually orthogonal), a sum-rate of 36 bits/channel use is achieved in the first scenario, and a sum-rate of 31.3 bits/channel use is achieved in the second scenario (see the vertical dashed lines in Fig. 7.6). When no user is dropped, by employing the proposed array (black), the 5th percentile sum-rate is improved significantly (9.90 bits/channel use) compared to that of the ULA with $\delta = \lambda/2$ (blue). This improvement becomes 1.43 bits/channel use when 1 user is dropped. By dropping 1 user, the 5th percentile ZF sum-rate of all the arrays is improved significantly, which shows it is necessary to drop 1 user. To reduce the aperture size, the array with δ_{n_1} (red) can be used instead of $\delta^\star$ with a loss in performance, i.e., 3.30 bits/channel use loss in *No Dropping* scenario and 0.09 bits/channel use in *Drop* 1 *user* scenario.

7.5 Conclusions

In this letter, we use probability analysis to find an improved uniform linear array for LOS massive MIMO. For the case of two users, the proposed ULA has the minimum probability that the correlation of the users being above a given threshold. For more users, we present the simulation results for a known linear precoder, i.e., ZF to show the effectiveness of the proposed ULA compared to half-wavelength ULA.

CHAPTER 8

Paper D
An Improved Dropping Algorithm for Line-Of-Sight Massive MIMO with Max-Min Power Control

Abstract

In line-of-sight massive MIMO, there is a nonnegligible probability that two users become highly correlated, which leads to a reduction in the achievable sum-rates of linear precoders. In this paper, threshold values of a previously proposed dropping algorithm are found analytically to avoid repeating a large number of simulations to find the optimal threshold. These thresholds allow us to improve conjugate beamforming (CB) and zero-forcing (ZF) sum-rates with max-min power control. By using the proposed threshold values, the CB and ZF sum-rates are maximized, when there are only two correlated users. In addition, by using the derived thresholds, a modified dropping algorithm is proposed for channels with any number of correlated users. The results of the simulation scenarios show that at signal to noise ratio of 20 dB and 120 antennas at the base station, the modified algorithm improves the average CB and ZF sum-rates up to 36% and 5%, respectively.

8.1 Introduction

Massive MIMO is a promising technology for 5G wireless networks [29]. One of the key properties massive MIMO relies on is favorable propagation (FP) [39], which implies that the channel vectors to the users become mutually orthogonal when the number of antennas at the base station (BS) tends to infinity. FP provides a large number of spatial degrees of freedom, which results in high data throughput and radiated-energy efficiency [39, 73]. Moreover, in FP environments, linear precoders, e.g., conjugate beamforming (CB) or zero-forcing (ZF), are optimal in terms of downlink capacity [39].

Studying line-of-sight (LOS) environments is of great importance since the real propagation environment is likely to fall between LOS and independent and identically distributed Rayleigh [69]. Under LOS propagation environments, it is of great interest to provide uniformly good service to all the users [33]. This is achieved by using max-min power control, which maximizes the fairness among the users.

In LOS environments, there is a nonnegligible probability that two users become highly correlated [39]. This makes the propagation environment unfavorable, which leads to a reduction in the downlink capacity and the sum-rate of linear precoders [70,71]. To improve CB and ZF sum-rates with max-min power control, a dropping algorithm was proposed in [33]. In the algorithm in [33], the BS drops some users to make the correlation between the channel vectors of the remaining users be less than a threshold. This threshold is found via numerical simulations for a large number of realizations with the same scenario, i.e., the number of users, the path loss, and total transmit power. The drawback of this approach is that new simulations are required for every new scenario. A similar approach is used in [91] for parallelogram planar arrays, and in [92] for a scheduling algorithm in massive MIMO.

In this paper, the dropping problem is analyzed for CB and ZF with max-min power control in LOS environments. We are interested in maximizing the minimum signal to interference plus noise ratio (SINR) among the served users. The contributions of this paper are as follows. First, we derive the threshold values used in the dropping algorithm of [33]. The derived thresholds avoid repeating numerical simulations as done in [33,91]. Second, we prove that by using the derived thresholds, the CB and ZF sum-rates for a channel of K users with only two correlated users, are maximized. Lastly, the derived thresholds are used to modify the dropping algorithm in [33]. Numerical simulations show that the modified algorithm improves the CB and ZF sum-rates considerably.

This paper is organized as follows[1]. In Sec. 8.2, the system model is given. The dropping problem is analyzed in Sec. 8.3. The simulation results are presented in Sec. 8.4. Finally, Sec. 8.5 concludes the paper.

[1]The following notation is used throughout the paper. Lowercase letters, bold lowercase and bold uppercase letters denote scalars, column vectors and matrices, respectively. The symbols $\mathbb{R}^+$ and $\mathbb{C}$ denote real positive numbers and complex numbers. The symbols $|\cdot|$ and $\|\cdot\|$ denote the absolute value and l^2-norm operators. The superscripts *, ^{T} and ^{H} denote complex conjugate, un-conjugated transpose, and conjugated transpose, respectively. A diagonal matrix with diagonal entries taken from $\boldsymbol{p}$ is denoted by $\mathrm{diag}(\boldsymbol{p})$.

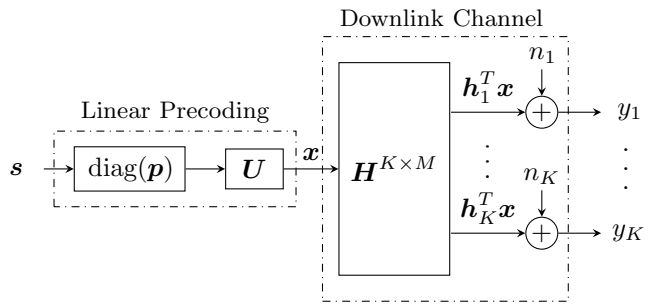

Figure 8.1: The model of the downlink channel with linear precoding.

8.2 System Model

The model for the downlink channel from an M-antenna BS to K single-antenna users with linear precoding is shown in Fig. 8.1. The intended zero-mean, uncorrelated and unit variance symbols $\boldsymbol{s} = (s_1, ..., s_K)^T \in \mathbb{C}^{K\times 1}$ are precoded by a diagonal matrix diag($\boldsymbol{p}$) and a linear precoding matrix $\boldsymbol{U} \in \mathbb{C}^{M\times K}$ with unit-norm column vectors $\boldsymbol{u}_i$. The power control vector is $\boldsymbol{p} = (\eta_1, ..., \eta_K)^T$, where $\eta_i \in \mathbb{R}^+$ with $i = 1, ..., K$ are the max-min power control coefficients. The power constraint at the BS is $\sum_{i=1}^{K} \eta_i^2 = P_{\text{tot}}$. The precoded vector $\boldsymbol{x} \in \mathbb{C}^{M\times 1}$ is transmitted through a general channel $\boldsymbol{H} = (\boldsymbol{h}_1, ..., \boldsymbol{h}_K)^T \in \mathbb{C}^{K\times M}$, where $\boldsymbol{h}_i$ is the channel vector from the BS to user i. The received signal for user i is:

$$y_i = \boldsymbol{h}_i^T \boldsymbol{u}_i \eta_i s_i + \sum_{\substack{j=1\\ j\neq i}}^{K} \boldsymbol{h}_i^T \boldsymbol{u}_j \eta_j s_j + n_i, \tag{8.1}$$

where n_i is complex AWGN noise with variance N_0. For a given channel matrix, SINR for each user can be expressed as

$$\text{SINR}_i = \frac{|\boldsymbol{h}_i^T \boldsymbol{u}_i|^2 \eta_i^2}{\sum_{j=1, j\neq i}^{K} |\boldsymbol{h}_i^T \boldsymbol{u}_j|^2 \eta_j^2 + N_0}. \tag{8.2}$$

To elaborate on the derived thresholds, we will focus on a specific channel in Sec. 8.3, which is defined as follows.

Definition 8.1. A correlated channel of size K is a channel with K single-antenna users in which user $K-1$ and user K are the only correlated users ($\|\boldsymbol{h}_{K-1}\| \geq \|\boldsymbol{h}_K\|$), and the other users are mutually orthogonal. The spatial correlation of user $K-1$ and user K is given by:

$$\rho = \frac{\boldsymbol{h}_K^H \boldsymbol{h}_{K-1}}{\|\boldsymbol{h}_K\| \|\boldsymbol{h}_{K-1}\|}. \tag{8.3}$$

Consider a correlated channel of size K. If the BS with the power constraint P_{tot} drops user (DU) K, user 1 to user $K-1$ will experience FP. Therefore, the following sum-rate R^{DU} is achieved with CB or ZF with max-min power control using the Lagrangian multiplier:

$$R^{\text{DU}} = (K-1)\log_2\left(1 + \frac{P_{\text{tot}}/N_0}{\sum_{i=1}^{K-1}\frac{1}{\|\boldsymbol{h}_i\|^2}}\right). \tag{8.4}$$

In what follows, the CB and ZF sum-rates for a correlated channel of size K are derived.

8.2.1 The CB Sum-Rate

To find the CB sum-rate, we need to find the SINR of each user with CB. The unit-norm column vectors of CB are found by:

$$\boldsymbol{u}_i^{\text{CB}} = \frac{\boldsymbol{h}_i^*}{\|\boldsymbol{h}_i\|}, \quad i = 1, ..., K. \tag{8.5}$$

Replacing (8.5) in (8.2), the following SINRs are found for the users:

$$\text{SINR}_i^{\text{CB}} = \frac{\|\boldsymbol{h}_i\|^2\eta_i^2}{N_0}, \quad i = 1, ..., K-2 \tag{8.6}$$

$$\text{SINR}_{K-1}^{\text{CB}} = \frac{\|\boldsymbol{h}_{K-1}\|^2\eta_{K-1}^2}{\|\boldsymbol{h}_{K-1}\|^2|\rho|^2\eta_K^2 + N_0}, \tag{8.7}$$

$$\text{SINR}_K^{\text{CB}} = \frac{\|\boldsymbol{h}_K\|^2\eta_K^2}{\|\boldsymbol{h}_K\|^2|\rho|^2\eta_{K-1}^2 + N_0}. \tag{8.8}$$

The max-min power control coefficients, $\eta_i, i = 1, ..., K$ are found by maximizing the minimum SINR among the users given by (8.6)–(8.8) using bisection method as explained in [33]. However, due to FP of user 1 to user $K-2$, the CB SINR corresponding to the max-min power control is derived analytically by solving a quadratic equation. The largest root always results in a negative power allocation for the correlated users, while the smallest root always results in a positive power allocation for all the users. The smallest root is found by:

$$z = \frac{P_{\text{tot}}}{2N_0\gamma_1} + \frac{1+\frac{\gamma_2}{\gamma_1}}{2|\rho|^2} - \sqrt{\left(\frac{P_{\text{tot}}}{2N_0\gamma_1} + \frac{1+\frac{\gamma_2}{\gamma_1}}{2|\rho|^2}\right)^2 - \frac{P_{\text{tot}}}{N_0\gamma_1|\rho|^2}}, \tag{8.9}$$

where

$$\gamma_1 = \sum_{i=1}^{K-2}\frac{1}{\|\boldsymbol{h}_i\|^2} \quad \text{and} \quad \gamma_2 = \frac{1}{\|\boldsymbol{h}_{K-1}\|^2} + \frac{1}{\|\boldsymbol{h}_K\|^2}. \tag{8.10}$$

Using (8.9) for the CB SINR, R^{CB} is found as:

$$R^{\text{CB}} = K\log_2(1+z). \tag{8.11}$$

8.2.2 The ZF Sum-Rate

To find the ZF sum-rate, we need to find the ZF SINR values. The pseudo-inverse of the channel $\boldsymbol{A} = \boldsymbol{H}^H(\boldsymbol{H}\boldsymbol{H}^H)^{-1}$ is required to find $\boldsymbol{u}_i^{\text{ZF}}$. Due to the definition of the correlated channel of size K, there are only two off-diagonal elements for $(\boldsymbol{H}\boldsymbol{H}^H)^{-1}$, which makes it simple to find $\boldsymbol{A}$. Then, each column of $\boldsymbol{A}$ is normalized to have unit-norm, which results in the following $\boldsymbol{u}_i^{\text{ZF}}$:

$$\boldsymbol{u}_i^{\text{ZF}} = \frac{\boldsymbol{h}_i^*}{\|\boldsymbol{h}_i\|}, \quad i = 1, ..., K-2 \tag{8.12}$$

$$\boldsymbol{u}_{K-1}^{\text{ZF}} = \frac{1}{\sqrt{1-|\rho|^2}}\left(\frac{\boldsymbol{h}_{K-1}^*}{\|\boldsymbol{h}_{K-1}\|} - \rho^* \frac{\boldsymbol{h}_K^*}{\|\boldsymbol{h}_K\|}\right), \tag{8.13}$$

$$\boldsymbol{u}_K^{\text{ZF}} = \frac{1}{\sqrt{1-|\rho|^2}}\left(\frac{\boldsymbol{h}_K^*}{\|\boldsymbol{h}_K\|} - \rho \frac{\boldsymbol{h}_{K-1}^*}{\|\boldsymbol{h}_{K-1}\|}\right). \tag{8.14}$$

Replacing (8.12)–(8.14) in (8.2), the SINR for user i is found by:

$$\text{SINR}_i^{\text{ZF}} = \frac{\|\boldsymbol{h}_i\|^2 \eta_i^2}{N_0}, \quad i = 1, ..., K-2 \tag{8.15}$$

$$\text{SINR}_{K-1}^{\text{ZF}} = \frac{\|\boldsymbol{h}_{K-1}\|^2 (1-|\rho|^2)\eta_{K-1}^2}{N_0}, \tag{8.16}$$

$$\text{SINR}_K^{\text{ZF}} = \frac{\|\boldsymbol{h}_K\|^2 (1-|\rho|^2)\eta_K^2}{N_0}. \tag{8.17}$$

By maximizing the minimum SINR among the users same as (8.4), the following ZF sum-rate R^{ZF} is found:

$$R^{\text{ZF}} = K \log_2\left(1 + \frac{P_{\text{tot}}/N_0}{\frac{\gamma_2}{1-|\rho|^2} + \gamma_1}\right). \tag{8.18}$$

8.3 Improved Dropping Algorithm

8

For a correlated channel of size K, the following Theorem gives the optimal dropping strategy in terms of the sum-rate.

Theorem 8.1. Consider a correlated channel of size K with ρ. If a BS with P_{tot} drops one of the correlated users based on

$$\begin{cases} \text{drop user } K & \text{when } |\rho| > |\rho^{\text{ZF}}| \\ \text{no dropping} & \text{when } |\rho| \leq |\rho^{\text{ZF}}|, \end{cases} \tag{8.19}$$

where $|\rho^{\text{ZF}}|$ is given by:

$$|\rho^{\text{ZF}}| = \sqrt{1 - \frac{\gamma_2}{\frac{P_{\text{tot}}/N_0}{(2^\alpha - 1)} - \gamma_1}}, \tag{8.20}$$

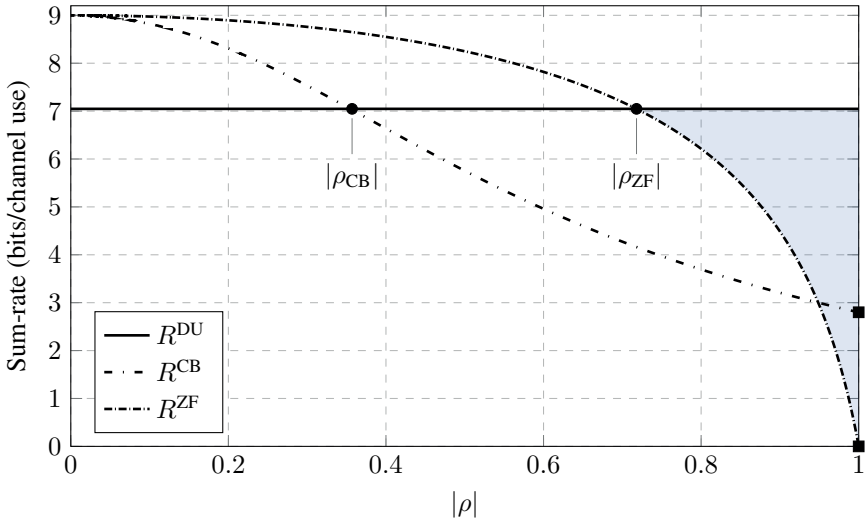

Figure 8.2: The comparison of R^{DU} (8.4), R^{CB} (8.11), and R^{ZF} (8.18) as a function of $|\rho|$ for a correlated channel of size 3 at SNR $= 7$ when $M = 64$. The shaded area shows the extra sum-rate that the BS can achieve by using the proposed threshold for the dropping with ZF.

and $\alpha = R^{\text{DU}}/K$, then, the ZF sum-rate with max-min power control is maximized.

Proof. By solving $R^{\text{DU}} \geq R^{\text{ZF}}$ for $|\rho^{\text{ZF}}|$ using (8.4) and (8.18), one can verify (8.20), which shows that the ZF sum-rate is maximized by using the dropping algorithm. □

8

The results of Theorem 8.1 are true for any channel matrix. However, our emphasis is on LOS environments in which there is a nonnegligible probability that two users become highly correlated [39]. The same analysis can be done for CB, while $|\rho^{\text{CB}}|$ is found by solving $R^{\text{CB}} = R^{\text{DU}}$ using the bisection method [42, sec. 7.1.1.]. This is possible since z (see (8.9)), and consequently R^{CB} (see (8.11)) are strictly decreasing functions of $|\rho|$.

In Fig. 8.2, R^{DU}, R^{CB}, and R^{ZF} are shown as a function of $|\rho|$ for a correlated channel of size 3. The threshold value for CB (and ZF) is found using the bisection method (and using (8.20)), which is exactly the intersection of R^{DU} and R^{CB} (and R^{ZF}) in Fig. 8.2 shown by a black circle. By using the derived threshold, the BS with CB (and ZF) can achieve R^{DU} when $|\rho| > |\rho^{\text{CB}}|$ (and $|\rho| > |\rho^{\text{ZF}}|$). Thus, compared to a BS, which does not drop any user, the dropping with the proposed threshold values avoids a large losses in the sum-rate (for instance, the shaded area in Fig. 8.2 is the loss in the ZF sum-rate). More importantly, by using the derived thresholds, the maximum CB and ZF sum-rates are achieved.

Although R^{CB} is lower than R^{ZF} for most values of $|\rho|$ (see Fig. 8.2), R^{CB} becomes close to 1 bit/channel use for each user when $|\rho| \to 1$ while R^{ZF} tends to zero. By

analyzing (8.11) and (8.18), the behaviors of R^{CB} and R^{ZF} when $|\rho| \to 1$ are found as:

$$\lim_{|\rho|\to 1} R^{\text{CB}} = K \log_2(1 + \frac{\|\boldsymbol{h}_K\|^2 \eta^2_{K(|\rho|=1)}}{\|\boldsymbol{h}_K\|^2 \eta^2_{K(|\rho|=1)} + N_0}), \tag{8.21}$$

$$\lim_{|\rho|\to 1} R^{\text{ZF}} = 0, \tag{8.22}$$

which explains the behavior in Fig. 8.2 (see the black squares).

We conclude this section by modifying the dropping algorithm in [33] using the proposed thresholds. This is explained for ZF in Algorithm 4. By having the channel matrix $\boldsymbol{H}$, the maximum spatial correlation among the users $|\rho^{\text{max}}|$ is found:

$$|\rho^{\text{max}}| = \max_{i,j\neq i} |\rho_{ij}|. \tag{8.23}$$

If $|\rho^{\text{max}}|$ is larger than $|\rho^{\text{ZF}}|$, one of the correlated users, who has the highest sum correlation (considering the distance difference) to the remaining users (see lines 4-5 of Algorithm 4), is dropped. Then, the channel matrix, $|\rho^{\text{max}}|$, and $|\rho^{\text{ZF}}|$ are updated to check whether dropping is still required. This procedure is repeated until there is no need for dropping any user. The same algorithm is found for CB using $|\rho^{\text{CB}}|$. The simulation results in the next section show the effectiveness of the modified dropping algorithm.

Algorithm 4 Modified Dropping algorithm for a channel of K users with ZF

Input: $\boldsymbol{H}, K, P_{\text{tot}}/N_0$
1: find $|\rho^{\text{max}}|$ using $\boldsymbol{H}$
2: find $|\rho^{\text{ZF}}|$ based on (8.20)
3: **while** $|\rho^{\text{max}}| > |\rho^{\text{ZF}}|$ **do**
4: find m and n the indexes of users associated with $|\rho^{\text{max}}|$
5: **if** $\sum_{l\neq m,n} \frac{|\rho_{ml}|}{\|\boldsymbol{h}_m\|} > \sum_{l\neq n,m} \frac{|\rho_{nl}|}{\|\boldsymbol{h}_n\|}$ **then**
6: drop user m
7: **else**
8: drop user n
9: **end if**
10: $K = K - 1$
11: update $\boldsymbol{H}$ by removing the row of the dropped user
12: update $|\rho^{\text{max}}|$ using $\boldsymbol{H}$
13: find $|\rho^{\text{ZF}}|$ based on (8.20)
14: **end while**

8.4 Simulations

Consider a channel of $K = 8$ users, where the users are uniformly distributed in a field-of-view (FoV) of $[30°, 150°]$. The carrier frequency is set to 30 GHz. A single-cell

is analyzed, where the users are assumed to be at the cell-edge (200 m) to study the worst case scenarios. The minimum distance between the two users is assumed to be a wavelength (λ). In LOS environments, the element ij of $\boldsymbol{H}$, denoted by h_{ij} is modeled by [35, Sec. 7.2.2.]

$$h_{ij} = \frac{\sqrt{\beta_i}}{\sqrt{M}} e^{-\jmath k d_i} e^{+\jmath k (j-1)\Delta \cos(\phi_i)}, \quad j = 1, ..., M, \tag{8.24}$$

where β_i is the large-scale fading, $k = 2\pi/\lambda$ is the wave number, d_i is the distance from user i to the array, Δ is the spacing between the antenna elements, and ϕ_i specifies the direction of user i with respect to the array (see [35, fig. 7.3. (b)]). The antenna spacing is assumed to be $\Delta = \lambda/2$. Two scenarios where the BS has $M = 40$ and $M = 120$ antennas are considered to evaluate the advantages of using the modified dropping algorithm for CB and ZF. The threshold values $|\rho^{\text{CB}}|$ and $|\rho^{\text{ZF}}|$ are found for each SNR in the modified dropping algorithm. The simulation is run for 10000 random realizations.

The average R^{CB} and R^{ZF} over SNR for the modified dropping algorithm (solid lines) compared to when the BS does not drop any user (dashed lines) are shown in Fig. 8.3 and Fig. 8.4 for $M = 40$ and $M = 120$, respectively. The modified dropping algorithm improves the sum-rate in all SNRs for both CB and ZF. For instance, at SNR $= 20$ dB, R^{CB} and R^{ZF} for $M = 40$ are improved by 101% and 19%, respectively (see Fig. 8.3). By increasing the antenna at the BS to $M = 120$, the improvements become 36% and 5% for CB and ZF, respectively. For $M = 120$ the transmit power at the BS is reduced 3 times to have a fair comparison with $M = 40$. By increasing M, the expected spatial correlation among the users decreases [33, Theorem 13.]. This shows for $M = 120$ fewer users are dropped, which limits the improvement for $M = 120$ compared to $M = 40$. The results show that the modified dropping algorithm is beneficial for the BS, especially for small M. The average sum-rates with the dropping algorithm of [33] using the optimal threshold are shown in Fig. 8.3 and Fig. 8.4. By using the modified dropping algorithm, one can avoid searching for the optimal threshold as in the dropping algorithm of [33] with a negligible loss in the average sum-rate.

8.5 Conclusions

In this paper, the dropping problem is analyzed for the CB and ZF with max-min power control in LOS environments. Threshold values are analytically derived to be used in the previously proposed dropping algorithm to avoid repeating a large number of simulations to find the optimal threshold. By using the derived threshold for the dropping, the sum-rate is maximized when there are only two correlated users. Furthermore, a modified dropping algorithm is proposed for channels with any number of correlated users. The results of the simulation scenarios show that at SNR of 20 dB and 120 antennas at the BS, the modified dropping algorithm improves the average CB and ZF sum-rates up to 36% and 5%, respectively.

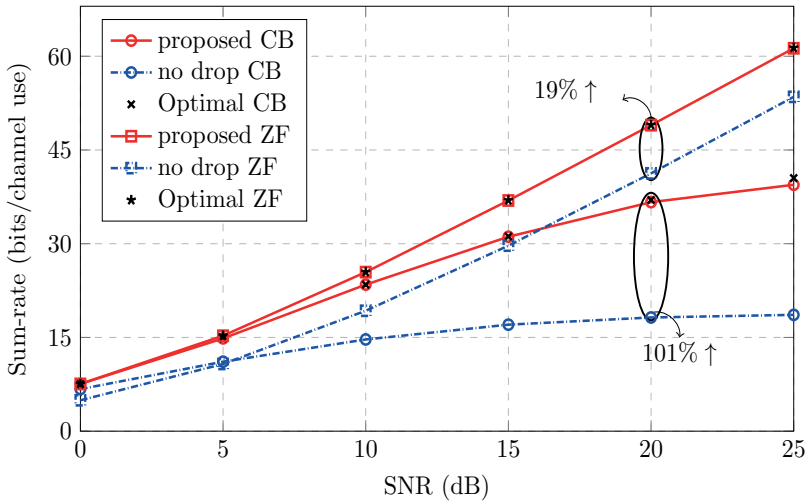

Figure 8.3: The average R^{CB} and R^{ZF} using the modified dropping algorithm (solid lines) compared to no dropping (dashed lines) for $K = 8$ and $M = 40$. At SNR = 20 dB, R^{CB} and R^{ZF} are improved by 101% and 19%, respectively.

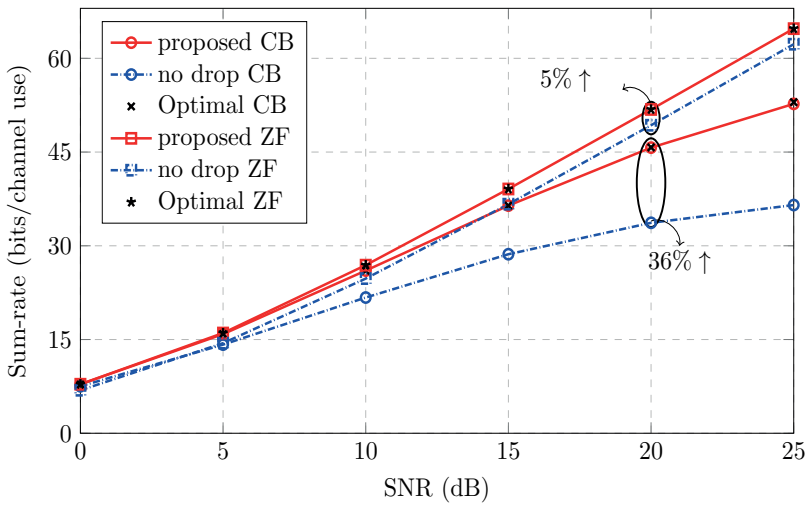

Figure 8.4: Same as Fig. 8.3 for $M = 120$.

CHAPTER 9

Paper E
An Improved Dropping Algorithm for Line-of-Sight Massive MIMO with Tomlinson-Harashima Precoding

Abstract

One of the problems in line-of-sight massive MIMO is that a few users can have correlated channel vectors. To alleviate this problem, a dropping algorithm has been proposed in the literature, which drops some of the correlated users to make the spatial correlation among the remaining users be less than a certain threshold. Thresholds were found by running a large number of simulations. In this paper, the same dropping algorithm is analyzed for a known *nonlinear* precoder: Tomlinson-Harashima precoder. Instead of simulation-based thresholds, closed-form analytical expressions are derived in this paper for two power allocation schemes: max-min and equal received power control schemes. It is shown that the derived thresholds are optimal in terms of achievable sum-rate when there is only one correlated pair of users. For channels with multiple pairs of correlated users, simulation results show that using the derived thresholds improves the 5th percentile sum-rate. Due to the fairness criterion of max-min, the improvement for max-min power control is much higher than equal received power control.

9.1 Introduction

One of the key properties of radio channels exploited in massive MIMO systems is favorable propagation (FP) [26, 39]. FP is defined as the mutual orthogonality among the channel vectors from the base station (BS) to the users [39]. FP can be observed both in line-of-sight (LOS) and independent and identically distributed Rayleigh fading environments [33]. In LOS environments, there is a nonnegligible probability that the channel vectors of a few users become highly correlated [39], which leads to a reduction in the downlink capacity and the achievable sum-rates of linear precoders [70, 71].

To improve the achievable sum-rates of linear precoders such as conjugate beamforming (CB) and zero-forcing (ZF) with max-min power control, a correlation-based dropping (CD) algorithm was proposed in [33] for LOS environments. In the CD algorithm, the BS drops some users and reschedules them in another coherence interval to make the spatial correlation between the channel vectors of the remaining users be less than a certain threshold. The threshold is found by repeating extensive numerical simulations for the same scenario. A similar criterion was used in [91, 93]. Instead of simulation-based thresholds as in [33], thresholds are derived in [3] for CB and ZF with max-min power control.

To improve the achievable sum-rate of a BS, which uses the CD algorithm, nonlinear precoders can be used instead of linear precoders. Tomlinson-Harashima precoding (THP) is a known nonlinear precoder [52, 94] for which an efficient implementation with a computational complexity order equal to that of ZF exists [41, Sec. 4.3.1]. In this paper, we analyze the combination of CD algorithm and THP from a theoretical viewpoint for two different power allocation schemes: max-min and equal received power control schemes. To the best of our knowledge, this is the first time the CD algorithm is analytically characterized in combination with THP.

The contribution of this paper is twofold. First, we derive closed-form analytical thresholds for the CD algorithm with THP and the two aforementioned power allocation schemes. Furthermore, we prove that using the derived thresholds when there is only one correlated pair of users, results in the optimal dropping strategy. The second contribution of this paper is to use the derived thresholds for channels with multiple pairs of correlated users. Numerical simulations show that near-optimum performance is achieved if a 100-antenna BS serving 10 single-antenna users employs the derived thresholds. By employing the CD algorithm for a BS with THP, the achievable sum-rates of both power control schemes are improved.[1]

[1] Lowercase, bold lowercase, and bold uppercase letters denote scalars, column vectors, and matrices, respectively. $|\cdot|$ and $\|\cdot\|$ denote the absolute value and l^2-norm operators. The superscripts *, ^{T}, and ^{H} denote complex conjugate, un-conjugated transpose, and conjugated transpose, respectively. $\mathrm{diag}(\boldsymbol{p})$ denotes a diagonal matrix with diagonal entries taken from $\boldsymbol{p}$.

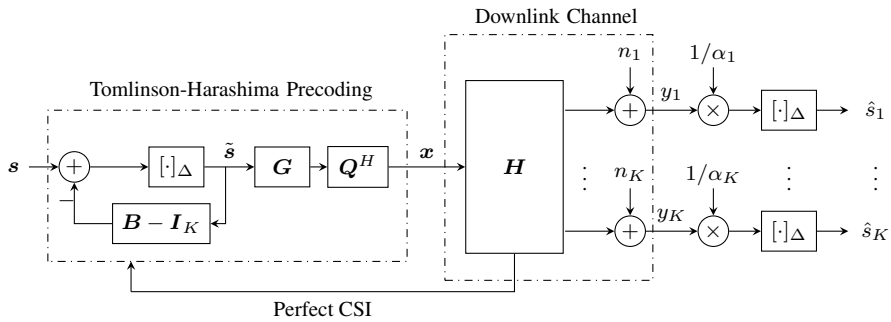

Figure 9.1: The model of the downlink channel with Tomlinson-Harashima precoding.

9.2 System Model and Preliminaries

In this section, THP with two power allocation schemes is reviewed. The THP sum-rates of the two power allocation schemes are derived for a "correlated channel of size K" defined in [3, Definition 1]. In this type of channel, user $K-1$ and user K are the only correlated pair of users. Perfect channel state information (CSI) is assumed at the BS. We then compare the aforementioned sum-rates with the sum-rate achieved when the BS simply drops one of the correlated users.

9.2.1 Tomlinson-Harashima Precoding

The model for the downlink channel from an M-antenna BS, which uses THP to communicate with K single-antenna users, is shown in Fig. 9.1. The intended zero-mean, uncorrelated and unit variance symbols $\boldsymbol{s} = (s_1, ..., s_K)^T \in \mathbb{C}^{K\times 1}$ are encoded to $\tilde{\boldsymbol{s}} = (\tilde{s}_1, ..., \tilde{s}_K)^T \in \mathbb{C}^{K\times 1}$ by using the feedback filter $\boldsymbol{B} - \boldsymbol{I} \in \mathbb{C}^{K\times K}$ and the modulo operator $[\cdot]_\Delta$ with divisor Δ. Then, by using the power control matrix $\boldsymbol{G} = \text{diag}(\sqrt{d_1}, ..., \sqrt{d_K})$ and feedforward filter $\boldsymbol{Q}^H \in \mathbb{C}^{M\times K}$, the precoded vector $\tilde{\boldsymbol{x}} \in \mathbb{C}^{M\times 1}$ is generated (for more details on THP see [41, Sec. 5.4.4]). The average power constraint at the BS is $\mathbb{E}[\|\boldsymbol{x}\|^2] = P_{\text{tot}}$. The transmitted vector $\boldsymbol{x}$ at the BS goes through the channel $\boldsymbol{H} = (\boldsymbol{h}_1, ..., \boldsymbol{h}_K)^T \in \mathbb{C}^{K\times M}$, where $\boldsymbol{h}_i$ is the channel vector from the BS to user i.

For THP, the LQ decomposition of the channel $\boldsymbol{H} = \boldsymbol{LQ}$ is used, where $\boldsymbol{Q}^H$ is used for the feedforward filter, and $\boldsymbol{L}$ is a lower triangular matrix with positive diagonal elements l_{ii}. The matrix $\boldsymbol{L}$ is used to find $\boldsymbol{B} = \boldsymbol{LG}$ for the feedback filter. The received signal for user i can be shown to be:

$$y_i = l_{ii}\sqrt{d_i}\tilde{s}_i + \sum_{j=1}^{i-1} l_{ij}\sqrt{d_j}\tilde{s}_j + n_i, \tag{9.1}$$

where n_i is complex AWGN noise with variance N_0. By using the scalar $\alpha_i = l_{ii}\sqrt{d_i}$, and using the modulo operator at the receiver, the estimated symbol for user i is:

$$\hat{s}_i = \left[\frac{y_i}{\alpha_i}\right]_\Delta = \left[\tilde{s}_i + \sum_{j=1}^{i-1} \frac{l_{ij}\sqrt{d_j}}{\alpha_i}\tilde{s}_j + \frac{n_i}{\alpha_i}\right]_\Delta . \tag{9.2}$$

By encoding $\tilde{s}_i = [s_i - \sum_{j=1}^{i-1} \frac{l_{ij}\sqrt{d_j}}{\alpha_i}\tilde{s}_j]_\Delta$ (see the feedback loop in Fig. 9.1), the estimated symbol becomes:

$$\hat{s}_i = \left[s_i + \frac{n_i}{\alpha_i}\right]_\Delta . \tag{9.3}$$

In high signal to noise ratios (SNRs), the modulo loss [53] can be ignored. Therefore, the following sum-rate (in bits/channel use) is achieved using inflated lattice strategies [54], where the shaping loss is neglected:

$$R_{\text{THP}} = \sum_{i=1}^{K} \log_2\left(1 + \frac{d_i}{N_0} l_{ii}^2\right). \tag{9.4}$$

Max-min power control coefficients are found by maximizing the minimum SNR among the users as:

$$d_{i,\text{max-min}} = \frac{P_{\text{tot}}}{l_{ii}^2 \sum_{j=1}^{K} \frac{1}{l_{jj}^2}}, \quad i = 1, ..., K. \tag{9.5}$$

The equal received power control coefficients considering the difference in the channel norms of the users are found by:

$$d_{i,\text{equ.}} = \frac{P_{\text{tot}}}{\|\boldsymbol{h}_i\|^2 \sum_{j=1}^{K} \frac{1}{\|\boldsymbol{h}_j\|^2}}. \tag{9.6}$$

In the case of mutual orthogonality among the K users, $d_{i,\text{max-min.}}$ and $d_{i,\text{equ.}}$ are equivalent since $l_{ii}^2 = \|\boldsymbol{h}_i\|^2$ (see Appendix 9.5 for more details). In this case, each user achieves the same SNR denoted by γ:

$$\gamma = \frac{P_{\text{tot}}}{N_0 \sum_{i=1}^{K} \frac{1}{\|\boldsymbol{h}_i\|^2}}. \tag{9.7}$$

For THP, the order of users for encoding $\boldsymbol{s}$ to $\tilde{\boldsymbol{s}}$ has to be optimized to maximize the sum-rate given the power control schemes. In this paper, the algorithm described in [41, Sec. 5.4.5] is used for THP with max-min power control to find an appropriate order of users. For equal received power control, we use the algorithm in [41, Sec. 5.4.8].

9.2.2 Sum-Rate Comparison

Consider a correlated channel of size K with the spatial correlation given by:

$$\rho = \frac{\boldsymbol{h}_K^H \boldsymbol{h}_{K-1}}{\|\boldsymbol{h}_K\| \|\boldsymbol{h}_{K-1}\|}, \tag{9.8}$$

where without loss of generality we assume that $\|h_{K-1}\| \geq \|h_K\|$. If the BS drops user (DU) K,[2] user 1 to user $K-1$ will experience FP. Thus, due to mutual orthogonality of the users, the following sum-rate R_{DU} is achieved (with either max-min or equal received power control) using (9.7) for $K-1$ users:

$$R_{\text{DU}} = (K-1)\log_2\left(1 + \frac{P_{\text{tot}}}{N_0 \sum_{i=1}^{K-1} \frac{1}{\|\boldsymbol{h}_i\|^2}}\right). \tag{9.9}$$

If the BS does not drop user K, the following sum-rates are achieved replacing (9.5) and (9.6) in (9.4):

$$R_{\text{max-min}} = K\log_2\left(1 + \frac{P_{\text{tot}}}{N_0 \sum_{i=1}^{K} \frac{1}{l_{ii}^2}}\right), \tag{9.10}$$

$$R_{\text{equ.}} = \sum_{i=1}^{K} \log_2\left(1 + \frac{P_{\text{tot}} l_{ii}^2}{N_0 \sum_{j=1}^{K} \frac{\|\boldsymbol{h}_i\|^2}{\|\boldsymbol{h}_j\|^2}}\right). \tag{9.11}$$

Max-min power control equalizes the SNR among the users by sacrificing the good users for the worst users. However, equal received power control only takes the channel norms into account, which is not as strict as max-min power control. Thus, it is expected that max-min power control achieves a lower sum-rate compared to equal received power control, i.e., $R_{\text{max-min}} \leq R_{\text{equ.}}$. In Fig. 9.2, R_{DU}, $R_{\text{max-min}}$, and $R_{\text{equ.}}$ are shown as a function of $|\rho|$ for a correlated channel of size $K = 3$, where the users have the same channel norms (i.e., $\|\boldsymbol{h}_1\| = \|\boldsymbol{h}_2\| = \|\boldsymbol{h}_3\|$). The horizontal black line shows R_{DU}, where the BS drops one of the correlated users regardless of $|\rho|$. For low $|\rho|$, $R_{\text{max-min}}$ (blue curve) and $R_{\text{equ.}}$ (red curve) are above R_{DU} since the users are almost orthogonal, and there is no need for dropping. By increasing $|\rho|$, both $R_{\text{max-min}}$ and $R_{\text{equ.}}$ reduce. When $|\rho| > \rho_{\text{max-min}}$ (shown by a black circle), $R_{\text{max-min}}$ falls below R_{DU}. Thus, the BS with max-min power control should drop the user only when $|\rho| > \rho_{\text{max-min}}$ to avoid the loss in the sum-rate (blue shaded area). Similarly, when $|\rho| > \rho_{\text{equ.}}$ (shown by a black circle), $R_{\text{equ.}}$ falls below R_{DU}, and the BS with equal received power control should drop the user. When $|\rho| \to 1$, $R_{\text{max-min}}$ converges to 0 bits/channel use (shown by a black square), which shows it is essential for the BS with the max-min power control to drop

[2] Dropping user K, results in a higher R_{DU} when $\|\boldsymbol{h}_{K-1}\| > \|\boldsymbol{h}_K\|$. In case of $\|\boldsymbol{h}_{K-1}\| = \|\boldsymbol{h}_K\|$, user $K-1$ or user K can be dropped.

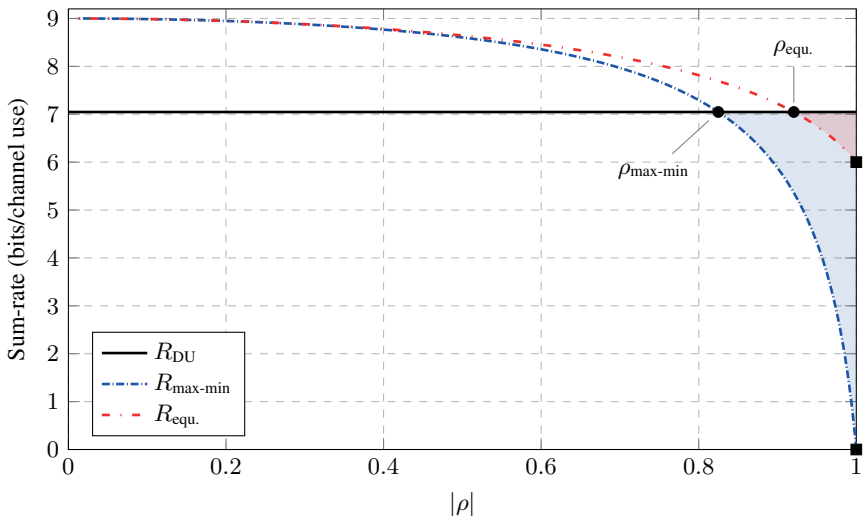

Figure 9.2: R_{DU} (9.9), $R_{\text{max-min}}$ (9.10), and R_{equ} (9.11) as a function of $|\rho|$ for a correlated channel of size 3 when $M = 100$ and $\gamma = 7$. The blue (red) shaded area shows the extra sum-rate that the BS can achieve by dropping the user with max-min power control (equal received power control).

the correlated users. However, when $|\rho| \to 1$, $R_{\text{equ.}}$ becomes close to 6 bits/channel use (shown by a black square). By dropping the user when $|\rho| > \rho_{\text{max-min}}$ ($|\rho| > \rho_{\text{equ.}}$), the BS can achieve R_{DU}, which shows that the sum-rate with max-min power control (or equal received power) is maximized. Comparing the sum-rates reveals the goal of the CD algorithm, which is to drop the correlated user only when it leads to a higher sum-rate for the remaining users with a given power allocation scheme.

9.3 Analytical Thresholds for the CD algorithm

In this section, analytical expressions for the thresholds $\rho_{\text{max-min}}$ and $\rho_{\text{equ.}}$ are derived for a correlated channel of size K, which has only one pair of correlated users. Then, simulations are presented to study the derived thresholds and how the CD algorithm performs with the derived thresholds for channels with multiple pairs of correlated users.

9.3.1 Analytical Expressions for the Thresholds

The following Theorem gives the optimal dropping strategy in terms of the THP sum-rate with max-min and equal received power control.

Theorem 9.1. Consider a correlated channel of size K, with spatial correlation ρ between user $K-1$ and user K ($\|\boldsymbol{h}_{K-1}\| \geq \|\boldsymbol{h}_K\|$). The sum-rate with max-min and equal received power control is maximized if the BS drops user K, when $|\rho| > \rho_{\text{max-min}}$ and $|\rho| > \rho_{\text{equ.}}$, respectively, where

$$\rho^2_{\text{max-min}} = 1 - \frac{1}{\|\boldsymbol{h}_K\|^2 \left(\frac{P_{\text{tot}}}{N_0(2^a-1)} - \sum_{j=1}^{K-1} \frac{1}{\|\boldsymbol{h}_j\|^2} \right)}, \tag{9.12}$$

with $a = R_{\text{DU}}/K$ (R_{DU} is given by (9.9)), and

$$\rho^2_{\text{equ.}} = 1 - \frac{N_0 \eta (2^b - 1)}{P_{\text{tot}}}, \tag{9.13}$$

with $\eta = \sum_{i=1}^{K} \frac{1}{\|\boldsymbol{h}_i\|^2}$, and b:

$$b = R_{\text{DU}} - (K-1)\log_2\left(1 + \frac{P_{\text{tot}}}{N_0 \eta}\right). \tag{9.14}$$

Proof. See Appendix 9.5. □

The derivation of thresholds is true for any channel matrix with only one pair of correlated users. Our emphasis is on LOS environments in which there is a nonnegligible probability that a few users become correlated [39, Sec. 4.3].

9.3.2 Simulation Results

In this section, the derived thresholds in Theorem 9.1 are studied as a function of γ. Then, the use of the derived thresholds in the CD algorithm for channels with multiple pairs of correlated users is studied. The details of the simulation scenario are as follows. A BS with a uniform linear array of $M = 100$ antennas with a half-wavelength spacing is assumed, which serves $K = 10$ single-antenna users. A single-cell is assumed with a field-of-view of $[30°, 150°]$. The carrier frequency is set to 30 GHz. The users are uniformly distributed at the cell-edge (200 m) to study the worst-case performance of the system (with no shadowing). The minimum distance between two users is assumed to be a wavelength. For LOS environments, we use [35, eq. (7.26)] for the channel matrix.

Fig. 9.3 shows $\rho_{\text{max-min}}$ (see (9.12)) and $\rho_{\text{equ.}}$ (see (9.13)) as a function of γ for $K = 10$. As can be seen in Fig. 9.3, by increasing γ, both $\rho_{\text{max-min}}$ and $\rho_{\text{equ.}}$ increase. This is due to using a higher transmit power at the BS, which can overcome a higher correlation. Furthermore, $\rho_{\text{equ.}}$ is higher than $\rho_{\text{max-min}}$ for all SNRs. More importantly, by increasing γ, $\rho_{\text{equ.}}$ converges to 1, which means that dropping the correlated user may not be required for equal received power control at high SNRs.

The CD algorithm is applied on 100000 realizations of the channel to find the cumulative distribution function (CDF) of THP sum-rate. In Fig. 9.4, the CDF of the THP sum-rate with max-min power control with no dropping is compared to CD algorithm with

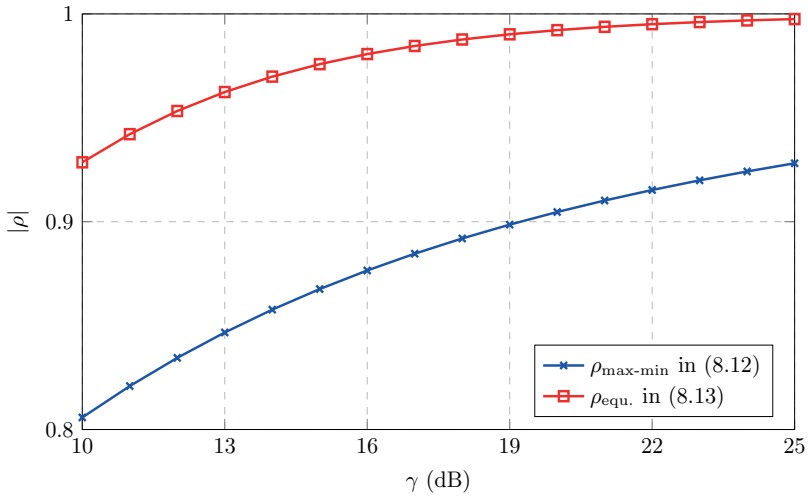

Figure 9.3: The thresholds for the max-min $\rho_{\text{max-min}}$ (9.12) and equal received power control $\rho_{\text{equ.}}$ (9.13) as a function of γ for $K = 10$.

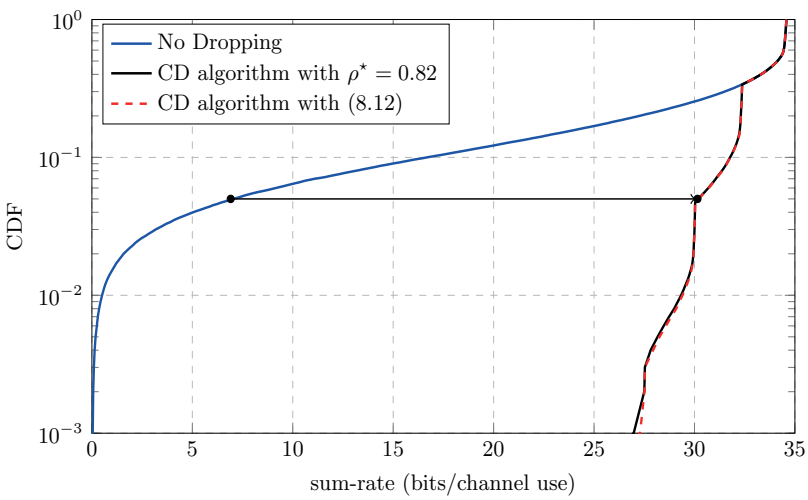

Figure 9.4: CDF of THP sum-rate with max-min power control with no dropping, compared to CD algorithm with two different thresholds for $K = 10$, $M = 100$, and $\gamma = 10$. The first threshold is found by (9.12), whereas the second threshold $\rho^\star = 0.82$ is found by repeating the simulations. The arrow shows the improvement of the 5th percentile sum-rate by using CD algorithm.

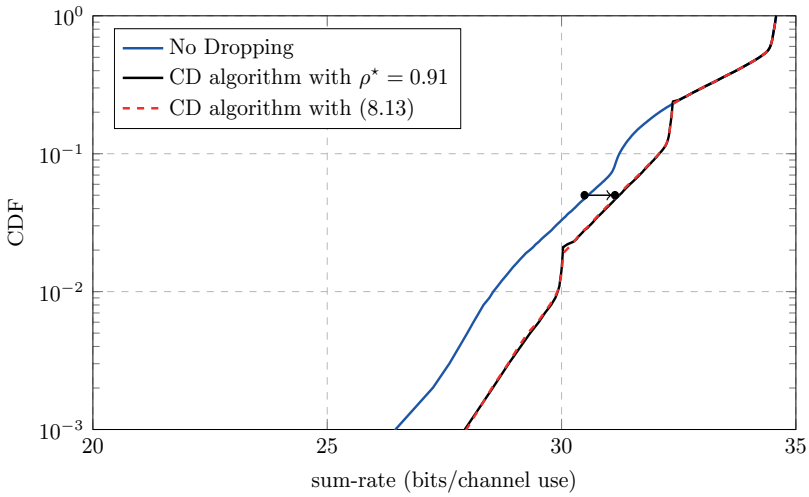

Figure 9.5: Same as Fig. 9.4 for equal received power control with $\rho^\star = 0.91$.

two different thresholds. The first threshold denoted by $\rho^\star$ is found by repeating the simulations to maximize the 5th percentile sum-rate, whereas the second threshold is found by (9.12). The same curves are presented for equal received power control in Fig. 9.5. In Fig. 9.4 and Fig. 9.5, the 5th percentile sum-rates are shown by black circles. As can be seen in Fig. 9.4, dropping the correlated users is essential for the max-min power control since the 5th percentile sum-rate is improved from 6.91 to 30.16 bits/channel use. This very high improvement is due to the max-min criterion in which the users are sacrificed for the highly correlated users (see the blue shaded area in Fig. 9.2). On the other hand, the 5th percentile sum-rate for equal received power control is improved from 30.49 to only 31.15 bits/channel use (see Fig. 9.5). This improvement can be explained by the red shaded area in Fig. 9.2. Furthermore, as can be seen in Fig. 9.4 and 9.5, the obtained CDF using the derived threshold for the CD algorithm, almost overlaps with the CDF obtained by $\rho^\star$ for both power allocation schemes.

9.4 Conclusions

In this paper, a previously proposed dropping algorithm for LOS massive MIMO is combined with THP with max-min and equal received power control. The main contribution of our paper is to derive analytical thresholds for the CD algorithm with THP, which avoids extensive numerical simulations. The derived thresholds are optimal when there is only one correlated pair of users. For scenarios with multiple pairs of correlated users, simulation results showed that using the derived thresholds for the drop-

ping algorithm has near-optimum performance. Furthermore, simulation results showed the CD algorithm with the derived threshold improved the 5th percentile sum-rate for both max-min and equal received power control, while the improvement for the max-min power control was much higher due to the max-min criterion. Thus, using the CD algorithm with the derived threshold is essential for max-min power control.

9.5 Proof of Theorem 9.1

To derive $l_{ii}^2, i = 1, ..., K$ for a correlated channel of size K, recall the LQ decomposition of the channel $\boldsymbol{H} = \boldsymbol{LQ}$. Then, $\boldsymbol{HH}^H = \boldsymbol{LQQ}^H\boldsymbol{L}^H = \boldsymbol{LL}^H$. For a correlated channel of size K, the diagonal elements of $\boldsymbol{HH}^H$ are $\|\boldsymbol{h}_i\|^2$ and the off-diagonal elements are 0 except:

$$\left[\boldsymbol{HH}^H\right]_{K-1,K} = \left[\boldsymbol{HH}^H\right]^H_{K,K-1} = \|\boldsymbol{h}_{K-1}\|\|\boldsymbol{h}_K\|\rho. \tag{9.15}$$

By comparing the first $K-2$ rows of $\boldsymbol{HH}^H$ and $\boldsymbol{LL}^H$, the corresponding elements of $\boldsymbol{L}$ are found. The diagonal elements of $\boldsymbol{LL}^H$ are found as $l_{ii}^2 = \|\boldsymbol{h}_i\|^2, i = 1, ..., K-2$, and all the off-diagonal elements of $\boldsymbol{LL}^H$ are 0 for $i = 1, ..., K-2$. By comparing the last two rows of $\boldsymbol{HH}^H$ and $\boldsymbol{LL}^H$, l_{K-1K-1}, l_{KK} and l_{KK-1} are found. This is done by introducing the following matrices:

$$\boldsymbol{A} = \begin{bmatrix} \|\boldsymbol{h}_{K-1}\|^2 & \|\boldsymbol{h}_{K-1}\|\|\boldsymbol{h}_K\|\rho \\ \|\boldsymbol{h}_{K-1}\|\|\boldsymbol{h}_K\|\rho^H & \|\boldsymbol{h}_K\|^2 \end{bmatrix}, \tag{9.16}$$

and

$$\boldsymbol{B} = \begin{bmatrix} l_{K-1K-1}^2 & l_{K-1K-1}l_{K-1K}^H \\ l_{K-1K-1}^H l_{K-1K} & |l_{K-1K}|^2 + l_{KK}^2 \end{bmatrix}. \tag{9.17}$$

By solving $\boldsymbol{B} = \boldsymbol{A}$ for l_{K-1K-1} and l_{KK}, the following solutions are found as:

$$l_{K-1K-1}^2 = \|\boldsymbol{h}_{K-1}\|^2, \;\; l_{KK}^2 = \|\boldsymbol{h}_K\|^2(1-|\rho|^2). \tag{9.18}$$

Thus, the diagonal elements of $\boldsymbol{LL}^H$ are found as $l_{ii}^2 = \|\boldsymbol{h}_i\|^2, i = 1, ..., K-1$ and $l_{KK}^2 = \|\boldsymbol{h}_K\|^2(1-|\rho|^2)$. Next step is to solve $R_{\text{DU}} \geq R_{\text{max-min}}$ for $\rho_{\text{max-min}}$ using (9.9) and (9.10) for the sum-rates and using the derived l_{ii}^2. Therefore, the following inequality is solved for $\rho_{\text{max-min}}$:

$$R_{\text{DU}} > K\log_2\left(1 + \frac{P_{\text{tot}}}{N_0\sum_{i=1}^K \frac{1}{l_{ii}^2}}\right). \tag{9.19}$$

By defining $a = R_{\text{DU}}/K$, we have:

$$(2^a - 1) > \frac{P_{\text{tot}}}{N_0\sum_{i=1}^K \frac{1}{l_{ii}^2}} \Rightarrow \frac{P_{\text{tot}}/N_0}{(2^a-1)} < \sum_{i=1}^K \frac{1}{l_{ii}^2}. \tag{9.20}$$

By replacing l_{ii}^2, (9.20) is simplified to:

$$\begin{aligned} \frac{P_{\text{tot}}/N_0}{(2^a-1)} &< \frac{1}{\|\boldsymbol{h}_K\|^2(1-|\rho|^2)} + \sum_{i=1}^{K-1} \frac{1}{\|\boldsymbol{h}_i\|^2} \\ \frac{P_{\text{tot}}/N_0}{(2^a-1)} - \eta_1 &< \frac{\eta_2}{1-|\rho|^2}, \end{aligned} \tag{9.21}$$

where $\eta_1 = \sum_{i=1}^{K-1} \frac{1}{\|\boldsymbol{h}_i\|^2}$ and $\eta_2 = \frac{1}{\|\boldsymbol{h}_K\|^2}$. If we assume that $\frac{P_{\text{tot}}/N_0}{(2^a-1)} - \eta_1 > 0$, (9.21) is simplified to:

$$\frac{\eta_2}{\frac{P_{\text{tot}}/N_0}{(2^a-1)} - \eta_1} > 1 - |\rho|^2 \Rightarrow |\rho|^2 > 1 - \frac{\eta_2}{\frac{P_{\text{tot}}/N_0}{(2^a-1)} - \eta_1}. \tag{9.22}$$

To show the assumption is always true, we need to show:

$$\frac{P_{\text{tot}}/N_0}{(2^a-1)} - \eta_1 > 0 \Rightarrow \frac{P_{\text{tot}}}{\eta_1 N_0} > (2^a-1). \tag{9.23}$$

We need to simplify 2^a:

$$2^a = 2^{\frac{(K-1)}{K}\log_2\left(1+\frac{P_{\text{tot}}}{N_0\eta_1}\right)} = \left(1+\frac{P_{\text{tot}}}{N_0\eta_1}\right)^{\frac{(K-1)}{K}}. \tag{9.24}$$

Therefore, using (9.24), (9.23) is simplified to:

$$1+\frac{P_{\text{tot}}}{\eta_1 N_0} > \left(1+\frac{P_{\text{tot}}}{N_0\eta_1}\right)^{\frac{(K-1)}{K}}, \tag{9.25}$$

which is always true. Thus, by replacing η_1 and η_2 in (9.22), (9.12) is achieved.

For the equal received power control, $\rho_{\text{equ.}}$ is found by solving $R_{\text{DU}} > R_{\text{equ.}}$ as follows:

$$R_{\text{DU}} > \sum_{i=1}^{K} \log_2\left(1+\frac{P_{\text{tot}} l_{ii}^2}{N_0\left(\sum_{j=1}^{K}\frac{\|\boldsymbol{h}_i\|^2}{\|\boldsymbol{h}_j\|^2}\right)}\right). \tag{9.26}$$

By using the derived l_{ii}, (9.26) is simplified to:

$$R_{\text{DU}} > \log_2\left(1+\frac{P_{\text{tot}}(1-|\rho|^2)}{N_0\eta}\right) + \sum_{i=1}^{K-1}\log_2\left(1+\frac{P_{\text{tot}}}{N_0\eta}\right), \tag{9.27}$$

where $\eta = \sum_{i=1}^{K}\frac{1}{\|\boldsymbol{h}_i\|^2}$. Furthermore, by defining:

$$b = R_{\text{DU}} - (K-1)\log_2\left(1+\frac{P_{\text{tot}}}{N_0\eta}\right), \tag{9.28}$$

(9.27) is simplified to:

$$\begin{aligned} 2^b &> \left(1 + \frac{P_{\text{tot}}(1-|\rho|^2)}{N_0\eta}\right) \\ \frac{N_0\eta(2^b-1)}{P_{\text{tot}}} &> 1-|\rho|^2 \Rightarrow |\rho|^2 > 1 - \frac{N_0\eta(2^b-1)}{P_{\text{tot}}}, \end{aligned} \tag{9.29}$$

which results in (9.13). □

CHAPTER 10

Paper F
DropNet: An Improved Dropping Algorithm Based On Neural Networks for Line-of-Sight Massive MIMO

Abstract

In line-of-sight massive MIMO, the downlink channel vectors of few users may become highly correlated. This high correlation limits the sum-rates of systems employing linear precoders. To constrain the reduction of the sum-rate, few users can be dropped and served in the next coherence intervals. The optimal strategy for selecting the dropped users can be obtained by an exhaustive search at the cost of high computational complexity. To alleviate the computational complexity of the exhaustive search, a correlation-based dropping algorithm (CDA) is conventionally used, incurring a sum-rate loss with respect to the optimal scheme. In this paper, we propose a dropping algorithm based on neural networks (DropNet) to find the set of dropped users. We use appropriate input features required for the user dropping problem to limit the complexity of DropNet. DropNet is evaluated using two known linear precoders: conjugate beamforming (CB) and zero-forcing (ZF). Simulation results show that DropNet provides a trade-off between complexity and sum-rate performance. In particular, for a 64-antenna base station and 10 single-antenna users: (i) DropNet reduces the computational complexity of the exhaustive search by a factor of 46 and 3 for CB and ZF, respectively, (ii) DropNet improves the

5th percentile sum-rate of CDA by 0.86 and 2.33 bits/s/Hz for CB and ZF, respectively.

10.1 Introduction

The mutual orthogonality of the channel vectors from the base station (BS) to the users is known as favorable propagation (FP) [39]. Line-of-sight (LOS) environments exhibit FP both in theory and practice [33, 71]. There are important use cases (e.g., stadiums or exhibitions), in which the channel vectors of some users become highly correlated [32], which in turn results in a non-FP environment. In these non-FP environments, the high correlation yields a reduction in the achievable sum-rates of linear precoders [70, 71]. In particular, this reduction is non-negligible when the max-min power control is employed due to the fairness criterion, as shown in our previous papers [3, 4].

To limit the reduction in the achievable sum-rates of linear precoders, a correlation-based dropping algorithm (CDA) for LOS environments with max-min power control is proposed in [33]. In CDA, the BS drops a few users to constrain the spatial correlations between the remaining users up to a predefined threshold, which is optimized using extensive simulations. We previously derived this threshold for two known linear precoders: (i) conjugate beamforming (CB) and (ii) zero-forcing (ZF) in [3], and for a known non-linear precoder, i.e., Tomlinson-Harashima precoding [52, 94] in [4]. Employing CDA with the thresholds given in [3, 4] for channels with only one pair of correlated users (any other pairs are orthogonal) yields the optimal dropping strategy. However, when there are more than one pair of correlated users, the CDA approach is suboptimal. The optimal strategy in such a scenario can be found via an exhaustive search at the cost of significantly high computational complexity. Therefore, a low-complex yet near-optimal dropping strategy is required when there are more than one pair of correlated users. To the best of our knowledge, this problem has not been studied in the literature.

In this paper, we propose a dropping algorithm based on neural networks (DropNet) to find the set of dropped users that maximizes the achievable sum-rate of the remaining users with max-min power control. DropNet is inspired by the universal function approximation property of neural networks (NNs) [95–97]. By employing NN, we study the user dropping problem in a general scenario for LOS massive MIMO, when there might be more than one pair of correlated users. We find appropriate input features for the NN by studying the signal to noise plus interference ratio (SINR) of CB and ZF. We treat the user dropping as a classification problem, where each output class of the NN represents a possible set of dropped users. To achieve a near-optimal 5th percentile achievable sum-rate with low complexity compared to the exhaustive search, we adjust the hyperparameters of the NN. DropNet lifts the need for employing a predefined threshold to find the set of dropped users as opposed to [3, 4, 33]. Simulation results for two known linear precoders with max-min power control show that DropNet provides a good trade-off between performance in terms of achievable sum-rate and computational complexity.

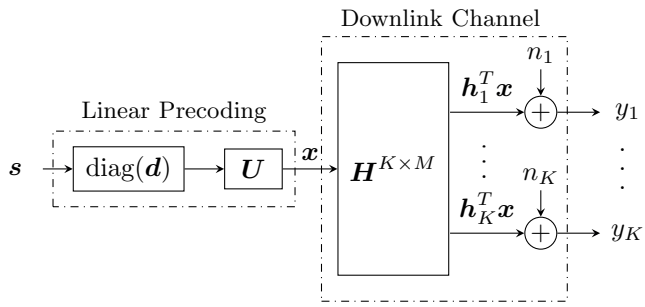

Figure 10.1: The model of the downlink channel with linear precoding.

10.2 System Model

The schematic of the massive MIMO downlink channel with linear precoding is shown in Fig. 10.1, where an M-antenna BS serves K single-antenna users in a time division duplexing manner. The symbol of the users is $\boldsymbol{s} = (s_1, s_2, ..., s_K)^T \in \mathbb{C}^{K\times 1}$, where the components of $\boldsymbol{s}$ are assumed to be zero-mean, uncorrelated, and unit variance. [1] The diagonal power control matrix $\boldsymbol{D} = \text{diag}(\boldsymbol{d})$ and a linear precoding matrix $\boldsymbol{U} = (\boldsymbol{u}_1, \boldsymbol{u}_2, ..., \boldsymbol{u}_K) \in \mathbb{C}^{M\times K}$ (with unit-norm column vectors $\boldsymbol{u}_i$) precode $\boldsymbol{s}$ to $\boldsymbol{x} \in \mathbb{C}^{M\times 1}$. The power control vector $\boldsymbol{d} = (\sqrt{d_1}, \sqrt{d_2}, ..., \sqrt{d_K})^T$ has the coefficients $d_i \in \mathbb{R}^+$ with $i = 1, 2, ..., K$ with the total power constraint $\sum_{i=1}^{K} d_i = P$. The transmit vector $\boldsymbol{x}$ is found by

$$\boldsymbol{x} = \boldsymbol{U}\boldsymbol{D}\boldsymbol{s}. \tag{10.1}$$

Then, $\boldsymbol{x}$ is transmitted through the propagation channel denoted by $\boldsymbol{H} = (\boldsymbol{h}_1, \boldsymbol{h}_2, ..., \boldsymbol{h}_K)^T \in \mathbb{C}^{K\times M}$, where $\boldsymbol{h}_i$ is the channel vector from the BS antennas to user i.

The received signal at user i is given as

$$y_i = \boldsymbol{h}_i^T\boldsymbol{x} + n_i = \boldsymbol{h}_i^T\boldsymbol{u}_i\sqrt{d_i}s_i + \sum_{\substack{j=1\\ j\neq i}}^{K} \boldsymbol{h}_i^T\boldsymbol{u}_j\sqrt{d_j}s_j + n_i, \tag{10.2}$$

where n_i is zero mean complex Gaussian noise with the variance of N_0. Assuming perfect channel state information at the BS, the SINR for user i denoted by γ_i is given as

$$\gamma_i = \frac{|\boldsymbol{h}_i^T\boldsymbol{u}_i|^2 d_i}{\sum_{j=1, j\neq i}^{K} |\boldsymbol{h}_i^T\boldsymbol{u}_j|^2 d_j + N_0}. \tag{10.3}$$

[1] **Notation**: Lowercase, bold lowercase, and bold uppercase letters denote scalars, column vectors, and matrices, respectively. $|\cdot|$ and $\|\cdot\|$ denote the absolute value and l^2-norm operators. The superscripts *, ^{T}, and ^{H} denote complex conjugate, un-conjugated transpose, and conjugated transpose, respectively. diag($\boldsymbol{p}$) denotes a diagonal matrix with diagonal entries taken from $\boldsymbol{p}$. The operator $\otimes$ denotes the kronecker product.

In this paper, we consider two known linear precoders: CB and ZF. To find the precoding matrix $\boldsymbol{U}$ for CB and ZF, we first find $\boldsymbol{G} = \boldsymbol{H}^H$ and $\boldsymbol{G} = \boldsymbol{H}^\dagger = \boldsymbol{H}^H(\boldsymbol{H}\boldsymbol{H}^H)^{-1}$, respectively. The precoding matrix $\boldsymbol{U}$ is then found for each precoder by normalizing $\boldsymbol{G}$ to have unit-norm column vectors, i.e., $\boldsymbol{u}_i = \boldsymbol{g}_i/\|\boldsymbol{g}_i\|$. By replacing CB and ZF filters, the following SINR is obtained for each user:

$$\gamma_i^{\text{CB}} = \frac{\|\boldsymbol{h}_i\|^2 d_i}{\|\boldsymbol{h}_i\|^2 \sum_{j=1,j\neq i}^{K} |\rho_{ij}|^2 d_j + N_0}, \tag{10.4}$$

$$\gamma_i^{\text{ZF}} = \frac{|\boldsymbol{h}_i^T \boldsymbol{u}_i|^2 d_i}{N_0} = \frac{d_i}{\|\boldsymbol{g}_i\|^2 N_0}. \tag{10.5}$$

For a given set of filters $\boldsymbol{u}_i, i = 1, 2, ..., K$, we are interested in finding the coefficients $d_i, i = 1, 2, ..., K$, that maximize the minimum γ_i among the users, which is referred to as max-min power control [42, Sec. 7.1]. Employing the max-min power control equalizes the throughput of all users [33], i.e., $\gamma_i^{\text{CB}} = \gamma^{\text{CB}}$ and $\gamma_i^{\text{ZF}} = \gamma^{\text{ZF}}$ for $i = 1, 2, ..., K$. The power control vector $\boldsymbol{d}^*$ is found by solving

$$\boldsymbol{d}^* = \underset{d_1,d_2,...,d_K \in \mathbb{R}^+}{\text{argmax}} \quad \min_{i\in\{1,2,...,K\}} \quad \gamma_i, \tag{10.6}$$

where γ_i is given by (10.3). To solve (10.6), we use the bi-section method (see [33, Algorithm 2]) for CB, and we use the Lagrangian multiplier for ZF.

10.3 DropNet: Proposed Dropping Algorithm Based On Neural Networks

In this section, we present details of DropNet. DropNet is designed to find the set of users that shall be dropped such that the achievable sum-rate of the remaining users is maximized. At the end of this section, a complexity analysis is given to compare the complexity of DropNet with the exhaustive search and the previous CDA.

10.3.1 Design Methodology

We model the user dropping as a classification problem. In the classification problem, we consider one class representing the case where no user is dropped, $\binom{K}{i}$ classes representing the cases where i users out of K users are dropped. We assume $1 \leq i \leq n_{\text{max}}$, where n_{max} is the maximum number of users that we allow to be dropped. Overall, the total number of classes is

$$n_{\text{out}} = 1 + \binom{K}{1} + \binom{K}{2} + ... + \binom{K}{n_{\text{max}}}. \tag{10.7}$$

Each class denotes a neuron in the output layer. Thus, the number of neurons corresponding to the output layer is n_{out}.

We choose the inputs of the NN as follows assuming a real-valued NN. For a given channel realization $\boldsymbol{H}$, the chosen inputs should correspond to a meaningful metric related to the users to be dropped. Moreover, as will be shown in Sec. 10.3.2, the computational complexity of the resulting NN is directly related to the number of input and output neurons. Therefore, the number of inputs should be as small as possible. In general, for a fixed transmit power P, one can employ the elements of $\boldsymbol{H}$ as the inputs of the NN, as $\boldsymbol{H}$ contains all the information required for the dropping algorithm. However, the number of elements of $\boldsymbol{H}$ is $2MK$,[2] which scales linearly with both the number of antennas M and the number of users K. This is not desirable because in massive MIMO $M >> K$. Thus, it is beneficial to find appropriate input features for which the number of input nodes does not scale with M. Previous dropping algorithms [3, 4, 33] use the absolute value of the pair-wise normalized spatial correlation of the users ρ_{ij}

$$\rho_{ij} = \frac{\boldsymbol{h}_j^H \boldsymbol{h}_i}{\|\boldsymbol{h}_i\|\|\boldsymbol{h}_j\|}, \quad i, j \neq i \in \{1, 2, ..., K\}, \tag{10.8}$$

to drop some of the users. There are $\binom{K}{2}$ values of $|\rho_{ij}|$, i.e., $(K^2 - K)/2$, which is much less than $2MK$ values of $\boldsymbol{H}$. Thus, $|\rho_{ij}|$ values are possible candidates for the inputs of the NN. By studying (10.4) and (10.5), we propose to use $|\rho_{ij}|$ and $\|\boldsymbol{h}_i\|^2$ as the input features of the NN as explained in the following.

To find the SINR for CB as in (10.4), we need to use bisection method to find the power control coefficients, for which $\|\boldsymbol{h}_i\|$ and $|\rho_{ij}|$ are required. Therefore, $\|\boldsymbol{h}_i\|$ and $|\rho_{ij}|$ provide enough information to find the set of dropped users for CB. To find the SINR for ZF as in (10.5), we need to use Lagrangian multiplier to find the power control coefficients for which $\|\boldsymbol{g}_i\|^2$ the diagonal elements of $(\boldsymbol{H}\boldsymbol{H}^H)^{-1}$ are required. To compute the diagonal elements of $(\boldsymbol{H}\boldsymbol{H}^H)^{-1}$, we need $\|\boldsymbol{h}_i\|$ and ρ_{ij}. Thus, for ZF, we need the complex values of ρ_{ij} rather than $|\rho_{ij}|$ as for CB. However, by using $|\rho_{ij}|$ instead of ρ_{ij}, we can further reduce the number of input nodes for ZF. Thus, in this paper, we use $|\rho_{ij}|$ and $\|\boldsymbol{h}_i\|^2$ as the input features for both CB and ZF. Overall, the number of input nodes becomes:

$$n_{\text{in}} = \binom{K}{2} + K = \frac{K^2 + K}{2}, \tag{10.9}$$

which is much lower than $2MK$. For instance, assuming $K = 10$ and $M = 100$, $\binom{K}{2} + K = 55$, while $2MK = 2000$. We emphasize that by using $|\rho_{ij}|$ and $\|\boldsymbol{h}_i\|^2$ values, we remove the dependency of the number of inputs to M and therefore, reduce the complexity of NN considerably. Hence, such input selection is practical for massive MIMO systems. We investigated different NNs with more than one hidden layer, however, to limit the computational complexity of the designed NN we use only one hidden layer instead. The number of neurons in the hidden layer is the design parameter, which provides a performance-complexity trade-off in DropNet.

[2] Note that the factor 2 is due to considering a real-valued NN.

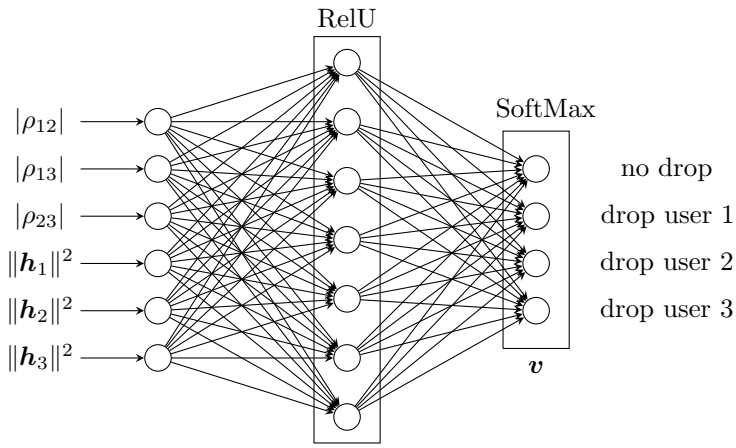

Figure 10.2: The schematic of a NN for DropNet when $K = 3$ and $n_{\text{max}} = 1$ with inputs $|\rho_{12}|, |\rho_{13}|, |\rho_{23}|, \|\boldsymbol{h}_1\|^2, \|\boldsymbol{h}_2\|^2, \|\boldsymbol{h}_3\|^2$ and output one-hot vector $\boldsymbol{v}$.

As an example, the NN of DropNet for $K = 3$, $n_{\text{max}} = 1$ is illustrated in Fig. 10.2. There are $\binom{3}{2} + 3 = 6$ input nodes and there are $1 + \binom{3}{1} = 4$ output nodes with 7 nodes in the hidden layer. In DropNet, we employ "Relu" as the activation function for the hidden layer and "Softmax" as the activation function for the output layer (see Fig. 10.2). The output of Softmax represents the probability of each class for a given set of input features. The output of NN is represented by a one-hot vector $\boldsymbol{v}$ of size $n_{\text{out}} \times 1$, where the component corresponding to the class of dropped users is "1" and all the other components are "0". We employ cross-entropy as the cost function, as NN is used to find the set of dropped users with a high probability. The standard back-propagation algorithm [98] is used for optimizing the parameters of NN.

To train (test) the NN, we generate the training (test) set for a given precoder as follows. We generate a large number of realizations of $\boldsymbol{H}$ for the training (test) set. For each realization of $\boldsymbol{H}$, we compute $\binom{K}{2}$ values of $|\rho_{ij}|$ and K values of $\|\boldsymbol{h}_i\|^2$ associated with $\boldsymbol{H}$. We find the optimal set of dropped users corresponding to $\boldsymbol{H}$ with an exhaustive search. The solution of the exhaustive search is stored as a one-hot vector $\boldsymbol{v}$ of size $n_{\text{out}} \times 1$, where the component corresponding to the class of dropped users is "1" and all the other components are zero. The vector $\boldsymbol{v}$ serves as the NN output corresponding to the computed input nodes. After the training phase, the trained NN is evaluated using the test set. We evaluate the complexity of the designed NN in the sequel.

10.3.2 Complexity Analysis

We first explain the computational complexity of the exhaustive search for CB and ZF precoding, then, we compute the corresponding complexity of DropNet. For the complexity analysis, it is assumed that each complex addition costs 2 floating point operations

(FLOPS) and each complex multiplication costs 6 FLOPS [63]. To drop i out of K users, there are $\binom{K}{i}$ possibilities. In the exhaustive search, one requires to check all possible sets of dropped users. For each set of dropped users, we need to find the SINR with max-min power control of the remaining users to compute the corresponding sum-rate. For CB, it is required to use the bi-section method to compute the max-min SINR denoted by γ^{CB} for the users. At each iteration of the bi-section method, an inverse of a $K \times K$ matrix is required, which entails $K^3/2 + 3K^2/2$ multiplications and $K^3/2 - K^2/2$ additions and K square roots operations[3] [82]. For a given n_{max}, the complexity of the exhaustive search for CB in FLOPS is given as

$$C^{\text{CB}} = \sum_{i=0}^{n_{\text{max}}} \binom{K}{i} I_i (4(K-i)^3 + 8(K-i)^2 + (K-i)), \tag{10.10}$$

where I_i is the number of iterations used to run the bi-section method, which depends on the search interval for γ_{CB} and the required accuracy for γ_{CB} [99, Th. 2.1]. For instance, for $n_{\text{max}} = 2$ and $I_0 = I_1 = I_2 = K$ with accuracy of 0.01, C^{CB} has complexity of $\mathcal{O}(K^6)$.

The max-min SINR for ZF is given as [69, eq. (14)]:

$$\gamma^{\text{ZF}} = \frac{P}{N_0 \operatorname{tr}(\boldsymbol{H}\boldsymbol{H}^H)^{-1}}. \tag{10.11}$$

As can be seen from (10.11), the trace of $(\boldsymbol{H}\boldsymbol{H}^H)^{-1}$ for computing γ_{ZF} needs to be calculated. It is known that the trace of $(\boldsymbol{H}\boldsymbol{H}^H)^{-1}$ is equal to the sum of the eigenvalues of $(\boldsymbol{H}\boldsymbol{H}^H)^{-1}$ [100, Ch. 4]. To find the eigenvalues of $(\boldsymbol{H}\boldsymbol{H}^H)^{-1}$, it is enough to find the eigenvalues of $\boldsymbol{H}\boldsymbol{H}^H$ and then inverse them. Consequently, the computational complexity of evaluating γ^{ZF} is equal to the complexity of finding the eigenvalues of a $K \times K$ symmetric matrix, which is $16/3K^3$ [63]. Overall, the complexity of the exhaustive search for ZF in FLOPS is given as

$$C^{\text{ZF}} = \sum_{i=0}^{n_{\text{max}}} \binom{K}{i} \frac{16}{3} (K-i)^3. \tag{10.12}$$

For instance, for $n_{\text{max}} = 2$, C^{ZF} has complexity of $\mathcal{O}(K^5)$.

The complexity of DropNet depends on the number of multiplications and additions in the forward propagation of the NN at the test phase.[4] We consider real-valued NN, where the multiplications and additions are all real operations. Recall that the input and output layers of NN have n_{in} (see (10.9)) and n_{out} (see (10.7)) neurons. Let us assume that the hidden layer contains l neurons. The number of multiplications for computing the value of a given neuron in the hidden and output layers are n_{in} and l, respectively,

[3] We assume that each square root operation costs 1 FLOP [82].

[4] Back-propagation is performed offline at the training phase, thus, only the complexity of the forward propagation is considered at the test phase.

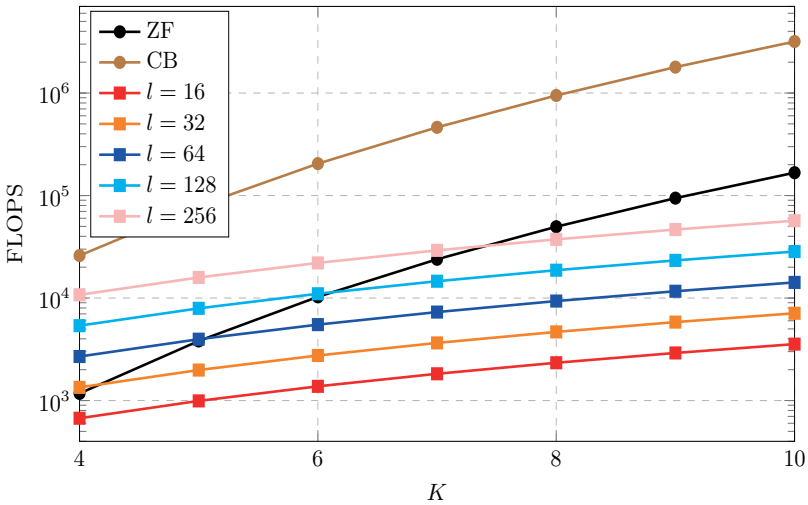

Figure 10.3: The computational complexity of the exhaustive search for CB and ZF compared to the DropNet with different number of nodes (16 to 256) as a function of the number of users K with $n_{\text{max}} = 2$.

rendering a total of $n_{\text{in}}l + ln_{\text{out}}$ multiplications in the forward propagation. Assuming a bias term for the hidden and output layers, the total number of additions in the forward propagation becomes the same as the number of multiplications, i.e., $n_{\text{in}}l + ln_{\text{out}}$. As each real-value multiplication and addition require one FLOP, the total number of FLOPs for the forward propagation is given as

$$\begin{aligned} C^{\text{DropNet}} &= 2n_{\text{in}}l + 2ln_{\text{out}}, \\ &= 2l\left(\frac{K^2+K}{2} + \sum_{i=0}^{n_{\text{max}}}\binom{K}{i}\right) \end{aligned} \tag{10.13}$$

For instance, for $n_{\text{max}} = 2$ and $l = K^2$, C^{DropNet} has complexity of $\mathcal{O}(K^4)$, which is lower than that of CB and ZF for the same n_{max}.

In Fig. 10.3, the complexity (FLOPS) of DropNet as a function of K is compared with that of the exhaustive search for $n_{\text{max}} = 2$ for both CB and ZF. The number of nodes in the hidden layer for DropNet changes from 16 to 256. Although by increasing the number of nodes in the hidden layer, the complexity of DropNet increases, the slope of DropNet is much lower than the exhaustive search for both CB and ZF. To compute the complexity of CB in Fig. 10.3 for a given number of users, we use the average I_i found by running a large number of simulations. For instance for $K = 10$ and accuracy of 0.01, $I_0 = 24.2$, $I_1 = 21.4$ and $I_2 = 19.9$. We use the results in Fig. 10.3 to find an

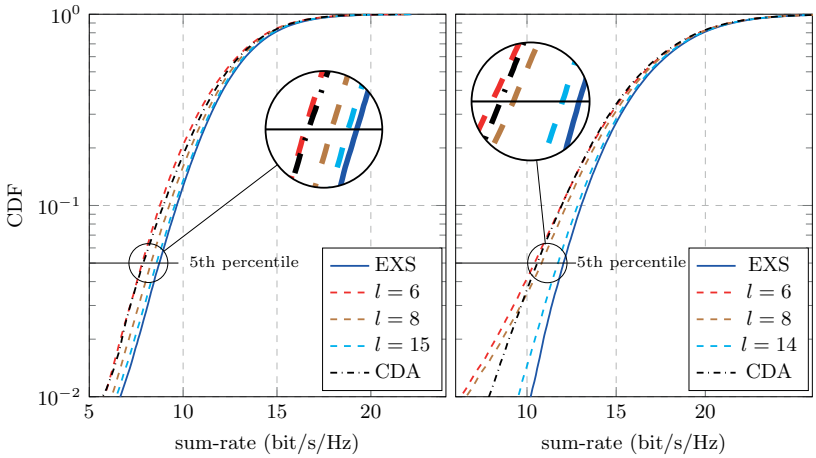

(a) CB (9,4) (b) ZF (9,4)

Figure 10.4: The CDF plots of sum-rates for exhaustive search (EXS), CDA and DropNet with different l when a 3×3 UPA serves 4 users $(M = 9, K = 4)$ with CB and ZF.

appropriate number of neurons for the hidden layer in DropNet that considerably reduces the computational complexity of the exhaustive search.

10.4 Simulation Results

We consider a single-cell massive MIMO, where a BS with a uniform planar array (UPA) of $\sqrt{M} \times \sqrt{M}$ antennas located at x-y plane with half-wavelength spacing (carrier frequency of 30 GHz) serving K single-antenna users. The users are uniformly distributed in the cell (10-200 m). The channel matrix $\boldsymbol{H}$ is computed using the LOS model given in [36, eq. (5)]. Moreover, shadowing effect (log-normal shadow fading with the variance of 12 dB) is considered. The azimuth and elevation angles of the users are uniformly distributed in the intervals $(0, 2\pi)$ and $(0, \pi/2)$, respectively. The minimum distance between two users is set to a wavelength. We set the transmit power (without loss of generality) at the BS such that in FP, $\gamma_{\text{CB}} = \gamma_{\text{ZF}} = 15$ is achieved and we consider $n_{\text{max}} = 2$ for all the dropping algorithms. This means for each dropping algorithm, the maximum number of users that is allowed to be dropped is 2. For the training set 3.9M (97.5% of dataset) and for the test set 100K realizations (2.5% of dataset) of the channels are used. We present the cumulative distribution function (CDF) of CB and ZF achievable sum-rate for DropNet compared to the exhaustive search and previous CDA [3, Algorithm 1].

In Fig. 10.4, the CDF of the sum-rate is shown for CB and ZF for a BS with a 3×3 UPA serving 4 users $(M = 9, K = 4)$ employing the exhaustive search (blue solid line),

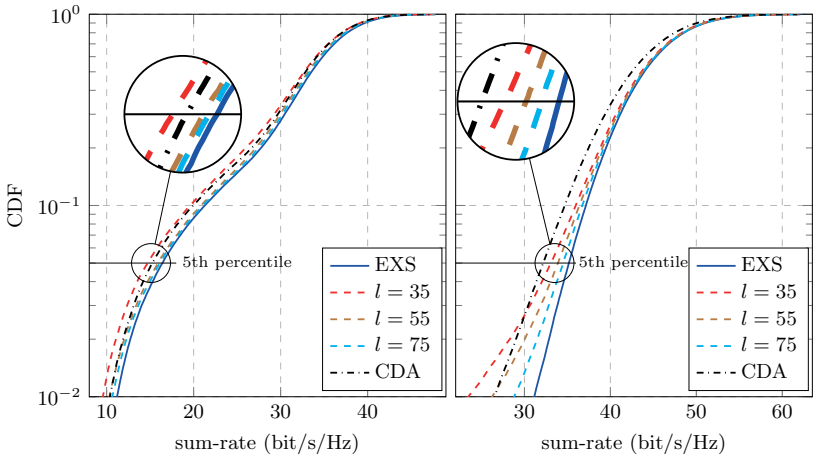

(a) CB (64,10) (b) ZF (64,10)

Figure 10.5: The CDF plots of sum-rates for exhaustive search (EXS), CDA and DropNet with different l when a 8×8 UPA serves 10 users ($M = 64, K = 10$) with CB and ZF.

CDA (black dash-dotted) and DropNet with three different l (dashed lines) to drop some of the users. The 5th percentile sum-rate is magnified for a better comparison for all the scenarios. In addition, in Fig. 10.5, the same curves are presented for a BS with a 8×8 UPA serving 10 users ($M = 64, K = 10$). The following conclusions are inferred from Fig 10.4 and Fig. 10.5. First, there is a gap between the CDF of the sum-rate of the exhaustive search and CDA. Second, by employing DropNet with an appropriate l, one can improve the CDF of CDA and reduce the gap to the exhaustive search. Third, for a given l, the designed NN for CB has a performance much closer to the exhaustive search compared to ZF. For ZF, the gap to the exhaustive search can be further reduced by using ρ_{ij} instead of $|\rho_{ij}|$ as the input features, however, with extra complexity.

We compare the 5th percentile sum-rate of DropNet with a given l with the exhaustive search and CDA in Table 10.1. We use simulation scenarios in Fig. 10.4 and Fig. 10.5. The improvement of DropNet for ZF is more than that of CB for both MIMO systems. In terms of the 5th percentile sum-rate, by employing DropNet, the gap (loss) to the exhaustive search is smaller than the gap (improvement) to CDA. We further compare the computational complexity (FLOPS) of DropNet for a given l with the exhaustive search and CDA in Table 10.2 for the same scenarios as in Table 10.1. Note that computing $|\rho_{ij}|$ for CDA and DropNet costs $8MK^2$ FLOPS. The complexity reduction of DropNet for CB is much more than that of ZF for both MIMO systems. For both CB and ZF, by employing DropNet, the complexity of the exhaustive search is reduced.

The results in Table 10.1 and Table 10.2 show that DropNet provides a 5th percentile sum-rate close to that of the exhaustive search while its complexity is close to

Table 10.1: 5th percentile sum-rate comparison between DropNet, exhaustive search, and CDA dropping schemes for the simulation scenarios of Fig. 10.4 and Fig. 10.5.

Case study	Number of neurons in hidden layer (l)	5th percentile sum rate gap w.r.t. EXS (bit/s/Hz)	5th percentile sum rate improvement w.r.t. CDA (bit/s/Hz)
CB ($M = 9, K = 4$)	15	0.15	0.70
CB ($M = 64, K = 10$)	75	0.30	0.86
ZF ($M = 9, K = 4$)	14	0.31	1.16
ZF ($M = 64, K = 10$)	75	0.67	2.33

Table 10.2: Complexity (FLOPS) comparison between DropNet, exhaustive search, and CDA dropping schemes for the simulation scenarios of Fig. 10.4 and Fig. 10.5. To find the complexity reduction (increase) ratio, we compute (10.10) for CB, (10.12) for ZF and (10.13) for DropNet.

Case study	Number of neurons in hidden layer (l)	Complexity reduction ratio w.r.t. EXS	Complexity increase ratio w.r.t. CDA
CB ($M = 9, K = 4$)	15	14.57	1.55
CB ($M = 64, K = 10$)	75	46.89	1.33
ZF ($M = 9, K = 4$)	14	1.34	1.51
ZF ($M = 64, K = 10$)	75	3.22	1.33

that of CDA. Therefore, DropNet provides an interesting trade-off between complexity and sum-rate performance.

We further present the CDF of sum-rates for CB and ZF in Fig. 10.6 for $M = 64$ and $K = 10$ when there is no shadowing. In this case, the gap between CDA and the exhaustive search is smaller. Similar to the shadowing scenarios, by employing DropNet, we can approach the exhaustive search performance.

10.5 Conclusions

In this paper, a dropping algorithm based on neural networks is proposed for LOS massive MIMO. We show that the proposed dropping algorithm provides a performance-complexity trade-off between conventional correlation-based dropping algorithms and the optimal dropping strategy found by an exhaustive search. The proposed dropping algorithm outperforms the correlation-based dropping algorithm and achieves a 5th percentile sum-rate close to that of the exhaustive search with up to a factor of 46 and 3 lower computational complexity compared to the exhaustive search for CB and ZF, respectively.

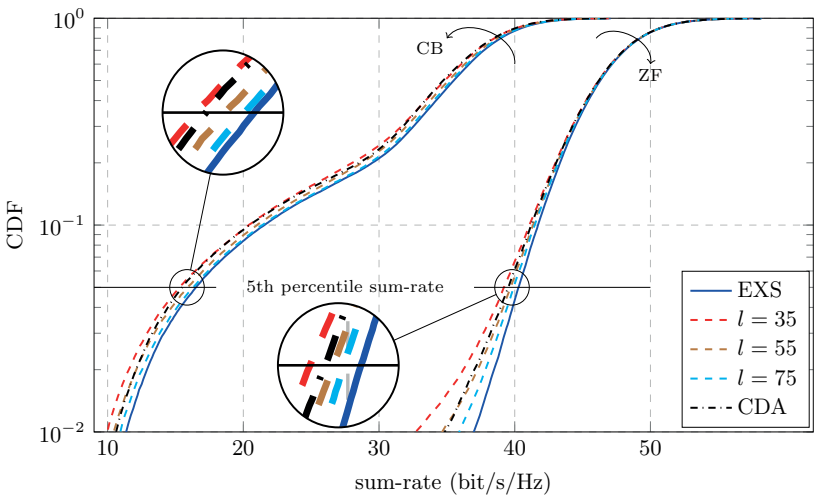

Figure 10.6: The CDF plots of the sum-rates for the exhaustive search (EXS), CDA and DropNet with $l = 35, 55, 75$ when a 8×8 UPA serves 10 users ($M = 64, K = 10$) with CB (left curves) and ZF (right curves) with no shadowing effect.

CHAPTER 11

Paper G
An Improved Successive Filter-Based Dropping Algorithm for Massive MIMO with Max-Min Power Control

Abstract

In line-of-sight massive MIMO, there are use cases where the channel vectors of some users become highly correlated. Highly correlated users lead to a large reduction in the sum-rate of linear and nonlinear precoders with max-min power control. To alleviate the loss in the sum-rate, some users can be dropped and rescheduled. The optimal dropping strategy can be found by an exhaustive search. In this paper, a successive filter-based dropping algorithm (SFDA) is proposed, which improves upon the existing dropping algorithms in the literature. At each step, the user with the highest filter norm is dropped. By comparing the sum-rate of all the steps, the best set of dropped users is found. In contrast to previous threshold-based algorithms in the literature, SFDA does not require a predefined threshold for the spatial correlation of users. Compared to an exhaustive search, the complexity of SFDA is reduced. Simulations results show when a 100 antennas base station serves 10 users, SFDA improves the 5th percentile sum-rate compared to previous algorithms in the literature up to 6 bits/channel use.

11.1 Introduction

When the number of antennas at the base station (BS) of a massive MIMO system increases, the channel vectors from the BS to the users are more likely to become mutually orthogonal. Mutual orthogonality among the channel vectors is known as favorable propagation (FP) [39]. FP is observed both in line-of-sight (LOS) and independent and identically distributed Rayleigh fading environments [33]. In LOS environments, there are some use cases (e.g., "open exhibition") where the channel vectors of a few users become highly correlated [32, 39]. In these highly correlated scenarios, the achievable sum-rates of linear and nonlinear precoders decrease considerably [3, 4, 70, 71].

To avoid the loss in the achievable sum-rates of linear and nonlinear precoders, one can optimize the inter-element spacing of the BS antenna arrays [2] or can use a dropping algorithm to drop and reschedule some of the correlated users [33, 91–93]. For LOS environments with max-min power control, a correlation-based dropping algorithm (CD algorithm) was proposed in [33]. In the CD algorithm of [33], the BS drops a few users and reschedules them in another coherence interval to make the spatial correlation among the channel vectors of the remaining users to be less than a threshold. The threshold is found by rerunning a large number of numerical simulations with the same configuration. A similar method was used in [91, 93]. Instead of predefined thresholds as in [33], thresholds are derived in [3, 4] for conjugate beamforming (CB) and zero-forcing (ZF), and a known nonlinear precoder, i.e., Tomlinson-Harashima precoding (THP) [94] with max-min power control. By using the thresholds in [3, 4] for channels with only one pair of correlated users (the other pairs are mutually orthogonal), the optimal dropping strategy is achieved. However, when there are more correlated pairs of users, the available CDAs may be far from the optimal dropping strategy, which can be found by an exhaustive search. An exhaustive search entails a high computational complexity. In [75], an improved dropping algorithm based on neural networks is proposed, which provides a trade-off between computational complexity and sum-rate performance. Nevertheless, to the best of our knowledge, a low-complexity dropping strategy with a better sum-rate performance has not been proposed in the literature.

In this paper, we propose a novel successive filter-based dropping algorithm (SFDA) for massive MIMO systems with max-min power control. The proposed SFDA finds the set of dropped users such that the achievable sum-rate of the remaining users with max-min power control is maximized. At each step of SFDA, the user with the highest filter norm is dropped. By comparing the sum-rate of all the steps, the best set of dropped users is found.

The main contribution of the paper is to propose a new dropping algorithm for LOS massive MIMO systems that does not require a threshold or any preprocessing. Although the proposed SFDA can be used for non-LOS scenarios, we focus on LOS scenarios in this paper for the following reason. In LOS environments, it is essential to employ dropping algorithms to drop a few users to achieve nearly orthogonal channel vectors [3, 4, 33, 75, 92]. One appealing feature of SFDA is that it allows the selection of the maximum number of users that could be dropped and rescheduled. This number can

be set based on the sum-rate requirements of the users or the computational complexity. By increasing this number, a higher sum-rate can be achieved with more computations, which makes the algorithm flexible as it trades-off performance vs. complexity. Simulation results show that SFDA achieves almost the same performance as an exhaustive search with much lower complexity. For instance, when at maximum two out of K users shall be dropped, the complexity of SFDA is $\mathcal{O}(K^3)$, which is much lower than that of the exhaustive search, which is $\mathcal{O}(K^5)$.

11.2 System Model

The model for the downlink channel with linear precoding for an M-antenna BS that serves K single-antenna users is shown in Fig. 10.1. The intended zero-mean, uncorrelated and unit variance symbols $\boldsymbol{s} = (s_1, s_2, ..., s_K)^T \in \mathbb{C}^{K\times 1}$ are precoded by a diagonal power control matrix $\boldsymbol{D} = \text{diag}(\boldsymbol{d})$ and a linear precoding matrix $\boldsymbol{U} \in \mathbb{C}^{M\times K}$ with unit-norm column vectors $\boldsymbol{u}_i$[1]. The power control vector is $\boldsymbol{d} = (\sqrt{d_1}, \sqrt{d_2}, ..., \sqrt{d_K})^T$, where $d_i \in \mathbb{R}^+$ with $i = 1, 2, ..., K$ are power control coefficients. The radiated power constraint at the BS is $\sum_{i=1}^{K} d_i = P$. The precoded vector $\boldsymbol{x} \in \mathbb{C}^{M\times 1}$ is found by:

$$\boldsymbol{x} = \boldsymbol{U}\boldsymbol{D}\boldsymbol{s}. \tag{11.1}$$

Then, $\boldsymbol{x}$ is transmitted through the wireless channel, which is modeled using a matrix $\boldsymbol{H} = (\boldsymbol{h}_1, \boldsymbol{h}_2, ..., \boldsymbol{h}_K)^T \in \mathbb{C}^{K\times M}$, where $\boldsymbol{h}_i$ is the channel vector from the BS to user i.

The received signal for user i is given by:

$$y_i = \boldsymbol{h}_i^T \boldsymbol{x} + n_i = \boldsymbol{h}_i^T \boldsymbol{u}_i \sqrt{d_i} s_i + \sum_{\substack{j=1 \\ j\neq i}}^{K} \boldsymbol{h}_i^T \boldsymbol{u}_j \sqrt{d_j} s_j + n_i, \tag{11.2}$$

where n_i is complex AWGN noise with variance N_0. Assuming a perfect channel state information for a given channel realization, the signal to noise plus interference ratio (SINR) for each user can be expressed as:

$$\gamma_i = \frac{|\boldsymbol{h}_i^T \boldsymbol{u}_i|^2 d_i}{\sum_{j=1, j\neq i}^{K} |\boldsymbol{h}_i^T \boldsymbol{u}_j|^2 d_j + N_0}. \tag{11.3}$$

For a given set of filters $\boldsymbol{u}_i, i = 1, 2, ..., K$, we are interested in finding the coefficients $d_i, i = 1, 2, ..., K$, that maximize the minimum γ_i among the users, a.k.a., max-min power control:

$$\boldsymbol{d} = \underset{d_1, d_2, ..., d_K}{\text{argmax}} \quad \min_i \quad \gamma_i, \tag{11.4}$$

[1] Lowercase, bold lowercase, and bold uppercase letters denote scalars, column vectors, and matrices, respectively. $|\cdot|$ and $\|\cdot\|$ denote the absolute value and l^2-norm operators. The superscripts *, ^{T}, and ^{H} denote complex conjugate, un-conjugated transpose, and conjugated transpose, respectively. diag($\boldsymbol{p}$) denotes a diagonal matrix with diagonal entries taken from $\boldsymbol{p}$. $\boldsymbol{H}^\dagger$ denotes the pseudo-inverse of the matrix $\boldsymbol{H}$.

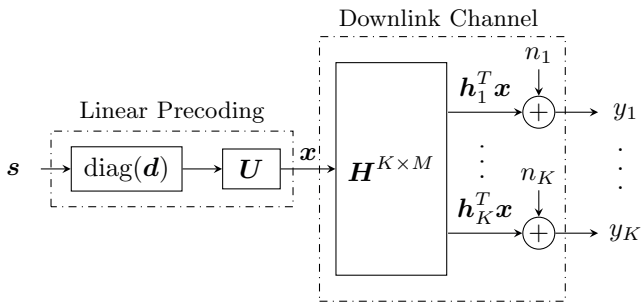

Figure 11.1: The model of the downlink channel with linear precoding.

where γ_i is given by (11.3). Using the max-min power control in (11.4), uniformly good service for all the users is achieved [33].

The ZF filters and corresponding max-min power control are found as follows. The ZF filters $\boldsymbol{u}_i$ are found, by normalizing the ith column of the pseudo-inverse of the channel $\boldsymbol{H}^\dagger = (\boldsymbol{g}_1, \boldsymbol{g}_2, ..., \boldsymbol{g}_K) = \boldsymbol{H}^H(\boldsymbol{H}\boldsymbol{H}^H)^{-1}$ to have a unit-norm column vector. By using the ZF filters $\boldsymbol{u}_i = \frac{\boldsymbol{g}_i}{\|\boldsymbol{g}_i\|}$, (11.3) becomes:

$$\gamma_i = \frac{d_i}{\|\boldsymbol{g}_i\|^2 N_0}. \tag{11.5}$$

By employing Lagrangian multiplier to solve (11.4), the max-min power control coefficients are found to be

$$d_i = \frac{P\|\boldsymbol{g}_i\|^2}{\sum_{j=1}^K \|\boldsymbol{g}_j\|^2}, \tag{11.6}$$

which lead to the following γ for each user:

$$\gamma = \frac{P}{N_0 \sum_{j=1}^K \|\boldsymbol{g}_j\|^2}. \tag{11.7}$$

By employing THP with max-min power control at the BS, one can improve the signal to noise ratio (SNR) at the users compared to linear precoders. By using the results in [4, 41], the following γ is found for the users:

$$\gamma = \frac{P}{N_0 \sum_{j=1}^K \|\boldsymbol{w}_j\|^2}, \tag{11.8}$$

where $\boldsymbol{w}_j$ is the corresponding filter used in THP (see [41, Sec. 5.4.5] for more details). The algorithm described in [41, Fig. 5.18] is used to find an appropriate order of users for THP that maximizes γ among the users.

In the case of mutual orthogonality among the K users, ZF and THP achieve the same SNR denoted by γ_0 as follows:

$$\gamma_0 = \frac{P}{N_0 \sum_{i=1}^{K} \frac{1}{\|\boldsymbol{h}_i\|^2}}. \tag{11.9}$$

For ZF or THP, the sum-rate

$$R = K \log_2 (1 + \gamma) \tag{11.10}$$

can be achieved using (11.7) or (11.8), respectively.

11.3 Proposed SFDA

We are interested in finding the set of up to n_{max} users that shall be dropped such that the sum-rate with max-min power control is maximized for the remaining users. The parameter n_{max} can be set based on the sum-rate requirements for the users or the computational complexity at the BS. For a given channel with K users, the set of all users is denoted by $\mathcal{U} = \{1, 2, ..., K\}$, and the set of dropped users is denoted by $\mathcal{A}^\star$ with $|\mathcal{A}^\star| \leq n_{\text{max}}$. For ZF, the set of dropped users is found by

$$\mathcal{A}^\star = \underset{\mathcal{A} \in \mathcal{S}}{\text{argmax}} \quad (K - |\mathcal{A}|) \log_2 \left(1 + \frac{P/N_0}{\sum_{j \in \mathcal{U} \setminus \mathcal{A}} \|\boldsymbol{g}_j\|^2} \right), \tag{11.11}$$

where $\mathcal{S}$ is the set of all the subsets of $\mathcal{U}$ with up to n_{max} elements. For instance, when $K = 3$ and $n_{\text{max}} = 2$, $\mathcal{S} = \{\varnothing, \{1\}, \{2\}, \{3\}, \{1, 2\}, \{1, 3\}, \{2, 3\}\}$.

For a given n_{max}, (11.11) can be solved by an exhaustive search as follows. The set $\mathcal{S}$ is split to disjoint subsets $\mathcal{S}_0, \mathcal{S}_1, ..., \mathcal{S}_{n_{\text{max}}}$, where $|\mathcal{S}_i|$ is the set of all the subsets of $\mathcal{U}$ with exactly i elements (any $\mathcal{A} \in \mathcal{S}_i$ has i elements). Given $\mathcal{S}_i$, (11.11) becomes

$$\mathcal{A}_i^\star = \underset{\mathcal{A} \in \mathcal{S}_i}{\text{argmax}} \quad \frac{P/N_0}{\sum_{j \in \mathcal{U} \setminus \mathcal{A}} \|\boldsymbol{g}_j\|^2}, \tag{11.12}$$

which is equivalent to

$$\mathcal{A}_i^\star = \underset{\mathcal{A} \in \mathcal{S}_i}{\text{argmin}} \quad \sum_{j \in \mathcal{U} \setminus \mathcal{A}} \|\boldsymbol{g}_j\|^2. \tag{11.13}$$

After finding the solutions $\mathcal{A}_0^\star, \mathcal{A}_1^\star, ..., \mathcal{A}_{n_{\text{max}}}^\star$, the solution to (11.11) is the one, which results in the highest sum-rate. Employing the exhaustive search to solve (11.11) for large K entails huge computational complexity. For example, for $K = 10$ and $n_{\text{max}} = 2$, $\mathcal{S}$ has 56 subsets that need to be searched as in (11.11).

To alleviate the complexity burden of the exhaustive search, we propose a successive filter-based dropping algorithm (SFDA) to heuristically solve (11.11). The idea of SFDA is to reduce the number of searches from $|\mathcal{S}| = |\mathcal{S}_0| + |\mathcal{S}_1| + ... + |\mathcal{S}_{n_{\text{max}}}|$ (with $|\mathcal{S}_i| = \binom{K}{i}$)

to $n_{\text{max}} + 1$. Besides, we use the filter norms $\|\boldsymbol{g}_i\|$ (see the summation in (11.13)) to choose the set of dropped users, and heuristically solve (11.11).

The proposed SFDA for ZF is presented in Algorithm 1. The inputs for the algorithm are $\boldsymbol{H}$, the channel matrix, P, the BS total transmit power, and n_{max}, the maximum number of users that is allowed to be dropped. After running SFDA, the set of dropped users $\mathcal{A}^\star$ is found. Note by setting n_{max} to a higher number, more users could be dropped and thus, a higher sum-rate can be achieved for the users (see (11.7)). However, to drop more users, more computations are required.

The proposed SFDA is explained as follows. When no users are dropped, the set of active users, the channel matrix and corresponding sum-rate are denoted by $\mathcal{A}^{(0)}$, $\boldsymbol{H}^{(0)}$ and $r^{(0)}$, respectively (see line 1-3). In each step of the the main loop (line 4-10), one user is dropped. To find which user shall be dropped, we first need to find the filters $\boldsymbol{G}$ using $\boldsymbol{H}^{(j)}$ (line 5). The user with the highest filter norm $\|\boldsymbol{g}_i\|$ is dropped (line 6). By dropping the user with the highest filter norm, we heuristically minimize the summation of filter norms for the remaining users (see (11.13)). Then, $\mathcal{A}^{(j+1)}$, the set of the remaining users, $\boldsymbol{H}^{(j+1)}$, the channel matrix, and $r^{(j+1)}$, corresponding sum-rate are found (line 7-9). Finally, by finding the maximum sum-rate, the set of dropped users $\mathcal{A}^\star$ is found (line 11-12).

The main complexity of SFDA is to find the filter norms $\|\boldsymbol{g}_i\|$ (line 5-6). For the channel matrix $\boldsymbol{H}$, $\|\boldsymbol{g}_i\|^2$ are found by finding the diagonal elements of:

$$\boldsymbol{G}^H\boldsymbol{G} = (\boldsymbol{H}\boldsymbol{H}^H)^{-1}. \tag{11.14}$$

Therefore, one only needs to find the diagonal elements of a $K \times K$ matrix, which has the complexity order of $\mathcal{O}(K^3)$. Consequently, at each step of the algorithm (line 4-10), diagonal elements of a $(K-j) \times (K-j)$ matrix are found, which has the complexity of $\mathcal{O}(K-j)^3$. If n_{max} is small enough compared to K, the complexity of the algorithm is $\mathcal{O}(K^3)$. On the other hand, the complexity of the exhaustive search is much higher. To drop n_{max} users, there are $\binom{K}{n_{\text{max}}}$ cases (complexity order of $\mathcal{O}(K^{n_{\text{max}}})$ for $n_{\text{max}} << K$) that have to be checked for which the complexity is $\mathcal{O}(K^3)$. Thus, the complexity order of the exhaustive search is $\mathcal{O}(K^{n_{\text{max}}+3})$. Although, the complexity of CDA is lower than SFDA, the complexity of finding the ZF filters is the same for all the algorithms, i.e., $\mathcal{O}(MK^2)$. Therefore, the complexity of finding the active users and corresponding ZF filters is the same for SFDA and CDA, while for the exhaustive search is $\mathcal{O}(\max(MK^2, K^{n_{\text{max}}+3}))$.

Note that by increasing n_{max} the computations required for SFDA increases while the same or a higher sum-rate can be achieved for the remaining users. In the case of $n_{\text{max}} = K$, the computational complexity of SFDA is increased to $\mathcal{O}(K^4)$. In this case, it is guaranteed that the highest sum-rate is achieved for the active users with the highest computations. However, one can reduce n_{max} to trade-off complexity vs. performance.

We can use Algorithm 1 for THP as well. However, for THP, the order that the users are dropped may change the SNR (different set of $\boldsymbol{w}_j$ in (11.8)), and consequently the sum-rate. This means that we may need to check a different set for dropping the users.

Algorithm 1 Proposed SFDA for ZF

Input: $\boldsymbol{H}$, P, n_{max}
Output: $\mathcal{A}^{\star} \subset \{1, 2, ..., K\}$
1: $\mathcal{A}^{(0)} = \{1, 2, ..., K\}$
2: $\boldsymbol{H}^{(0)} = \boldsymbol{H}$
3: find sum-rate $r^{(0)}$ for $\mathcal{A}^{(0)}$ using $\boldsymbol{H}^{(0)}$ (see (11.7) and (11.10))
4: **for** $j = 0, 1, 2, ..., n_{\text{max}} - 1$ **do**
5: $\quad \boldsymbol{G} = (\boldsymbol{g}_1, \boldsymbol{g}_2, ..., \boldsymbol{g}_{K-j}) = (\boldsymbol{H}^{(j)})^{\dagger}$
6: $\quad i = \text{argmax}_k \ \ \|\boldsymbol{g}_k\|$
7: $\quad$ remove row i from $\boldsymbol{H}^{(j)}$ to find $\boldsymbol{H}^{(j+1)}$
8: $\quad \mathcal{A}^{(j+1)} \leftarrow \mathcal{A}^{(j)} \setminus \{i\}$
9: $\quad$ find sum-rate $r^{(j+1)}$ for $\mathcal{A}^{(j+1)}$ using $\boldsymbol{H}^{(j+1)}$
10: **end for**
11: $n^{\star} = \text{argmax}_l \ \ r^{(l)}$
12: $\mathcal{A}^{\star} \leftarrow \mathcal{A}^{(0)} \setminus \mathcal{A}^{(n^{\star})}$

For THP, we propose to run Algorithm 1 two times. Then, we compare the sum-rate associated with the two runs to find the set of dropped users that leads a higher achievable sum-rate. Once, as it is explained in Algorithm 1, and once with a small modification. The modification is as follows. For $j = 0$ in the main loop of the algorithm (line 4-10), the second user with the highest $\|\boldsymbol{g}_i\|$ is dropped instead of the user with the highest $\|\boldsymbol{g}_i\|$. The rest steps of the loop remains unchanged.

11.4 Simulation Results

A BS with a uniform planar array (UPA) of 10×10 antennas with a half-wavelength spacing is assumed, which serves K single-antenna users. The users are uniformly distributed at the cell-edge (200 m) to study the worst-case performance of the system considering shadow fading (log-normal shadow fading with the variance of 12 dB) with the azimuth angle of $\phi \in (0, 2\pi)$ and polar angle of $\theta \in (0, \pi)$. The carrier frequency is set to 30 GHz. The minimum distance between two users is assumed to be a wavelength ($\lambda = 0.01$ m). For LOS environments, we use [35, eq. (7.26)] for the channel matrix. The Monte Carlo simulation runs for 100K realizations of the channel. We compare the cumulative distribution function (CDF) of the achievable sum-rate of SFDA with CDA in [3, Algorithm 1], the neural network based dropping algorithm (DropNet) of [75] and the optimal dropping strategy found by an exhaustive search in the two following scenarios.

In the first scenario, the goal is to compare the dropping algorithms when the BS is allowed to drop up to n_{max} users such that the achievable sum-rate of the remaining users is maximized using max-min power control. For instance, for $n_{\text{max}} = 2$, the BS can drop 1 or 2 or no users. The BS serves $K = 12$ users and the transmit power is fixed

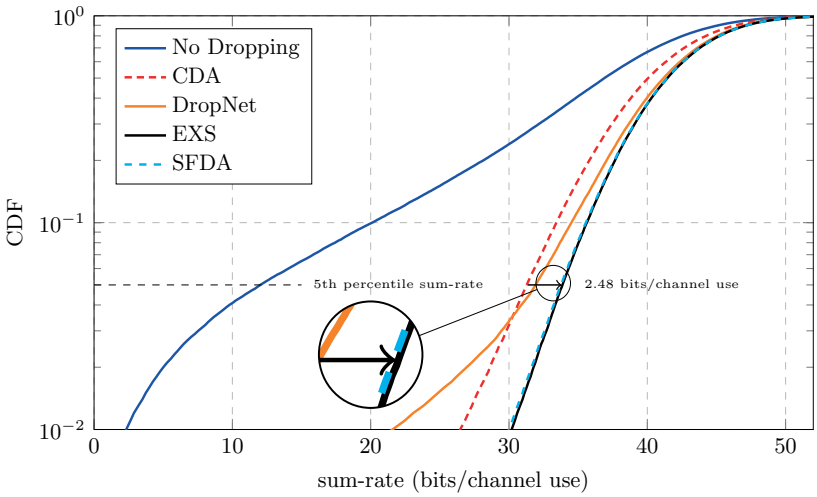

Figure 11.2: Sum-rate CDF for ZF when a 10×10 UPA serves 12 single-antenna users employing no dropping algorithm compared to CDA, DropNet, SFDA and exhaustive search with $n_{\max} = 2$ and $\gamma_0 = 15$. SFDA improves the 5th percentile of CDA and DropNet by 2.48 and 1.82 bits/channel use, respectively.

such that when the users are mutually orthogonal $\gamma_0 = 15$ is achieved. In Fig. 11.2, the sum-rate CDF for ZF when no user is dropped (No Dropping) is compared with that of when the BS uses CDA, DropNet, SFDA and exhaustive search to drop up to $n_{\max} = 2$ users. We chose the number of hidden nodes for DropNet such that the complexity of DropNet is the same as the complexity of the proposed SFDA. When the BS does not employ any dropping algorithm, the 5th percentile ZF sum-rate is the worst (12.22 bits/channel use). By employing CDA (dashed red curve), the 5th percentile ZF sum-rate is improved considerably to 31.27 bits/channel use, which shows that it is essential for the BS with the max-min power control to drop and reschedule some of the users to avoid the loss in the achievable sum-rate. The achievable sum-rate of CDA is still far from that of the exhaustive search (solid black curve), which is 33.85 bits/channel use. By employing DropNet (solid orange curve), the 5th percentile ZF sum-rate of CDA is improved from 31.27 to 31.93 bits/channel use, however, it is still far from that of the exhaustive search. By employing SFDA (dashed cyan curve), the 5th percentile ZF sum-rate is 33.75 bits/channel use. As shown in Fig. 11.2, SFDA achieves almost the same CDF as the exhaustive search.

The same simulation is run for THP, and the results are shown in Fig. 11.3. By employing the CDA, the 5th percentile THP sum-rate is improved from 26.64 bits/channel use (No Dropping) to 32.86 bits/channel use, while by employing DropNet (with the same complexity as the proposed SFDA), it is 33.89 bits/channel use. By using SFDA

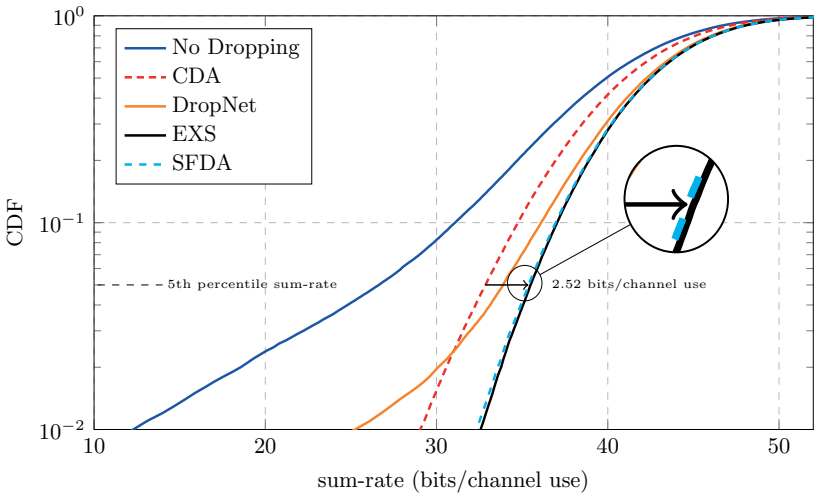

Figure 11.3: Sum-rate CDF for THP when a 10×10 UPA serves 12 single-antenna users employing no dropping algorithm compared to CDA, DropNet, SFDA and exhaustive search with $n_{\text{max}} = 2$ and $\gamma_0 = 15$. SFDA improves the 5th percentile of CDA and DropNet by 2.52 and 1.49 bits/channel use, respectively.

and the exhaustive search, the 5 percentile THP sum-rate is 35.38 and 35.50 bits/channel use, respectively. Similar to ZF, the results in Fig. 11.3 show that it is essential for the BS with THP to drop and reschedule some of the users. By using THP at the BS, the CDF of achievable sum-rate is improved compared to ZF, which shows that THP is a better candidate compared to ZF.

In Fig. 11.2 and Fig. 11.3, DropNet and the proposed SFDA have the same complexity, however, the proposed SFDA provides a higher 5th percentile sum-rate. More importantly, SFDA achieves almost the optimal performance, which makes SFDA a better alternative in terms of performance. Note, for DropNet a neural network has to be trained for each simulation scenario with different parameters, e.g., the number of users, the transmit power at the BS, etc. This feature of DropNet limits its flexibility for the simulations in the second scenario.

In the second scenario, the goal is to compare the dropping algorithms when the BS drops exactly n users. This implies that after dropping n users, the number of served users is the same for the dropping algorithms. The sum-rate CDF when the BS uses CDA, SFDA and exhaustive search to drop exactly n users is shown for ZF and THP in Fig. 11.4 and Fig. 11.5, respectively. We present the results for three different examples, i.e., when exactly $n = 1$, $n = 2$ and $n = 3$ users are dropped. The number of users after dropping n users is 10 for all the examples. The transmit power is fixed at the BS such that after dropping $n = 1$ users and when the users are mutually orthogonal, $\gamma_0 = 15$ is

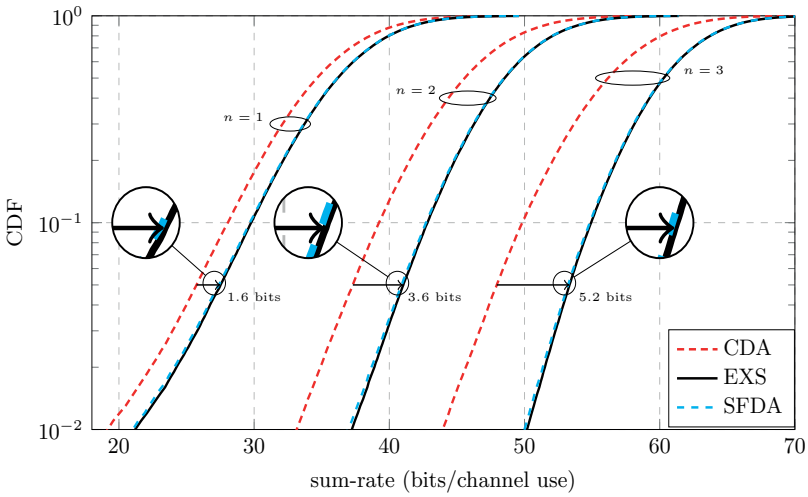

Figure 11.4: Sum-rate CDF for ZF using CDA, SFDA, and exhaustive search (EXS) to drop exactly $n = 1$ (left curves), $n = 2$ (middle curves), $n = 3$ (right curves) users. After dropping n users, K is equal to 10 in all the examples. SFDA improves the 5th percentile sum-rate of CDA by 1.66, 3.6 and 5.28 bits/channel use, for $n = 1$, $n = 2$ and $n = 3$, respectively.

achieved. For $n = 2$ and $n = 3$, the transmit power is changed accordingly to achieve $\gamma_0 = 31$ and $\gamma_0 = 63$, respectively. Note the transmit power for different n is changed for a better comparison.

The results in Fig. 11.4 and Fig. 11.5 show that by employing SFDA instead of CDA, the 5th percentile ZF achievable sum-rate is improved in all the examples (see the arrows). More importantly, the SFDA achieves almost the same CDF of the exhaustive search. The same simulation is run for THP in Fig. 11.5. Similar to the ZF results, SFDA achieves almost the same performance as the exhaustive search for THP in all the examples.

11.5 Conclusions

In this paper, a successive filter-based dropping algorithm is proposed for LOS massive MIMO with max-min power control. The main advantage of SFDA is that it does not require a predefined threshold or any preprocessing. By tuning the maximum number of users that may be dropped, one can trade-off performance and complexity. Simulation results show that SFDA improves the 5th percentile achievable sum-rate compared to previous dropping algorithms both for ZF and THP, while achieving almost the same performance as the optimal dropping strategy.

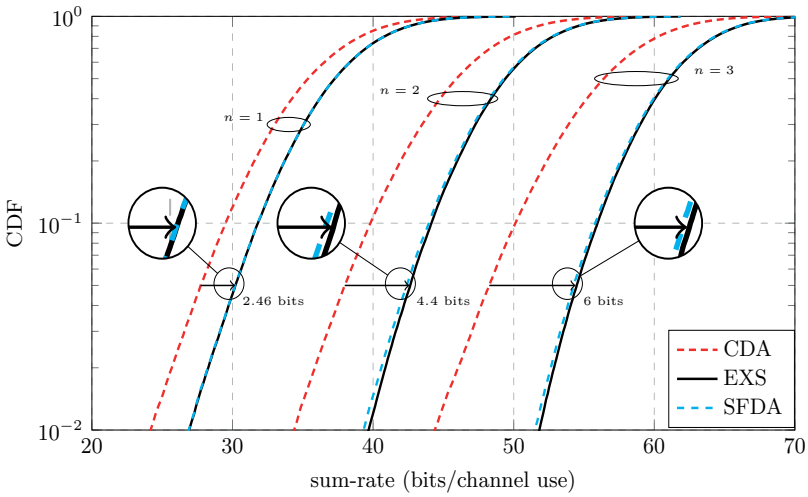

Figure 11.5: Sum-rate CDF for THP using CDA, SFDA, and exhaustive search (EXS) to drop exactly $n = 1$ (left curves), $n = 2$ (middle curves), $n = 3$ (right curves) users. After dropping n users, K is equal to 10 in all the examples. SFDA improves the 5th percentile sum-rate of CDA by 2.46, 4.4 and 6 bits/channel use, for $n = 1$, $n = 2$ and $n = 3$, respectively.

CHAPTER 12

Conclusion

In this thesis, we investigated three research questions to address dealing with correlated scenarios in LOS massive MIMO systems. For each research question, we employ a different strategy (see Fig. 1.4). Applying the proposed strategies improves the outage performance in various use cases such as stadiums, shopping malls, open-air festivals, etc.

The first research question was

- **RQ1**:
  What are the precoding techniques that trade-off complexity vs. performance for LOS massive MIMO systems while improving the performance of linear precoding?

We addressed RQ1 in [C1] and [J1] by proposing low-complexity precoders. We proposed a low-complexity linear precoder in [C1] and we proposed a low-complexity hybrid linear and nonlinear precoder in [J1]. In [C1] (Chapter 5), we proposed a low-complexity linear precoder that switches between CB and ZF based on the channel condition. The proposed idea is to predict and use the precoder, which results in the highest sum-rate for a given channel. We showed analytically that the achievable sum-rate of the proposed precoder is higher than both CB and ZF. Furthermore, by presenting two examples, we showed that the computational complexity of the proposed precoder is lower than that of ZF.

In [J1] (Chapter 6), probability analysis is presented for LOS massive MIMO to study the probability that there is at least one pair of correlated users and to study the average number of correlated users. The presented probability analysis shows that it is more probable that there are only one or two pairs of correlated users in LOS massive MIMO systems. We proposed a hybrid linear and nonlinear precoder with max-min power control for which a modified THP method is proposed to reduce the complexity of nonlinear precoders. We proposed a grouping scheme where users are divided into two groups. For

the first group, modified THP is used, while for the second group, linear precoding is employed. In the end, the precoded vectors of the two groups are combined. The presented simulation results show that the proposed hybrid linear and nonlinear precoder reduces the required transmit power at the BS to ensure a given average BLER for NR-LDPC codes using 16QAM and 64QAM compared to ZF. In summary

- We proposed a switching-based linear precoder based on CB and ZF that achieves a sum-rate higher than both CB and ZF, and entails a computational complexity lower than that of ZF.
- We derived the probability that there is at least one pair of correlated users in LOS massive MIMO systems. Besides, we showed by simulation results that it is more probable in LOS massive MIMO systems that there are only one or two pairs of correlated users.
- We proved that when the number of antennas tends to infinity, the probability that there is at least one pair of correlated users is asymptotically equivalent to the probability that there is exactly one pair of correlated users.
- We proposed a low-complexity hybrid linear and nonlinear precoder for which simulation results with NR-LDPC codes were presented to show its effectiveness for LOS massive MIMO systems.

The second research question was

- **RQ2**:
  What is the inter-element spacing for the ULA at the BS that has the optimal outage performance, i.e., minimizes the probability of occurrence of the correlated scenarios?

We addressed RQ2 in [J2] by designing an optimized ULA. In [J2] (Chapter 7), we proposed to employ a ULA with an optimized inter-element spacing at the BS to reduce the occurrence of correlated scenarios with the cost of increasing the aperture size at the BS. For a given ULA with an arbitrary inter-element spacing, we derived the probability that the correlation among the channel vectors of two users is above a threshold. The inter-element spacing of the proposed ULA is the one for which the derived probability is minimized. The proposed ULA has the best outage performance when there are only two users. For more users, we presented simulation results that demonstrate the effectiveness of the proposed array compared to the conventional half-wavelength ULA with a known linear precoder, i.e., ZF. In summary

- We derived the probability that the spatial correlation of a pair of users becomes higher than a given threshold as a function of the inter-element spacing of the ULA.
- We found the inter-element spacing that minimizes the mentioned probability, i.e., optimizes the outage performance, when there are only two users.

- We proposed to use the optimized inter-element spacing for the case with more than two users for which simulation results were presented to show its effectiveness.

The third research question was

- **RQ3**:
  What are the dropping algorithms that can achieve near-optimal performance with feasible computational complexity?

We addressed RQ3 in [J3]-[J6] (Chapter 8- 11) by studying the dropping problem. In [J3] (Chapter 8), the dropping problem was analyzed for the CB and ZF with max-min power control in LOS environments. Threshold values were analytically derived to be used in the previously proposed dropping algorithm to avoid repeating a large number of simulations to find the optimal threshold. By using the derived threshold for the dropping, the sum-rate is maximized when there are only two correlated users. For more users, we present the simulation results to show the effectiveness of employing our derived threshold. Furthermore, a modified dropping algorithm was proposed that improves the previously proposed dropping algorithm. In [J4] (Chapter 9), we studied the problem for THP with two different power control strategies, i.e., max-min power control and equal received power control.

We proposed two dropping algorithms in [J5] (Chapter 10) and [J6] (Chapter 11) that do not rely on a predefined threshold and achieve better performance compared to the previous dropping algorithms. In (Chapter 10), we proposed DropNet to find the users that shall be dropped. By employing DropNet, we reduced the complexity of the exhaustive search and achieved better sum-rate performance compared to the previous correlation-based dropping algorithms. We trained the neural network in DropNet using a large number of channel realizations, where the input features are the spatial correlation and the norm of the channel vectors of the users. By presenting the simulation results, we showed that DropNet trade-offs complexity vs. performance.

In (Chapter 11), we proposed an iterative filter-based dropping algorithm, which achieves near-optimal performance. At each iteration, the user with the highest filter norm is dropped. By comparing the sum-rate of all the iterations, the best set of dropped users is found. In contrast to previous algorithms in the literature, our proposed IFDA does not require a predefined threshold for the spatial correlation of the users or any preprocessing. Compared to an exhaustive search, the complexity of IFDA is reduced significantly. We presented simulation results to show the effectiveness of the proposed IFDA with ZF and THP. In summary

- We derived the thresholds of the spatial correlation with CB, ZF and THP for the previously proposed dropping algorithm in the literature to avoid repeating a large number of simulations to find the threshold.

- We proposed a modified correlation-based dropping algorithm that improves the previously proposed dropping algorithm.

- We proposed a neural-network based dropping algorithm that trades-off complexity vs. performance.
- We proposed an iterative filter-based dropping algorithm that does not require a predefined threshold and achieves near-optimal performance.

By investigating these three research questions, we addressed dealing with correlated scenarios from three different perspectives. The proposed strategies can be combined to further improve the outage performance in the correlated scenarios. For instance, a low-complexity precoder can be employed, while the inter-element spacing of the BS antenna array is optimized and a few users are dropped. In this way, the system benefits from all the proposed three strategies, i.e., the outage performance of the system becomes closer to that of favorable propagation with a low computational complexity.

References

[1] A. Farsaei, A. Alvarado, F. M. J. Willems, and U. Gustavsson, "A low-complexity hybrid linear and nonlinear precoder for line-of-sight massive MIMO with max-min power control," *submitted to IEEE Transactions on Wireless Communications*.

[2] A. Farsaei, N. Amani, R. Maaskant, U. Gustavsson, A. Alvarado, and F. M. J. Willems, "Uniform linear arrays with optimized inter-element spacing for LOS massive MIMO," *IEEE Communications Letters*, vol. 25, no. 2, pp. 613–616, Feb. 2021.

[3] A. Farsaei, A. Alvarado, F. M. J. Willems, and U. Gustavsson, "An improved dropping algorithm for line-of-sight massive MIMO with max-min power control," *IEEE Communications Letters*, vol. 23, no. 6, pp. 1109–1112, Jun. 2019.

[4] ——, "An improved dropping algorithm for line-of-sight massive MIMO with Tomlinson-Harashima Precoding," *IEEE Communications Letters*, vol. 23, no. 11, pp. 2099–2103, Nov. 2019.

[5] A. Farsaei, A. Sheikh, U. Gustavsson, A. Alvarado, and F. M. J. Willems, "DropNet: an improved dropping algorithm based on neural networks for line-of-sight massive MIMO," *IEEE Access*, vol. 9, pp. 29 441–29 448, 2021.

[6] A. Farsaei, N. Amani, R. Maaskant, U. Gustavsson, A. Alvarado, and F. M. J. Willems, "A near-optimal dropping algorithm for line-of-sight massive MIMO with max-min power control," *submitted to IEEE Communications Letters*.

[7] A. Farsaei, F. Willems, A. Alvarado, and U. Gustavsson, "A reduced-complexity linear precoding strategy for massive MIMO base stations," in *2018 25th International Conference on Telecommunications (ICT)*, Jun. 2018, pp. 121–126.

[8] A. Farsaei, A. Alvarado, F. M. J. Willems, and U. Gustavsson, "Multi-user precoding: Low-complexity precoding for highly correlated scenarios," PCT patent application,PCT/EP2020/059238, April 1, 2020.

[9] ——, "Multi-user precoding: Low-complexity precoding, compute the correlation-limit," PCT patent application, PCT/EP2020/059241, April 1, 2020.

[10] A. Farsaei, A. Sheikh, A. Alvarado, F. M. J. Willems, and U. Gustavsson, "Neural network for MU-MIMO user selection," PCT patent application, PCT/EP2021/053718, February 16, 2021.

[11] A. Farsaei, A. Alvarado, F. M. J. Willems, and U. Gustavsson, "User selection for MU-MIMO," PCT patent application, PCT/EP2021/053713, February 16, 2022.

[12] A. Farsaei, N. Amani, A. Alvarado, F. M. J. Willems, U. Gustavsson, and R. Maaskant, "On the outage performance of line-of-sight massive MIMO with a fixed-length uniform linear sparse array," in *2019 IEEE-APS Topical Conference on Antennas and Propagation in Wireless Communications (APWC)*, 2019, pp. 345–348.

[13] T. A. H. Bressner, A. Farsaei, M. Fozooni, U. Johannsen, M. N. Johansson, and A. Bart Smolders, "MIMO performance evaluation of isotropic, directional and highly-directional antenna systems for mm-wave communications," in *2019 13th European Conference on Antennas and Propagation (EuCAP)*, 2019, pp. 1–5.

[14] T. Marinovic, A. Farsaei, R. Maaskant, A. L. Lavieja, M. N. Johansson, U. Gustavsson, and G. A. E. Vandenbosch, "Effect of antenna array element separation on capacity of MIMO systems including mutual coupling," in *2019 IEEE International Symposium on Antennas and Propagation and USNC-URSI Radio Science Meeting*, 2019, pp. 415–416.

[15] N. Amani, A. Farsaei, U. Gustavsson, T. Eriksson, F. M. J. Willems, M. V. Ivashina, and R. Maaskant, "Array configuration effect on the spatial correlation of MU-MIMO channels in NLoS environments," in *2020 14th European Conference on Antennas and Propagation (EuCAP)*, 2020, pp. 1–4.

[16] N. Amani, A. Farsaei, S. Rezaei Aghdam, T. Eriksson, M. V. Ivashina, and R. Maaskant, "Sparse array synthesis including mutual coupling for MU-MIMO average capacity maximization," *submitted to IEEE Transaction on Antennas and Propagation*.

[17] A. Zaidi, F. Athley, J. Medbo, U. Gustavsson, G. Durisi, and X. Chen, *5G Physical Layer: Principles, Models and Technology Components*, 1st ed. USA: Academic Press, Inc., 2018.

[18] Ericsson, "Ericsson mobility report," Jun. 2020.

[19] Ericsson, "5G systems: Enabling the transformation of industry and society," Jan. 2017, available at http://www.ericsson.com/res/docs/whitepapers/wp-5g.

[20] S. Parkvall, E. Dahlman, A. Furuskar, and M. Frenne, "NR: The New 5G Radio Access Technology," *IEEE Communications Standards Magazine*, vol. 1, no. 4, pp. 24–30, 2017.

[21] Ericsson, "5G wireless access: an overview," Apr. 2020, available at https://www.ericsson.com/498a10/assets/local/reports-papers/white-papers/whitepaper-5g-wireless-access.pdf.

[22] E. Björnson, E. G. Larsson, and T. L. Marzetta, "Massive MIMO: ten myths and one critical question," *IEEE Communications Magazine*, vol. 54, no. 2, pp. 114–123, Feb. 2016.

[23] G. Interdonato, "Cell-free massive MIMO: Scalability, signal processing and power control," Ph.D. dissertation, Linköping university, Linköping, Sweden, 2020.

[24] F. Boccardi, B. Clerckx, A. Ghosh, E. Hardouin, G. Jöngren, K. Kusume, E. Onggosanusi, and Y. Tang, "Multiple-antenna techniques in LTE-advanced," *IEEE Communications Magazine*, vol. 50, no. 3, pp. 114–121, Mar. 2012.

[25] E. Dahlman, S. Parkvall, and J. Skold, *5G NR: The Next Generation Wireless Access Technology*. Elsevier Science, 2018.

[26] T. L. Marzetta, "Noncooperative cellular wireless with unlimited numbers of base station antennas," *IEEE transactions on wireless communications*, vol. 9, no. 11, pp. 3590–3600, 2010.

[27] Ericsson. (2018) Going massive with mimo. Available at https://www.ericsson.com/en/news/2018/1/massive-mimo-highlights.

[28] E. Björnson, L. Sanguinetti, H. Wymeersch, J. Hoydis, and T. L. Marzetta, "Massive MIMO is a reality—What is next?: Five promising research directions for antenna arrays," *Digital Signal Processing*, vol. 94, pp. 3 – 20, 2019, special Issue on Source Localization in Massive MIMO.

[29] T. L. Marzetta, "Massive MIMO: An introduction," *Bell Labs Technical Journal*, vol. 20, pp. 11–22, Mar. 2015.

[30] Ericsson, "5G wireless access: an overview," Apr. 2020, available at http://www.ericsson.com/res/docs/whitepapers/wp-5g.

[31] R. W. Heath, N. González-Prelcic, S. Rangan, W. Roh, and A. M. Sayeed, "An Overview of Signal Processing Techniques for Millimeter Wave MIMO Systems," *IEEE Journal of Selected Topics in Signal Processing*, vol. 10, no. 3, pp. 436–453, April 2016.

[32] A. Osseiran *et al.*, "Scenarios for 5G mobile and wireless communications: the vision of the METIS project," *IEEE Communications Magazine*, vol. 52, no. 5, pp. 26–35, May 2014.

[33] H. Yang and T. L. Marzetta, "Massive MIMO with max-min power control in line-of-sight propagation environment," *IEEE Transactions on Communications*, vol. 65, no. 11, pp. 4685–4693, Nov. 2017.

[34] ——, "A macro cellular wireless network with uniformly high user throughputs," in *2014 IEEE 80th Vehicular Technology Conference (VTC2014-Fall)*, Sept 2014, pp. 1–5.

[35] D. Tse and P. Viswanath, *Fundamentals of Wireless Communication*. New York, NY, USA: Cambridge University Press, May 2005.

[36] W. Tan, S. D. Assimonis, M. Matthaiou, Y. Han, X. Li, and S. Jin, "Analysis of different planar antenna arrays for mmwave massive mimo systems," in *2017 IEEE 85th Vehicular Technology Conference (VTC Spring)*, 2017, pp. 1–5.

[37] T. M. Cover and J. A. Thomas, *Elements of Information Theory*. New York, U.S.: Wiley, 1991.

[38] E. G. Larsson, O. Edfors, F. Tufvesson, and T. L. Marzetta, "Massive MIMO for next generation wireless systems," *IEEE Communications Magazine*, vol. 52, no. 2, pp. 186–195, Feb. 2014.

[39] H. Q. Ngo, E. G. Larsson, and T. L. Marzetta, "Aspects of favorable propagation in Massive MIMO," in *2014 22nd European Signal Processing Conference (EUSIPCO)*, Sep. 2014, pp. 76–80.

[40] E. Agrell, T. Eriksson, A. Vardy, and K. Zeger, "Closest point search in lattices," *IEEE Transactions on Information Theory*, vol. 48, no. 8, pp. 2201–2214, Aug. 2002.

[41] C. Windpassinger, "Detection and precoding for multiple input multiple output channels," Ph.D. dissertation, Dept. Inst. Inf. Transmiss., Univ. Erlangen-Nuremberg, Erlangen, Germany, 2004.

[42] E. Björnson, J. Hoydis, and L. Sanguinetti, "Massive MIMO networks: Spectral, energy, and hardware efficiency," *Foundations and Trends® in Signal Processing*, vol. 11, no. 3-4, pp. 154–655, 2017.

[43] T. L. Marzetta, E. G. Larsson, H. Yang, and H. Q. Ngo, *Fundamentals of Massive MIMO*. Cambridge, U.K.: Cambridge Univ. Press, 2016.

[44] P. Viswanath and D. N. C. Tse, "Sum capacity of the vector Gaussian broadcast channel and uplink-downlink duality," *IEEE Transactions on Information Theory*, vol. 49, no. 8, pp. 1912–1921, Aug. 2003.

[45] N. Jindal, S. Vishwanath, and A. Goldsmith, "On the duality of Gaussian multiple-access and broadcast channels," *IEEE Transactions on Information Theory*, vol. 50, no. 5, pp. 768–783, May 2004.

[46] G. Caire and S. Shamai, "On the achievable throughput of a multiantenna Gaussian broadcast channel," *IEEE Transactions on Information Theory*, vol. 49, no. 7, pp. 1691–1706, July 2003.

[47] M. Costa, "Writing on dirty paper (Corresp.)," *IEEE Transactions on Information Theory*, vol. 29, no. 3, pp. 439–441, May 1983.

[48] H. Yang and T. L. Marzetta, "Performance of Conjugate and Zero-Forcing Beamforming in Large-Scale Antenna Systems," *IEEE Journal on Selected Areas in Communications*, vol. 31, no. 2, pp. 172–179, Feb. 2013.

[49] S. Shi and M. Schubert, "MMSE transmit optimization for multi-user multi-antenna systems," in *Proceedings. (ICASSP '05). IEEE International Conference on Acoustics, Speech, and Signal Processing, 2005.*, vol. 3, 2005, pp. iii/409–iii/412 Vol. 3.

[50] Y. Zhao, I. G. Niemegeers, and S. H. De Groot, "Power allocation in cell-free massive MIMO: A deep learning method," *IEEE Access*, vol. 8, pp. 87 185–87 200, 2020.

[51] M. Alodeh, D. Spano, A. Kalantari, C. G. Tsinos, D. Christopoulos, S. Chatzinotas, and B. Ottersten, "Symbol-level and multicast precoding for multiuser multiantenna downlink: a state-of-the-art, classification, and challenges," *IEEE Communications Surveys Tutorials*, vol. 20, no. 3, pp. 1733–1757, 2018.

[52] R. F. H. Fischer, *Precoding and signal shaping for digital transmission*. New York: Wiley, 2002.

[53] W. Yu, D. P. Varodayan, and J. M. Cioffi, "Trellis and convolutional precoding for transmitter-based interference presubtraction," *IEEE Transactions on Communications*, vol. 53, no. 7, pp. 1220–1230, Jul. 2005.

[54] U. Erez, S. Shamai, and R. Zamir, "Capacity and lattice strategies for canceling known interference," *IEEE Transactions on Information Theory*, vol. 51, no. 11, pp. 3820–3833, Nov. 2005.

[55] B. M. Hochwald, C. B. Peel, and A. L. Swindlehurst, "A vector-perturbation technique for near-capacity multiantenna multiuser communication-part II: perturbation," *IEEE Transactions on Communications*, vol. 53, no. 3, pp. 537–544, 2005.

[56] C. Ling and W. H. Mow, "A unified view of sorting in lattice reduction: From V-BLAST to LLL and beyond," in *2009 IEEE Information Theory Workshop*, 2009, pp. 529–533.

[57] R. F. H. Fischer, S. Stern, and J. B. Huber, "Lattice-reduction-aided and integer-forcing equalization: Structures, criteria, factorization, and coding," *Found. Trends Commun. Inf. Theory*, vol. 16, no. 1-2, pp. 1–155, 2019.

[58] Schmidt, Joham, and Utschick, "Minimum mean square error vector precoding," in *2005 IEEE 16th International Symposium on Personal, Indoor and Mobile Radio Communications*, vol. 1, 2005, pp. 107–111.

[59] S. Jacobsson, G. Durisi, M. Coldrey, T. Goldstein, and C. Studer, "Quantized Precoding for Massive MU-MIMO," *IEEE Transactions on Communications*, vol. 65, no. 11, pp. 4670–4684, Nov. 2017.

[60] NTT DOCOMO, 3GPP TSG RAN WG1 Meeting 87, R1-1700594, "Discussion on non-linear precoding scheme for NR," Jan. 2017.

[61] S. Zarei, W. H. Gerstacker, R. Weigel, M. Vossiek, and R. Schober, "Robust MSE-balancing hierarchical linear/Tomlinson-Harashima precoding for downlink massive MU-MIMO systems," *IEEE Transactions on Wireless Communications*, vol. 17, no. 11, pp. 7309–7324, Nov. 2018.

[62] H. Nishimoto, A. Taira, H. Iura, S. Uchida, A. Okazaki, and A. Okamura, "Nonlinear block multi-diagonalization precoding for high SHF wide-band massive MIMO in 5G," in *2016 IEEE 27th Annual International Symposium on Personal, Indoor, and Mobile Radio Communications (PIMRC)*, 2016, pp. 1–7.

[63] M. Arakawa, "Computational workloads for commonly used signal processing kernels," MIT, Cambridge, MA, USA, DTIC Document, Tech. Rep., 2006.

[64] A. Wiesel, Y. C. Eldar, and S. Shamai, "Zero-Forcing Precoding and Generalized Inverses," *IEEE Transactions on Signal Processing*, vol. 56, no. 9, pp. 4409–4418, Sep. 2008.

[65] D. P. Palomar, J. M. Cioffi, and M. A. Lagunas, "Joint Tx-Rx beamforming design for multicarrier MIMO channels: a unified framework for convex optimization," *IEEE Transactions on Signal Processing*, vol. 51, no. 9, pp. 2381–2401, Sep. 2003.

[66] C. Shepard, N. Anand, and L. Zhong, "Practical performance of MU-MIMO precoding in many-antenna base stations," in *Proceeding of the 2013 workshop on Cellular networks: operations, challenges, and future design*. ACM, Jun. 2013, pp. 13–18.

[67] D. Zhu, B. Li, and P. Liang, "Normalized volume of hyperball in complex Grassmann manifold and its application in large-scale MU-MIMO communication systems," *arXiv preprint arXiv:1402.4543*, Feb. 2014.

[68] D. Tse and P. Viswanath, *Fundamentals of wireless communication*. Cambridge, U.K.: Cambridge University Press, 2005.

[69] H. Yang and T. L. Marzetta, "Max-min SINR dependence on channel correlation in line-of-sight Massive MIMO," in *2017 IEEE Global Communications Conference (GLOBECOM)*, Dec. 2017, pp. 1–6.

[70] X. Gao, O. Edfors, F. Rusek, and F. Tufvesson, "Linear pre-coding performance in measured very-large MIMO channels," in *2011 IEEE Vehicular Technology Conference (VTC Fall)*, Sep. 2011, pp. 1–5.

[71] ——, "Massive MIMO performance evaluation based on measured propagation data," *IEEE Transactions on Wireless Communications*, vol. 14, no. 7, pp. 3899–3911, Jul. 2015.

[72] E. Karipidis, J. Lorca, and E. Björnson, "D1.1: System scenarios and requirements specifications," *MAMMOET, Utrecht, The Netherlands,Tech. Rep. ICT-619086-D1.1*, 2015.

[73] J. Flordelis, F. Rusek, X. Gao, G. Dahman, O. Edfors, and F. Tufvesson, "Spatial separation of closely-located users in measured Massive MIMO channels," *IEEE Access*, vol. 6, pp. 40 253–40 266, 2018.

[74] H. Yang, "User scheduling in massive MIMO," in *2018 IEEE 19th International Workshop on Signal Processing Advances in Wireless Communications (SPAWC)*, 2018, pp. 1–5.

[75] A. Farsaei, A. Sheikh, U. Gustavsson, A. Alvarado, and F. M. J. Willems, "DropNet: An Improved Dropping Algorithm Based On Neural Networks for Line-of-Sight Massive MIMO," *IEEE Access*, to be published.

[76] N. Brahmi, O. N. C. Yilmaz, K. W. Helmersson, S. A. Ashraf, and J. Torsner, "Deployment strategies for ultra-reliable and low-latency communication in factory automation," in *2015 IEEE Globecom Workshops (GC Wkshps)*, 2015, pp. 1–6.

[77] Nokia, Alcatel-Lucent Shanghai Bell, 3GPP TSG RAN WG1 NR Ad-Hoc Meeting, R1-1701087, "On MU MIMO nonlinear precoding in NR," Jan. 2017.

[78] Mitsubishi Electric, 3GPP TSG RAN WG1 Meeting 88, R1-1702754, "Summary of analysis of nonlinear precoding schemes for NR," Feb. 2017.

[79] S. Zarei, W. Gerstacker, and R. Schober, "Low-complexity hybrid linear/Tomlinson-Harashima precoding for downlink large-scale MU-MIMO systems," in *2016 IEEE Globecom Workshops (GC Wkshps)*, Dec. 2016, pp. 1–7.

[80] ETSI, "Study on channel model for frequencies from 0.5 to 100 GHz," *3GPP TR 38.901 version 14.1.1 Release 14*, Aug. 2017.

[81] W. Feller, *An Introduction to Probability Theory and Its Applications*, 3rd ed. Wiley, 1968, vol. 1.

[82] R. Hunger, "Floating point operations in matrix-vector calculus," Technische Universität München, München, Germany, Tech. Rep. TUM-LNS-TR-05-05, Oct. 2005.

[83] D. Hui, S. Sandberg, Y. Blankenship, M. Andersson, and L. Grosjean, "Channel coding in 5G New Radio: a tutorial overview and performance comparison with 4G LTE," *IEEE Vehicular Technology Magazine*, vol. 13, no. 4, pp. 60–69, Dec. 2018.

[84] S. Kinjo, "A low complexity soft demapping method for expanded M-QAM constellations," in *2014 IEEE Asia Pacific Conference on Circuits and Systems (APCCAS)*, 2014, pp. 137–140.

[85] E. C. Y. Peh and Y. Liang, "Power and modulo loss tradeoff with expanded soft demapper for LDPC coded GMD-THP MIMO systems," *IEEE Transactions on Wireless Communications*, vol. 8, no. 2, pp. 714–724, Feb. 2009.

[86] E. Hecht, *Optics*, ser. Pearson education. Addison-Wesley, 2002.

[87] C. A. Balanis, *Antenna theory: analysis and design*. John wiley & sons, 2016.

[88] S. Pratschner, E. Zöchmann, H. Groll, S. Caban, S. Schwarz, and M. Rupp, "Does a large array aperture pay off in line-of-sight massive MIMO?" in *2019 IEEE 20th International Workshop on Signal Processing Advances in Wireless Communications*, Jul. 2019, pp. 1–5.

[89] N. Amani, A. A. Glazunov, M. V. Ivashina, and R. Maaskant, "Per-antenna power distribution of a zero-forcing beamformed ULA in pure LOS MU-MIMO," *IEEE Communications Letters*, vol. 22, no. 12, pp. 2515–2518, Dec. 2018.

[90] D. Pinchera, M. D. Migliore, F. Schettino, and G. Panariello, "Antenna arrays for line-of-sight massive MIMO: Half wavelength is not enough," *Electronics*, vol. 6, no. 3, p. 57, 2017.

[91] T. Arai, A. Ohta, S. Kurosaki, K. Maruta, T. Iwakuni, and M. Iizuka, "Correlation-based user scheduling and multi-planar parallelogram array for massive antenna systems," in *2016 IEEE 27th Annual International Symposium on Personal, Indoor, and Mobile Radio Communications (PIMRC)*, Sep. 2016, pp. 1–6.

[92] H. Yang, "User scheduling in Massive MIMO," in *19th IEEE International Workshop on Signal Processing Advances in Wireless Communications, SPAWC*, Jun. 2018.

[93] S. Sigdel and W. A. Krzymien, "Simplified fair scheduling and antenna selection algorithms for multiuser MIMO orthogonal space-division multiplexing downlink," *IEEE Transactions on Vehicular Technology*, vol. 58, no. 3, pp. 1329–1344, Mar. 2009.

[94] R. F. H. Fischer, C. Windpassinger, A. Lampe, and J. B. Huber, "Tomlinson-Harashima precoding in space-time transmission for low-rate backward channel," in *2002 International Zurich Seminar on Broadband Communications Access - Transmission - Networking (Cat. No.02TH8599)*, 2002, pp. 7–7.

[95] G. Cybenko, "Approximation by superpositions of a sigmoidal function," *Math. Control Signal Systems*, vol. 2, p. 303–314, 1989.

[96] A. Pinkus, "Approximation theory of the MLP model in neural networks," *Acta Numer*, vol. 8, p. 143–195, 1999.

[97] T. L. P. Kidger, "Universal approximation with deep narrow networks," *arXiv preprint arXiv:1905.08539v2*, May 2019.

[98] D. E. Rumelhart, G. E. Hinton, and R. J. Williams, "Learning representations by back-propagating errors," *nature*, vol. 323, no. 6088, pp. 533–536, 1986.

[99] R. L. Burden and J. D. Faires, *Numerical Analysis*, 4th ed. Boston: PWS-Kent Publishing Company, 1989.

[100] G. Hartman, *Fundamentals of Matrix Algebra*, 3rd ed. Virginia Military Institute, 2011.

Acknowledgments

I would like to thank all of the people who helped me during the past four years. It would never be possible without the supports of my lovely family and friends, and supervision of my promoters at Eindhoven university of technology and my advisor in Ericsson Research, and all the colleagues in SILIKA project. Thanks for supporting me on this journey.

Frans, I'm very grateful that I did my Ph.D. under your supervision. I learned a lot from your personality as well as your smart ideas and the way you approach the research problems. I hope you will be at the university more often and we can keep in touch in the future. Alex, thanks for helping me during these four years. Your supervision helped me to enhance the quality of my works. It would never be possible to publish a couple of papers without your support. Ulf, it was my pleasure to be under your supervision during my Ph.D. The time I spent in Sweden will never be forgotten. I really felt at "home" in Sweden and you were one of the reasons. Thanks for all your supports and ideas that helped me to publish papers and patent applications, and thanks for all the nice conversations that we had during my stay in Sweden.

I would like to thank all the people in wing 62 in Ericsson Research, Gothenburg. Colette, as I said earlier, I felt at "home" in Sweden and you were another reason for that. Thanks for all your supports and your warm-hearted attitude. Milad, thanks for being a supervisor as well as a supportive friend. I really enjoyed the time in Ericsson with you. Your energy cheered me up during my stay in Sweden. Martin, I enjoyed the moments in wing 62 with you, all the technical discussions that we had as well as our chats during lunch and coffee time. Sven, thanks for being a nice friend. I wish I could publish a paper with you, but unfortunately, it did not happen. Anyway, I enjoyed all the technical discussions that we had. I will never forget the nice memories in Sweden with you from playing football or having lunch in Lindholmen. I would like to thank all the other people in wing 62, Jonas Hansryd, Anders, Aidin, Lars, Astrid, Henrik, Fredrik, Keerthi, Jonas Fridén, Sven Petersson, Mona and Behrooz.

I would like to thank all the supervisors in SILIKA projects. Particularly, Bart and

Ulf J. for organizing the project. In addition, I would like to thank Rob Maaskant for all the supports and ideas for our joint papers. I would like to thank Thomas Eriksson for all his ideas and the nice and fruitful discussions we had during SILIKA project meetings.

I would like to thank all the early stage researchers in SILIKA projects. Navid, thanks for all your supports during my Ph.D. I really enjoyed all our discussions and all the walks we had in Gothenburg, Eindhoven, Leuven, and even in Granada. I'm very proud of our joint papers. Adrián, thanks for being a nice flatmate and a supportive colleague. I learned a lot from you. I hope I did not bother you that much in Svängrumsgatan 8. I'll never forget those times that we had in Sweden, Ericsson and all the other SILIKA meetings. Thomas, I enjoyed all the memories during SILIKA and all the discussions we had. Your always smiling attitude cheered me up. Amr, I really enjoyed the time we spent in SILIKA and also in Svängrumsgatan 8. I wish all the best for all of you in your future career.

I would like to thank the members of my defense committee, Robert Fischer, Christoph Studer, Sonia Heemstra de Groot. Thank you for taking the time to review my thesis and for providing valuable comments.

I would like to thank all the colleagues of the SPS group. Jan, thanks for your supports during my Ph.D. Carla, Marieke and Sabine, thanks for your supports and the very nice conversations that we had during coffee times. I would like to thank all the people in ICT Lab, Wim, Hamdi, Bin, Lieneke, Yunus, Firat, Gabriele, Vinícius, Franz, Astrid, Kaiquan, Sebastiaan and Mehrangiz. Last but not least, I would like to thank Alireza for all your supports. Not only I learned a lot from your ideas, but also I enjoyed the collaboration that we had a lot. I would like to thank Yunus, particularly for his template for writing this thesis. I would like to thank the so-called "cultural group", Astrid, Simon, Franz, Mochi and Kaiquan for all the beauties in the cultural exchange that we had.

I would like to thank all the people in Eindhoven who cheered me up during my Ph.D. When I came to the Netherlands, playing football on weekends was the only "flow" on weekends. Thanks Hamed and Mehdi for introducing those football games to me. Then, I would like to thank all the players in "international team" in chronological order, Amin, Amirreza, Jilal, Vahid, Hamid, Mohsen, Alfonso, Reza Refaei, and Reza Z. Last but not least, "Shelem Emshab" group was the other "flow" during my Ph.D., thanks Mehdi, Mohsen and Hamideh, Amirabbas and Zahra, Hadi, and Farzad for your nice gatherings.

Finally, I would like to thank all the other people with which I had nice memories, Fatemeh, Faranak and Mohammad Reza, Naseh and Mana, Zabih and Roya, Reza and Shila, Mohammad Emad, Saeid, Roohollah, Aref and Fereshteh, Mehrdad, Parsa, Hadi S., Amin J., Ali Mehrabi, Ali and Niousha. I would like to thank all of my friends in Gothenburg, Sweden, Ali Mirani, Mohammad (Manzar), Ahad, Kamran and Parisa, Sina, Mohammad Hossein and Yasaman, Nima and Marzieh, Fazele, Masoud, Bita, Fatemeh. I would like to thank my friends in Stockholm, Mohammad Reza and Afsane, Hasan, and Alireza for their nice memories in Stockholm. Last but not least, I would like to thank my B.Sc. friends who are located in different continents who joined our Skype meetings every now and then, especially, Ehsan M., Sepehr H. M., Amirmasoud, Soheil,

Ali P., Mohammad Rayiati, Ramin F., Mahdiar, Saman, Sahar, Mehrdad, Mehdi Khalili. Furthermore, I would like to thank my high school friends in Germany, i.e., Ehsan and Amirhossein, and especially, Mohammad Yasseri for his warm and peaceful conversations.

I would like to thank my father and my mother for all their supports. I'm very proud of being your son, for everything you gave me with your love and kindness. I would like to thank my gorgeous sister, Anahita, for her supports during my Ph.D. and my supportive brother and my sister-in-law, Arash and Elnaz as well. Last but not least, I would like to thank Maedeh who changed my life with her love and her support.

Ashkan Farsaei,
Eindhoven, May 2020.

About the Author

Amirashkan Farsaei was born in Tehran, Iran, in 1991. He finished high school in Mofid 2 educational complex. In 2009, he started his B.Sc. in the Electrical Engineering department of Sharif University of Technology, Tehran, Iran. He was offered to join M.Sc. in the Electrical Engineering department of Sharif University of Technology without entrance exam in 2013. He finished his M.Sc. in Digital Electronics under the supervision of Prof. Shabany and Prof. Kavehvash. From 2015-2016, he was a researcher at Sharif University of Technology, where he was involved in developing a millimeter-wave imaging system.

In 2016 he was awarded Marie Curie Fellowship by Eindhoven University of Technology, Eindhoven, The Netherlands to start his industrial doctorate. During Ph.D., he published several conference and journal papers and four patent applications under the supervision of Prof. Willems and Prof. Alvarado in Eindhoven University of Technology and under the supervision of Dr. Gustavsson from Ericsson Research. During his Ph.D., he was a research consultant at Ericsson Research, Gothenburg for more than two years. He further spent one month in QAMCOM research and technology, Gothenburg, working on RadComm. systems. He recently joined Imec in Eindhoven, Netherlands. His research interests are signal processing and wireless communication.